The roles of the neonatal Fc receptor and interferons in echovirus pathogenesis

by

Alexandra Isabella Wells

BS, Bucknell University, 2015

Submitted to the Graduate Faculty of the

School of Medicine in partial fulfillment

of the requirements for the degree of

Doctor of Philosophy

University of Pittsburgh

2022

UNIVERSITY OF PITTSBURGH

SCHOOL OF MEDICINE

This dissertation was presented

by

Alexandra Isabella Wells

It was defended on

February 28, 2022

and approved by

Christopher Bakkenist, PhD, Professor, Department of Radiation Oncology

Terence Dermody, MD, Professor, Department of Pediatrics

Timothy Hand, PhD, Assistant Professor, Department of Pediatrics

John Williams, MD, Professor, Department of Pediatrics

Dissertation Director: Carolyn Coyne, PhD, Professor, Department of Molecular Genetics and Microbiology, Duke University

The roles of the neonatal Fc receptor and interferons in echovirus pathogenesis

Alexandra Isabella Wells, PhD

University of Pittsburgh, 2022

Enterovirus infections are major sources of disease in humans. Echoviruses are a major subtype of enteroviruses and are especially devastating to neonates and young children. Despite the number of infections and potential adverse outcomes, the basic determinants of pathogenesis for echoviruses is poorly understood. This dissertation describes the identification of the neonatal Fc receptor (FcRn) as the entry receptor for echoviruses and the subsequent development of new *in vivo* models that fully recapitulate echovirus disease as well as establish the role of interferons during echovirus infections. Collectively, these studies show (1) that human FcRn is the entry receptor for echoviruses, (2) that human FcRn and type I interferons mediate infection in the liver, (3) that type I and III interferons play differential roles in infection of the gastrointestinal tract and dissemination to other tissues, (4) the meninges of the brain are the main target of echovirus infection and (5) that the host interferon stimulated genes that target enteroviruses function in pan-enterovirus- and enterovirus-species specific manners.

Table of Contents

List of Tables

List of Figures

1.0 Introduction

Enteroviruses are a major source of human disease, particularly in neonates and young children where infections can range from acute, self-limited febrile illness to meningitis, endocarditis, hepatitis, and acute flaccid myelitis. Enteroviruses primarily infect by the fecal-oral route and target the gastrointestinal epithelium early during their life cycles. These viruses bind to a proteinaceous receptor on the cell surface and begin the process of internalization. Once internalized, enteroviruses are detected by intracellular proteins that recognize common viral features and trigger antiviral innate immune signaling. These pathways often lead to the production of IFNs and interferon stimulated genes (ISGs). ISGs can directly or indirectly inhibit different stages of the viral lifecycle. However, co-evolution of enteroviruses with humans has allowed them to develop strategies to evade detection and/or to disrupt intracellular signaling. This chapter will discuss how enteroviruses infect the gastrointestinal tract, the mechanisms by which cells detect enterovirus infections to induce IFNs and ISGs, and the strategies enteroviruses use to escape this detection.

1.1 Interferons at barrier surfaces

Barrier surfaces such as the epithelium lining the respiratory and gastrointestinal (GI) tracts, the endothelium comprising the blood-brain barrier (BBB), and placental trophoblasts provide key physical and immunological protection against viruses. These barriers utilize nonredundant mechanisms to suppress viral infections including the production of interferons

(IFNs), which induce a strong antiviral state following receptor binding. The innate immune system is activated by the recognition of 'non-self' from 'self' through diverse pattern recognition receptors. This recognition of a foreign substance induces complex signaling pathways that are essential for mounting an immune response to the pathogen and, if necessary, to induce the adaptive immune response. Interferons (IFNs) are key cytokines induced during innate immune detection of viral infections. IFNs play a primary role in barrier defenses and are important for barrier function and integrity in the face of viral infections. However, whereas type I IFNs control infection systemically, type III IFNs (IFN-λs) control infection locally at barrier surfaces and are often preferentially induced by these cells. In this chapter, we focus on the role of type I and III IFNs at barrier surfaces, focusing on the respiratory and GI tracts, the BBB, and the placenta and how these IFNs act to suppress viral infections.

1.1.1 Barrier Surfaces

Cellular barriers establish both physical and immunological defenses to prevent viruses from breaching key entry portals into the human body. These barriers can include the epithelium lining the gastrointestinal (GI) and respiratory tracts, the microvasculature that forms the blood brain barrier (BBB), and fetal-derived trophoblasts that constitute the placental barrier during pregnancy **(Figure 1)**. In addition to forming a physical barrier, these cell types sometimes also function as conduits at key cellular interfaces in order to exchange gases, small molecules, and nutrients. Thus, cell types that constitute barrier surfaces have evolved unique mechanisms to defend against viral infections, while retaining their critical role in maintaining cellular homeostasis. Breakdown of these barriers can have far-reaching impacts. For example, disruption

of the placental barrier could allow for pathogenic microorganisms to gain access to the fetal compartment, which can induce fetal demise and/or congenital malformations in some cases[1].

Each of the barrier cell types mentioned above have evolved unique defense mechanisms to limit access by viruses. In addition, these cell types have, in some cases, also co-evolved shared defensive strategies despite their disparate locations throughout the body. These shared mechanisms include goblet cell-derived mucus secretions in the GI and respiratory tracts, which coat the cell surface with a protective barrier, the formation of junctional complexes that limits paracellular transport, and the formation of complex apical actin networks that limit direct passage across the cell surface, amongst others[2,3]. Secondary to physical (or natural) protective strategies is the innate immune system. The innate immune system is essential for alerting the body to pathogen infection and is highly evolutionarily conserved. The innate immune system is activated by the recognition of 'non-self' from 'self' through diverse pattern recognition receptors. This recognition of a foreign substance induces complex signaling pathways that are essential for mounting an immune response to the pathogen and, if necessary, to induce the adaptive immune response. Interferons (IFNs) are key cytokines induced during innate immune detection of viral infections. IFNs play a primary role in barrier defenses and are important for barrier function and integrity in the face of viral infections. In this review, we discuss disparate barrier surfaces in the body and how type III IFNs play a critical role in antiviral defenses at these surfaces.

1.1.2 Interferon discovery

IFNs are a diverse family of cytokines with potent antiviral activity against many classes of viruses[4]. IFNs consist of three families: type I, type II, and type III IFNs. In this review, we will

focus mainly on the antiviral activities of type I and III IFNs given their involvement at the interface of barrier surfaces. Type I IFN was discovered in 1957 by Isaacs and Lindenmann, who named the factor because of its ability to interfere with viral replication[5]. This family of IFNs includes many different subtypes, including 13 IFN-α subtypes and a single IFN-β subtype. Type I IFNs are located on chromosome 9 in humans and on chromosome 4 in mice[6]. In humans, type I IFN is located in an intron-less region of the chromosome where the alpha subtypes are on the 3' end, with IFN-β on the 5' end of the locus[7,8]. Type I IFNs signal through the heterodimeric type I IFN receptor (IFNAR1/2) complex to induce hundreds of antiviral interferon stimulated genes (ISGs). IFNAR is expressed on all nucleated cells, which allows type I IFNs to produce a potent systemic antiviral state.

Type III IFNs are the most recently discovered family of IFNs. This family includes IFN-λ1, IFN-λ2, and IFN-λ3, also known as interleukin IL-29, IL-28A, and IL-28B[9,10]. In 2013, a fourth type III IFN, IFN-λ4, was discovered[11,12]. IFN-λ4 has been shown to be antiviral against hepatitis C virus in cultured Huh7 liver cells[12]. However, it is nonfunctional in a large subset of the world's human population due to a single nucleotide polymorphism (SNP) that causes a frameshift in the gene[11,12]. Type III interferons are located on chromosome 19 in humans and on chromosome 7 in mice[13]. Unlike the type I IFN locus, the type III genetic cluster consists of introns and exons within each IFN-λ gene[13,14]. Each IFN-λ gene has 5 exons; this characteristic shares homology to the IL-10 cytokine family[15]. Type III IFNs share homology with the IL-10 cytokine family and share the IL-10R2 receptor subunit, leading to the speculation that these cytokines might be evolutionarily related[4,16]. The receptor is heterodimeric and includes the other lambda receptor subunit, IFNLR1. However, whereas virtually all cells express the functional type I IFN receptor IFNAR, the expression of the type III receptor IFNLR complex is most commonly restricted to cells at mucosal

and other barrier surfaces[17]. Although the full repertoire of immune cells that do or do not respond to type III IFNs has yet to be fully elucidated, it is becoming clear that some immune cell populations may not be responsive to type III IFNs due to their lack of IFNLR expression[18]. Neutrophils are one of the few immune cell that expresses the IFNLR and can respond to IFN-λ and represent an important bridge between innate and adaptive immunity[19,20]. Thus, whereas type I IFNs function in a broad systemic manner, type III IFNs produce a more localized antiviral state, which may be largely restricted to barrier-associated cell types **(Figure 1)**.

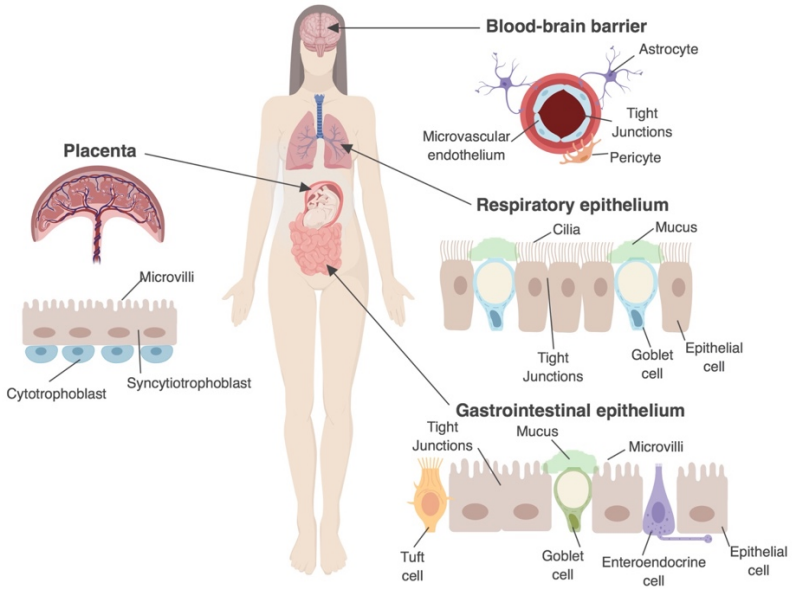

Figure 1 Protective cellular barriers of the human body

The cell composition of the blood-brain barrier, respiratory tract, gastrointestinal tract, and placenta are shown. The blood-brain barrier is made up in part of microvascular endothelial cells which form a physical barrier between the brain and the blood. The respiratory epithelium is composed of epithelial cells and goblet cells, which secrete mucus. The respiratory epithelial cells have cilia which beat in concert to clear mucus. The gastrointestinal tract contains enterocytes which have microvilli and goblet cells which secrete mucus. The human placenta is composed in part by the outermost syncytiotrophoblasts and inner cytotrophoblasts. Syncytiotrophoblasts form a dense brush border, but unlike the respiratory and GI epithelium, does not contain junctional complexes between cells (as the syncytium is a continuous layer). Figure was made with Biorender.com.

1.1.3 Interferon induction and signaling

Both type I and III IFNs are induced through the recognition of pathogen associated molecular patterns (PAMPs) or damage associated molecular patterns (DAMPs) by pattern recognition receptors (PRRs). PRRs, such as Toll-like receptors (TLRs), recognize common features of microorganisms, which thus provides them with a strategy to detect diverse and unrelated pathogens[21]. When PRRs recognize a PAMP, an intracellular signaling cascade is induced, thus altering the transcriptional profile of the cell and leading to the upregulation of transcription factors such as Interferon Regulatory Factors (IRFs) and NF-κB, which in turn induce IFNs **(Figure 2)**. The induction of each class of IFNs has been shown to require slightly different proteins to bind to the promotor of a given gene[22]. For example, IFN-β induction requires the binding of NF-κB, AP-1, and phosphorylated IRF3[23]. IRF7 does not typically bind to the promotor of IFN-β in unstimulated cells, largely due to the fact that it is itself an ISG and must be upregulated before it can become fully expressed and activated. If IRF7 is present and phosphorylated, it can then bind to the IFN-β promoter in the place of IRF3[22,23]. On the other hand, a recent study showed that the IFN-λ1 promoter has multiple NF-κB binding sites, suggesting that binding of multiple NF-κB proteins can induce expression. This study concluded that IFN-λ1 can be induced by the binding of multiple NF-κB proteins to the binding sites within the promoter region, without the requirement for IRF3 binding or another factor[24]. Once IFNs are expressed, they then initiate a positive feedback loop that can act in both autocrine and paracrine manners[25].

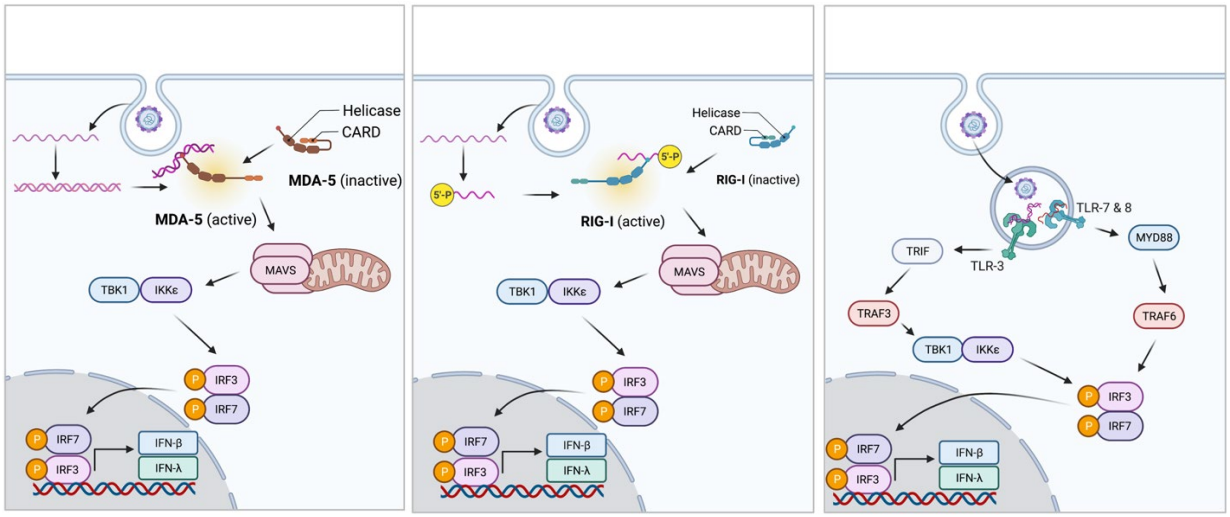

Figure 2 Interferon induction pathway

When the host cell detects a foreign nucleic acid, a signaling cascade begins to induce interferons. Cytoplasmic detection includes MDA-5 (left) and RIG-I (center). Endosomal detect includes TLR-7 and TLR-8 (right). MDA-5 and RIG-I trigger a signaling cascade through MAVS to induce IFNs. The left shows viral RNA detection by TLRs within the endosome. A signaling pathway is triggered leading to the induction of interferons. Figure was made with biorender.com.

As discussed above, type I IFNs signal through the heterodimeric IFN-α/β receptor (IFNAR1/2) whereas type III IFNs signal through the heterodimeric IFN-λ receptor (IFNLR1/IL10R2)[26]. However, despite their distinct induction differences and usage of receptor complexes, once type I or III IFNs bind to their respective receptors, the downstream signaling process is almost identical and leads to the induction of hundreds of ISGs through the canonical signaling pathway **(Figure 3)**[26,27]. However, the kinetics of ISG induction have been shown to differ in some cell types. For example, hepatocytes express IFNLR and are able to respond to type III IFN, however, type I and III IFNs vary in the magnitude and induction pattern of ISGs they induce in these cells[28]. Another group showed that both whereas both type I and III IFNs induce a

similar number of ISGs, type III IFN induced a slightly different subset of ISGs in a polarized murine intestinal epithelial cell line[29]. Other studies have indicated that human stem cell-derived enteroids treated with either IFN-β or IFN-λ induce ISGs in a similar manner[30]. These results indicate that ISG induction by type I and III IFN is dependent on many factors, such as IFN concentration, cell and tissue type, and time points assessed. Together, these studies show that the presence of IFN and ISGs trigger a state of antiviral immune response in cells.

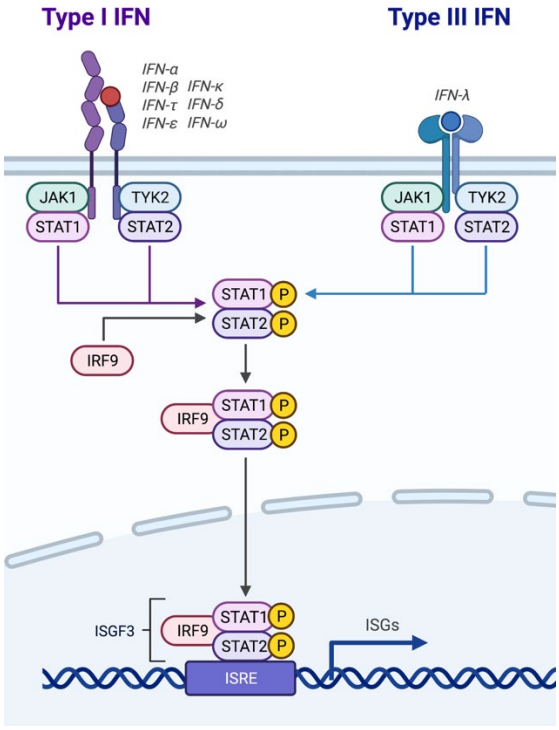

Figure 3 ISG induction pathway

Once secreted, IFNs bind to their respective receptors on the cell surface of the cell. This triggers a signaling cascade through the Jak/Stat pathway leading to the induction of antiviral ISGs. Figure was made with biorender.com.

1.1.4 Antiviral activity of IFN-λs at epithelial and endothelial barriers

1.1.4.1 Respiratory Tract

The respiratory tract is a pseudostratified columnar epithelium composed of ciliated epithelial cells, mucus-secreting goblet cells, and basal cells **(Figure 1)**. The epithelium forms a physical barrier in part due to the presence of tripartite junctional complexes (composed of tight and adherens junctions, and desmosomes) that form between neighboring cells to restrict the free flow of ions and solutes[31]. Two mechanical defense mechanisms that the respiratory tract utilizes to defend against viral invasion are the beating of cilia on the apical surface of all ciliated cells and mucus secretion from goblet cells. Cilia beat in a synchronized motion to move mucus out of the respiratory tract in order to clear pathogens[32]. In contrast, junctional complexes form a belt-like structure along the apical-most domains of the paracellular cell surface to restrict virus access to the subcellular domains[3]. Collectively, these defensive strategies work in concert to directly clear viruses from the lungs or to prevent their penetration into the bloodstream should they bypass other physical defenses. However, if these physical barriers are breached or weakened, which can occur in the context of both normal and abnormal physiologic states, IFNs form a key antiviral defense.

The respiratory epithelium secretes type III IFNs as an antiviral response to viruses that might damaging this barrier[33–35]. Studies have shown that primary murine tracheal respiratory epithelial cells and murine lung epithelial cell lines are able to respond to both type I and III IFN[36,37]. Although these cells can respond to both types of IFNs, they preferentially induce type III IFNs in response to influenza A virus (IAV), respiratory syncytial virus (RSV), *M. tuberculosis*, and other viral infections[38–41]. In primary cultures of human airway epithelium grown at an air liquid interface (ALI), type III IFNs are preferentially secreted into both the apical and basolateral compartments in response to IAV infection[37,39]. Additionally, when ALI cultures were pretreated

with recombinant IFN-λ, IAV replication was reduced[36]. Although recombinant type I IFN can restrict IAV replication, it is not typically secreted by these cells during a natural infection[36,42]. In mice, type III IFNs are also preferentially induced by IAV infection[33] and mice deficient in IL28RA exhibit higher levels of IAV replication compared to wild type controls[43]. Similar findings have been shown in the context of RSV infection[41]. Collectively, these studies show that IFN-λ is an important mediator of antiviral defenses in the respiratory tract.

1.1.4.2 Gastrointestinal tract

The GI tract is a complex surface that acts as a protective and immunological barrier in a diverse microbial environment. The GI epithelium is composed of at least seven distinct cell types, including Paneth cells, goblet cells, enterocytes, and enteroendocrine cells, amongst others **(Figure 1)**. The physical barriers that comprise the respiratory epithelial barrier (described above) are largely shared by the GI epithelium, with the exception of beating cilia. In contrast to beating cilia, the GI epithelium contains a dense brush border at the apical surface of the epithelium, which is supported by a dense cortical actin network that acts to prevent viral access to the cytosol[3].

Historically, the role of IFNs in the GI tract has mostly been studied in the context of cell lines[44]. These cell line-based studies have shown that both type I and III IFNs can be rapidly induced upon the recognition of PAMPs and that these cells are able to mount an antiviral response against enteric viruses[29,45]. Type III IFNs have been shown to induce ISGs in intestinal-derived cell culture models in response to many important enteric viruses, including rotavirus, reovirus, norovirus and enteroviruses in the GI tract[46–49]. These studies have shown that IFN-λ has an important role at the GI epithelium, however, immortalized cell lines are often derived from

malignancies, in which native healthy cell signaling pathways are inherently altered and that these lines do not recapitulate the diversity of cell types present in the epithelium.

Recently, new advances in primary intestinal stem cell-derived *in vitro* enteroid and organoid models have provided new systems to study enteric virus infections in the setting of a multicellular GI epithelium. Several studies have shown the ability of human intestinal enteroids and organoids to respond to both type I and III IFNs and to induce IFNs and/or ISGs in response to enteric viral infections[47–51]. However, although human intestinal organoids induce the expression of both type I and III IFNs at the transcript level in response to rotavirus infections, only type III IFNs are secreted from infected cells[52,53], suggesting that the GI epithelial cells are preferentially secreting type III IFNs over type I IFNs. When intestinal enteroids or organoids are pretreated with either type I or III IFN, rotavirus replication is decreased, indicating that type I and III may induce similar antiviral states[46,51,54]. In mice, IFN-λ restricts norovirus and reovirus replication in the intestine[47,48,53]. Thus, a growing body of work in cell lines, primary stem cell-derived organoids, and *in vivo* demonstrate the prominent role of type III IFNs in restricting enteric virus infections.

1.1.4.3 Blood brain barrier

The BBB is composed of microvascular endothelial cells, pericytes, and astrocytes and is a selective transport membrane that serves as the protective barrier surrounding the brain **(Figure 1)**. The BBB protects the central nervous system from a wide variety of toxins and microorganisms in the blood, while allowing for the selective exchange of ions and solutes. Similar to polarized epithelial cells, the microvascular endothelial cells that comprise the BBB are connected by junctional complexes between adjacent cells. In addition to its barrier properties, the BBB microvasculature is important for the exchange of signals between the brain and the circulatory

system. Beneath the endothelium is a continuous basement membrane that connects the microvasculature to the pericytes and endfoot astrocytes that further limit permeability of the barrier[55]. Disruption of the BBB is induced by infection by several neurotropic viruses, such as West Nile Virus (WNV), and is caused by both host and viral factors[56,57].

Type III IFNs play important roles in antiviral defenses at the BBB[56,58]. However, the mechanisms by which type III IFNs restrict viral infections at this barrier site may be unique. Unlike the canonical mechanism of IFN-induced antiviral defenses through ISG induction, type III IFNs also function to protect mice from WNV infection through non-ISG-dependent mechanisms. Mice lacking functional type III IFN signaling (*Ifnlr1*$^{-/-}$) exhibit increased BBB permeability and higher viral titers after WNV infection relative to wild type controls[56]. However, unlike the canonical pathway of ISG induction, IFN-λ appears to exert its antiviral activity at least in part from a direct increase in endothelial barrier properties. Treatment of cultured brain microvascular cells with recombinant IFN-λ increases transendothelial resistance values (TEER) *in vitro,* a measure of the ability of the endothelium to resist ion flow, through a transcription-independent mechanism[56]. This study suggests that these IFNs may defend against viral infection of barrier cell types through ISG-independent mechanisms, however, whether this property is shared amongst other barrier cell types has yet to be determined.

The role of type III IFNs in the human BBB are less clear, owing in part to the difficulties of modeling this complex system *ex vivo*. Studies utilizing cultured human BBB microvascular endothelial cells suggests that type III IFNs also play a key role in human BBB endothelial cells and respond to synthetic ligands of viral RNA or to viral infections by potently inducing type III IFNs[59]. When immortalized human BBB microvascular endothelial cells are stimulated with the synthetic vRNA ligand poly(I:C), they respond by secreting high concentrations of IFN-λ

compared to mock-treated cells. At low doses of poly(I:C), these cells also secrete higher concentrations of IFN-λ than IFN-β compared to mock-treated cells, suggesting that type III IFNs are preferentially released in these cells similar to epithelial-derived cell types[59].

1.1.5 Concluding remarks on interferons at barrier surfaces

In addition to their role as a physical barrier, it is becoming clear that the cell types that comprise the barriers in the human body are also dynamic and highly reactive chemical barriers that use type III IFNs to protect these sites from viral infections. The role of IFN-λ in the protection of the BBB and the GI and respiratory tracts have clearly established these molecules as essential in antiviral defenses in these critical tissues.

1.2 Enterovirus Biology

The enterovirus genus includes poliovirus, coxsackieviruses, echoviruses, enterovirus 71, and enterovirus D68. Enteroviruses primarily infect by the fecal-oral route and target the gastrointestinal epithelium early during their life cycles. In addition, spread via the respiratory tract is possible and some enteroviruses such as enterovirus D68 are preferentially spread via this route. Following infection in the primary site of infection, enteroviruses disseminate to secondary target sites in the body where these viruses cause clinical disease.

1.2.1 Enterovirus infections in humans

According to the Centers for Disease Control and Prevention, enteroviruses cause at least 10-15 million symptomatic infections in the United States each year[60]. These viruses belong to the *Picornaviridae* family and are small, non-enveloped viruses that have a single stranded positive sense RNA genome. The enterovirus genus includes poliovirus (PV), coxsackieviruses, echoviruses, enterovirus 71 (EV71), enterovirus D68 (EV-D68) and rhinoviruses. These viruses are spread primarily through the fecal-oral route, but some species can be spread through respiratory secretions (e.g. EV-D68 and rhinovirus). Nonpolio enteroviruses are typically asymptomatic or cause minor clinical symptoms which include hand-foot-and-mouth disease and respiratory illness. In some cases, enteroviruses can cause severe complications which include acute flaccid myelitis, myocarditis, encephalitis, pancreatitis, hepatitis, and even death[61–64].

The pediatric and neonatal populations can develop severe symptoms and grave clinical outcomes of enterovirus infections[65–67]. In fact, enteroviruses are one of the top viral pathogens that cause outbreaks in neonatal intensive care units (NICUs) across the United States each

year[68,69] and infections in infants and neonates are associated with high morbidity and mortality. Additionally, enterovirus infections particularly impact young children during outbreaks, as seen in the EV71 outbreak in China from 2008 to 2012. This outbreak was responsible for over 7 million infections with a majority of infections in children under the age of five[70]. In addition to EV71 outbreaks, EV-D68 outbreaks have been intensifying throughout the world with outbreaks in 2014, 2016, and 2018[71]. EV-D68 outbreaks also typically impact neonates and children and have caused many cases of acute flaccid myelitis (AFM) in the United States including 120 confirmed cases across 34 states in 2014[72,73]. Although these severe outcomes are the focus of many studies, most individuals infected with enteroviruses are asymptomatic. Overall, enteroviruses are a significant public health concern, particularly in the pediatric population, due to severe complications from infection in children and neonates.

The immune response to enteroviruses is imperative for successful host clearance. A sufficient immune response to clear enterovirus infection includes the activation of innate immune signaling and a strong B cell response. The antibody response can be extremely important to clear an enterovirus infection. Previous studies have shown that about 50% of adults and older children have neutralizing antibodies against at least two non-polio enteroviruses and over 75% of adults and children have neutralizing antibodies to PV serotypes[74,75]. Neutralizing antibodies to PV arise from vaccination-induced long lived memory B cells and neutralizing antibodies that are protective against infection[76,77]. This suggests that neutralizing antibodies are important for protection from re-exposure and may explain why children and neonates are most likely to experience severe infection since they likely lack these antibodies[74]. Consistent with this, individuals with X-linked agammaglobulinemia, where the patient has little to no B cells, are highly susceptible to enterovirus infection[78,79]. In addition, mice deficient in B cells have high coxsackievirus B (CVB)

titers in their tissues and experience chronic infection and an inability to clear the virus[80]. Thus, the concerted actions of the innate and adaptive immune response allow for the clearance of enteroviruses.

1.2.2 Enterovirus infections of the gastrointestinal tract

Enteroviruses are primarily transmitted through the fecal-oral route and target the GI epithelium. Enteroviruses are typically ingested through contact with contaminated surfaces, food, and/or water. These viruses are not thought to cause gastrointestinal illness such as severe vomiting or diarrhea, but GI-associated complications may occur[81]. However, most cases of enterovirus infection are asymptomatic[82]. Once they infect the GI epithelium, enteroviruses can disseminate into secondary target tissues and can cause clinical disease in some cases. Enteroviruses have specific secondary tissue tropism that vary between enterovirus species. EV71 has been shown to disseminate into the skin and brain causing hand, foot and mouth disease and aseptic meningitis or acute flaccid myelitis, respectively[83]. On the other hand, coxsackievirus B (CVB) can disseminate to the heart and pancreas to cause myocarditis and pancreatitis[64,84,85]. Additionally, echoviruses target the liver as well as the brain causing acute liver failure and aseptic meningitis[63,86]. Despite these differences in secondary target tissues, most enteroviruses, with the exception of rhinoviruses and EV-D68, replicate in the GI epithelium. Enteroviruses target the epithelium for replication and therefore this barrier surface is an important defense mechanism for preventing the dissemination of these viruses into secondary target tissues.

1.2.2.1 The gastrointestinal tract

The gastrointestinal (GI) tract is a key defensive barrier against pathogenic bacteria and viruses. The GI tract is divided into different subsections: the duodenum, jejunum, ileum, which make up the small intestine, large intestine and colon. The GI tract is composed of an epithelial layer that forms a physical cellular barrier as well as a lamina propria that contains immune cells[87]. The lamina propria is essential to elicit an adaptive immune response to pathogens that breach the epithelium. This region contains dendritic cells and macrophages that are able to present viral antigens well as many other immune cells which are important for initiating a cellular immune response **(Figure 4A)**. In addition to these two compartments, specialized subsections of the epithelium and the lamina propria contain Peyer's patches. Peyer's patches contain organized lymphoid structures that sample the intestinal lumen to initiate mucosal immune responses. The formation and role of Peyer's patches in mucosal immunity have been extensively reviewed elsewhere[88–90].

The GI tract, like many barrier surfaces, has important defense mechanisms to prevent microbial invasion. The cells that comprise the epithelium are polarized, meaning they have a distinct apical and basolateral surfaces that contain distinct lipid and protein components. The apical surface of enterocytes, which make up a high proportion of the epithelium, contain microvilli that create a dense brush border. The GI epithelium forms a physical barrier due to junctional complexes composed of tight and adherens junctions as well as desmosomes **(Figure 4B)**[91]. These junctional complexes are important for restricting the free flow of ions and solutes[92]. In addition, differentiated enterocytes have a dense cortical actin network that is critical for preventing pathogens from gaining access to the subcellular domain[3]. Finally, the epithelium utilizes chemical defenses and secretes type I and III interferons (IFNs) to trigger an antiviral state

during viral infections[45,93,94]. The concerted actions of the epithelium and the cells that comprise the lamina propria are essential in the defense against enteric pathogens.

The GI epithelium has villus and crypt structures that influence the morphology of the intestine **(Figure 4A)**. The villi project into the intestinal lumen and are mainly composed of enterocytes with other cell types scattered throughout the villi. The base of the crypts contain stem cells that are responsible for the renewal of all the cell types of the GI epithelium[95,96]. The LGR5+ stem cells at the base of the crypt are lined by Paneth cells, which are critical for maintaining stem cell homeostasis (growth factor production) and the secretion of antimicrobial peptides[97,98]. Other cell types are also critical for stem cell differentiation, including crypt-specific fibroblasts[99]. In addition to stem cells and Paneth cells, the epithelium is composed of at least six distinct cell types that help execute the barrier's essential functions. The cell types can be broken into two main subgroups: those of absorptive and secretory lineages. The absorptive lineage is comprised mainly of enterocytes and microfold (M) cells. M cells are grouped into the absorptive lineage due to their role as conduits between luminal contents and immune cells in the lamina propria and Peyer's patches[100]. The secretory lineage includes enteroendocrine cells, Paneth cells, and goblet cells[101]. As the name suggests, cells comprising the secretory lineage mainly secrete proteins into the lumen of the GI tract. Goblet cells produce and secrete mucus which covers the epithelium and has a protective function against pathogens[2]. On the other hand, enteroendocrine cells produce hormones that are thought to provide signals to stem cells. Each cell type is responsible for separate functions to maintain homeostasis of the GI epithelium. Without each cell type, the delicate balancing act of protecting against pathogens, maintaining correct equilibrium with the microbiome, and the absorption of nutrients would be disrupted.

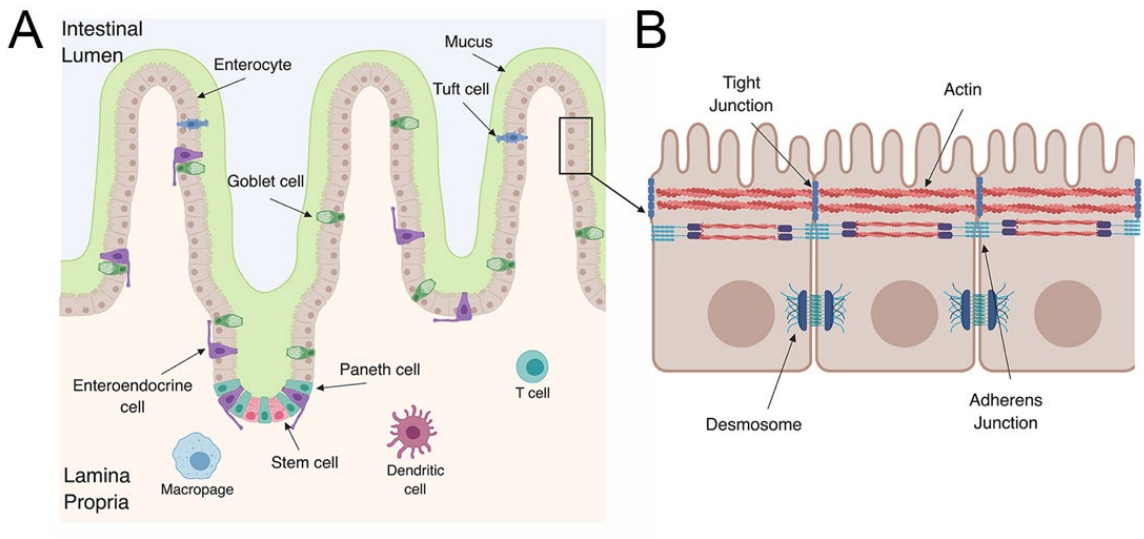

Figure 4 The gastorintestinal tract defenses

(A) The gastrointestinal tract is composed of numerous cell types which are important for immune activation and barrier surface defenses. The gastrointestinal epithelium is composed of enterocytes, goblet cells, Paneth cells, enteroendocrine cells, tuft cells, and stem cells. In contrast, the lamina propria is composed of immune cells such as dendric cells, T cells, and macrophages. (B) Polarized intestinal epithelial cells have distinct apical and basolateral domains. The apical domain contains microvilli and is closely associated with the actin cytoskeletal network. Figure was made with Biorender.com.

1.2.2.2 Enterovirus entry and replication

Enteroviruses initiate entry into a host cell by binding to cell surface receptors and undergoing receptor-mediated endocytosis. Entry receptors vary between enteroviruses and include scavenger receptor B2 (SCARB2) and P-selectin glycoprotein ligand 1 (PSGL-1) for EV71[102–104], the coxsackievirus and adenovirus receptor (CAR) for CVB[105–107], the poliovirus receptor (PVR/CD155) for PV[108], and the neonatal Fc receptor (FcRn) for echoviruses[109], amongst others **(Table 1)**. In some cases, enteroviruses bind to additional attachment factors, the most common of which is decay accelerating factor (DAF)/CD55[110,111]. Despite differences in cellular receptors, enteroviruses have generally well-conserved life cycles **(Figure 5)**. In intestinal epithelial cell lines, CVB binding to DAF has been proposed to facilitate the induction of cell

signaling from the apical domain, which in turn facilitates delivery of viral particles to their primary receptors[112]. Similarly, echovirus binding to DAF has also been proposed to facilitate entry into intestinal epithelial cell lines, although the role of intracellular cell signaling and the primary echovirus receptor in this process remains unclear[113].

After binding and entry, enteroviruses undergo uncoating in order to release the viral genome. Uncoating occurs either after the virus binds to the cell receptor or is initiated through a pH change in the endosome. This uncoating process allows the RNA genome to be released from the protective capsid into the cytoplasm or endosome. Several studies have investigated the speed at which PV virions uncoat in nonpolarized cells using either fluorescently labeled capsids and viral RNA (vRNA) or neutral red incorporated vRNA. These studies reveled that vRNA is released from the capsid within 30 minutes of entry[114,115]. However, other studies using polarized cells of the blood brain barrier with apical and basolateral domains suggest that uncoating is a slower process that requires actin cytoskeleton remodeling[116]. Additionally, the speed of uncoating may differ between enteroviruses based on the requirements of attachment factors, such as DAF, or other cellular proteins required for entry[112].

Once viral RNA has entered the cytoplasm it is translated by host ribosomes **(Figure 5)**. Historically, it was thought that the viral RNA was translated into a single polyprotein. However, a recent study discovered a second open reading frame (ORF) in some enterovirus genomes[117]. This study found a small ORF that is located in the 5' end of the untranslated region and is suggested to be important in replication in intestinal epithelial cells[117]. Regardless of whether it is a single polyprotein or two proteins, the resulting product is then proteolytically cleaved by the viral proteases 2A and 3C. The resulting proteins include 10 proteins such as capsid proteins and other replication proteins including the RNA-dependent RNA polymerase 3D ($3D^{pol}$). $3D^{pol}$

initiates the synthesis of the negative-stranded copy of the genome making a dsRNA intermediate which becomes the template to generate new positive-stranded genomes. Replication of viral RNA occurs in replication organelles that derive from host membranes that are induced upon viral infection[118]. These replication organelles can protect the RNA and replication intermediates from cytosolic localized innate immune pattern recognition receptors (PRRs) that are important for the detection of foreign RNA[118]. The newly synthesized positive-stranded genome is packaged into virions for release out of the cell. The virions are assembled into protomers and pentamers using the capsid proteins VP0, VP1 and VP3. After the RNA is packaged into the virion, VP0 is processed into VP2 and VP4 which results in mature enterovirus virions[82,119].

Classically, enteroviruses have been thought to exit the cell through a lytic form of cell death where the cell undergoes lysis and releases the progeny virions to infect neighboring cells[82] **(Figure 5)**. Recently, new studies have suggested that enteroviruses can also exit the host cell through non-lytic pathways[120–122]. These studies showed that during infection of PV and a related Picornavirus, hepatitis A virus, progeny virions are able to acquire host cell membranes to exit the cell in a vesicle in order to infect new cells[120,121]. These studies have shifted how enterovirus release is considered, but more work is needed to establish whether all enterovirus species are able to undergo non-lytic release and whether GI-derived cells permit this form of release.

Table 1 Enterovirus receptors and attachment factors

Host Protein	EV Serotype	Role	Reference
PVR (CD155)	PV	Uncoating	[108]
CAR	CVB1, CVB2, CVB3, CVB4, CVB5 & CVB6	Uncoating	[105–107]
DAF	CVA21, CVB1, CVB3, CVB5, E3, E6, E7, E11, E12, E13, E19, E19, E20, E21, E25, E29 & E30	Attachment	[110,111]
SCARB2	EV71, CVA7, CVA14 & CVA16	Uncoating	[102]
PSGL1	EV71, CVA2, CVA7, CVA10, CVA14 & CVA16	Attachment	[103,123]
KREMEN1	CVA10	Binding, entry, uncoating (?)	[124]
Sialic acid	EV71	Attachment	[125]
ICAM5	EV-D68	Binding, entry, uncoating (?)	[126]
Integrin $\alpha_2\beta_1$ (VLA-2)	E1	Uncoating	[127]
FcRn	E5, E6, E7, E9, E11, E13 & E30, others	Binding, entry, uncoating (?)	[109,128]

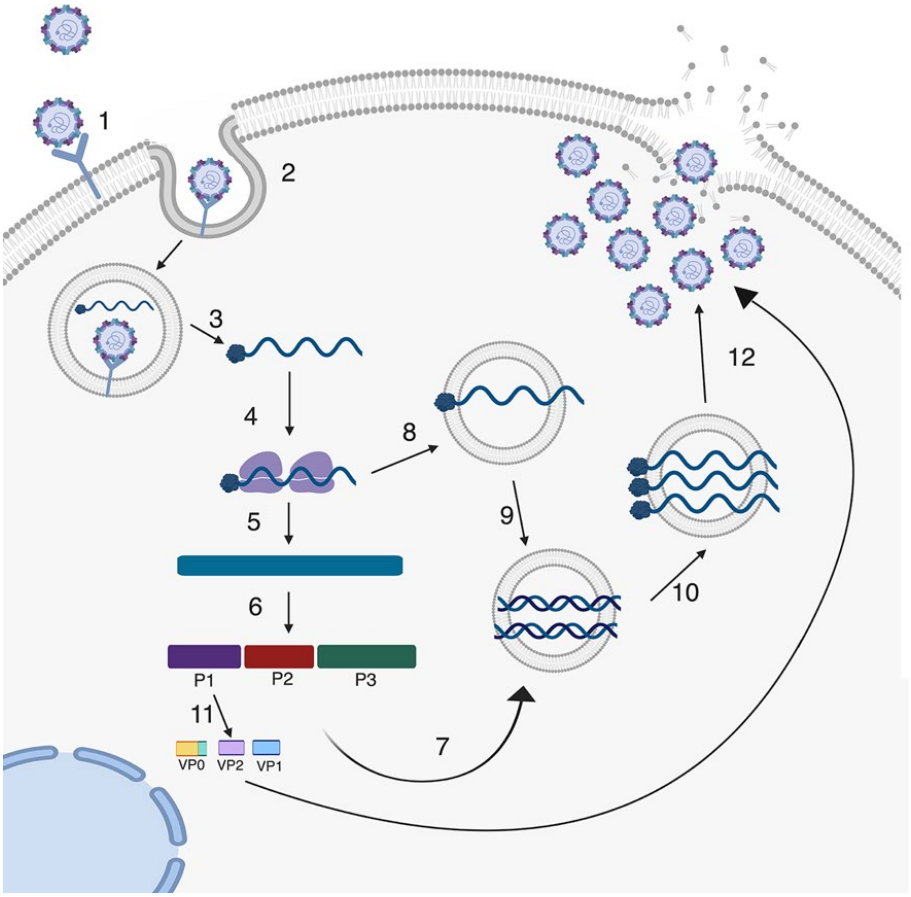

Figure 5 Enterovirus life cycle

Enteroviruses enter the cell through receptor mediated endocytosis (1). Following endocytosis, uncoating of the virion occurs in the endosome and the positive stranded RNA along with the covalently linked VPg protein is released into the cytoplasm (2 & 3). Viral RNA is translated by host ribosomes making a single polyprotein that is catalytically cleaved by enterovirus proteases $2A^{pro}$ and $3C^{pro}$ (4, 5, 6). After production and accumulation of non-structural proteins, including the viral polymerase, viral RNA is then replicated using the virally encoded RNA dependent RNA polymerase to generate a double stranded RNA (8 & 9). The negative sense RNA serves as the template to make more positive sense RNA. This newly produced RNA can be the template to produce more positive sense RNAs or serve as the genome for progeny viruses (10). Capsid proteins assemble and newly synthesized positive strand viral RNA is packaged into virion (11). Finally, new progeny virions are released either by non-lytic release where virions are released in vesicles (not shown) or are released when the cell undergoes lysis (lytic release) (12).

1.2.3 Detection of Enteroviruses by pattern recognition receptors

Detection of pathogens by the host immune system is an important first step in the clearance of viral pathogens. Previous studies have shown that echovirus 11 (E11), EV71 and CVB induce a robust innate immune response in intestinal epithelial cell lines and primary cells[49,129,130]. Viruses can be detected by the innate immune system in a variety of ways. PRRs are imperative in the detection and response to viral pathogens and are germ line encoded. PRRs detect pathogen associated molecular patterns (PAMPs) and respond by inducing an antiviral state.

1.2.3.1 Detection by TLRs

One class of PRRs is Toll-like receptors (TLRs). TLRs are a class of 10 transmembrane PRRs that recognize a variety of PAMPs. Within the TLR family, two additional categories exist, which are TLRs that are localized to the cell surface as well as TLRs that are localized to the endosome[131]. Generally, TLRs have a PAMP binding domain on the N terminal region of the protein that is either on the extracellular domain or in the endosomal lumen and an intracellular signaling region on the C terminal end[132]. Here we will only discuss TLRs which detect RNA viruses but note other TLRs exist to sense DNA virus and bacterial derived PAMPs, such as TLR5 (flagellin), which have been extensively reviewed elsewhere[132–134].

TLR3 is primarily expressed on the endosome and recognizes dsRNA[135]. TLR3 is expressed under basal conditions in most cells and is not typically induced by interferon (IFN) or enterovirus infection **(Figure 6)**[136]. TLR3 mediates an IFN response through Toll/IL-1 receptor domain-containing adaptor inducing interferon-beta (TRIF) and interferon regulatory factor (IRF)-3. The antiviral response mediated through TLR3 has been shown to be important in controlling PV, coxsackievirus A16 (CVA16) and coxsackievirus B3 (CVB3)[137–139]. In fact, the interferon

stimulated genes (ISGs) that are produced by the induction of type I IFNs downstream of TLR3 are directly antiviral against CVA16. When expression of TLR3 is knocked out in mice, these animals have a more severe CVA16 infection compared to wild type control animals and develop severe paralysis and death[138]. Others have shown that TLR3 is also imperative for antiviral signaling during PV infection in mice[140]. Additionally, *in vitro* studies have shown that when cells are depleted of TRIF, a downstream adaptor molecule of TLR3, EV71 replication increases[141]. Although a rare polymorphism in TLR3 was identified in a patient who developed CVB-associated myocarditis, genetic variants in TLR3 or other IFN-associated factors are not commonly found in patients with viral-associated myocarditis[142,143]. Instead, these patients often express variants in genes associated with inherited cardiomyopathies, suggesting that TLR3 signaling is not the sole determinant of CVB-induced myocarditis. Nonetheless, *in vitro* and *in vivo* studies provide strong evidence that TLR3 is important for the detection and antiviral control of many enterovirus species.

Several studies provide support that TLR3 is an essential TLR in enterovirus infection. However, other TLRs can also play significant roles. Although, TLR4 is thought to be key during bacterial infection since it mainly senses lipopolysaccharide (LPS), a protein found on gram negative bacteria, TLR4 plays an important role in secondary target tissues (tissues other than the route of entry) of enterovirus infection. TLR4 is localized to the cell surface where it can detect extracellular bacterial pathogens and has been shown to be important in myocarditis associated with CVB3 infection[144,145]. Studies have shown the TLR4 activation induces proinflammatory cytokines which is seen in dilated cardiomyopathy and a positive correlation between TLR4 and enterovirus RNA in endomyocardial biopsy tissues[145]. Furthermore, coxsackievirus B4 (CVB4) has been shown to induce proinflammatory cytokines through TLR4 in the pancreas which leads to the progression of type I diabetes[146]. It is still unclear how TLR4 detects enterovirus infection,

however evidence points to a role of TLR4 in the induction of proinflammatory cytokines and clinical pathology during infection.

Both TLR7 and TLR8 sense ssRNA and are localized to the endosome[147]. Typically, these TLRs are not thought to be ISGs and therefore their expression is independent of IFN induction. However, a number of studies have demonstrated that TLR7 and TLR8 can be induced upon enteroviral infection. CVB3 can induce TLR7 and TLR8 expression after 48hrs of infection at a low multiplicity of infection (MOI)[136]. Additionally, EV71 induces expression of TLR8 in cell lines and expression of TLR7 and TLR8 are increased in lung and brain tissues from children who died from EV71 infection[129,148]. Although the role of TLR7 and TLR8 have not been extensively studied during enterovirus infection, it is becoming clear that these PRRs may play key roles in the induction of proinflammatory cytokines. In fact, CVB is known to cause myocarditis due to chronic inflammation of the myocardium. This release of inflammatory cytokines has been linked to TLR8 and TLR4[149,150]. These studies suggest that TLR7 and TLR8 play a significant role in enterovirus infection.

1.2.3.2 Detection by RLRs

TLRs play a key role in the detection of extracellular and endosomal localized pathogens, but RIG-I like receptors (RLRs) are arguably the crucial sensors for the detection of enteroviruses due to their localization to the cytoplasm. RLRs that are able to detect RNA virus infection are Retinoic acid-inducible gene I (RIG-I) and Melanoma differentiation-associated antigen 5 (MDA5). Both MDA5 and RIG-I have two caspase recruitment domains (CARD-like domains) at the N terminus as well as a DExD box RNA helicase, which is important for the detection of viral PAMPs[151]. RIG-I is a cytosolic PRR that recognizes RNA ligands such as 5' triphosphate RNA (5' pppRNA) **(Figure 6)**[152]. *In vitro* data suggests that RIG-I is not always activated by enterovirus

infection due to the VPg protein binding to the free 5' triphosphate RNA, which would normally activate RIG-I[82]. However, recent studies have suggested a role of RIG-I in CVB3 infection[153,154]. Feng *et al* suggests that the 5' clover leaf of CVB3 is able to activate RIG-I since it contains triphosphate containing RNA[154]. However, this may be specific to CVB3 in cell line models since mice that are deficient in RIG-I have no difference in susceptibility to enterovirus infection compared to WT controls[155].

MDA5 detects long cytoplasmic dsRNA[156–158]. Several studies have indicated that MDA5 specifically interacts with enterovirus dsRNA, a replication intermediate, during CVA, CVB, EV71 and other enteroviruses[159–162]. Moreover, a polymorphism in MDA5 has been suggested to be a risk factor for more severe EV71 infection[163]. Children with this polymorphism exhibited more severe symptoms during EV71 infection compared to children without the polymorphism, suggesting a role of MDA5 in the detection of enterovirus infection. Furthermore, mice that are deficient in MDA5 are more susceptible to enterovirus infection and succumb to disease much more rapidly[161,164]. In addition to this increase in susceptibility, MDA5 deficient animals infected with CVB3 display severe hepatic necrosis of the liver[161]. Collectively, these studies point to the essential role of MDA5 in the detection of enteroviruses.

The adaptor protein for both RIG-I and MDA5 is the mitochondrial antiviral-signaling protein (MAVS) which is localized to the mitochondria and peroxisomes. When RIG-I or MDA5 are activated by dsRNA, the CARD domains become ubiquitinated[165,166], leading to the formation of MAVS aggregates in the mitochondrial membrane[167]. Aggregation of MAVS leads to the activation of NF-κB and IRF3, which then induce IFN[168]. *In vitro* studies have concluded that overexpression of MAVS can inhibit CVB3 replication by increasing the amount of IFN induction[169]. Although some studies have showed that MAVS deficient mice do not have an

increased CVB3 viral load compared to WT controls, these animals succumb to infection much earlier than WT animals, suggesting that MAVS signaling and MDA5 dependent activation of IFN is imperative to host response to infection[161]. Overall, these PRRs and adaptor molecules have been shown to be imperative for sensing enterovirus infections.

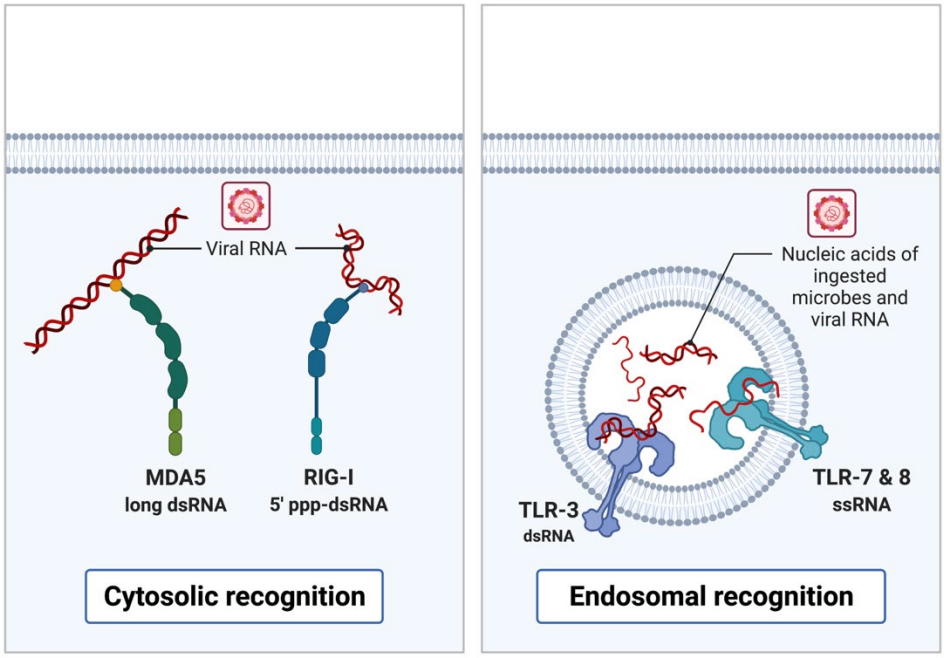

Figure 6 Cellular localization of pattern recognition receptors

Cellular pattern recognition receptors have different localizations to detect pathogen products. PRRs that detect enterovirus products are localized to the cytosol or endosome. Cytosolic PRRs include MDA5, which senses long dsRNA, and RIG-I, which detects 5' ppp-dsRNA, shown on the left. Endosomal localized PRRs include TLR-3, TLR-7, and TLR-8, shown on the right. Figure was made with Biorender.com.

1.2.4 Evasion of innate immunity by enteroviruses

Viruses have evolved mechanisms to evade the induction of the antiviral state of the cell. Viral protease-mediated cleavage of PRRs allow enteroviruses to impact downstream signaling cascades resulting in loss or reduced induction of IFN or interferon stimulated genes (ISGs). Table

2 summarizes these specific events and will be detailed below. As a result of these cleavage events, viruses are able to replicate more efficiently in the cell. Each species of enterovirus has developed its own set of mechanisms of evasion. Here, we will discuss current knowledge of evasion mechanisms of enteroviruses and how they antagonize host innate immune signaling.

1.2.4.1 Evasion of TLRs by enteroviruses

Enteroviruses are very efficient at disrupting downstream innate immune signaling (Figure 7**)** We have previously shown that in human embryonic kidney cells (HEK293), CVB3 3C protease ($3C^{pro}$) cleaves TRIF, a downstream adaptor molecule of TLR3[170]. Cleavage of TRIF results in loss of TLR3 dependent induction of IFN and NF-κB. Other groups have shown that EV-D68 and EV71 $3C^{pro}$ can also cleave TRIF resulting in decreased signaling downstream of TLR3[171,172]. These studies, which include many different enterovirus species, show that TLR3 dependent IFN induction is antiviral against enteroviruses and is a key evasion target for these viruses (**Figure 7**). In addition to TLR3, TLR7 has been shown to be targeted by some enterovirus species, but the mechanisms that they use to target it are not well understood. As discussed previously, some enteroviruses such as CVB3 can induce expression of TLR7 during infection. However, other enteroviruses seem to target TLR7. The detection of vRNA by TLR7 has been shown to increase autophagic flux[173]. In fact, one study showed that in human bronchial epithelial cells (16HBE), TLR7 dependent type I IFN induction is reduced by EV71 and CVA16[174]. This study concluded that autophagy induced by these viruses reduces endosome formation, resulting in the decreased expression of TLR7 to evade TLR7 dependent induction of autophagic flux in this cell type. This finding potentially demonstrates that some enterovirus species evade detection by TLR7, but others benefit from the induction of proinflammatory cytokines by TLR7.

1.2.4.2 Evasion of RLRs by enteroviruses

In addition to TLRs, enteroviruses also target members of the RLR family for cleavage to evade innate immune signaling **(Figure 7 and Table 2)**. MDA5, which is important for the sensing of enteroviruses in the host cell, is a target of viral proteases in many different studies. CVB3 $2A^{pro}$ has been shown to cleave MDA5 in HeLa cells[175]. However, this study does not determine whether the cleavage products are still able to induce IFN signaling or whether cleavage of MDA5 hinders MDA5-depedent IFN induction. Similar studies using CVA16, CVA6, and EV-D68 have indicated that $3C^{pro}$ cleaves MDA5[176]. Although the authors show that IFN signaling is disrupted when cells were transfected with $3C^{pro}$, they do not specifically show that the cleavage products are not functional in inducing an IFN response. Additionally, MDA5 has been shown to be cleaved in PV infected HeLa cells[177]. However, unlike the prior studies, this study concluded that the cleavage was not dependent on viral proteases but was instead mediated by cellular caspases activated during infection[177]. Furthermore, EV71 is able to cleave MDA5, but the mechanism is less clear[160]. Apart from the different mechanisms enteroviruses use to disrupt MDA5 signaling, infected cell lines have been shown to have cleavage products resulting in the inhibition of IFN induction.

RIG-I has also been shown to be cleaved in cells infected with different enteroviruses. Since RIG-I mainly detects 5' pppRNA, the reason why enteroviruses would target this RLR is not well understood but as discussed before, new evidence suggests that RIG-I may detect enteroviruses. PV $3C^{pro}$ is able to cleave RIG-I in infected HeLa cells by 6 hours post infection[178]. In addition to viral protease-mediated cleavage of these sensors, EV71 alters IFN induction by targeting the ubiquitination of RIG-I[179], which is critical for downstream signaling[179,180]. Previous studies have shown that CYLD (cylindromatosis), a deubiquitinating enzyme, is a negative regulator of RIG-I[181]. During viral infection, a cellular microRNA, miR-526a, is upregulated and

induces the downregulation of negative regulator, CYLD, leading to enhanced signaling of RIG-I. However, EV71 is able to downregulate miR-526a resulting in normal levels of CYLD[182]. As a result, RIG-I ubiquitination decreases inhibiting IFN induction. Further research to delineate the specific enterovirus PAMP that RIG-I is able to detect to induce IFN and the mechanisms enteroviruses use to target RIG-I will be needed to understand this aspect of enterovirus infection.

Numerous studies have investigated the viral protease mediated cleavage of MAVS. Targeting MAVS, the adaptor protein of RIG-I and MDA5, ablates IFN induction of both RIG-I and MDA5 making this protein an essential target of many enteroviruses. CVB3 $2A^{pro}$ and $3C^{pro}$ cleave MAVS in various cell lines[170,175]. The resulting cleavage products are nonfunctional and are deficient in NF-κB and IFN signaling[170]. EV71 $2A^{pro}$ is able to cleave MAVS in HeLa cells[175,183]. These studies showed that, similar to CVB infection, the products of MAVS in EV71 infected cells are deficient in NF-κB and IFN signaling[175,183]. However, since these studies are mainly performed in cell lines, further research is needed to determine if enteroviruses behave similarly in primary cells such as those of the GI tract.

Table 2 Enterovirus targets of PRRs

Host Protein	EV Serotype	Mechanism of Cleavage	Reference
TRIF	CVB3	$3C^{pro}$	170
	EV-D68	$3C^{pro}$	172
	EV71	$3C^{pro}$	171
RIG-I	EV71	Decreases ubiquitination of RIG-I inhibitin recruitment to MAVS	179,180
	PV	$3C^{pro}$	178
MDA5	CVA6	$3C^{pro}$	176
	CVA16	$3C^{pro}$	176
	CVB3	$2A^{pro}$	175
	EV-D68	$3C^{pro}$	176
	EV71	Unknown	160
	PV	Caspase Dependent	177
MAVS	CVB3	$2A^{pro}$, $3C^{pro}$	170,175
	EV71	$2A^{pro}$	175,183

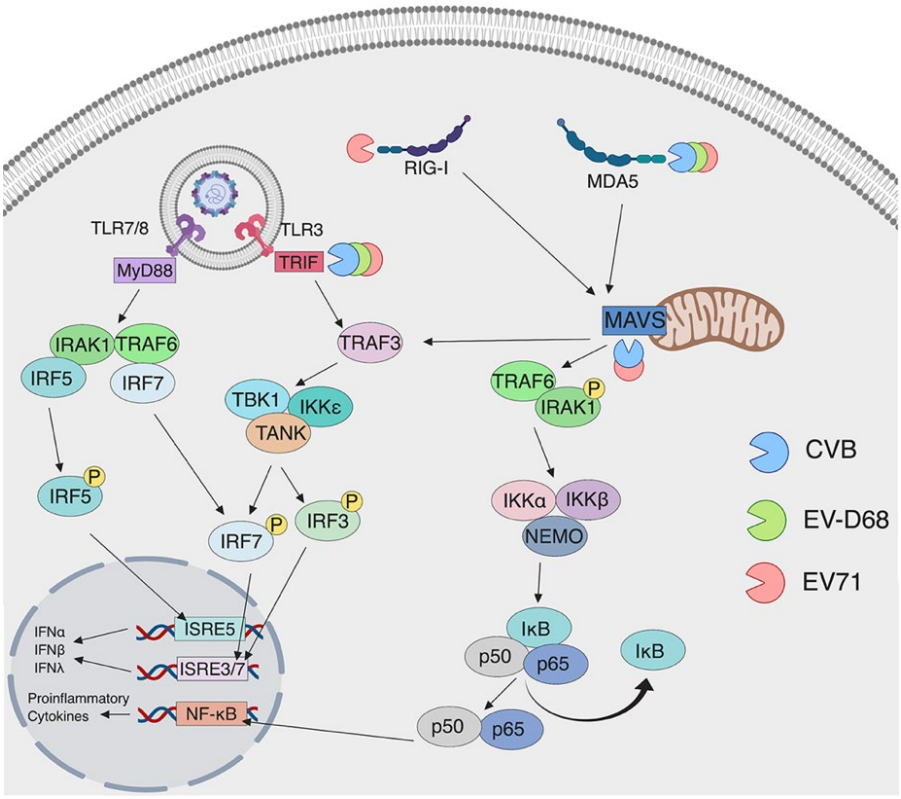

Figure 7 Enterovirus evasion strategies of PRR-mediated signaling

Enteroviruses target innate immune signaling proteins through cleavage by the viral proteases 2A and 3C. Shown are the targets for the CVB (blue), EV-D68 (green) and EV71 (red) proteases. All three viral proteases target MDA5 and the TLR adaptor protein, TRIF as mechanisms to halt antiviral innate immune signaling in infected cells.

1.2.5 Existing models to study enteroviruses in the gastrointestinal tract

1.2.5.1 *in vitro* and *ex vivo* models to study enterovirus infection

Many different models to study enteroviruses in the GI tract exist. These include cell lines, three-dimensional cell culture-based models, mouse models, and non-human primate models. Cell lines that model the GI tract and have been applied to enterovirus research include Caco-2, HT-29, T84, MODE-K (murine), and IEC-6 (rat) cells. The main cell line that has historically been

used to model enteroviral infections of the human intestinal epithelium is Caco-2 cells. Caco-2 cells have characteristics of enterocytes, which includes a brush border and tight junctions[44]. In addition to standard culture systems that utilize Caco-2 cells, we have also developed a three-dimensional culture model using Caco-2 cells grown on beads in a rotating wall vessel bioreactor that exhibit the properties of the intestinal epithelium and have applied this system to model enterovirus infections in the GI tract[184].

Other 3-D culture model systems include organoids. Organoids are 3-D enterospheres that are derived from pluripotent stem cells or embryonic stem cells [185]. Organoids are spherical structures that are hollow in the middle, have apical and basolateral polarity, and form a spherical layer of epithelium[186,187]. Pluripotent stem cells are differentiated into ectoderm, then hindgut ectoderm, and finally form spheroids with the addition of correct growth factors [54,185]. In addition, organoids contain a mesenchymal cell layer that develops under the organoid. Studies have shown that organoids are able to differentiate into the absorptive and secretory lineages of the GI epithelium[185]. However, this culture model has not yet been applied to enterovirus research.

In addition to organoids, enteroids are used as another 3D system to model the GI epithelium. Enteroids are formed through the isolation of intestinal crypts from whole human and murine intestinal tissues[188], which contain LGR5+ stem cells[96]. The crypts can be isolated and plated in Matrigel, where they from 3D spherical enteroids, or on transwells, where they form 2D monolayers that exhibit barrier function **(Figure 8)**[49,130,189]. Enteroids that are plated in matrigel have an 'inside out' phenotype, where the apical surface is facing into the lumen and the basolateral surface is on the outside of the structure[130]. This makes the Matrigel model a difficult model for studying viruses that use receptors that are localized to the apical surface since the apical surface is not accessible without disruption of the 3-D nature of these structures. To overcome this

limitation, we and others have developed a transwell-based model system in order to gain access to both the apical and basolateral surfaces[130,190,191]. These transwell models allow for infection at either the apical or basolateral surfaces and for collection of growth medium from these distinct compartments. We have applied both Matrigel- and transwell-based enteroid models to study enterovirus-GI interactions (**Figure 8**). Using these systems, we have identified differences in the cell-type specificity by which enterovirus target the GI epithelium. For example, whereas E11 preferentially infects enterocytes and enteroendocrine cells, EV71 replication is largely restricted to goblet cells[49,130]. In addition, using a transwell-based model, we have shown that enteroviruses also exhibit differences in the polarity by which they enter into and egress from the epithelium, with E11 exhibiting a basolateral polarity of entry and a bidirectional manner of egress whereas EV71 both enter and is released preferentially from the apical domain[130]. Perhaps most striking in these models is the robust antiviral response elicited in response to enterovirus infections. In contrast to most cell lines, which induce little to no IFN signaling, primary human enteroid models potently induce an antiviral response to enteroviral infections[130]. Perhaps not surprisingly given their role in barrier defenses, these models almost exclusively induce antiviral type III IFNs in response to infection. Collectively, these data highlight the potential relevance of primary-based intestinal cell systems to model enterovirus infections. Although these *in vitro* models recapitulate the multicellular complexity of the small intestine making them a more physiologically relevant model compared to cell lines, however they lack bacterial interactions, which can impact enteroviral infection. *In vitro* studies have shown that PV virions can bind to bacteria and that some bacterial strains can facilitate enterovirus infection[192]. In fact, bacteria can aid in co-infection of different enteroviruses, which allows for genetic recombination[192]. Other studies have shown that certain species of bacteria can increase thermal stabilization of PV and CVB[193]. This leads to

the question of whether other enteroviruses are also impacted by bacterial co-infection and what impact this has on pathogenesis *in vivo*. Studies investigating the role of the microbiome on enteroviruses are imperative to understand *in vivo* pathogenesis.

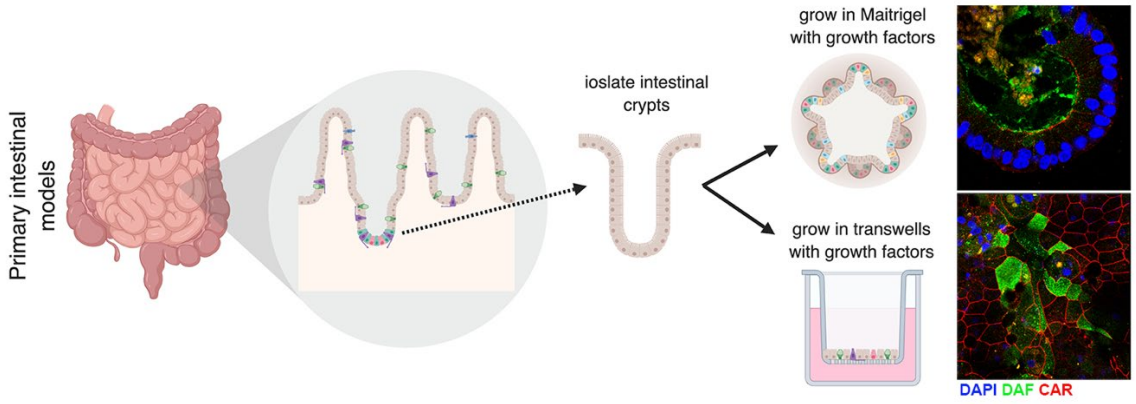

Figure 8 Primary intestinal models to study enterovirus infection

Intestinal crypts are isolated from the small intestine and plated either in Matrigel or on transwells. Crypts plated in Matrigel form a 3D structure called enteroids. When plated in Matrigel, enteroids have an 'inside-out' structure, where the apical domain faces inward, and the basolateral domain is facing outward. When crypts are plated on transwells, they form a monolayer that has apical and basolateral polarity. Images shown are from crypts that were plated in Matrigel (top) or on a transwell (bottom) and stained with DAF (green) and CAR (red), which are involved in CVB attachment, uncoating, and entry. Figure was made in biorender.com.

1.2.5.2 *in vivo* models to study enterovirus infection

While the above-described *in vitro* models have provided many insights into various aspects of enterovirus infections of the GI tract, *in vivo* models are also needed to understand complex interactions that occur during enteroviral infections, such as the interaction of viral particles with bacteria or the complex interaction with the immune system. One of the first mouse models to study enterovirus infection was the transgenic PV receptor mouse. The authors demonstrated that mice expressing the human homologue of the poliovirus receptor (PVR) were able to be infected with PV through intracerebral injection, where they displayed signs of paralysis similar to human disease[194]. Due to the route of infection, animals did not need to be

immunosuppressed such as blocking and depleting type I interferon receptor (IFNAR). Since this model was established, others have developed models for other enterovirus infection using a variety of different methods. Many mouse models of enterovirus infection use 'humanized' mice that express the human form of the viral receptor. Since mice are not the natural host of enteroviruses, the mouse homologs of the entry receptors are often not sufficient for infection or the affinity of viruses much less. Several groups have used this strategy, including generating 'knock in' animals expressing human SCARB2 for EV71 infection[195]. Very commonly, ablation of IFNAR or oral infection at high viral doses is required to generate *in vivo* mouse models of enteroviruses[196–198]. These strategies allow the infection of enteroviruses in mice, which normally do not support robust replication. However, many of these models are based on IP injection or other non-oral infection routes. However, this route of administration bypasses the primary site of infection observed in humans. Thus, models that include oral infection are imperative to understand how enteroviruses infect the GI tract and disseminate into secondary target tissues causing clinical disease.

Several models of oral infection have been established for a E11, PV, CVB, and EV71, and have been shown to recapitulate human disease[109,197,199–201]. An adult model of oral infection of CVB using IFNAR-deficient mice investigated the pathogenesis of a mutant CVB virus which emerged after passage through a mouse that exhibited a large plaque phenotype[196]. In addition to adult mouse models of oral infection, several studies have established neonatal infection models for a number of enteroviruses. We recently established a neonatal model for E11 infection by the enteral route in human transgenic mice expression the human homolog of FcRn[109] and showed that only transgenic mice exhibited viral replication in the small intestine, liver and blood seven days post oral infection[109]. An oral infection model of PV was established using transgenic animals

expressing the human homolog of PVR and using IFNAR deficient mice [197]. Neonatal, transgenic, IFNAR-deficient mice infected with PV exhibit viral replication in the blood and small intestine 2 and 3 days post oral infection[197]. In addition to E11 and PV, multiple neonatal model of oral EV71 infection have been established[200,201]. One study established an oral infection model using chimeric receptor-expressing transgenic mice, showing that oral infection of clinical isolates of EV71 leads to viral replication in the stomach, small intestine, colon and brain seven days post infection[200]. Another model of EV71 infection using outbred mice showed seven day old outbred mice that were orally infected with EV71 displayed skin rashes early during infection which progressed to hind limb paralysis[201].

In addition to mouse models, several studies have used non-human primate models to study EV71, CVB, and PV pathogenesis. One study showed that rhesus monkeys can be infected with EV71 through the intravenous, respiratory, and oral routes but had limited viral replication in the blood after intracerebral infection[202]. This study showed that EV71 disseminated to the brain and causes neuropathological damage[202]. Moreover, oral infection models of EV71 have been established in cynomolgus monkeys which showed degeneration and necrosis of neurons in the central nervous system of infected monkeys[203]. Additionally, neonatal rhesus monkeys animals infected with EV71 show signs of clinical hand, foot, and mouth disease as seen in humans[204]. Furthermore, a model of CVB-induced myocarditis was established using cynomolgus monkeys which exhibited viral myocarditis similar to human disease. This study showed that following intravenous inoculation with CVB, animals experienced myocardial injury and inflammatory cells infiltration in the heart of infected animals[205]. Another study using patas monkeys showed that intravenous CVB infection caused abnormalities in blood glucose as well as impaired insulin secretion[206]. In addition to EV71 and CVB, several models to study PV have been established

which include oral, subcutaneous, intravenous, intraspinal, and intracerebral infection[207–211]. These models were incredibly important for understanding the immune response to the PV vaccine[76,212]. One study showed that rhesus, cynomolgus, and bonnet macaques were all susceptible to oral PV infection[210]. When these macaques were fed PV, they developed paralysis[210]. Other studies have shown that infant cynomolgus monkeys that were fed PV developed paralytic poliomyelitis[213]. Together, the use of *in vitro* models and *in vivo* models, including mouse models and non-human primate models, will aid in our understanding of enterovirus entry, detection by the host immune response, and evasion mechanisms these viruses use to subvert the innate immune response.

1.2.6 Summary of enterovirus biology

Enteroviruses remain a significant global public health concern. The field has made significant progress in determining how enteroviruses are detected by host cells and the mechanisms they use to evade this detection. With the continued development of *in vitro*, *ex vivo*, and *in vivo* models that fully recapitulate the GI epithelium, we will gain a better understanding of the mechanisms used by enteroviruses to breach the intestinal barrier. These models could also facilitate the development of novel therapeutic targets and/or strategies to prevent or treat enterovirus infections and ultimately alleviate morbidity and mortality caused by these infections.

1.3 Concluding remarks

Many previous studies have determined the pathogenesis of enteroviruses such as CVB, EV71 and EVD68, however few studies have been able to determine the mechanisms of

pathogenesis for echoviruses. Some of these studies have also investigated the role of interferons in enterovirus infection, such as many studies have shown that in order to infect mice with various enteroviruses, these mice have to be deficient in type I interferon signaling. Additionally, many studies using cell lines or intestinal organoid technology have shown that interferons and ISGs play an important role in controlling infection. These studies have been limited in terms of echoviruses, especially in pathogenesis in a mouse. The work presented here helps progress our knowledge on echovirus entry and pathogenesis in mice as well as how the innate immune system control infection. First, we identify the viral receptor for echoviruses, the neonatal Fc receptor (FcRn). Additionally, we establish two models of echovirus infection by two different routes of inoculation, intraperitoneal (IP) or oral gavage (PO) to study echovirus pathogenesis in adult mice and suckling pups. Finally, we identify specific ISGs which have the ability to control enterovirus infection.

2.0 The neonatal Fc receptor is a pan-echovirus receptor

Echoviruses are amongst the most common causative agents of aseptic meningitis worldwide and are particularly devastating in the neonatal population, where they are associated with severe hepatitis, neurological disease, including meningitis and encephalitis, and even death. Here, we identify the neonatal Fc receptor (FcRn) as a pan-echovirus receptor. We show that loss of expression of FcRn or its binding partner beta 2 microglobulin (β2M) renders cells resistant to infection by a panel of echoviruses at the stage of virus attachment, and that a blocking antibody to β2M inhibits echovirus infection in cell lines and in primary human intestinal epithelial cells. We also show that expression of human, but not mouse, FcRn renders non-permissive human and mouse cells sensitive to echovirus infection and that the extracellular domain of human FcRn directly binds echovirus particles and neutralizes infection. Lastly, we show that neonatal mice expressing human FcRn are more susceptible to echovirus infection by the enteral route. Our findings thus identify FcRn as a pan-echovirus receptor, which may explain the enhanced susceptibility of neonates to echovirus infections.

2.1 Introduction

Echoviruses are small (~30 nm) single-stranded RNA viruses belonging to the Picornaviridae family. These viruses make up the largest subgroup of the Enterovirus genus and consist of ~30 serotypes. Enteroviruses are the main causative agents of aseptic meningitis worldwide, with echovirus 9 (E9) and echovirus 30 (E30) among the most commonly circulating

serotypes[214]. The neonatal and infant populations are at greatest risk for developing severe echovirus-induced disease, and infection within the first few weeks of life can be fatal[66,215]. In neonates, vertical transmission may occur before or at the time of delivery following a maternal infection[216]. Echovirus infections in utero, both at late and earlier stages of pregnancy, have also been associated with fetal death[217–221].

Echoviruses are primarily transmitted through the fecal–oral route where they target the gastrointestinal (GI) epithelium. In primary human fetal-derived enteroids, echoviruses exhibit a cell type specificity of infection and preferentially infect enterocytes[49]. The basis for this cell type-specific tropism is unclear. Decay accelerating factor (DAF/CD55) functions as an attachment factor for some echoviruses[222], but DAF expression does not sensitize nonpermissive cells to infection[223], suggesting that another cell surface molecule functions as the primary receptor. While integrin VLA-2 (α2β1) is a primary receptor for E1[127], it does not serve as a receptor for other echoviruses. Other work has implicated a role for MHC class I receptors in echovirus infections due to inhibition of viral binding, entry, or infection by monoclonal antibodies to MHC class I and/or beta 2 microglobulin (β2M)[223–225], which is required for efficient cell surface trafficking of MHC class I receptors. However, the primary receptor for most echoviruses is unknown.

Here, we identify the human neonatal Fc receptor (FcRn) as a primary echovirus receptor. We show that human cells deficient in FcRn expression are resistant to echovirus infection and infection is restored by FcRn expression. Concomitantly, expression of human FcRn renders murine-derived cell lines and primary cells permissive to echovirus infection. In contrast, expression of the murine homolog of FcRn has little effect on viral infection in either human or mouse cells, suggesting a species-specific role for FcRn in echovirus infection. In addition, we show that a monoclonal antibody recognizing β2M, which noncovalently associates with FcRn

and is required for FcRn cell surface expression, significantly reduces echovirus infection in primary intestinal epithelial cells and that recombinant FcRn in complex with β2M neutralizes echovirus infection and directly interacts with viral particles. Lastly, we show that neonatal mice expressing human FcRn are more susceptible to echovirus infection by the enteral route. Our data thus identify FcRn as a primary receptor for echoviruses, which has important implications for echovirus pathogenesis.

2.2 Results

2.2.1 Human cell deficient in FcRn are nonpermissive to echovirus infection

We screened a panel of cell lines for their susceptibility to echovirus infection and found that human placental choriocarcinoma JEG-3 cells were resistant to infection by seven echoviruses (E5, E7, E9, E11, E13, and E30) but were highly permissive to the related enterovirus coxsackievirus B3 (CVB) **(Figure 9A)**. Levels of echovirus infection in JEG-3 cells were comparable to those observed in mouse embryonic fibroblasts (MEFs), which are resistant to echovirus infection, and were significantly less than those observed in permissive cell types, including human intestinal Caco-2, HeLa, human brain microvascular endothelial cells (HBMECs), and human osteosarcoma U2OS cells **(Figure 9A** and **Figure 40A-C)**. The resistance of JEG-3 cells to echovirus infection occurred at the level of viral binding or entry, as infection was restored when cells were transfected with infectious viral RNA (vRNA) **(Figure 40D)**.

We performed RNAseq-based transcriptomics analyses between nonpermissive JEG-3 cells and permissive cell types, including Caco-2 cells, HBMECs, and primary human enteroids

harvested from fetal small intestines, which are highly sensitive to echovirus infection (10), to identify cell surface receptors differentially downregulated in JEG-3 cells. Because JEG-3 cells arise from choriocarcinomas and express many placental-specific transcripts, we also included JAR cells in our analyses, another human choriocarcinoma line that is more permissive to echovirus infection than JEG- 3 cells **(Figure 40E)**. Using this approach, we identified 118 transcripts differentially down-regulated in JEG-3 cells ($P < 0.001$, $\log_2$ z score less than -2) **(Figure 9B and C)**. Of these 118 transcripts, the neonatal Fc receptor (FCGRT, referred to here as FcRn), was the most significantly down-regulated cell surface receptor in JEG-3 cells ($P < 0.001$, $\log_2$ z score less than -2), **(Figure 9D and Figure 40F)**. We confirmed the significantly lower levels of expression of FcRn in JEG-3 cells relative to permissive cell lines (HBMEC, HeLa, and JAR) and primary human fetal enteroids by RT-qPCR **(Figure 40G)**. In contrast, there were no differences in expression of β2M, which is required to traffic FcRn to the cell surface **(Figure 9D and Figure 40G)**.

To determine if the lack of FcRn expression was directly responsible for the low levels of echovirus infection in JEG-3 cells, we ectopically expressed human FcRn (hFcRn). Expression of hFcRn in JEG-3 cells significantly increased their susceptibility to infection by E5, E11, and E30 (∼10,000-fold) **(Figure 9E and Figure 40H)**. In contrast, expression of the related MHC class I or MHC class I-like molecules HLA-A and HLA-C and hemochromatosis protein (HFE), which also require β2M for cell surface expression, had no effect on infection **(Figure 9E and Figure 40 H & I).** These data show that expression of hFcRn restores echovirus infection in nonpermissive human cells.

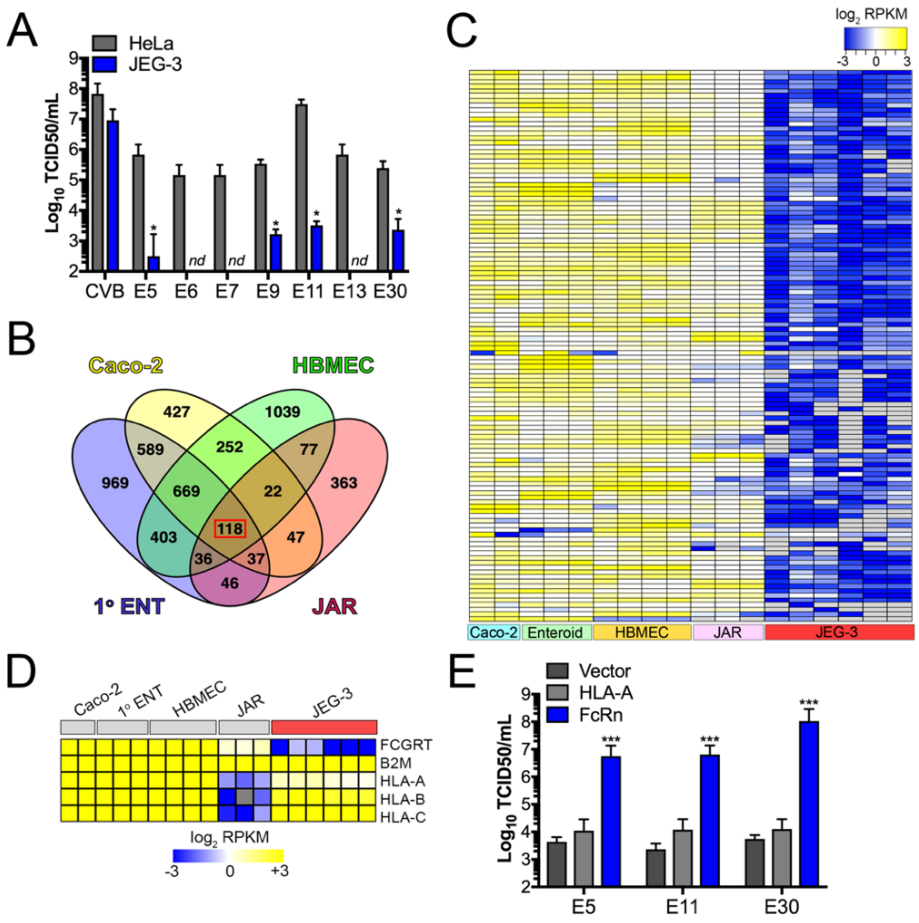

Figure 9 Human Cells Deficient in FcRn Are Nonpermissive to Echovirus Infection

JEG-3 cells are resistant to echovirus infection due to low FcRn expression. **(A)** JEG-3 cells (blue bars) or HeLa cells (gray bars) were infected with the indicated echovirus (1 pfu/cell) for ~24 h. Viral titers (log10 TCID50/mL) from the indicated cell types are shown as mean ± SD. Significance was determined using a standard t test (*P < 0.05). **(B)** Venn diagram from differential expression analysis using the DeSeq2 package in R between JEG-3 cells and either primary human fetal-derived enteroids (blue), HBMEC (green), Caco-2 cells (yellow), or JAR cells (red). There were 118 shared genes differentially down-regulated between JEG-3 cells and these cell types (red square). **(C)** Heatmap of 118 genes differentially down-regulated in JEG-3 cells and the indicated cell type (at Bottom) based on log2 reads per kilobase of transcript, per million mapped reads (RPKM) values. Transcripts with no reads are shown in gray. **(D)** Heatmap of FcRn, B2M, HLA-A, -B, or -C expression in the indicated cell type (based on log2 RPKM values). **(E)** JEG-3 cells were transfected with vector control (pcDNA), human HLA-A, or FcRn for 24 h, and then infected with the indicated echovirus for 24 h. Viral titers (log10 TCID50/mL) are shown as mean ± SD with significance

determined with a one-way ANOVA with Dunnett's test for multiple comparisons (***P < 0.001). Data in A and E are shown as mean ± SD. Data were generated by Stefanie Morosky and Carolyn Coyne.

2.2.2 Expression of human FcRn restores echovirus infection in mouse cells

Echoviruses do not infect mouse cells efficiently **(Figure 40A and B)**. Since ectopic expression of hFcRn in human cells in which endogenous levels were low restored their susceptibility to infection, we next determined whether the murine homolog of FcRn (mFcRn) was also sufficient to promote infection. Whereas expression of hFcRn in JEG-3 cells restored infection of a panel of echoviruses (E5, E7, E11, E13, and E30) by ~10,000-fold, expression of mFcRn had no significant effect **(Figure 10A and Figure 41A and B)**. Similarly, we found that expression of hFcRn, but not mFcRn, rendered MEFs and Chinese hamster ovary (CHO) cells highly susceptible to echovirus infection **(Figure 10B and Figure 41D)**. Collectively, these data show that expression of human, but not mouse, FcRn is sufficient to confer cellular susceptibility to echovirus infection, indicating a species-specific role for FcRn in echovirus infections.

2.2.3 Loss of FcRn expression renders cell resistant to echovirus infection

We next determined whether loss of FcRn expression rendered cells expressing FcRn less susceptible to infection. For these studies, we used RNAi-mediated silencing or CRISPR/Cas9-mediated depletion of FcRn. We found that RNAi-mediated silencing of FcRn expression in HBMECs, an immortalized human blood–brain barrier cell line that expresses high levels of FcRn by two independent siRNAs, led to significant (~1,000- to 10,000-fold) decreases in echovirus

infection but had no effect on CVB infection **(Figure 10C and Figure 42A and B)**. Similar results were obtained in human osteosarcoma U2OS cells **(Figure 42C)**. In addition, silencing of β2M expression led to comparable reductions in infection **(Figure 10C and Figure 42A-C)**. In contrast, RNAi-mediated silencing of other cell surface molecules that require β2M for trafficking, such as HLA-A, HLA-B, HLA-C, and HFE had no significant effect on echovirus infection in HBMECs **(Figure 42D)**. Importantly, echovirus replication in β2M- and hFcRn-RNAi transfected cells was restored when cells were transfected with infectious vRNA **(Figure 42E)**, supporting that the inhibition occurred at the stage of virus binding or entry. Moreover, we found that infection of many echoviruses (E5–E7, E9, E11, E13, E25, E29, and E30–E32) was reduced by β2M siRNA and FcRn siRNAs using a high content imaging- based screen **(Figure 42G)**.

Next, we utilized CRISPR/Cas9-mediated gene editing to knock out FcRn expression. We found that infection of E5, E11, and E30 was significantly reduced in two clones of U2OS cells in which FcRn was knocked out **(Figure 10D and Figure 43A and B)**. In contrast, infection by CVB was unchanged **(Figure 10D and Figure 43A and B)**.

Consistent with a role for FcRn in echovirus infection, blocking antibodies to β2M inhibited infection by E5, E7, E9, E11, E13, and E30 in a cell line (U2OS) **(Figure 43C)** and significantly reduced E7, E11, and E30 infection in primary intestinal epithelial cell monolayers derived from human fetal small intestines **(Figure 10E)**, where FcRn localizes to the subapical domain **(Figure 43D**). Collectively, these data show that FcRn expression is required for echovirus infection.

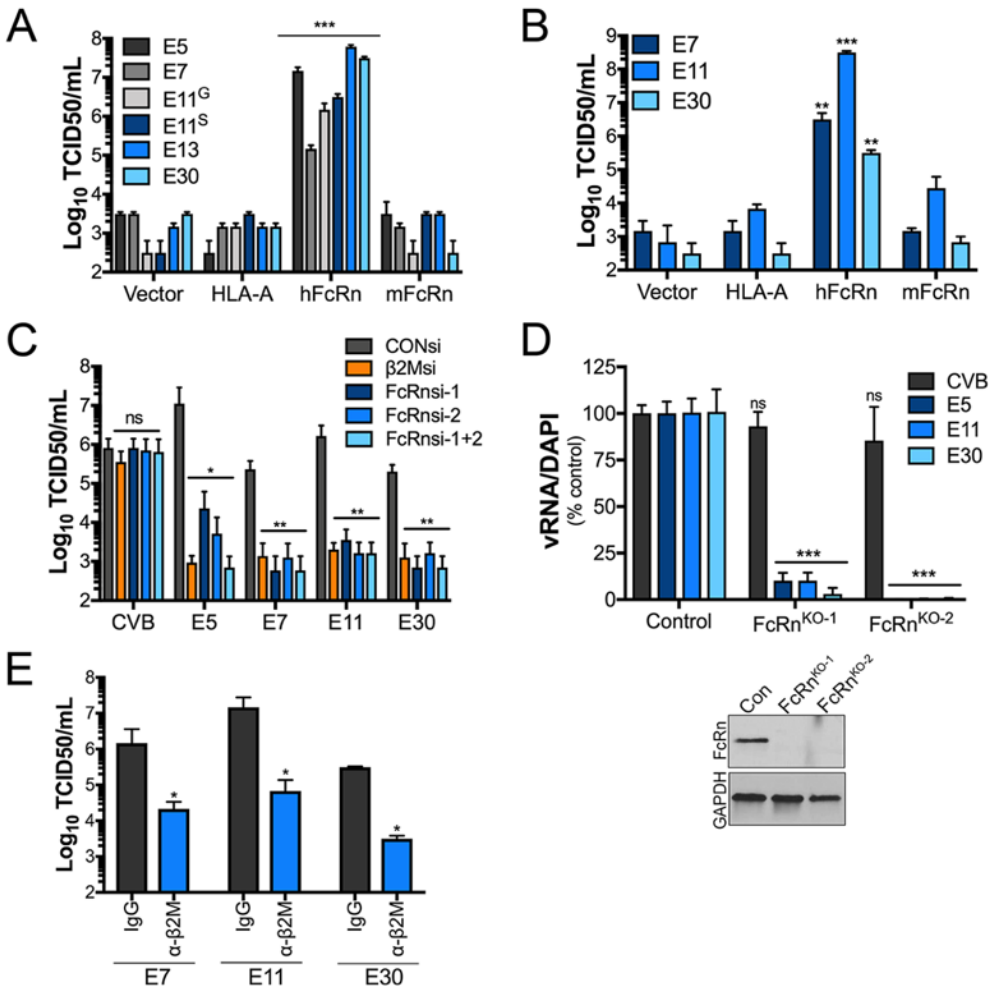

Figure 10 Expression of human FcRn restores echovirus infection in mouse cells while loss of FcRn expression renders cells resistant to echovirus infection

Loss of FcRn expression reduces echovirus infection. **(A)** JEG-3 cells were transfected with vector control (pcDNA), human HLA-A, human FcRn (hFcRn), or mouse FcRn (mFcRn) for 24 h and then infected with the indicated echovirus for 24 h (E11G Gregory strain and E11S Silva strain). Viral titers (log10 TCID50/mL) are shown as mean ± SD with significance determined with a Kruskal–Wallis test with a Dunn's test for multiple com- parisons (***P < 0.001). The relative expression of HLA-A, hFcRn, and mFcRn is shown in SI Appendix, Fig. S2B. (B) MEFs were transfected with pcDNA, human HLA-A, or either hFcRn or mFcRn, respectively, for 24 h and then infected with the indicated echovirus for 24 h. Viral titers (log10 TCID50/mL) are shown as mean ± SD with significance determined with a Kruskal–Wallis test with Dunn's test for multiple comparisons (**P < 0.01; ***P < 0.001). The relative expression of HLA-A, hFcRn, and mFcRn is shown in S2C Fig. **(C)** HBMECs were transfected with an siRNA against β2M

(orange bar) or two independent siRNAs against FcRn (FcRn-1 and FcRn-2) alone or in combination (FcRn 1+2) (blue bars), or scrambled control siRNA (CONsi, gray bars) for 48 h and then infected with CVB or the indicated echovirus for an additional 16 h. Shown are viral titers (log10 TCID50/mL) as mean ± SD with significance determined with a Kruskal–Wallis test with Dunn's test for multiple comparisons (*P < 0.05; **P < 0.01; ***P < 0.001; ns, not significant). **(D)** At Top, control (WT) U2OS cells or two clones of U2OS cells depleted of FcRn expression by CRISPR/Cas9-mediated gene editing (FcRnKO-1, FcRnKO-2) were infected with the indicated echoviruses, or with CVB as a control, for ~20 h. Levels of infection were assessed by immunostaining for double-stranded viral RNA and are shown as %positive cells over DAPI-stained nuclei. Significance was determined by a one-way ANOVA with a Dunnett's test for multiple comparisons (***P < 0.001). At Bottom, immunoblotting for FcRn in control (Con) or FcRnKO-1 and FcRnKO-2 cells. GAPDH is shown at bottom as a loading control. **(E)** Primary human intestinal epithelial cells were incubated with anti-β2M monoclonal antibody (blue bars) or isotype control antibody (gray bars) (2 μg/mL for both) for 30 min before infection with the indicated echovirus in the presence of antibody for an additional 24 h. Shown are viral titers (log_{10}TCID50/mL) as mean ± SD from three independent HIE preparations with significance determined with a t test (*P < 0.05). Data are shown as mean ± SD. Data were generated by Stefanie Morosky and Carolyn Coyne.

2.2.4 FcRn facilitates echovirus attachment and directly interacts with viral particles

We found that echovirus infection in cells depleted of FcRn could be restored by transfection of cells with vRNA, which suggested that this inhibition occurred at the stage of viral binding or entry. We therefore determined whether down-regulation of FcRn expression would alter echovirus binding. We found that silencing of FcRn expression in HBMECs significantly reduced cell surface binding of E5, E7, E9, E11, and E30 to HBMECs **(Figure 11A)**. In contrast, this silencing had no effect on CVB binding **(Figure 11A)**. Residual levels of viral binding in HBMECs may be mediated by cell surface factors such as DAF that facilitate binding of some

echoviruses (11). We also found that echovirus binding to primary mouse fibroblasts isolated from transgenic mice expressing human, but not mouse FcRn under the control of the endogenous human promoter [B6.Cg-Fcgrttm1Dcr Tg(FCGRT)32Dcr/DcrJ, hereafter referred to as $hFcRn^{Tg}$] **(Figure 44A)**[226,227] was significantly higher than in cells isolated from wild-type (WT) (C56Bl/6) mice **(Figure 11B)**, indicating that human FcRn facilitates echovirus cell surface attachment.

To determine whether FcRn directly interacts with echovirus particles, we used a recombinant protein approach with a purified heterodimer containing the extracellular domain of FcRn in complex with β2M (rFcRn-β2M). We found that incubation of viral particles with rFcRn-β2M before infection neutralized both E11 and E30 infection **(Figure 11C and D)**. In contrast, incubation with purified β2M alone, or recombinant HLA-A or HLA-C had no effect **(Figure 11C and D)**. To determine whether there was a direct interaction between FcRn and echoviral particles, we performed in vitro binding assays using rFcRn-β2M. Using this approach, we found that rFcRn-β2M coprecipitated with purified E11 and E30 in in vitro binding assays, **(Figure 11E)**, demonstrating a direct interaction between FcRn and echovirus particles.

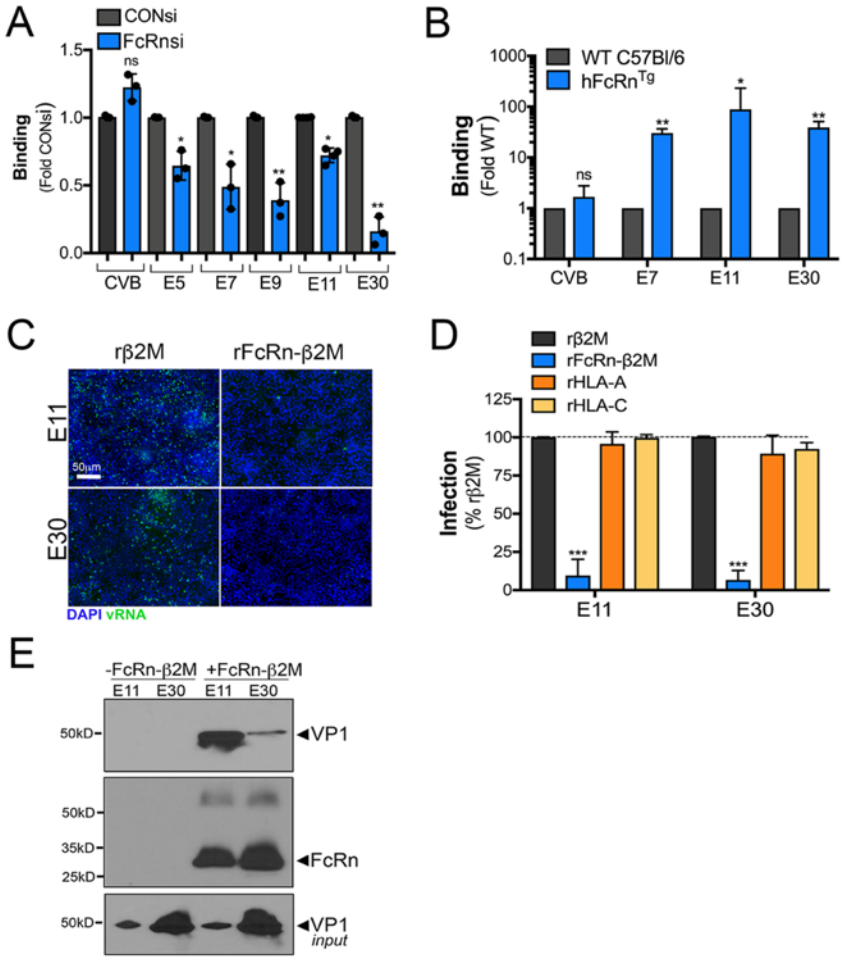

Figure 11 FcRn facilitates echovirus attachment and directly interacts with viral particles

FcRn mediates echovirus binding. **(A)** HBMECs were transfected with an siRNA against FcRn (FcRn-1, blue bars) or scrambled control siRNA (CONsi, gray bars) for 48 h and then the extent of viral binding of CVB or the indicated echovirus (50 pfu/cell) as assessed by a RT-qPCR–based binding assay. The extent of binding is shown as a fold from CONsi control (mean ± SD). Significance was determined using a t test (*P < 0.05; **P < 0.01; ns, not significant). **(B)** The extent of viral binding of CVB or the indicated echovirus (50 pfu/cell) was assessed in primary fibroblasts isolated from WT C57BL/6 mice (gray bars) or from hFcRn^{Tg} mice using a RT-qPCR–based binding assay. Shown is the extent of binding in cells isolated from four mice of each type, which is shown as mean ± SD. Significance was determined using a t test (*P < 0.05; **P < 0.01; ns, not significant). **(C)** E11 or E30 (10^6 particles) were incubated with recombinant β2M (rβ2M, 2.5 μg/mL) or the extracellular domain of FcRn in complex with β2M (rFcRn-β2M, 2.5 μg/mL) for 1 h at 4 °C, preadsorbed to HBMECs for 1 h at 4 °C, washed, and then cells infected for 16 h. Shown

are representative immunofluorescence images for double-stranded viral RNA (a replication intermediate, green). DAPI-stained nuclei are shown in blue. **(D)** E11 or E30 (10^6 particles) were incubated with rβ2M (2.5 μg/mL), rFcRn-β2M (2.5 μg/mL), HLA-A (2.5 μg/mL), or HLA-C (2.5 μg/mL) for 1 h at 4 °C, preadsorbed to HBMECs for 1 h at 4 °C, washed, and then cells infected for 16 h. The level of infection was assessed by immunostaining for vRNA normalized to DAPI-stained nuclei. Shown is the percent of infection normalized to rB2M controls from experiments performed in triplicate (>1,000 cells total) as mean ± SD. Significance was determined with a Kruskal–Wallis test with Dunn's test for multiple comparisons (***P < 0.001). **(E)** E11 or E30 (10^8 particles) were incubated with rβ2M (5 μg/mL) or 6x His-tagged extracellular domain of FcRn in complex with β2M (rFcRn-β2M, 5 μg/mL) for 1 h at 4 °C, then incubated with Ni-NTA agarose beads for 1 h at 4 °C. Following extensive washing, immunoblots were performed for the viral capsid protein VP1 (Top) and then membranes were stripped and reprobed with an antibody recognizing the extracellular domain of FcRn (Middle). In parallel, level of input virus was immunoblotted with anti-VP1 antibody (Bottom). Data in A, B, and D are shown as mean±SD. Data were generated by Stefanie Morosky and Carolyn Coyne.

2.2.5 FcRn promotes infection in neonatal mice by the enteral route

We found that exogenously overexpressed hFcRn rendered murine- derived cells sensitive to echovirus infection **(Figure 10B and Figure 41D)**. To further define the role of FcRn in echovirus infection, we compared echovirus infection in primary fibroblasts isolated from WT C57BL/6 and $hFcRn^{Tg}$ mice. Primary fibroblasts isolated from WT mice were resistant to echovirus infection, as expected **(Figure 12A and Figure 44B)**. In contrast, cells isolated from $hFcRn^{Tg}$ mice were highly permissive to echovirus infection and exhibited >10,000-fold enhanced susceptibility to infection **(Figure 12A and Figure 44B)**.

To define the role of FcRn in echovirus pathogenesis, we developed an in vivo model of E11 infection of WT and $hFcRn^{Tg}$ neonatal mice by the enteral route. FcRn is expressed at high

levels throughout the intestinal tract, liver, and endothelium in hFcRn^{Tg} mice[228,229]. We infected 7-d-old WT or hFcRn^{Tg} mice with 10^6 infectious particles of E11 by oral gavage and then collected tissues (brain, liver, small intestine, large intestine, and stomach) at 3 or 7 d post inoculation. We did not detect any infectious virus as determined by TCID50 assays when tissues were collected at 3 d post inoculation **(Figure 44C)**. However, at 7 d post inoculation, we detected significantly higher titers of E11 in the blood and livers of hFcRn^{Tg} mice compared with WT control mice **(Figure 12B)**. In addition, we also detected infectious E11 in the small intestines, large intestines, and stomachs of some hFcRn^{Tg}, but not WT, mice **(Figure 12B)**. There was no detectable E11 in tissue har- vested from WT mice **(Figure 12B)**. We confirmed E11 replication in isolated organs by performing immunohistochemistry using an antibody against the VP1 viral capsid protein. E11 infection was present in the livers of hFcRn^{Tg} mice, where viral replication was localized to select cell types **(Figure 12C)**, and in the epithelium lining the small intestine **(Figure 12D)**. In addition, E11 replication was localized to the muscle of both the colon and stomach, with no detectable replication in the epithelium **(Figure 45A and B)**. These data show that expression of hFcRn in neonatal mice is sufficient to permit E11 infection by the enteral route.

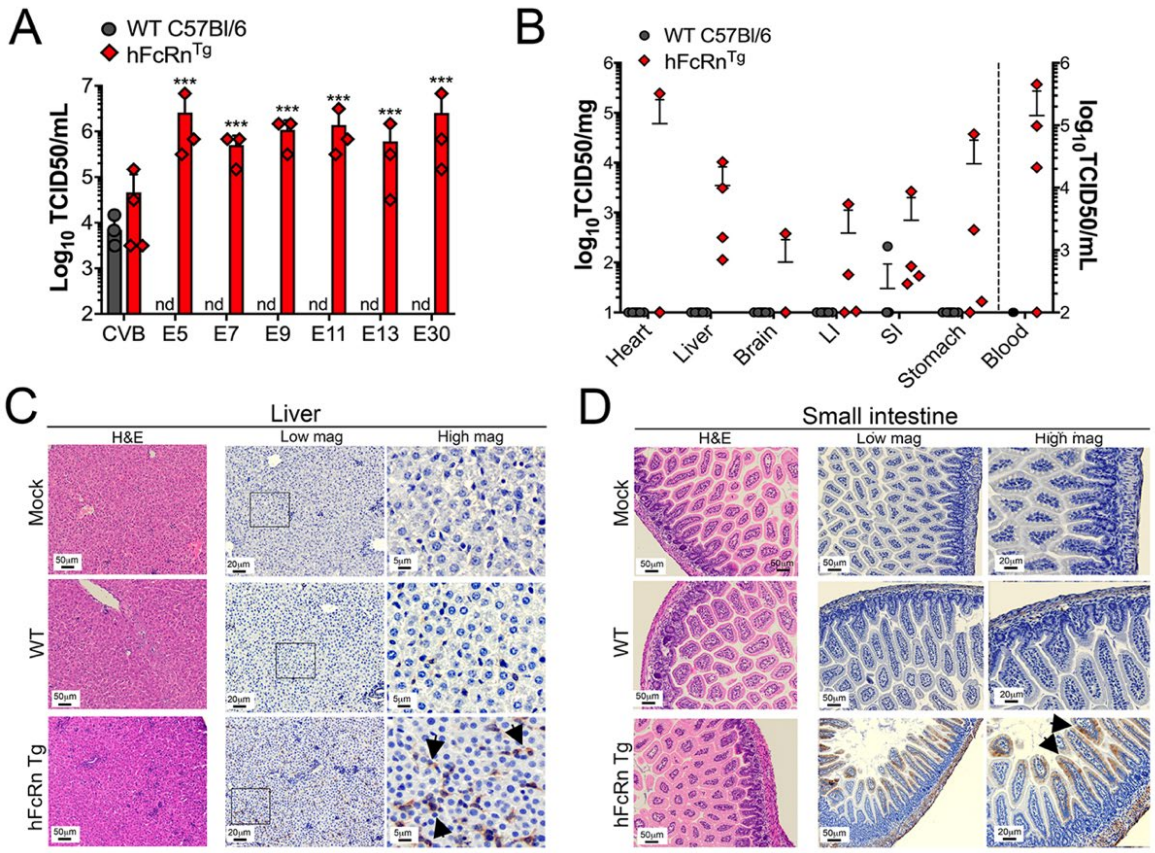

Figure 12 FcRn promotes infection in neonatal mice by the enteral route

Expression of human FcRn enhances E11 infection in vivo. **(A)** Primary fibroblasts isolated from WT C57BL/6 mice (gray bars) or hFcRn^{Tg} mice (red bars) were infected with the indicated echovirus, or with CVB as a control for 24 h. Viral titers (log10 TCID50/mL) are shown as mean ± SD from cells isolated from four mice of each type. Nd, not detected. Significance was determined using a standard t test (***P < 0.001). **(B)** E11 titers in the indicated tissues as determined by TCID50 assays from WT C57BL/6 mice (10 total) of hFcRn^{Tg} mice (9 total) infected for 7 d by oral gavage with 10^6 E11 particles. Titers were normalized to tissue weight (organs, Left y axis) or volume (blood, Right y axis). LI, large intestine; SI, small intestine. Data are shown as data points from individual mice as a mean ± SD with significance determined by a nonparametric Mann–Whitney U test (*P < 0.05; **P < 0.01; ns, nonsignificant). **(C and D)** Immunohistochemistry for E11 using an antibody recognizing the VP1 capsid protein from WT or hFcRn^{Tg} infected as indicated in B. Shown are H&E (Left) and IHC (Right) from liver (C) or small intestine (D). Scale bars are shown at Bottom Left.

2.3 Discussion

Here, we identify FcRn as a primary receptor for echoviruses. We show that expression of FcRn is necessary and sufficient for echovirus infection and that FcRn directly binds echovirus particles and facilitates viral binding. We also show that expression of human, but not mouse, FcRn restores echovirus infection in nonpermissive mouse and human cells and thereby identify a species-specific mechanism of infection. Our data show that a number of clinically relevant echoviruses commonly associated with human disease, including E9, E30, and E11, utilize FcRn as a receptor, suggesting a pan-echovirus role. In contrast, FcRn plays no role in the infection of related enteroviruses, including CVB and poliovirus (PV). Our findings provide important insights into the cellular receptor used by echoviruses to initiate their infections and into echovirus pathogenesis.

FcRn transports and regulates the circulating half-life of IgG throughout life[230]. In addition, FcRn is responsible for the development of passive immunity through the transfer of maternal-derived antibodies. In humans, expression of FcRn on the placenta[231] is solely responsible for the establishment of passive immunity in the fetus due to transport of maternal-derived IgG across the placental surface directly into fetal blood[232]. This differs in rodents, where passive immunity is established postnatally from maternal-derived IgG in milk/colostrum[233]. FcRn is expressed throughout life in a variety of cell types, including the small intestine, the microvasculature of the blood–brain barrier, myeloid cells, and hepatocytes, among others[230]. Although echoviruses are primarily transmitted via the fecal–oral route, viral-induced disease is associated with infection of secondary organs, most notably the liver and brain. Our in vivo studies support a role for FcRn at these sites of echovirus infection, as we identified E11 infection in the livers of $hFcRn^{Tg}$ neonatal mice. However, it is unclear whether the virus preferentially infects hepatocytes or Kupffer cells,

the specialized macrophages that line liver sinusoids, which express high levels of FcRn[228]. In addition, we found that E11 infection at other sites such as the colon and stomach was largely restricted to the subepithelial muscular layer, which also expresses FcRn[234]. The expression of FcRn on cell types present in the intestine, brain microvasculature, and liver may thus explain the tropism of echoviruses for these tissues and the viral mechanism to bypass the barriers presented by the cells comprising these sites.

In addition to IgG, FcRn also binds albumin, which regulates hepatic injury[235,236]. Of note, previous work has shown that albumin inhibits E7 infection at the stage of viral uncoating[237], suggesting that the interaction between echoviruses and FcRn may occur at the interface of albumin–FcRn binding. Although FcRn binds to albumin and IgG at distinct sites[238], both of these interactions occur within the low pH (≤6.5) environment of endosomes, with release occurring in the basic pH (≤7.5) of the bloodstream. In contrast, our findings suggest a direct interaction between echoviruses and FcRn that occurs at the neutral pH of the cell surface before viral entry, although it is unclear whether different echoviruses exhibit differences in affinity for the receptor. Indeed, our in vitro pulldown assays suggest that E11 might exhibit higher affinity for the receptor than E30. However, it is possible that differences in the ratio of infectious to noninfectious particles between echovirus preparations accounts for these differences. Once internalized, it is possible that the interaction between FcRn and echoviruses is altered by the low pH of endosomes, which may facilitate subsequent genome release and/or endosomal escape. We have shown that E11 preferentially infects enterocytes[49], with enhanced infection from the basolateral surface of human intestinal epithelial (HIE) cells[130]. This polarity of infection is consistent with the enhanced expression of FcRn in enterocytes in the intestine and its enrichment to the basolateral surface. Following replication, E11 is released bidirectionally from HIE from both the apical and

basolateral domains[130]. Given that FcRn mediates bidirectional transport[239], this raises the possibility that echoviruses could be transported from either the apical or basolateral domains to cross the intestinal barrier.

Echoviruses are associated with severe disease in neonates, particularly during the first 2 weeks of life and in those born prematurely. The vertical transmission of echoviruses is thought to occur at the time of delivery and be associated with maternal infection in the preceding days or weeks. However, fetal infections in utero have also been associated with disease and/or death[217–221], suggesting that vertical transmission might also occur during pregnancy. FcRn is highly expressed on syncytiotrophoblasts[240,241], the fetal-derived cells that comprise the outermost cellular barrier of the human placenta and which directly contact maternal blood. These cells are highly resistant to viral infections due to intrinsic antiviral defense pathways[231]. However, given that FcRn expressed on the surface of these cells transcytoses maternal-derived IgG directly into the underlying fetal blood, our identification of FcRn as an echovirus receptor raises the possibility that echoviruses might have higher rates of transplacental transfer than has been previously appreciated. In addition, it should be noted that the highest rates of transplacental IgG transfer occur in the third trimester, with the level of maternal-derived IgG greater in the fetus than in the mother[241]. Thus, a maternal echovirus infection in the later stages of pregnancy could potentially lead to FcRn-mediated placental infection or transplacental viral transport and expose the fetus to virus before delivery. Further defining the role of FcRn in echovirus infections in utero and postnatally will provide important insights into echovirus- induced fetal and neonatal disease.

Our work presented here identifies FcRn as a pan-echovirus receptor. Given that FcRn-based therapeutics have been developed to target a variety of human diseases[242], our findings also point to FcRn as a possible target for anti-echovirus therapeutics to ameliorate virus-induced

disease. Future studies identifying the mechanism by which echoviruses utilize FcRn to enter or bypass barrier tissues such as the GI epithelium, blood– brain barrier, and placenta will provide important insights into a variety of aspects of echovirus pathogenesis.

2.4 Materials and Methods

2.4.1 Cell lines

HBMECs were obtained from Kwang Sik Kim, Johns Hopkins University, Baltimore, MD, described previously[243], and grown in RPMI-1640 supplemented with 10% FBS (Invitrogen), 10% NuSerum (Corning), non- essential amino acids (Invitrogen), sodium pyruvate, MEM vitamin solution (Invitrogen), and penicillin/streptomycin. JEG-3, JAR, U2OS, and Caco-2 (BBE clone) cells were purchased from the American Type Culture Collection (ATCC) and cultured as described previously[184,244]. HeLa cells (clone 7B) were provided by Jeffrey Bergelson, Children's Hospital of Philadelphia, Philadelphia, PA, and cultured in MEM supplemented with 5% FBS and penicillin/streptomycin. Primary human intestinal epithelial cells were isolated from crypts isolated from human fetal small intestines as described[49].

2.4.2 Animals

All animal experiments were approved by the University of Pittsburgh Animal Care and Use Committee and all methods were performed in accordance with the relevant guidelines and regulations. Primary fibroblasts were generated from 4-wk-old B6.Cg-Fcgrt < tm1Dcr > Tg(CAG-

FCGRT) 276Dcr/DcrJ (cat. no. 004919) and control C57BL/6J (cat. no. 000664) mice purchased from The Jackson Laboratory. For collection of primary cells, mice were killed according to institution standards and ears and tail were removed, incubated in 70% ethanol for 5 min, and then rinsed twice in PBS + 50 μg/mL kanamycin for 5 min. Hair was removed and tissue was cut into small pieces and incubated in 9.4 mg/mL collagenase D (11088858001, Roche) and 1.2 mg/mL pronase (1088858001, Roche) in complete DMEM at 37 °C with shaking at 200 rpm for 90 min. The resulting cell suspensions were filtered through 70-μM cell strainers, collected at 580 g, resuspended in complete DMEM containing 10 units penicillin and 10 μg streptomycin/mL and 250 ng/mL amphotericin B and cultured at 37 °C in a humidified 5% CO2 incubator.

For animal infections, 3- or 7-d-old neonatal mice were infected with 10^6 pfu of E11 in 50 μL of 1× PBS by oral gavage using a 24-gauge round- tipped needle. Mice were killed at various intervals postinoculation and organs harvested into 500 μL–1 mL of DMEM and stored at −80 °C before TCID50 assay. Samples were thawed at 37 °C and homogenized with a TissueLyser LT (Qiagen) for 8 min, followed by brief centrifugation at 400 × g. Viral titers in organ homogenates were determined by TCID50 assay.

2.4.3 Viruses and Infections

Experiments were performed with CVB (RD strain), PV (Sabin strain, type 2), echovirus 5 (Noyce strain, E5), echovirus 6 (Burgess strain, E6), echovirus 7 (Wallace strain, E7), echovirus 9 (Hill strain, E9), echovirus 11 (Gregory or Silva strains, E11G and E11S), echovirus 13 (Del Carmen strain, E13), echovirus 25 (JV-4, E25), echovirus 29 (JV-10, E29), echovirus 30 (Bastianni strain, E30), echovirus 31 (Caldwell strain, E31), or echovirus 32 (PR-10 strain, E32) that were

provided by Jeffrey Bergelson and originally obtained from the ATCC. Viruses were propagated in HeLa cells and purified by ultracentrifugation over a sucrose cushion, as described[245].

Unless otherwise stated, infections were performed with 1 pfu/cell of the indicated virus. In some cases, viruses were preadsorbed to cells for 1 h at 4 °C in serum-free MEM supplemented with 10 mM Hepes followed by extensive washing in 1× PBS or complete media. Infections were then initiated by shifting cells to 37 °C for the times indicated. Viral titers were determined by TCID50 assays in HeLa cells using crystal violet staining.

Binding assays were performed by preadsorbing 50 pfu/cell of the indicated virus to cells for 1 h at 4 °C in serum-free MEM supplemented with 10 mM Hepes followed by extensive washing with 1× PBS. Immediately following washing, RNA was isolated and RT-qPCR performed for viral genome-specific primers, as described below.

For experiments using blocking antibodies, cells were incubated with the indicated antibodies (at 5 μg/mL) for 1 h at 4 °C in serum-free DMEM containing 10 mM Hepes. For anti-DAF IF7 blocking experiments, all incubations were performed in DMEM containing 10% FBS and 10 mM Hepes. Following this incubation, viruses were preadsorbed to cells in the presence of anti- bodies for an additional 1 h at 4 °C in serum-free or serum-containing medium, washed extensively, and then the cells were infected at 37 °C for the indicated time in the presence of antibodies.

2.4.4 High content RNAi screening

HBMEC were reverse transfected with the indicated siRNA in triplicate wells using Dharmafect-1 according to the manufacturer's instructions and then plated into black walled 96-well plates (Corning). Approximately 48hrs following transfection, cells were infected with the

indicated echovirus at 5 PFU/cell for 16hrs and then cells fixed with ice-cold methanol. Immunostaining for double-stranded viral RNA was performed using the J2 antibody and nuclei counterstained with DAPI. Images were captured using an inverted IX83 Olympus microscope using a motorized XY stage, with four independent sites captured per well. Automated image analysis was then performed using the Count and Measure package in CellSens software.

2.4.5 Immunohistochemistry

Tissue sections were deparaffinized with xylene and rehydrated with decreasing concentrations of ethanol (100%, 95%, 80%), then washed with ddH20. Peroxidase activity was blocked with hydrogen peroxide for 15 mins and antigen retrieval was performed with slides submerged in 10 mM citrate buffer (pH 6.0) and heated in a standard microwave for 3 – 5 min intervals. Slides were cooled to room temperature and immunostained with mouse monoclonal VP-1 antibody (Clone 5-D8/1, Leica Biosystems) using a Mouse on Mouse Polymer IHC Kit (Abcam, ab127055) according to the manufacturer's instructions. Following incubation with rodent block for 30 mins, sections were incubated with anti-VP1 antibody diluted 1:100 in TBS-T (Tris-buffered saline, 0.1% Tween 20) and slides incubated overnight in a humidified chamber at 4o C. Next, slides were exposed to mouse on mouse HRP Polymer for 15 mins and diaminobenzidine substrate for 1-5 mins; which was terminated with water incubation. Slides were counterstained with hematoxylin for 1 min, thoroughly rinsed with H2O, and incubated in 0.1% sodium bicarbonate in H2O for 5 mins. Slides were then dehydrated with increasing concentrations of ethanol, cleared with xylene and mounted with Vectamount Permanent Mounting Medium (Vector Biolabs, H-5000). Images were captured on an IX83 inverted microscope (Olympus) using a UC90 color CCD camera (Olympus).

2.4.6 Immunofluorescence microscopy

Cells were washed with PBS and fixed with ice-cold 100% methanol for immunostaining of viral infections or with 4% paraformaldehyde at room temperature, followed by 0.25% Triton X-100 to permeabilize cell membranes for a minimum of 15min at room temperature for all other immunostaining. Cells were incubated with primary antibodies for 1 hour at room temperature, washed with 1x PBS, and then incubated for 30 minutes at room temperature with Alexa-Fluorconjugated secondary antibodies (Invitrogen). Slides were washed and mounted with Vectashield (Vector Laboratories) containing 4′,6-diamidino-2-phenylindole (DAPI). Images were captured using a Zeiss LSM 710 inverted laser scanning confocal microscope or with inverted IX81 or IX83 Olympus fluorescent microscopes. Images were adjusted for brightness/contrast using Adobe Photoshop (Adobe). Image quantification for the extent of infection was performed using Fiji (Cell counter plugin) or the CellSens Count and Measure package, as indicated. A minimum of 1000 cells were quantified.

2.4.7 Antibodies

The following antibodies or reagents were used—recombinant anti-dsRNA antibody (provided by Abraham Brass, University of Massachusetts and described previously[246]), mouse monoclonal anti-VP1 (NCL-ENTERO, Leica), mouse monoclonal anti-FcRn (Santa Cruz Biotechnology, sc271745), rabbit polyclonal FcRn (Abcam ab139152, ab193148), rabbit monoclonal HLA-A (Abcam, ab52922), rabbit monoclonal HLA-C (Abcam, ab126722), PE-conjugated anti-HLA antibody (recognizing HLA A-C, HLA-E) (Novus, NBP2-68006PE), mouse monoclonal anti-b2M (Sigma, SAB4700010), and isotype control mouse monoclonal IgG

antibody (MOPC 21, Sigma, M5284). Alexa-fluor 594 conjugated phalloidin was purchased from Invitrogen (A12381). AntiDAF IF7 antibody was provided by Jeffrey Bergelson (Children's Hospital of Philadelphia).

2.4.8 Recombinant protein, *in vitro* pulldowns, and immunoblotting

Purified native b2M was purchased from Bio-rad (6240-0824) and was isolated from human urine. Recombinant HLA-A and HLA-C was purchased from Novus (H00003105 and NBP2-2310, respectively). Recombinant extracellular domain of FcRn in complex with b2M was purchased from Sino Biological (CT009-H08H) and was purified from HEK293 cells. For viral neutralization studies, purified viral particles (10^6) were incubated with the indicated recombinant protein (2μg) for 1hr at 4° C with constant rotation in serum-free MEM supplemented with 10mM HEPES. This complex was then added to cells for an additional 1hr at 4°C, cells washed extensively with 1x PBS, and infections initiated by shifting to 37°C for the 16-24hrs, as indicated in figure legends. In vitro pulldowns between E11 and E30 were performed by incubating purified virus particles (10^7) with 2μg of purified 6xHis tagged FcRn complex to β2M for 1hr at 4° C with constant rotation in buffer containing 100mM NaCl, 20mM Tris-Cl (pH 7.4), 0.5mM EDTA, and 0.5% (v/v Nonidet-40). Following this incubation, HiPur Ni-NTA agarose beads were added for an additional 1hr at 4°C with constant rotation. Bead complexes were then pelleted by centrifugation and washed 6x with wash buffer (10mM Tris-Cl (pH 8.0), 1mM EDTA, 1% Triton X-100, 0.1% SDS, and 140mM NaCl). Beads were then resuspended in denaturing sample buffer and immunoblots performed, as described below.

For immunoblotting, the lysates described above were loaded onto 4-20% Tris-HCl gels (Bio-Rad) and transferred to nitrocellulose membranes. Membranes were blocked in 5% nonfat

dry milk, probed with the indicated antibodies, and developed with horseradish peroxidaseconjugated secondary antibodies (Invitrogen), and SuperSignal West Dura chemiluminescent substrates (Pierce Biotechnology). Membranes were stripped for reprobing using ReBlot Strong antibody stripping solution (Millipore, 2504) according to the manufacturer's instructions. For FcRn immunblotting in CRISPR/Cas9 depleted U2OS cells, cells were lysed in RIPA buffer (20 mM Tris-HCl (pH 7.5). 150 mM NaCl, 1 mM Na2EDTA. 1 mM EGTA. 1% NP-40) containing protease inhibitors (Promega). Following brief centrifugation at 1200rpm, lysates were incubated with rabbit anti-FcRn antibody (Abcam, ab193148) for 1hr at 4ºC, then incubated with agarose-conjugated protein G beads (Millipore) for 1hr 4ºC with constant rotation. Bead-antibody complexes were pelleted by centrifugation at 3000rpm and washed four times with RIPA buffer. Immunoblotting was performed as described above using mouse anti-FcRn antibody (Santa Cruz sc-271745).

2.4.9 RT-qPCR

Total RNA was prepared using the Sigma GenElute total mammalian RNA miniprep kit, according to the protocol of the manufacturer. RNA was reverse transcribed with the iScript cDNA synthesis kit (Bio-Rad) following the manufacturer's instructions. A total of 1 µg of total RNA was reversed transcribed in a 20 µL reaction, and subsequently diluted to 100 µL for use. RT-qPCR was performed using the iQ SYBR Green Supermix or iTaq Universal SYBR Green Supermix (BioRad) on a CFX96 Touch Real-Time PCR Detection System (Bio-Rad). Gene expression was determined based on a ΔCQ method, normalized to human actin. Primer sequences to actin, CVB, and pan-echovirus primers have been described previously[184,247]. Primers to β2M,

FcRn, HLAA, HLA-B, HLA-C, and HFE were synthesized by Sigma and sequences can be found in Table 6.

2.4.10 RNAseq and differential expression analysis

Heat maps (based on log2(RPKM) values) were generated in Heatmapper[248] or MeV. Analysis of the transcriptional profile of cells were based on previously published datasets with files available in sequence read archives as follows: Caco-2 cells (SRP065330), primary human enteroids (SRP091501), HBMEC (PRJNA344703), JAR cells (SRP095402), and JEG3 cells (SRP109039). FASTQ data were processed and mapped to the human reference genome (hg38) using CLC Genomics Workbench 11 (Qiagen). Differential expression analysis was performed using the DeSeq2 package in R[249] with a statistical cutoff set to adjusted p-value (padj).

2.4.11 Plasmids, siRNA transfections, and CRISPR/Cas9 gene editing

Sequence verified vectors (pcDNA 3.1) expressing human HLA-A, HLA-C, FcRn or mouse FcRn were purchased from Genscript. EGFP-fused HFE (pCB6-HFE-EGFP) was a gift from Pamela Bjorkman (Addgene plasmid # 12104) and was described previously[250]. Plasmids were reverse (MEFs, CHO cells) or forward (JEG-3 cells) transfected with the indicated plasmids using Lipofectamine 3000 according to the manufacturer's instructions. Pooled siRNAs (four total) targeting HLA-A and HFE were purchased from Dharmacon (siGENOME, M-012850-01 and M-011051-02). Pooled siRNAs (four total) targeting HLA-B and HLA-C were purchased from Santa Cruz Biotechnology (sc-42922 and sc-105525). Control (scrambled) siRNA was purchased

from Sigma (Mission Universal, SIC001). Individual siRNAs targeting β2M and FcRn were synthesized by Sigma, with sequences as follows: (b2M UCCAUCCGACAUUGAAGUU; FcRn-1 CCACAGAUCUGAGGAUCAA; FcRn-2 ACUUUUGACUGUUAGUGAC). In all cell types, siRNAs were reverse transfected into cells using Dharmafect-1 (Dharmacon) according to the manufacturer's instructions. FcRn was deleted from U2OS cells using the following sgRNA sequence: ACCGCCAAGTTCGCCCTGAA in a pSpCas9 BB-2A-GFP plasmid (Genscript). Cells were reverse transfected using X-tremegene HP according to the manufacturer's instructions and single cell clones isolated by single cell sorting for GFP expression on a FACSAria II flow cytometer 48-hrs following transfection. FcRn deletion was verified by immunoblotting as described below and by Sanger sequencing.

2.4.12 Statistics

All statistical analysis was performed using GraphPad Prism. Data are presented as mean ± SD. A Student's t test or one-way ANOVA was used to determine statistical significance, as described in the figure legends. Parametric tests were applied when data were distributed normally based on D'Agostino–Pearson analyses; otherwise nonparametric tests (such as Mann–Whitney U tests) were applied. P values of <0.05 were considered statistically significant, with specific P values noted in the figure legends.

3.0 Human FcRn expression and Type I Interferon signaling control Echovirus 11 pathogenesis in mice

Neonatal echovirus infections are characterized by severe hepatitis and neurological complications that can be fatal. Here, we show that expression of the human homologue of the neonatal Fc receptor (hFcRn), the primary receptor for echoviruses, and ablation of type I interferon (IFN) signaling are key host determinants involved in echovirus pathogenesis. We show that expression of hFcRn alone is insufficient to confer susceptibility to echovirus infections in mice. However, expression of hFcRn in mice deficient in type I interferon (IFN) signaling, hFcRn-IFNAR$^{-/-}$, recapitulate the echovirus pathogenesis observed in humans. Luminex-based multianalyte profiling from E11 infected hFcRn-IFNAR$^{-/-}$ mice revealed a robust systemic immune response to infection, including the induction of type I IFNs. Furthermore, similar to the severe hepatitis observed in humans, E11 infection in hFcRn-IFNAR$^{-/-}$ mice caused profound liver damage. Our findings define the host factors involved in echovirus pathogenesis and establish *in vivo* models that recapitulate echovirus disease in humans.

3.1 Introduction

Echoviruses are small (~30 nm) single-stranded RNA viruses that belong to the *Picornaviridae* family. Echoviruses consist of approximately 30 serotypes and are members of the Enterovirus genus, which are primarily transmitted through the fecal-oral route. Infants and neonates are often most severely impacted by echovirus infections, with the majority of enterovirus

infections in infants below the age of two months caused by echoviruses[214,251]. Echovirus infections are particularly devastating in Neonatal Intensive Care Unit (NICU) outbreaks, where they account for 15-30% of nosocomial viral infections and can result in death of the neonate in as many as 25% of cases[67,69,252,253]. Echovirus 11 (E11) is one of the most common serotypes associated with outbreaks in NICUs across the world[68,254]. Despite the severe clinical outcomes associated with echovirus infections, the tissue tropism and pathogenesis of infection remain largely unknown due to the lack of established animal models to study E11 infection at secondary sites of infection, such as the liver and brain.

We and others previously identified the neonatal Fc receptor (FcRn) as a primary receptor for echoviruses[109,255]. Structural analysis has shown that the murine homologue of FcRn (mFcRn) does not support echovirus binding and entry[255], which has also been shown experimentally in murine-derived primary cells and cell lines[109]. However, ectopic expression of human FcRn (hFcRn) renders murine-derived primary cells susceptible to echovirus infections[109]. FcRn is important for establishing passive immunity from mother to child through IgG transport across the placenta during human pregnancy or across the small intestine after birth in mice[239]. Additionally, FcRn is important for albumin homeostasis in liver hepatocytes and regulates the response to hepatic injury[236]. FcRn expression is maintained throughout life in the liver and many other tissue types in the body[234]. We have previously demonstrated in an oral infection model of suckling mice that E11 disseminates from the gastrointestinal (GI) tract into the blood and liver, and that this dissemination is dependent on the expression of human FcRn[109]. Although the virus disseminated to the liver, very little detectable virus was observed in this and other tissues, occluding further studies of pathogenesis at secondary sites of infection.

The development of mouse models that recapitulate the hallmarks of enterovirus disease in humans has historically been challenging. Enteroviruses typically do not infect mice as the murine homolog of their receptors are often not sufficient for binding and entry. Others have developed mouse models of select enteroviruses including poliovirus, coxsackievirus B (CVB), and enterovirus 71 (EV71)[194–196]. These models often use immunodeficient humanized transgenic mice, which express the human homolog of the receptor while lacking expression of the interferon α/β receptor (IFNAR)[195–197,256,257]. Despite established *in vivo* models for other enteroviruses, echoviruses have few established mouse models. A previous echovirus 1 mouse model was established using transgenic mice expressing human integrin very late antigen 2 (VLA-2), the receptor for E1[127], which inoculated newborn mice intracerebrally, resulting in paralysis of the transgenic mice[258]. However, the host determinants involved in restricting echovirus infections *in vivo* remain largely unknown.

Here, we define the host determinants of echovirus infection and developed parallel adult and suckling mouse models of E11 infection. We show that immunocompetent animals that express hFcRn under the native human promotor ($hFcRn^{Tg32}$) are largely resistant to E11 infection following intraperitoneal (IP) inoculation. In addition, immunodeficient mice lacking IFNAR expression ($IFNAR^{-/-}$) alone are also refractory to infection. In contrast, $hFcRn^{Tg32}$ animals that are also deficient in IFNAR expression ($hFcRn^{Tg32}$-$IFNAR^{-/-}$) are highly permissive to E11 infection and high levels of viral replication occur in the liver and pancreas, which reflects the tissue sites most commonly targeted in infected human neonates[63,219]. Luminex-based multianalyte profiling of whole blood revealed that $hFcRn^{Tg32}$-$IFNAR^{-/-}$ infected animals induced a robust systemic immune response to infection, including high levels of type I IFNs. Using RNASeq-based transcriptional profiling, we also show that the livers of $hFcRn^{Tg32}$-$IFNAR^{-/-}$ mice mount a pro-

inflammatory and antiviral signaling cascade in response to infection. Additionally, elevated liver enzymes and histological analyses showed profound damage to the liver. Finally, using hybridization chain reaction (HCR) with specific probes against the E11 genome, we show that hepatocytes are the main cell type infected and both uninfected and infected cells in the liver produce IFN-β to mount an antiviral signaling in response to infection. Our data thus define hFcRn and type I IFN signaling as key host determinant of E11 pathogenesis in the liver and suggest that these factors could be targeted therapeutically to control infection.

3.2 Results

3.2.1 Human FcRn and Type I IFN signaling are key host determinants of E11 infection

Given that the most severe outcomes of E11 infections in humans are in neonates, we first performed studies in suckling (7 day old) mice. We inoculated immunocompetent wild-type C57BL/6 (WT) and hFcRn^{Tg32} suckling mice with 10^4 plaque forming units (PFU) of E11 by the IP route. Animals were sacrificed at 72 hours post inoculation (hpi) and tissues were collected for viral titration by plaque assay. Because an IP echovirus mouse model has not been established previously, we collected a diverse range of tissues (e.g. brain, liver, pancreas, small intestine) to determine the tissue tropism of E11 *in vivo*. WT and hFcRn^{Tg32} animals exhibited low to undetectable levels of infection in all of the tissues tested **(Figure 13A-F)**. For example, only 2 of 12 WT animals and 2 of 13 hFcRn^{Tg32} animals had any detectable virus in liver and 0 of 12 WT mice and 1 of 13 hFcRn^{Tg32} mice had detectable virus in the brain, although in both cases, viral titers were very low **(Figure 13B and F)**. Because many enteroviruses are restricted by type I IFN

signaling in small animal models and because we have previously shown that E11 is sensitive to recombinant IFN-β treatment [130], we reasoned that type I IFNs might play a key role in restricting E11 infection *in vivo*. To test this, we infected suckling mice deficient in type I IFN signaling (IFNAR$^{-/-}$) with 10^4 PFU E11 by the IP route. However, we found that these animals were also largely resistant to E11 infection, with most animals having no detectable circulating virus in blood or replicating virus in tissues (4 of 12 animals had detectable virus in the blood and liver) **(Figure 13A-F)**. These data show that expression of hFcRn or ablation of type I IFN signaling alone is insufficient to confer susceptibility to E11 replication.

We next determined whether expression of hFcRn in the context of ablation of IFNAR-mediated signaling would be sufficient for E11 infection in mice. To do this, we generated hFcRn^{Tg32} mice that are deficient in IFNAR expression (hFcRn^{Tg32}-IFNAR$^{-/-}$). Similar to the studies described above, we inoculated suckling hFcRn^{Tg32}-IFNAR$^{-/-}$ mice with E11 by IP inoculation. In contrast to animals expressing hFcRn or lacking IFNAR expression alone, we found that hFcRn^{Tg32}-IFNAR$^{-/-}$ suckling mice were highly permissive to E11 infection, with high levels of infectious virus circulating in blood **(**17 of 18 animals, **Figure 13A)**. Similarly, hFcRn^{Tg32}-IFNAR$^{-/-}$ animals had significantly more detectable infectious virus in livers compared to other genotypes **(**18 of 18 with detectable virus in liver**, Figure 13B).** In addition to liver, we also observed high viral loads in the pancreas of hFcRn^{Tg32}-IFNAR$^{-/-}$ animals **(**18 of 18 with detectable virus, **Figure 13C)**. We also observed increased viral titers in the stool, small intestine, and brain, which all contained moderate to high levels of viral infection in hFcRn^{Tg32}-IFNAR$^{-/-}$ mice **(Figure 13D-F)**. We monitored for any sex differences in our pup model and found no difference in viral replication. These results show that hFcRn^{Tg32}-IFNAR$^{-/-}$ suckling mice are highly permissive to E11 inoculation.

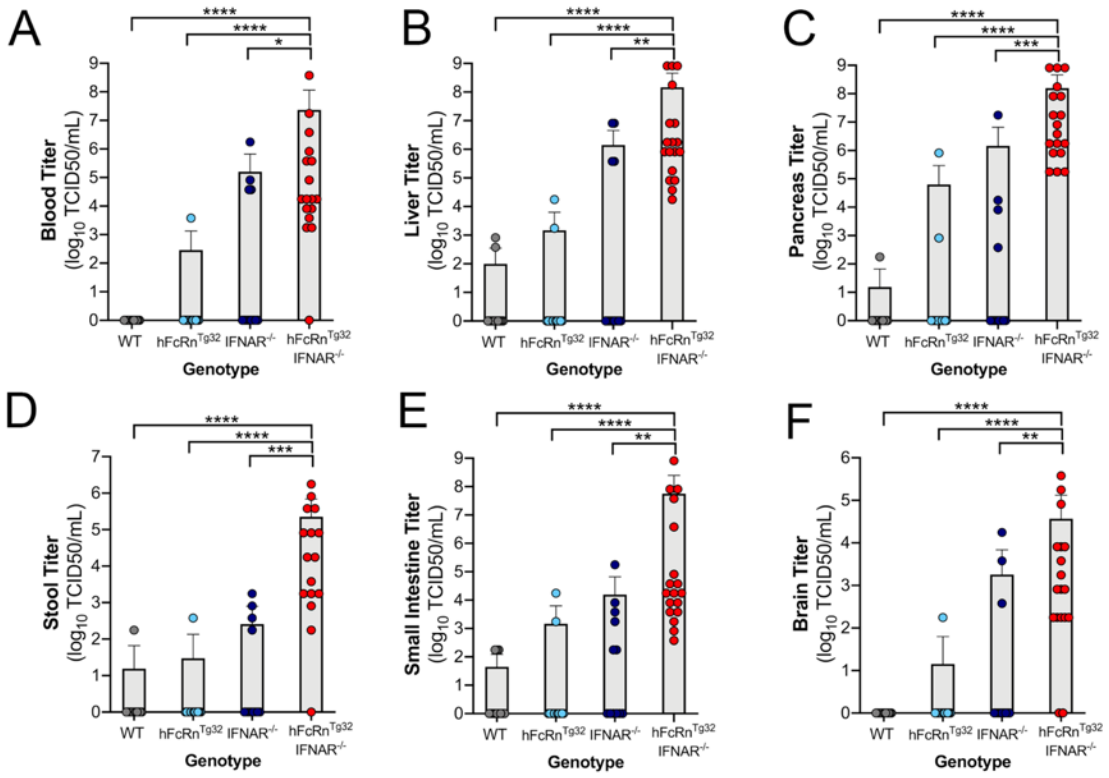

Figure 13 hFcRn^{Tg32}-IFNAR$^{-/-}$ suckling mice are permissive to E11 infection

C57Bl/6 (WT, gray), hFcRn^{Tg32} (light blue), IFNAR$^{-/-}$ (dark blue), or hFcRn^{Tg32}-IFNAR$^{-/-}$ (red) suckling mice were IP inoculated with 10^4 PFU of E11 and sacrificed 72 hours post inoculation. **(A-F)** Viral titers (log_{10}TCID50/mL) of suckling mice (WT – 12, hFcRn^{Tg32} – 13, IFNAR$^{-/-}$ – 12, hFcRn^{Tg32}-IFNAR$^{-/-}$ – 18 animals) in the blood (A), liver (B), pancreas (C), stool (D), small intestine (E), and brain (F) are shown as mean ± standard deviation and individual animals (points). Data are shown with significance determined with a Kruskal-Wallis test with a Dunn's test for multiple comparisons (*p<0.05, **p<0.005, ***p<0.0005, ****p<0.0001).

We next determined whether hFcRn and IFN signaling played a role in echovirus pathogenesis in adult (6-week-old) mice. Similar to our findings in suckling mice, we found that WT, hFcRn^{Tg32}, and IFNAR$^{-/-}$ mice were largely resistant to E11 infection **(Figure 14A-F)**. In contrast to suckling mice, immunocompetent animals (WT and hFcRn^{Tg32}) had no detectable circulating virus and a majority of IFNAR$^{-/-}$ animals also completely resisted infection (2 of 16 with detectable virus in

the blood) **(Figure 14A)**. In contrast, hFcRn^{Tg32}-IFNAR$^{-/-}$ animals had significant levels of viral replication in the blood (12 of 23 with detectable virus), liver (20 of 23 with detectable virus) and pancreas (13 of 23 with detectable virus), similar to what was observed in suckling pups **(Figure 14A-C)**. Additionally, these animals had low levels of detectable virus in the stool and small intestine suggesting this is not a main site of replication following IP inoculation **(Figure 14D and E)**. In contrast to suckling mice, adult hFcRn^{Tg32}-IFNAR$^{-/-}$ animals did not contain high levels of detectable virus in the brain (only 3 of 23 animals), suggesting age-related differences between adult and suckling mice **(Figure 14F)**. We monitored for any sex differences in our adult model and found no difference in viral replication. Additionally, we treated hFcRn^{Tg32} adult mice with an anti-IFNAR blocking antibody to ablate type I IFN signaling or an isotype control antibody. Similar to our results in hFcRn^{Tg32}-IFNAR$^{-/-}$ animals, hFcRn^{Tg32} animals treated with anti-IFNAR blocking antibody exhibited viral replication in the liver **(Figure 46A,** 4 out of 5 with detectable virus**)** with no isotype control antibody-treated animals having any detectable virus. In addition to liver, anti-IFNAR-, but not isotype control-, treated animals also had virus in their stool **(Figure 46B)**. Taken together, these data show that both hFcRn and type I IFNs are key regulators of E11 infection of suckling mice and adult mice and that the liver is a key target site of replication *in vivo*.

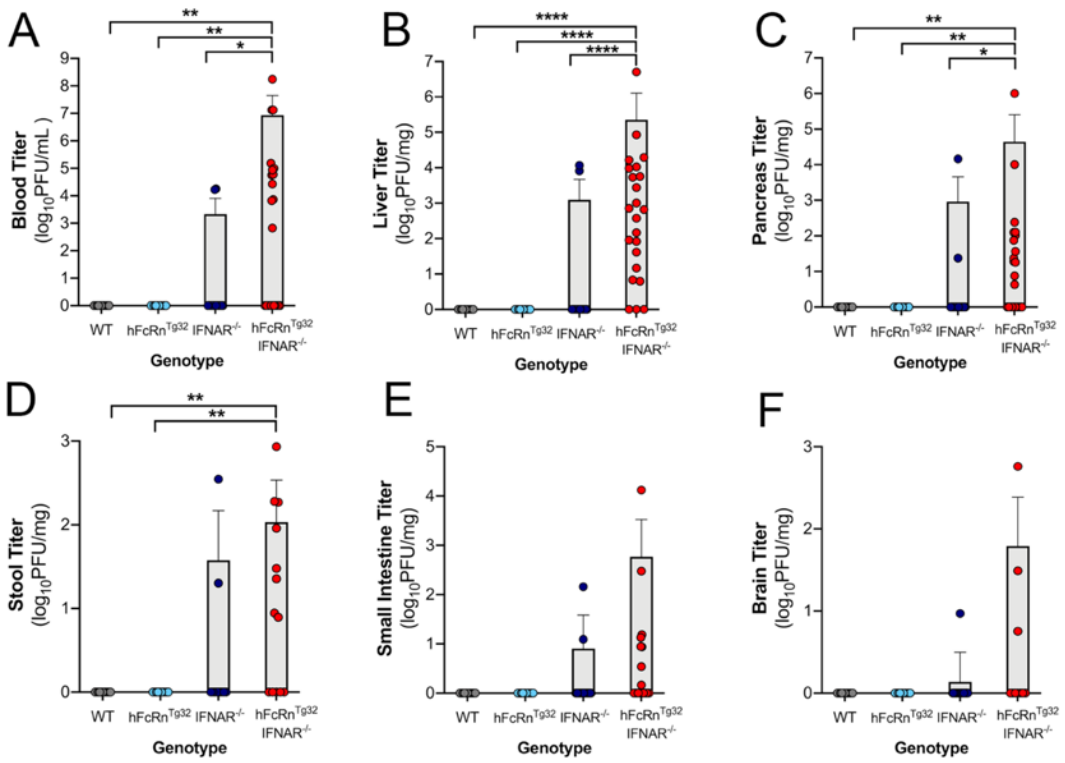

Figure 14 hFcRn^{Tg32}-IFNAR$^{-/-}$ adult mice are permissive to E11 infection

C57/BL6 (WT, gray), hFcRn^{Tg32} (light blue), IFNAR$^{-/-}$ (dark blue), and hFcRn^{Tg32}-IFNAR$^{-/-}$ (red) animals were IP inoculated with 10^4 PFU of E11 and sacrificed 72 hours post inoculation. **(A)** Viral titers in the blood (log_{10}PFU/mL) of adult animals (WT – 11, hFcRn^{Tg32} – 10, IFNAR$^{-/-}$ – 16, hFcRn^{Tg32}-IFNAR$^{-/-}$ – 23 animals). Viral titers in the liver **(B)**, pancreas **(C)**, stool **(D)**, small intestine **(E)**, and brain **(F)** (log_{10}PFU/mg) from adult mice are shown as mean ± standard deviation bars and individual animals (points). Data are shown with significance determined with a Kruskal-Wallis test with a Dunn's test for multiple comparisons (*p<0.05, **p<0.005, ***p<0.0005, ****p<0.0001).

3.2.2 hFcRn^{Tg32}-IFNR$^{-/-}$ animals induce a robust proinflammatory immune response to E11 infection

Due to the high levels of viremia in adult hFcRn^{Tg32}-IFNAR$^{-/-}$ mice, we next characterized the systemic immune response to E11 infection in these animals. To do this, we performed Luminex-based multiplex assays to assess the levels of 45 circulating cytokines and chemokines in the blood of adult animals infected with E11. Consistent with their low levels of infection, we observed no significant changes in the levels of circulating cytokines and chemokines in immunocompetent (WT, hFcRn^{Tg32}) or immunodeficient (IFNAR$^{-/-}$) mice **(Figure 15A)**. In contrast, the blood of infected hFcRn^{Tg32}-IFNAR$^{-/-}$ animals contained high levels of various cytokines and chemokines in response to infection, with 19 cytokines/chemokines induced ≥ 2-fold compared to uninfected controls **(Figure 15A)**. The two most induced cytokines were members of the type I IFN family, IFN-α and IFN-β. On average, 7,802pg/mL of IFN-β was circulating in the blood of hFcRn^{Tg32}-IFNAR$^{-/-}$ animals, while WT, hFcRn^{Tg32}, and IFNAR$^{-/-}$ animals had little to no circulating IFN-β **(Figure 15B)**. Similarly, hFcRn^{Tg32}-IFNAR$^{-/-}$ animals had an average of 165pg/mL circulating IFN-α in blood while WT, hFcRn^{Tg32}, and IFNAR$^{-/-}$ animals had very low to undetectable levels **(Figure 15C)**. In addition to type I IFN induction, a number of chemokines, including monocyte chemoattractant protein 1 (MCP-1/CCL2), B cell attracting chemokine 1 (BCA-1/CXCL13), IP-10/CXCL10, and IL-12(p40) were present at very high levels in E11 infected hFcRn^{Tg32}-IFNAR$^{-/-}$ mice **(Figure 15D-G)**. These data show adult hFcRn^{Tg32}-IFNAR$^{-/-}$ animals mount a potent immune response, including very high levels of type I IFNs, in response to E11 infection.

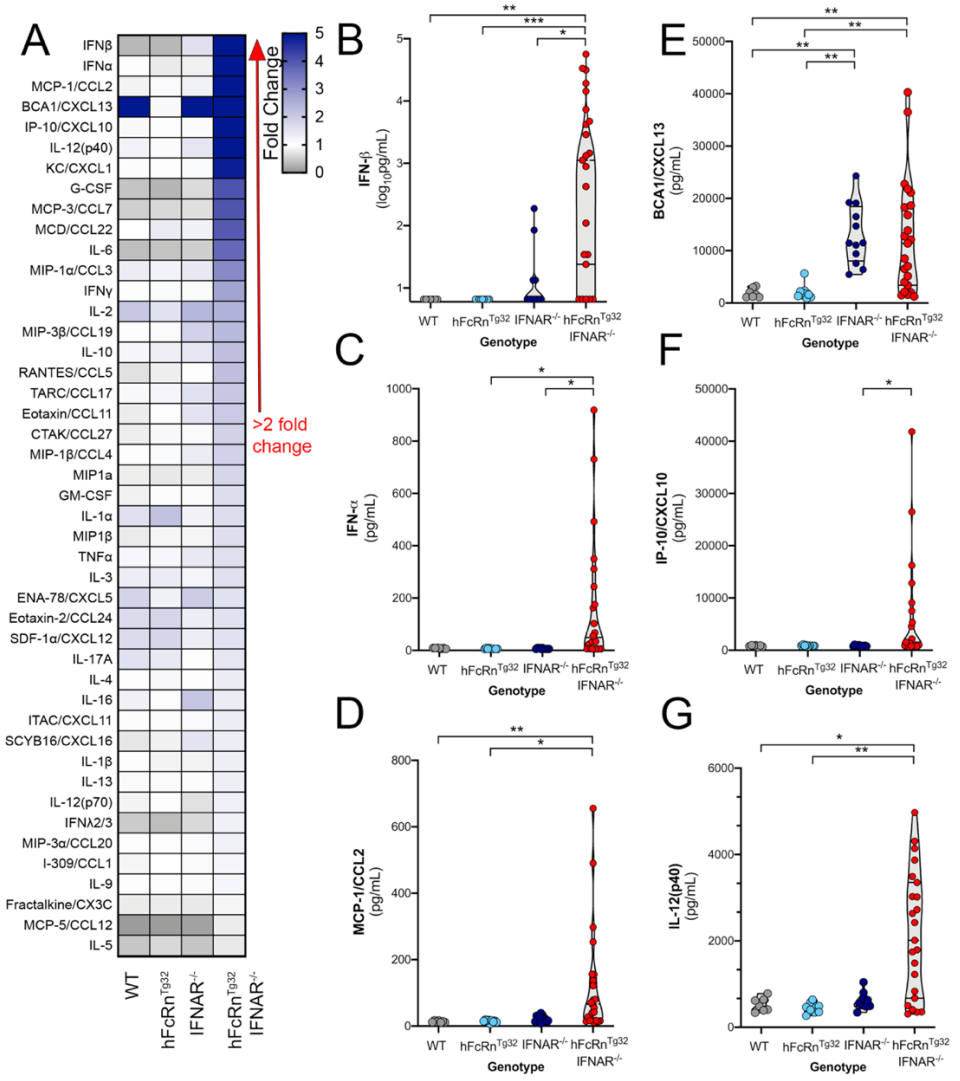

Figure 15 hFcRn^{Tg32}-IFNAR$^{-/-}$ animals induce a robust immune response to E11 infection

C57/BL6 (WT, gray), hFcRn^{Tg32} (light blue), IFNAR$^{-/-}$ (dark blue), and hFcRn^{Tg32}-IFNAR$^{-/-}$ (red) animals were IP inoculated with 10^4 PFU of E11 and sacrificed 72 hours post inoculation. Luminex-based multianalyte profiling of 45 cytokines was then performed from whole blood. **(A)** Heatmap demonstrating the induction (shown as fold-change from uninfected control) in E11-infected mice of the indicated genotype. Blue denotes significantly increased cytokines in comparison to untreated. Grey or white denote little to no changes (scale at top right). The red arrow demonstrates cytokines with greater than 2-fold upregulation observed in the average of separate experiments. Luminex assays were performed in duplicate. **(B-G)** IFN-β (B), IFN-α (C), MCL-1/CCL2 (D), BCA1/CXCL13 (E), IP-10/CXCL10, and IL12(p40) cytokine levels in the blood of E11 infected C57Bl/6 (WT, gray), hFcRn^{Tg32} (light blue), IFNAR$^{-/-}$ (dark blue), and hFcRn^{Tg32}-IFNAR$^{-/-}$ (red) animals. Symbols represent individual mice. Significance was determined with a Kruskal-Wallis test with a Dunn's test for multiple comparisons (*p<0.05, **p<0.005, ***p<0.0005).

3.2.3 Infection and immune responses peak at 72h post-inoculation

Next, we determined the kinetics of the immune responses to E11 infection in hFcRn^{Tg32}-IFNAR$^{-/-}$ mice. To do this, we infected hFcRn^{Tg32}-IFNAR$^{-/-}$ animals with E11 and sacrificed at either 24, 48, or 72hpi and measured viral titers by plaque assays and immune induction by Luminex-based multiplex assays for 34 cytokines and chemokines. We found that there were measurable levels of virus present in key target tissues such as the blood, liver and pancreas by as early as 24hpi, with levels peaking at 72hpi **(Figure 16A-D)**. Consistent with these kinetics, we found that the levels of circulating cytokines increased at 24hpi and peaked at 72hpi as assessed by multianalyte Luminex-based profiling (**Figure 16E**). Strikingly, IFN-β was induced over ~1,000pg/mL in animals infected for 24hrs and even higher in animals after 48hpi and 72hpi **(Figure 16F)**. In addition, IFN-α and IFN-λ2/3 were increased at 72hpi compared to control and 24hpi **(Figure 16G and H)**. In contrast to IFNs, other cytokines and chemokines including IP-10/CXCL10, MCP-1/CCL2, and KC/CXCL1 were induced at highest levels at 48hpi, with levels decreasing by 72hpi (**Figure 16I-K**). These data suggest that animals induce an immune response to infection very early following the initiation of viral replication.

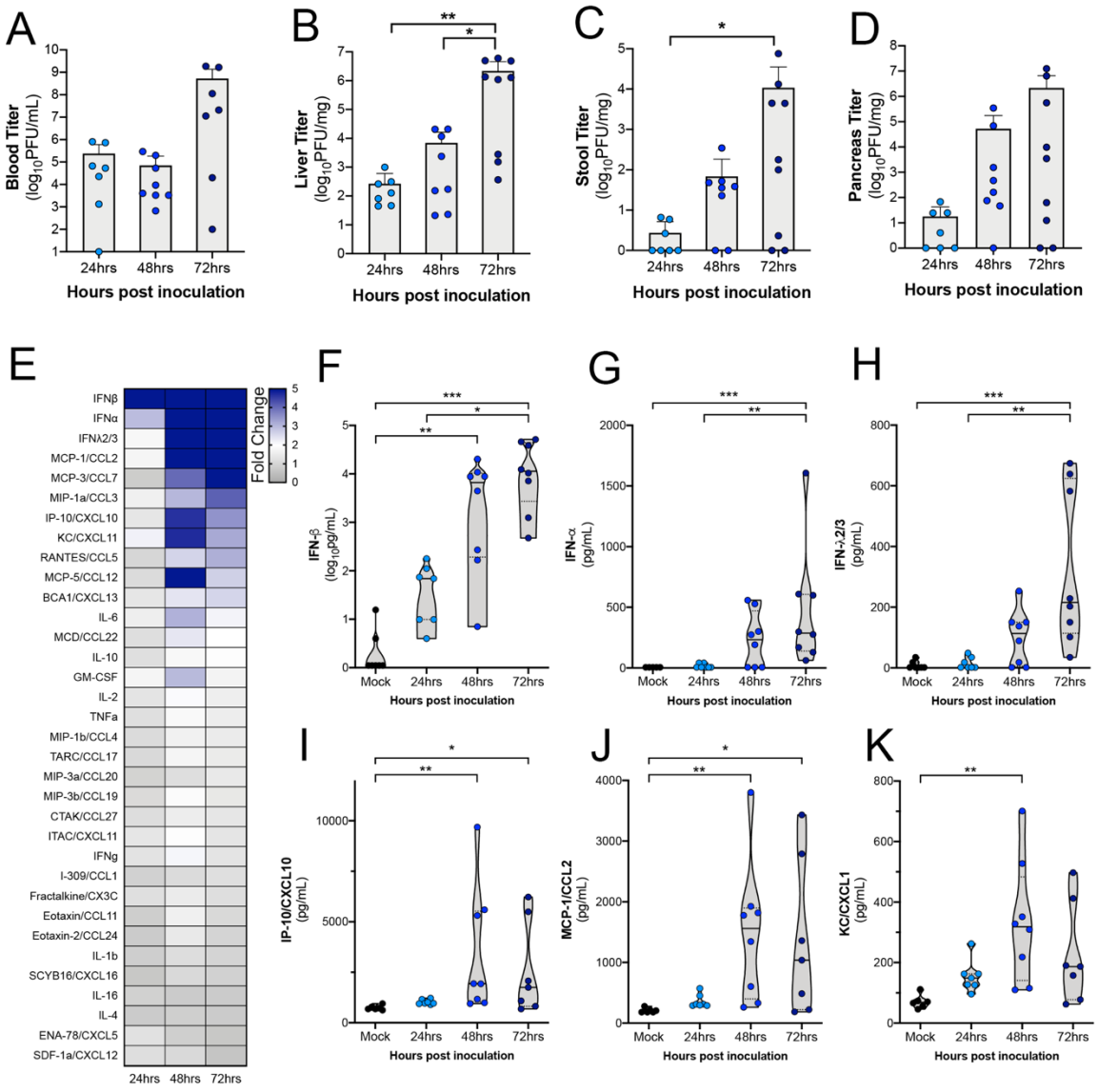

Figure 16 Cytokine levels increase with viremia in hFcRn^{Tg32}-IFNAR$^{-/-}$ animals

hFcRn^{Tg32}-IFNAR$^{-/-}$ animals IP inoculated with 10^4 PFU of E11 were sacrificed at 24 (light blue) 48 (blue), or 72 (navy) hours post inoculation. **(A)** Viral titers in the blood (log_{10}PFU/mL) of adult animals (24hpi – 7, 48hpi – 8, 72hpi – 9 animals) are shown as mean ± standard deviation bars) and individual animals (points). **(B-D)** Viral titers in the liver (B), stool (C), and pancreas (D), (log_{10}PFU/mg) from adult mice are shown as mean ± standard deviation bars and individual animals (points). **(E)** Heat map demonstrating the level of protein induction by Luminex-based assays shown as the fold change of from the average pg/mL of the uninfected animals to each individual animal concentration per protein then averaged within each timepoint. Proteins are sorted from largest fold change (blue) from uninfected to smallest fold change (gray) in 72hpi animals. **(F-K)** IFN-β (F), IFN-α (G), IFNλ2/3 (H), IP-10/CXCL10 (I), MCP-1/CCL2 (J), and KC/CXCL1 (K) protein levels expressed in the blood of each animal

shown by timepoint. Data are shown with significance determined with a Kruskal-Wallis test with a Dunn's test for multiple comparisons (*p<0.05, **p<0.005, ***p<0.0005, ****p<0.0001).

3.2.4 E11 infection induces damage and cell death in the livers of hFcRn^{Tg32}-IFNAR$^{-/-}$ animals

Echovirus infections in neonates commonly induces liver failure, which can be fatal [63]. In addition, our data suggested that the highest levels of E11 replication in hFcRn^{Tg32}-IFNAR$^{-/-}$ mice was in the liver. Thus, we focused on the impact of E11 infection on the liver as a contributor to disease. Blinded pathology scoring of H&E stained sections of infected livers revealed no histopathologic changes in immunocompetent animals or in IFNAR$^{-/-}$ adult or suckling mice infected with E11 **(Figure 17A and B and Figure 47A)**. In contrast, there was moderate to severe liver damage induced by E11 infection of adult hFcRn^{Tg32}-IFNAR$^{-/-}$ animals, including punctate hepatocytolysis and necrosis at 72hpi **(**Black arrows, **Figure 17A and Figure 47A)**. Other histopathological changes included increased immune cell infiltration, which was also observed in infected hFcRn^{Tg32}-IFNAR$^{-/-}$ adult and suckling mice (**Figure 17A,** white arrows; **Figure 47D**, black arrows). There were large areas of necrosis with degenerated neutrophils with little to no lymphocytes **(Figure 47B)**. While the portal areas consist mostly of lymphocytes with little to no neutrophils and macrophages **(Figure 47C)**. In addition to histopathology, we assessed the impact of infection on cell viability using an antibody specific for the cleaved (activated) version of caspase-3. Whereas E11 infection of immunocompetent and IFNAR$^{-/-}$ animals exhibited no cleaved caspase-3 staining as assessed by immunohistochemistry, E11-infected hFcRn^{Tg32}-IFNAR$^{-/-}$ adults **(**Black arrows, **Figure 17B)** and suckling mice **(Figure 47E)** exhibited

pronounced positive cleaved caspase-3 staining. Lastly, we measured the levels of liver enzymes in the blood of infected, which are released by damaged hepatocytes. By 48hpi hFcRn^{Tg32}-IFNAR$^{-/-}$ mice had a significant increase in circulating levels of aspartate transaminase (AST) and alkaline phosphatase (ALP), which occurred over time following infection **(Figure 17C and D)**. These data indicate that the livers of hFcRn^{Tg32}-IFNAR$^{-/-}$ animals undergo apoptosis and cell death leading to liver damage following E11 infection.

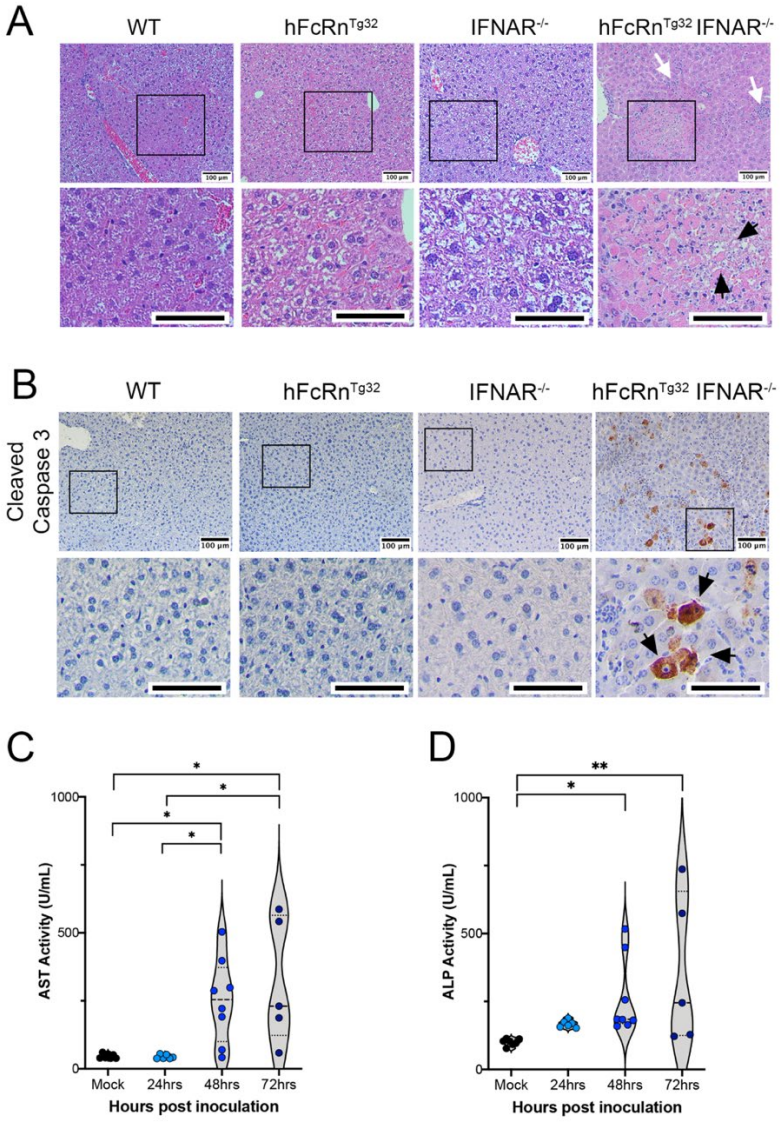

Figure 17 E11 infection induces histopathologic changes and cell death

C57Bl/6 (WT), hFcRn^{Tg32}, IFNAR$^{-/-}$, and hFcRn^{Tg32}-IFNAR$^{-/-}$ adult mice were IP inoculated with 10^4 E11 and sacrificed 72 hours post inoculation. **(A)** H&E staining of the livers in adult mice. White arrows denote immune cell infiltration and black arrows denote areas of hepatocytolysis. **(B)** Immunohistochemistry using an antibody recognizing the cleaved form of caspase 3 from the livers of a representative animal of each genotype as indicated. Black arrows denote positive staining. Scale bars (100μm) are shown at bottom right. Aspartate transaminase (AST) **(C)** or alkaline phosphatase (ALP) **(D)** levels in the serum of adult mice IP inoculated with 10^6 E11 and sacrificed at designated time shown. Data are shown with significance determined with a Kruskal-Wallis test with a Dunn's test for multiple comparisons (*$p<0.05$, **$p<0.005$).

3.2.5 E11 infection of hFcRn^{Tg32}-IFNAR$^{-/-}$ mice induces a robust local proinflammatory immune response in the liver

Because we found that the livers of hFcRn^{Tg32}-IFNAR$^{-/-}$ mice infected with E11 exhibited histopathologic changes and underwent cell death, we profiled other liver changes by RNAseq transcriptional profiling. Consistent with our Luminex-based profiling studies of circulating cytokines, we found that the livers of hFcRn^{Tg32}-IFNAR$^{-/-}$ animals infected with E11 robustly induced expression of the transcripts for type I IFNs, with less robust induction of type III IFNs **(Figure 18A)**. Levels of vRNA in infected animals mirrored our findings on infectious viral titers, with high levels in hFcRn^{Tg32}-IFNAR$^{-/-}$ mice **(Figure 18B)**. In addition to these changes, hFcRn^{Tg32}-IFNAR$^{-/-}$ infected animals also induced the expression of other pro-inflammatory and immunomodulatory factors, including chemokines (e.g. Ccl2, Cxcl1, Cxcl9), transcription factors (e.g. Stat1, Stat3, Socs1), and interferon stimulated genes (e.g. Isg15, Ifit1) **(Figure 18C and D)**.

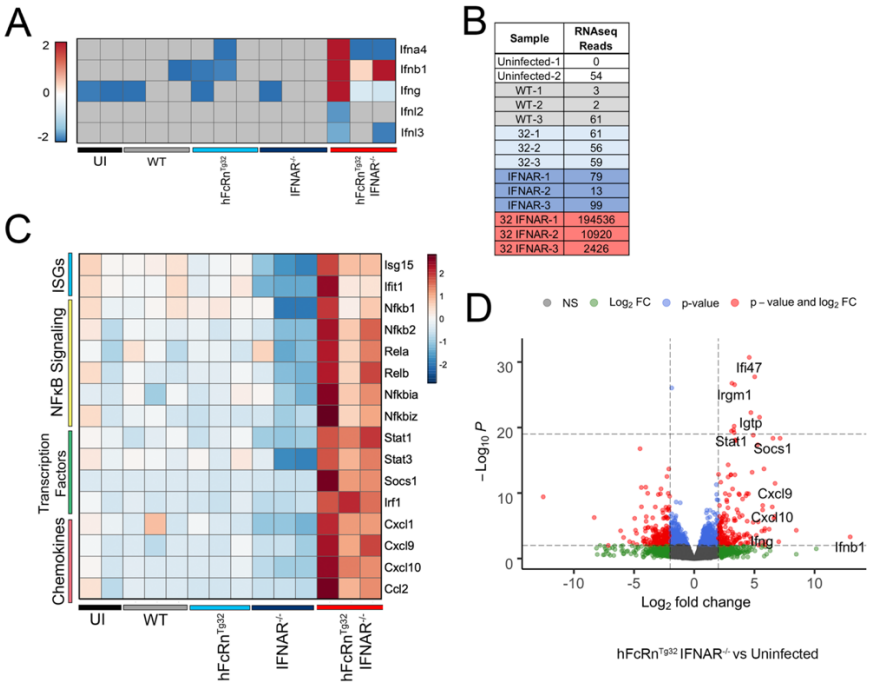

Sample	RNAseq Reads
Uninfected-1	0
Uninfected-2	54
WT-1	3
WT-2	2
WT-3	61
32-1	61
32-2	56
32-3	59
IFNAR-1	79
IFNAR-2	13
IFNAR-3	99
32 IFNAR-1	194536
32 IFNAR-2	10920
32 IFNAR-3	2426

Figure 18 Transcriptional profiling from the livers of E11 infected hFcRn^{Tg32}-IFNAR$^{-/-}$ animals reveals induction of a proinflammatory immune response to infection

RNAseq-based transcriptional profiling from RNA isolated from the livers of E11 infected C57Bl/6 (WT), hFcRn^{Tg32}, IFNAR$^{-/-}$ or hFcRn^{Tg32}-IFNAR$^{-/-}$ animals (3 animals each), or uninfected controls (2 animals) was performed. **(A)** Heatmap of log$_2$RPKM values for type I (Ifna4, Ifnb1), II (Ifng), and III (Ifnl2, Ifnl3) IFNs in the livers of the indicated genotypes 72hpi. Scale shown at left. **(B)** RPKM values mapped to the E11 genomic sequence in each genotype. Individual animals are shown. **(C)** Heatmap based on log$_2$RPKM values of select proinflammatory cytokines in the livers of following E11 infection of the indicated genotypes, or uninfected controls. Scale is shown at right. In (A) and (C), red indicates higher expression and blue indicates lower expression. Grey denotes no reads detected. **(D)** Volcano plot of differentially regulated genes in hFcRn^{Tg32}-IFNAR$^{-/-}$ adult animals compared to uninfected animals. Red indicates genes with a statistically significant upregulation or downregulation of > or < log$_2$ fold-change of 2 and $p<0.05$.

3.2.6 E11 specifically infects hepatocytes in hFcRn^{Tg32}-IFNAR$^{-/-}$ mice

Finally, we defined the cellular tropism of E11 within the liver. Using immunohistochemistry for the viral VP1 capsid protein, we found that E11 localized primarily in what appeared to be hepatocytes **(Figure 48A)**. No positive staining for VP1 was observed in any other three mouse strains **(Figure 48A)**. hFcRn^{Tg32}-IFNAR$^{-/-}$ suckling mice also displayed positive VP1 staining in the liver **(Figure 48B)**. Although VP1 staining suggested that E11 replication occurred primarily in hepatocytes, we developed a more sensitive approach to define the cellular tropism of E11 using hybridization chain reaction (HCRv3.0). HCR allows for multiplexed quantitative RNA fluorescence *in situ* hybridization (RNA-FISH) and the signal amplification inherent to the technique vastly enhances the dynamic range and sensitivity of conventional FISH-based approaches [259–261]. To do this, we designed probes specific for the E11 genome and performed HCR on liver sections from hFcRn^{Tg32}-IFNAR$^{-/-}$ mice infected with E11 (schematic, **Figure 19A**). To define the localization of E11 specifically to hepatocytes, we also developed probes to albumin, a specific marker of hepatocytes. Using HCR, we observed the presence of E11 vRNA in the livers of infected mice by 24hpi, with the numbers of positive cells increasing by 48-72hpi (**Figure 19B**). Interestingly, E11 vRNA positive cells exclusively colocalized with albumin, identifying hepatocytes as the main cellular target of infection in the liver. To confirm this, we quantified three fields at each time point and quantified colocalization between vRNA and albumin signals, which revealed a strong colocalization (Pearson's coefficient 24hpi – 0.73, 48hrs – 0.85, 72hpi – 0.84). We next applied HCR to determine whether infected and/or uninfected cells in the liver produce IFN-β. Using this approach, we found that although some infected cells produced low levels of IFN-β, the strongest signal was observed in uninfected neighboring cells **(Figure**

19C and D). Together, these data show that E11 replicates in liver hepatocytes and that uninfected neighboring cells may be a major source of IFN-β in hFcRn^{Tg32}-IFNAR$^{-/-}$ animals.

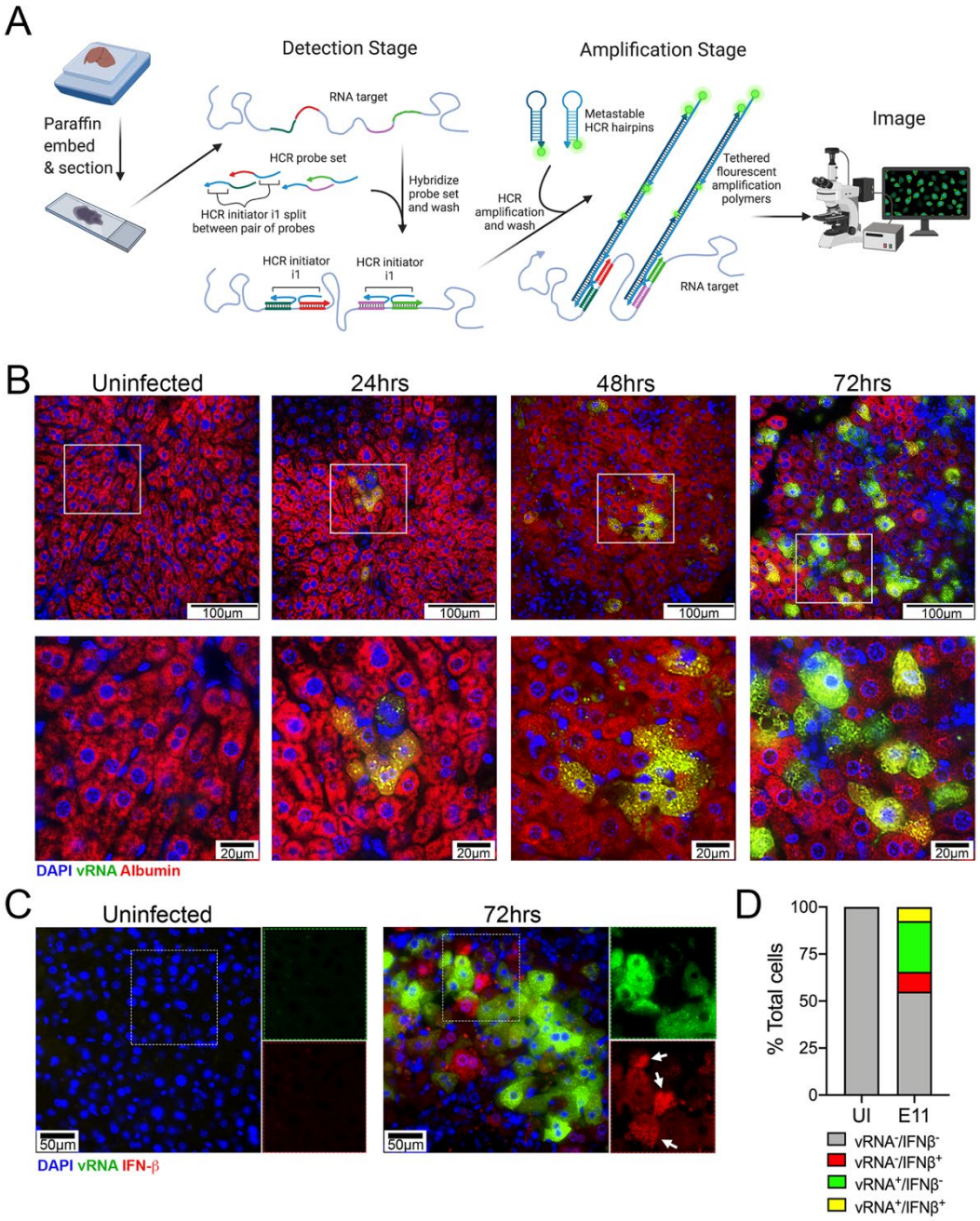

Figure 19 Hepatocytes are the primary site of E11 replication in the liver

(A) Schematic of the hybridization chain reaction (HCR) protocol used adapted from the Molecular Instruments HCR v3.0 protocol and created with BioRender.com. **(B)** HCR of hFcRn^{Tg32}-IFNAR$^{-/-}$ adult animals at the indicated dpi using probes against the E11 genome (green) and albumin (red). White boxes denote areas zoomed at bottom. Scale bars shown at bottom right (100µm at top and 20µm at bottom). Three unique fields were captured and colocalization between vRNA and albumin quantified, as indicated in the text. **(C)** HCR of hFcRn^{Tg32}-IFNAR$^{-/-}$ adult animals at the indicated dpi using probes against the E11 genome (green) and IFN-β (red). Separated channels are in the panels to the right of each image. Scale bars shown at bottom right. **(D)** Quantification

of HCR shown in (C) from uninfected control (704 total cells) or E11 infected (1064 total cells) animals. The total percentage of cells negative for both viral RNA (vRNA) and IFN-β ($vRNA^-/IFN\beta^-$) are shown in grey, negative for vRNA but positive for IFN-β ($vRNA^-/IFN\beta^+$) in red, positive for vRNA but negative for IFN-β ($vRNA^+/IFN\beta^-$) in green, and those positive for both vRNA and IFN-β ($vRNA^+/IFN\beta^+$). At least three unique fields from at least three unique animals were used in the analysis.

3.3 Discussion

Here, we show that human FcRn and type I IFN signaling are key host determinants that control E11 infection in the liver, a tissue site commonly associated with human disease. Through Luminex-based multianalyte and RNASeq-based transcriptional profiling, we also show that animals expressing hFcRn and ablated in type I IFN signaling initiate a systemic immune response to infection. Furthermore, we show that E11 replication in the liver induces histopathological changes leading to liver dysfunction and apoptotic cell death in hepatocytes. Finally, we show that neighboring hepatocytes rather than infected hepatocytes are also sources of IFN-β production. Our findings thus define pro-viral (hFcRn) and antiviral (type I IFN) host factors that control echovirus infections specifically in the liver. In addition, our studies provide a novel animal model that can be used to test anti-echovirus therapeutics.

Although FcRn has been identified as a pan-echovirus receptor[109,255], its role in mediating echovirus pathogenesis has remained unclear. Previous work has shown that FcRn is expressed in many different cell types in the body, including the small intestine[262,263] and in liver hepatocytes[235,264]. Despite what its name implies, FcRn is expressed on many cells throughout life, often at very high levels. Our results shown here define the organs targeted by E11 in an *in vivo* model, with high levels of replication in various tissues, such as the liver and pancreas. Our parallel adult and suckling pup models allowed us to compare age-related differences that might impact

sensitivity or responses to echovirus infections. Of note, the animals used in our studies express hFcRn under the control of the endogenous promoter, which might mimic age-related changes in expression observed in humans. Interestingly, although we detected high levels of echovirus replication in similar tissues between adults and suckling pups, there were age-related differences in viral infection in the brains of these mice. Whereas 16 of 18 of infected hFcRn^{Tg32}-IFNAR$^{-/-}$ suckling mice exhibited replication in the brain, only 3 of 23 adult animals did. Although this could be attributed to differences on the relative ratio of weight to viral inoculum, circulating viral titers in the blood were similar between suckling pups and adult mice. Given that echovirus infections are commonly associated with aseptic meningitis in neonates, these findings suggest that expression levels of hFcRn and type I IFN signaling could be key determinants of age-related susceptibility in key sites targeted in humans, such as the liver and brain.

The liver is a primary site of echovirus-associated disease, with hepatitis and acute liver failure commonly observed in infected infants and children and the majority of echovirus-associated death in neonates occurs due to overwhelming liver failure[265]. Our *in vivo* findings suggest that FcRn expression is required for this infection only when host type I IFN signaling is ablated. We hypothesize that although no IFNs were produced systemically in immunocompetent hFcRn^{Tg32}, that these animals produce a local response which restricts infection following inoculation. In addition to IFNs, we observed induction of a number of other immunomodulatory factors in infected animals. The role of cytokines in echovirus pathogenesis in humans is not known. However, immunodeficient individuals, including adults, are more susceptible to echovirus infections, which often induces hepatitis[266–269]. In addition, analysis of mutations in the E11 genome induced by selective pressure in an immunodeficient individual who developed chronic infection revealed strikingly high sequence conservation in the 3C virally-encoded protease which

often attenuates host cell innate immune signaling[269]. Our studies suggest that type I IFNs are the primary drivers of resistance to echovirus infections in the liver, which is supported by our RNASeq studies, in which low levels of the transcripts for type III IFNs were upregulated by infection. These findings are similar to those for the related enterovirus coxsackievirus B3 (CVB3), whose infection in the liver is also regulated primarily by type I IFN signaling[257]. Collectively, our studies show that expression of hFcRn in the setting of diminished type I IFN signaling is the primary driver of E11 infection in the liver.

Despite the clear hepatic tropism of echoviruses, little is known regarding the cell type(s) targeted by echoviruses in the liver or how these cells respond to infection. Moreover, the role of FcRn in mediating this tropism is unknown. The liver is composed of diverse cell types. In addition to hepatocytes, which comprise ~80% of total liver cells, tissue resident Kupffer Cells represent ~35% and liver sinusoidal endothelial cells comprise ~50% of non-parenchymal cells. FcRn is thought to be expressed in all of these cell types[228]. Our studies thus define the tropism of echoviruses specifically to hepatocytes and show that FcRn expression is a key determinant of this tropism. In addition, our studies suggest that echovirus infection of hepatocytes induces pronounced hepatic damage, characterized by apoptotic cell death, tissue damage, and the presence of elevated liver enzymes in the serum. These findings are consistent with what is observed in autopsy tissue isolated from echovirus infected neonates, which also indicates extensive infection-induced hepatocyte damage[63,216,268,270].

Consistent with high levels of infection in the liver, hFcRn^{Tg32}-IFNAR$^{-/-}$ infected animals also exhibited infectious virus present in the stool. Given that echoviruses are transmitted by the fecal-oral route, defining how viral particles are shed and subsequently transmitted is important for understanding pathogenesis and spread. Because infected animals did not have high titers in the

small intestine (~10^2 PFU/mg on average), our data indicate that shed virus does not result from direct intestinal infection, which is expected given the route of inoculation. The most likely scenario is via the gut-liver axis. Many studies have shown that the bacteria and bacterial products can reach the liver through the portal vein and liver secretory products, such as bile acids, IgA, and antimicrobial molecules, can leave the liver into the intestines through the biliary tract[271,272]. It is thus likely that infectious virus exits the liver through the biliary tract into the intestine where it exits the body in the stool, explaining the high stool titers with little to no infectious virus in the intestine itself.

There are currently no effective antiviral therapeutics to combat echovirus infections. Our work thus establishes *in vivo* models that full recapitulate echovirus infection in human neonates and could thus be used to develop and test antivirals. In addition, our studies define key roles for FcRn and type I IFN signaling in mediating echovirus pathogenesis and suggest these factors could be targeted to ameliorate or prevent infections. Collectively, this work defines fundamental aspects of echovirus biology that enhance our understanding of how infection, tissue targeting, and disease occurs.

3.4 Materials and Methods

3.4.1 Ethics Statement

All procedures were approved by the University of Pittsburgh institutional review boards. All mouse experiments were performed in accordance with the recommendations in the National

Institutes of Health Guide for the Care and Use of Laboratory Animals. Experiments were approved by the University of Pittsburgh Animal Care and Use Committee.

3.4.2 Cell lines and viruses

HeLa cells (clone 7B) were provided by Jeffrey Bergelson, Children's Hospital of Philadelphia, Philadelphia, PA, and cultured in MEM supplemented with 5% FBS, non-essential amino acids, and penicillin/streptomycin. Experiments were performed with echovirus 11 Gregory (E11), which was obtained from the ATCC. Virus was propagated in HeLa cells and purified by ultracentrifugation over a 30% sucrose cushion, as described previously[245].

3.4.3 Animals

All animal experiments were approved by the University of Pittsburgh Animal Care and Use Committee and all methods were performed in accordance with the relevant guidelines and regulations. C57BL/6J (WT, cat. no. 000664), B6.Cg-*Fcgr*^{tm1Dcr}Tg(FCGRT)32Dcr/DcrJ (hFcRn^{Tg32}, cat. no. 014565), B6(Cg)-Ifnar1$^{tm1.2Ees}$/J (IFNAR$^{-/-}$, cat. no. 028288) were purchased from The Jackson Laboratory. hFcRn^{Tg32}-IFNAR$^{-/-}$ mice were generated by crossing B6.129S2-Ifnar1^{tm1Agt}/Mmjax (cat no. 32045-JAX) with B6.Cg-Fcgrt^{tm1Dcr} Tg(FCGRT)32Dcr/DcrJ (cat no. 014565). Breeders were established that were deficient in mouse FcRn and IFNAR and were homozygous for the hFcRn transgene. All animals used in this study were genotyped by Transnetyx.

3.4.4 Adult animal infections

5-6-week-old mice were inoculated by the intraperitoneal route with 10^4 PFU of E11. An equal number of males and females were used in this study. Intraperitoneal inoculation was performed using a 1mL disposable syringe and a 25-gauge needle in 100µL of 1X PBS. Mice were euthanized at 3 days post inoculation, or at times specified in the figure legends, and organs harvested into 1mL of DMEM (viral titration) or RNA lysis buffer (RNA isolation) and stored at -80°C. Tissue samples for viral titration were thawed and homogenized with a TissueLyser LT (Qiagen) for 8 minutes, followed by brief centrifugation for 5 minutes at 5000 x g. Viral titers in organ homogenates were determined by plaque assay in HeLa cells overlayed with a 1:1 mixture of 1% agarose and 2x MEM (4% FBS, 2% pen/strep, 2% NEAA). Plaques were enumerated 40hpi following crystal violet staining.

3.4.5 Adult animal IFNAR blocking infections

5-6-week-old hFcRn^{Tg32} were injected by the intraperitoneal route with an anti-IFNAR blocking antibody (200µg) (BioXcell, #BP0241) or an isotype control antibody (BioXcell, #BP0083) 8hrs prior to inoculation with 10^6 PFU of E11. Mice were euthanized at 3 days post inoculation and tissues were used for viral titration assays, as described above.

3.4.6 Suckling pup infections

7-day-old mice were inoculated by the intraperitoneal route with 10^4 PFU of E11. Two separate litters were inoculated for each condition with an average ratio of 50:50 of male and

female pups. Intraperitoneal inoculation was performed using a 1mL disposable syringe and a 27-gauge needle in 50μL of 1X PBS. Mice were euthanized at 3 days post inoculation and organs harvested into 0.5mL of DMEM (viral titration) or RNA lysis buffer (RNA isolation) and stored at -80°C. Tissue samples for viral titration were thawed and homogenized with a TissueLyser LT (Qiagen) for 5 minutes, followed by brief centrifugation for 5 minutes at 8000 x g. Viral titers in organ homogenates were determined by TCID50 in HeLa cells and enumerated following crystal violet staining.

3.4.7 Immunohistochemistry

Tissues were fixed in 10% buffered formalin for 24hrs and then transferred to 70% ethanol. Tissues were embedded in paraffin and sectioned. Slides were stained with a monoclonal VP1 antibody, as described previously[109], or cleaved caspase 3. Tissue sections were deparaffinized with xylene and rehydrated with decreasing concentrations of ethanol (100%, 95%, 80%), then washed with ddH_20. Antigen unmasking was performed with slides submerged in 10 mM citrate buffer (pH 6.0) and heated in a steamer for 20 minutes at ~90°C. Slides were cooled to room temperature and slides were immunostained with cleaved caspase 3 using Vectastain Elite ABC HRP (Vector Biolabs, PK-6100), according to the manufacturer's instructions. Slides were incubated in 6% H_2O_2 in methanol for 30 min then washed 3 times for 5 minutes in H_2O. Avidin block (Vector, SP-2001) was applied for 15 minutes and washed twice in H_2O followed by biotin block (Abcam, ab156024) for 15 minutes and washed twice in H_2O. Finally, serum-free protein block was applied for 10 minutes and cleaved caspase 3 antibody was diluted 1:100 in TBS-T (Tris-buffered saline, 0.1% Tween 20) and slides incubated overnight in a humidified chamber at 4C. Next, slides were washed three times for 5 min in PBST and exposed to the goat anti-rabbit

biotinylated secondary antibody (Vector, BA-1000) for 30 min. Slides were rinsed in PBST three times for 5 min and the Vectastain Elite ABC HRP kit was applied for 30 min. Slides were rinsed in PBST for three times for 5 min and diaminobenzidine substrate for 5 mins; which was terminated with water incubation. Slides were counterstained with hematoxylin for 1 min, thoroughly rinsed with H_2O, and incubated in 0.1% sodium bicarbonate in H_2O for 5 mins. Slides were then dehydrated with increasing concentrations of ethanol, cleared with xylene and mounted with Cytoseal 60 (Thermo Scientific, 83104). Images were captured on an IX83 inverted microscope (Olympus) using a UC90 color CCD camera (Olympus).

3.4.8 Antibodies

The following antibodies were used- anti-VP1 (NCL-ENTERO, clone 5-D8/1, Leica Biosystems) and cleaved caspase 3 (Asp175) (9661, Cell Signaling).

3.4.9 HCR and Imaging

HCR was performed following the Molecular Instruments HCR v3.0 protocol for FFPE human tissue sections[259,261]. Briefly, tissue sections were deparaffinized with xylene and rehydrated with decreasing concentrations of ethanol (100%, 95%, 80%). Antigen unmasking was performed with slides submerged in 10 mM citrate buffer (pH 6.0) and heated in a steamer for 20 minutes at ~90°C. Slides were cooled to room temperature. Sections were treated with 10 µg/mL Proteinase K for 10 min at 37°C and washed with RNase free water. Samples were incubated for 10 minutes at 37°C in hybridization buffer. Sections were incubated overnight in a humidified chamber at 37°C with 0.4 pmol of initiator probes in hybridization buffer (Table 7 echovirus

probes, Table 8 albumin probes, Table 9 IFN-β probes). The next day, slides were washed in probe wash buffer and 5x SSCT for 4x 15 min, according to the manufacturer's instructions. Samples were incubated in a humidified chamber at 37°C for 30 minutes in amplification buffer. Fluorescent hair pins were heated to 95°C for 90 seconds and snap cooled at room temperature for 30 min. Hairpins and amplification buffer were added to the sample and incubated overnight at room temperature. Hairpins were washed off with 5x SSCT for 5 minutes, 15 minutes, 15 minutes, and 5 minutes. Slides were mounted in vectashield with DAPI. Slides were imaged an IX83 inverted microscope (Olympus) with ORCA-FLASH 4.0 camera. Olympus CellSens advanced imaging software with the deconvolution package, constrained iterative, was used. Image analysis was performed using FIJI.

3.4.10 RNA extraction and RNAseq

Total RNA was prepared using the Sigma GenElute total mammalian RNA miniprep kit with optional DNase step, according to the protocol of the manufacturer. RNA quality was assessed by Nanodrop and an Agilent RNA Screen Tape System, and 1ug was used for library preparation using RNA with Poly A selection kit (Illumina), as per the manufacturer's instructions. Sequencing was performed on an Illumina HiSeq. RNA-seq FASTQ data were processed and mapped to the mouse reference genome (GRCm38) using CLC Genomics Workbench 20 (Qiagen). Differential gene expression was performed using the DESeq2 package in R [249]. Heatmaps were made in R using the pheatmap: pretty heatmaps package shown as the $\log_2$RPKM. Raw sequencing files have been deposited in Sequence Read Archives (SUB8204864, PRJNA665496).

3.4.11 Luminex assays

Luminex profiling was performed on whole blood that was allowed to clot for 20 minutes and then spun down using a custom mouse IFN kit (IFN alpha, IFN beta, IL-28, Invitrogen), mouse cytokine 23-plex (Bio-Rad, M60009RDPD), and mouse chemokine 31-plex (Bio-Rad, 12009159), according to the manufacturer's protocol. Assays were read on a Millipore MagPix machine by the Luminex Corporation. Heat maps were generated using the fold change in concentration (picograms/milliliter) of each animal compared to the average of uninfected animals and was made in GraphPad Prism. Violin plots are shown as the concentration for each animal (one point) in picograms/milliliter.

3.4.12 Statistics

All statistical analysis was performed using GraphPad Prism version 8. Data are presented as mean ± SD. A one-way ANOVA was used to determine statistical significance, as described in the figure legends. Parametric tests were applied when data were distributed normally based on D'Agostino–Pearson analyses; otherwise nonparametric tests were applied. P values of <0.05 were considered statistically significant, with specific P values noted in the figure legends.

4.0 Enterovirus replication and dissemination are differentially controlled by type I and III interferons in the GI tract

Enteroviruses are amongst the most common viral infectious agents of humans and cause a broad spectrum of mild-to-severe illness. Enteroviruses are primarily transmitted by the fecal-oral route, but the events associated with their intestinal replication *in vivo* are poorly defined. Here, we developed a neonatal mouse model of enterovirus infection by the enteral route using echovirus 5 and used this model to define the differential roles of type I and III interferons (IFNs) in enterovirus replication in the intestinal epithelium and subsequent dissemination to secondary tissues. We show that human FcRn, the primary receptor for echoviruses, is essential for intestinal infection by the enteral route and that type I IFNs control dissemination to secondary sites, including the liver. In contrast, type III IFNs limit enterovirus infection in the intestinal epithelium and mice lacking this pathway exhibit persistent epithelial replication. Finally, we show that echovirus infection in the small intestine is cell-type specific and occurs exclusively in enterocytes. These studies define the type-specific roles of IFNs in enterovirus infection of the GI tract and the cellular tropism of echovirus intestinal replication.

4.1 Introduction

Enteroviruses are small (~30nm) single stranded RNA viruses that are comprised of coxsackieviruses (CVA and CVB), rhinoviruses, poliovirus (PV), enteroviruses 71 and D68 (e.g., EV-71, EV-D68), and echoviruses (which includes ~30 serotypes). Echoviruses can cause 15-30%

of nosocomial infections is Neonatal Intensive Care Units (NICUs) and often result in aseptic meningitis and liver failure, which can be fatal[67,69,252,253]. The National Enterovirus Surveillance System (NESS) indicates that between the years of 2014-2016 echoviruses were amongst the most commonly circulating enteroviruses in the U.S.[273]. Globally, outbreaks of other echoviruses including echovirus 5 (E5) have been associated with a range of clinical outcomes, with most severe disease occurring in infants and children[274–276].

Enteroviruses are primarily transmitted through the fecal-oral route and initiate host entry via the epithelial lining of the GI tract. We have previously shown that echoviruses robustly infect human stem cell-derived intestinal enteroids and exhibit a cell-type specificity of infection, with preferential infection in enterocytes and enteroendocrine cells[49,130]. Additionally, echovirus infections cause damage to barrier function in enteroid-derived intestinal epithelial monolayer cultures[130], suggesting that virus-mediated epithelial damage could contribute to dissemination from the intestine. The impact of host innate immune signaling on enteroviral infections in the intestinal epithelium is largely unknown. Previous studies in mouse models using PV and EV71 have shown that ablation of type I interferon (IFN) signaling by deletion of the IFNα/β receptor (IFNAR) is required for infection by the oral route[53,197,277], suggesting that these IFNs play a central role in the protection of the GI tract from enterovirus infection. Whether this enhancement was the result of increased infection in the intestinal epithelium directly and/or resulted from alterations in infection of non-epithelial cell types remains unclear. Other studies using CVB show that infection by the enteral route remains inefficient in IFNAR$^{-/-}$ animals, suggesting that these IFNs are not involved in intestinal innate immune responses[278]. Consistent with this, type III IFNs, which are comprised of IFN-λs 1-3 in humans, are preferentially induced in enterovirus-infected human enteroids[49,130]. For other enteric viruses, such as reoviruses, rotaviruses, and noroviruses, type III

IFNs specifically control viral replication in the intestinal epithelium *in vivo*, with type I IFNs impacting the lamina propria[46–48,53,279]. Thus, the roles of type I and III IFNs in the control of enteroviral infections *in vivo* remain unclear.

We and others previously identified the human neonatal Fc receptor (hFcRn) as a primary receptor for echoviruses[109,128]. In contrast, mouse FcRn does not function as an echovirus receptor and does not support replication *in vivo*[109,280]. FcRn is expressed at the apical membrane of polarized enterocytes, where it binds to IgG and albumin, is internalized by endocytosis, and delivers its cargo to early and late endosomes, with the eventual release of IgG and albumin into the interstitium[281]. However, expression of hFcRn alone is not sufficient for echovirus infection in adult or neonatal mice and ablation of IFNAR in hFcRn-expressing mice is required for infection following intraperitoneal (IP) inoculation[280]. However, the roles of hFcRn and IFN signaling following inoculation via the enteral route was not explored.

Here, we established *in vitro* and *in vivo* models to define the impact of hFcRn expression and type I and III IFN signaling in echovirus infections in the GI tract. To do this, we generated mice expressing hFcRn that are deficient in the type III IFN receptor (IFNLR) and compared their susceptibility to enteral echovirus infection to hFcRn-expressing mice lacking IFNAR expression, or immunocompetent animals expressing hFcRn alone. Whereas expression of hFcRn was necessary and sufficient to support echovirus replication in primary murine stem cell-derived enteroids, it was not sufficient for infection of immunocompetent mice following oral gavage. We show that hFcRn-expressing mice deficient in IFNLR expression are unable to control echovirus infection in the GI tract and exhibit persistent replication in the intestinal epithelium, which occurred exclusively in enterocytes. However, these animals did not exhibit any morbidity or mortality from infection and there was no dissemination to secondary tissues. In contrast, there

was robust dissemination in hFcRn-expressing mice deficient in IFNAR expression, which resulted in significant morbidity and mortality. However, we did not observe active replication in the intestinal epithelium of these animals. These findings define the differential roles of type I and III IFNs in the control of echovirus replication in the GI tract and in subsequent dissemination.

4.2 Results

4.2.1 Human FcRn is required for echovirus infection of murine-derived enteroids

To define the role of hFcRn in infections of the murine intestine, we generated neonatal enteroids from C57/BL6 (wild-type, WT) mice and mice expressing hFcRn ($hFcRn^{Tg32}$). $hFcRn^{Tg32}$ mice are deficient in expression of mouse FcRn and express human FcRn under the control of the native human promotor[227]. Stem cell-derived enteroids differentiated to form three-dimensional structures containing cells present in the epithelium *in vivo*, including enterocytes and mucin-secreting goblet cells (**Figure 20A**). Consistent with what has been described for murine fibroblasts derived from WT mice[109], enteroids derived from WT mice were resistant to E5 infection (**Figure 20B**). In contrast, enteroids derived from $hFcRn^{Tg32}$ mice were highly permissive to E5 infection, which peaked at ~ 24 hours post inoculation (hpi) (**Figure 20B**). To define the host response of E5-infected enteroids, we performed bulk RNASeq followed by differential expression analysis. Similar to previous results in human enteroids[49], murine-derived enteroids induced the selective expression of transcripts associated with the type III IFNs IFNλ-2 and IFNλ-3 (mice do not express IFN-λ1) (**Figure 20C**). Differential expression analysis revealed the induction of 48 transcripts in E5-infected $hFcRn^{Tg32}$ enteroids, 42 of which are classified as

interferon stimulated genes (ISGs) (**Figure 20D**), supporting a prominent role of IFN signaling in the intestinal innate immune response to echovirus infections.

The selective induction of type III IFNs in murine-derived enteroids suggests that these IFNs are key mediators in the control of echovirus infections in the intestinal epithelium. To test this, we derived enteroids from small intestine tissue of mice expressing hFcRn that are deficient in IFNAR expression ($hFcRn^{Tg32}$-$IFNAR^{-/-}$)[280]. To perform parallel studies in enteroids deficient in type III IFN signaling, we crossed $hFcRn^{Tg32}$ mice to mice deficient in IFNLR expression ($hFcRn^{Tg32}$-$IFNLR^{-/-}$). Enteroids were generated from the small intestines of immunocompetent $hFcRn^{Tg32}$, $hFcRn^{Tg32}$-$IFNAR^{-/-}$, and $hFcRn^{Tg32}$-$IFNLR^{-/-}$ mice and the levels of E5 replication compared between these genotypes. We did not detect any significant differences in E5 replication between hFcRn-expressing immunocompetent enteroids and those deficient in either IFNAR or IFNLR expression (**Figure 20E**). These data show that in *ex vivo* murine-derived enteroid models, hFcRn expression is necessary and sufficient for echovirus infection of the intestinal epithelium.

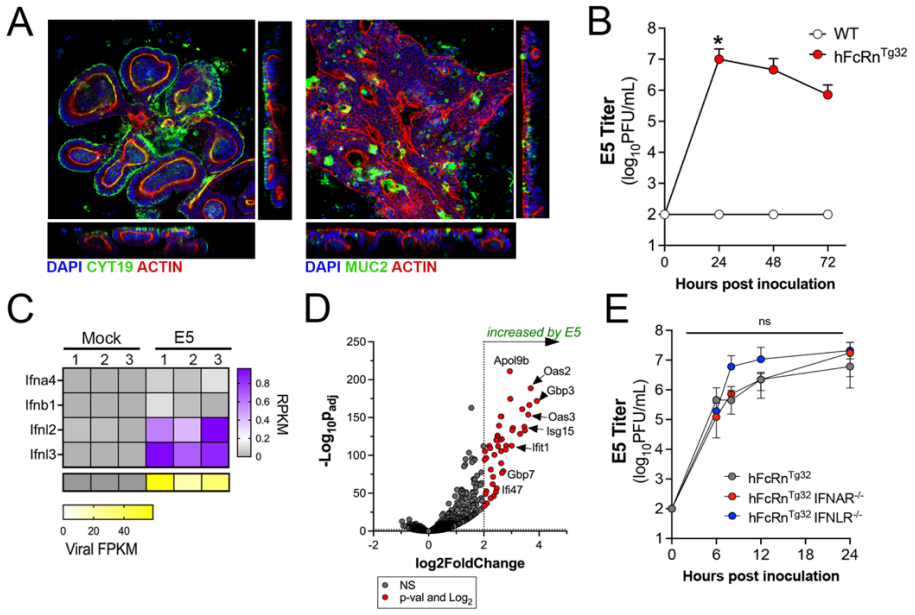

Figure 20 Human FcRn is necessary and sufficient for echovirus infection of murine-derived primary enteroids.

(A) Murine enteroids were generated Lgr5^{+} crypts isolated from the small intestines of five 10-day old neonatal C57BL/6J (WT) mice. Confocal microscopy of enteroids immunostained with cytokeratin-19 in green and actin in red (left) or mucin-2 in green and actin in red (right) ~10-days post-culturing. **(B)** WT (white) or hFcRn^{Tg32} (grey) enteroids were generated from small intestine tissue from 10-day old neonatal mice and infected with 10^6 PFU of neutral red incorporated E5. Viral titers (log_{10}PFU/mL) were assessed in cell culture supernatants at the indicated time points. **(C)** Heatmap of RPKM values of the type I IFNs Ifna4 and Ifnb1 and the type III IFNs Ifnl2 and Ifnl3 from bulk RNASeq of uninfected (mock)- or E5 infected hFcRn^{Tg32} enteroids at 24hrs post-infection. Key at right, purple indicates higher reads and grey denotes no reads detected. At bottom, viral FPKM values from samples shown at top. Yellow indicates high viral RNA reads and grey denotes no reads detected. **(D)** Volcano plot comparing differentially expressed transcripts in E5 infected hFcRn^{Tg32} enteroids compared to mock controls as determined by DeSeq2 analysis. Grey circles represent genes whose expression was not significantly changed. Red circles represent genes that were significantly changed by E5 infection. Significance was set at a $p<0.01$ and a log_2fold-change of ± 2. **(E)** Enteroids generated from the small intestine of hFcRn^{Tg32} (grey), hFcRn^{Tg32}-IFNAR$^{-/-}$ (red), or hFcRn^{Tg32}-IFNLR$^{-/-}$ (blue) were infected with 10^6 PFU of neutral red incorporated E5. Viral titers (log_{10}PFU/mL) are shown at indicated time points. In (B) and (E), data are shown as mean ± standard deviation from three independent replicates. Enteroids were isolated from at least five 10-day old neonatal mice and were pooled together during the LGR5^{+} crypt isolation. Significance in B was determined by a Kruskal-Wallis test with a Dunn's

test for multiple comparisons. Significance in D was determined using a two-way ANOVA with a Geisser-Greenhouse correction and a Tukey's multiple comparisons test. (*p<0.05, ns not significant.)

4.2.2 Human FcRn is necessary but not sufficient for echovirus infection of the intestine *in vivo*

As described above, *ex vivo* enteroid models suggested that echovirus infection of murine-derived intestinal cells depended on expression of hFcRn and were not controlled by either type I or III IFNs. However, enteroids may not fully recapitulate the events associated with infection *in vivo.* To address this, we used six genotypes of mice, including the humanized FcRn models described above (hFcRn^{Tg32}, hFcRn^{Tg32}-IFNAR$^{-/-}$, and hFcRn^{Tg32}-IFNLR$^{-/-}$) and animals expressing murine FcRn that were immunocompetent (C57/BL6, WT) or deficient in type I or III IFN signaling (IFNAR$^{-/-}$ or IFNLR$^{-/-}$, respectively) (**Figure 21A**). Neonatal (7-day old) mice were orally inoculated with 10^6 PFU of E5 and monitored daily for 7 days for signs of illness (e.g., inactivity, discoloration, lack of nursing, lack of parental care, and death). We observed death in approximately 50% of hFcRn^{Tg32}-IFNAR$^{-/-}$ animals by 3 days post-inoculation (dpi) and almost 100% lethality by 7dpi (**Figure 21B**). In contrast, there were no clinical symptoms of illness in any other genotype and all animals survived until 7dpi (**Figure 21B**). There were no significant differences in mortality between male and female hFcRn^{Tg32}-IFNAR$^{-/-}$ mice (**Figure 49A**).

We next determined the extent of viral replication in the GI tract of infected animals at 3dpi by measuring viral titers in stomach, small intestine (duodenum, jejunum, and ileum), large intestine, and stool. Infected hFcRn^{Tg32}-IFNAR$^{-/-}$ animals contained high levels of virus in all tissues collected, with half or more of animals having high viral loads in stomach (7 of 14 mice), duodenum (8 of 14 mice), jejunum (8 of 14 mice), ileum (7 of 14 mice), and large intestine (7 of

14 mice) (**Figure 21C-H**). In contrast, there was no detectable virus in any tissues isolated from mice not expressing hFcRn, including WT (0 of 10 mice), IFNAR$^{-/-}$ (0 of 11 mice), and IFNLR$^{-/-}$ (0 of 17 mice) (**Figure 21C-H**). There were low levels of virus detected in select tissues from immunocompetent hFcRn^{Tg32} animals, which included duodenum (3 of 8 mice), jejunum (2 of 8 mice), ileum (1 of 8 mice), and large intestine (3 of 8 mice). No virus was recovered from the stomachs of hFcRn^{Tg32} mice (0 of 8 mice). Similarly, low to mid-level titers were observed in hFcRn^{Tg32}-IFNLR$^{-/-}$ mice, with virus recovered from stomach (3 of 15 mice), duodenum (4 of 15 mice), jejunum (3 of 15 mice), ileum (3 of 15 mice), and large intestine (4 of 15 mice). Stool collected from all genotypes except for WT contained high levels of virus in stool, which may reflect remaining inoculum. There were no significant differences in titers between male and female hFcRn^{Tg32}-IFNAR$^{-/-}$ mice, although male mice did have overall higher titers in various regions of the small intestine (**Figure 49B**). These data show that hFcRn is necessary, but not sufficient, for echovirus infection of the intestine *in vivo* and that type I and III IFNs differentially control replication and pathogenesis.

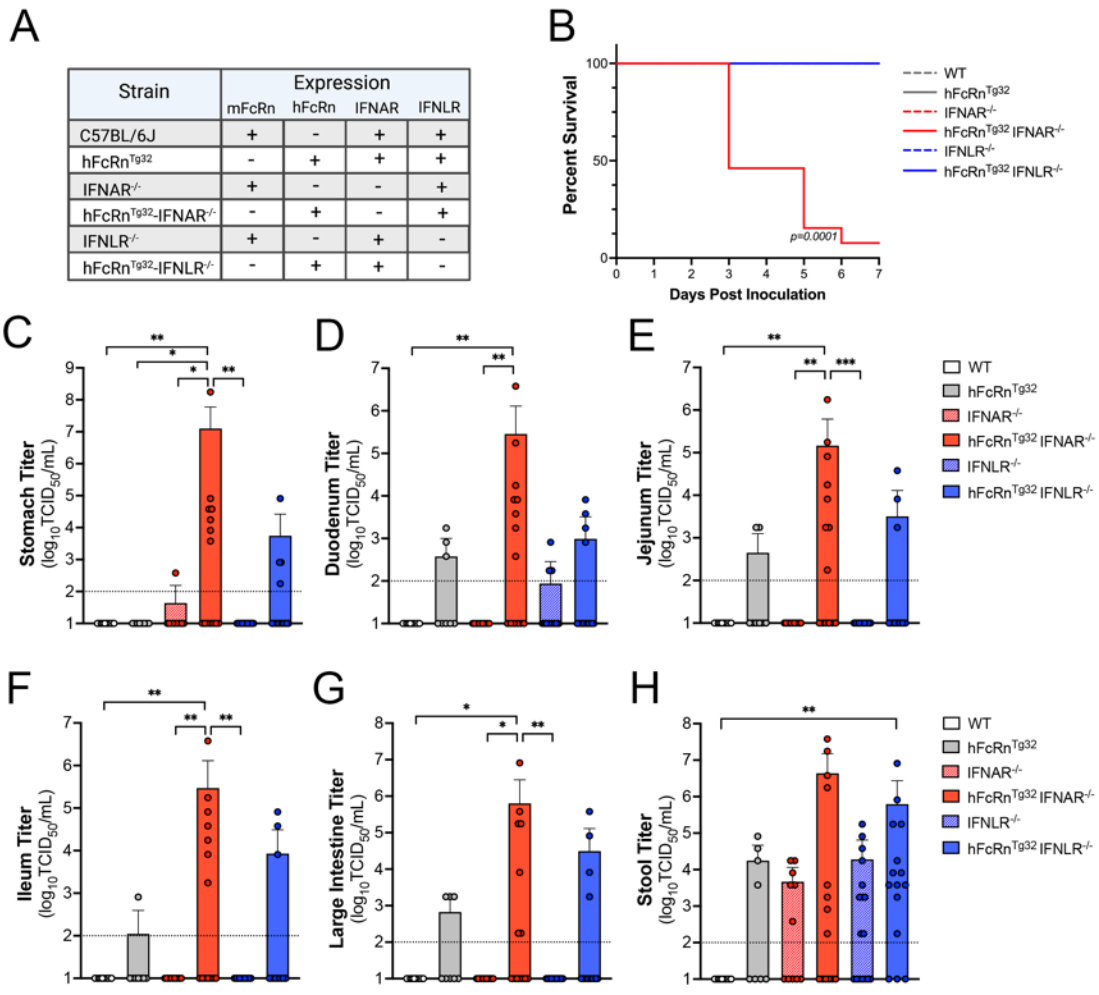

Figure 21 Expression of human FcRn is not sufficient for echovirus infection by the enteral route *in vivo*.

(A) Table of the six genotypes used in this study. Shown is the expression of mouse or human FcRn, IFNAR, and IFNLR amongst these genotypes. **(B)** Survival of the indicated genotype of mice inoculated with 10^6 E5 by oral gavage for 7 days post-inoculation. The log-rank test was used to analyze the statistical difference of the survival rate. **(C-H)**. At 3dpi, animals were sacrificed and viral titers in stomach **(C)**, duodenum **(D)**, jejunum **(E)**, ileum **(F)**, large intestine **(G)**, and stool **(H)** determined by TCID50 assays. In all, titers are shown as $\log_{10}$TCID50/mL with the limit of detection indicated by a dotted line. Data are shown as mean ± standard deviation with individual animals shown as each data point. Data are shown with significance determined with a Kruskal-Wallis test with a Dunn's test for multiple comparisons (*p<0.05, **p<0.005, ***p<0.0005).

4.2.3 Type I IFNs are the primary driver of dissemination outside of the GI tract

Given the high degree of mortality in orally inoculated hFcRn^{Tg32}-IFNAR$^{-/-}$ mice, we next assessed the levels of infection at key secondary sites of infection at 3dpi, including the liver, pancreas, and brain, which are all targeted by echoviruses in humans. hFcRn^{Tg32}-IFNAR$^{-/-}$ mice had higher levels of circulating virus (6 of 13 mice), which was not detected in any other genotype (**Figure 22A**). Consistent with this, we did not detect any virus in the livers, pancreases, or brains of WT, hFcRn^{Tg32}, IFNAR$^{-/-}$, IFNLR$^{-/-}$, or hFcRn^{Tg32}-IFNLR$^{-/-}$ animals (**Figure 22B-D**). In contrast, hFcRn^{Tg32}-IFNAR$^{-/-}$ mice contained very high titers in liver (7 of 14 mice) and pancreas (7 of 14 mice) and lower titers in brain (5 of 14 mice) (**Figure 22B-D**). There were no significant differences in titers between male and female mice, although male mice did have overall higher titers in the liver (**Figure 49B**). These data are consistent with our previous work data showing that hFcRn^{Tg32}-IFNAR$^{-/-}$ pups or adult mice inoculated by the IP route have high levels of echovirus infections in the liver and pancreas[280].

Next, we performed Luminex multiplex assays to determine the levels of twenty-five circulating cytokines in the blood of E5-infected animals. Consistent with their high levels of dissemination, we found that hFcRn^{Tg32}-IFNAR$^{-/-}$ mice induced pronounced antiviral and pro-inflammatory signaling in response to E5 infection, which included high levels of circulating type I IFNs (IFN-α and IFN-β), G-CSF, and IL-6 (**Figure 50A-D**). No other genotypes contained any significant increases in circulating cytokines (**Figure 50A-D**). These data are similar to our previous work where IP inoculated hFcRn^{Tg32}-IFNAR$^{-/-}$ animals had high levels of circulating type I IFNs[280].

Because we observed significant dissemination of E5 to the livers of orally inoculated hFcRn^{Tg32}-IFNAR$^{-/-}$ mice, we next determined if the cellular tropism of echoviruses is the same

between the IP and oral routes of inoculation. To do this, we performed hybridization chain reaction (HCR), which allows for multiplexed fluorescent quantitative RNA detection with enhanced sensitivity over conventional hybridization approaches[259,261]. Our previous work using this method showed that echoviruses exclusively target hepatocytes following IP inoculation[280]. We designed probes specific for the E5 genome and used probes to the hepatocyte marker albumin and performed HCR on liver sections from hFcRn^{Tg32}, hFcRn^{Tg32}-IFNAR$^{-/-}$, and hFcRn^{Tg32}-IFNLR$^{-/}$ mice orally inoculated with E5 at 3dpi. E5 vRNA positive cells exclusively colocalized with albumin, identifying hepatocytes as the main cellular target of infection in the liver following dissemination from the GI tract (**Figure 22E**). Collectively, these data show that type I IFNs are the primary drivers of echovirus dissemination from the GI tract to secondary sites including the liver and pancreas.

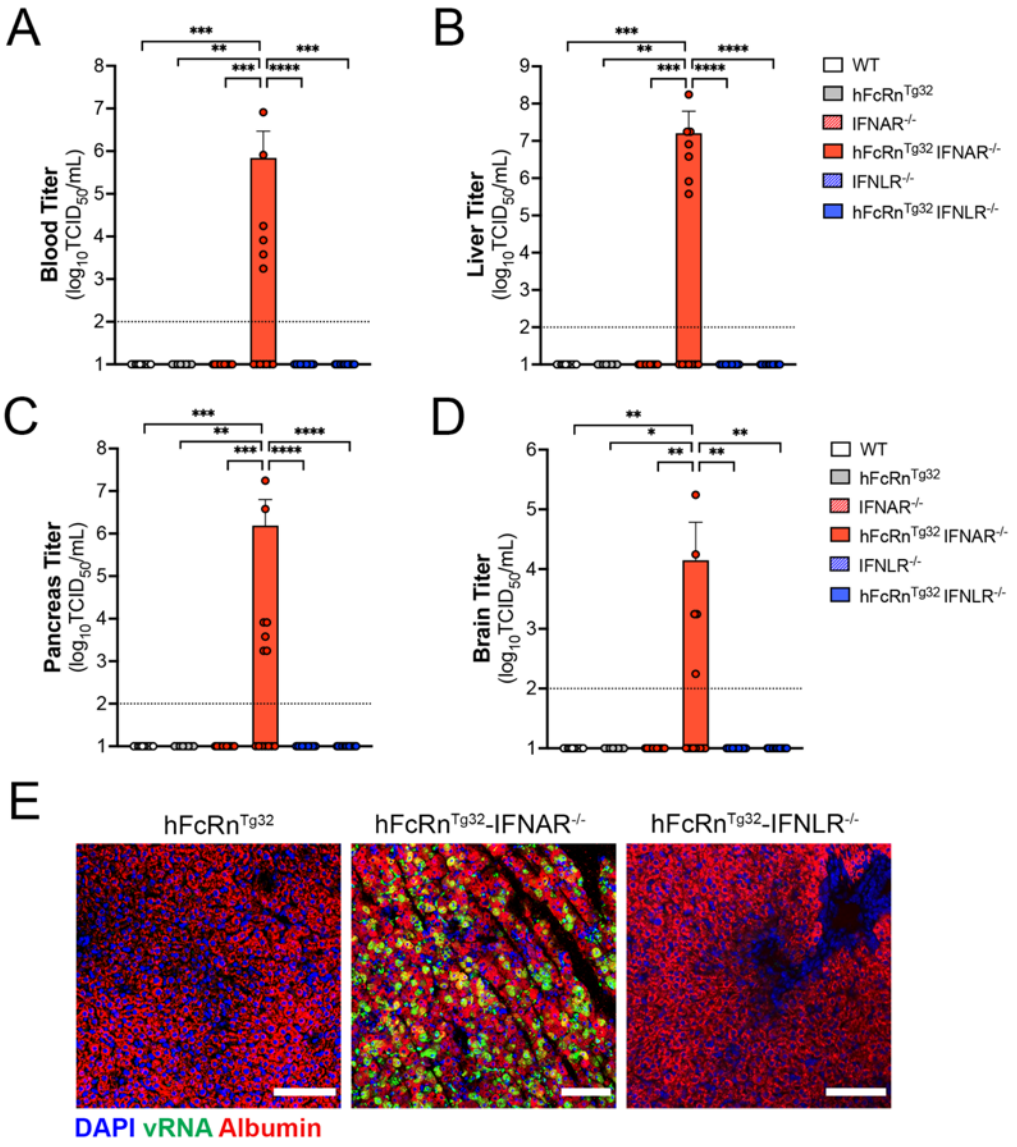

Figure 22 Type I IFNs control echovirus dissemination from the GI tract.

7-day old pups were orally inoculated with 10^6 PFU of E5 and at 3dpi, sacrificed for viral titration and histology. **(A-D),** Viral titers in the blood **(A)**, liver **(B)**, pancreas **(C)**, and brain **(D)** are shown. In all, titers are shown as log_{10}TCID50/mL with the limit of detection indicated by a dotted line. Data are shown as mean ± standard deviation with individual animals shown as each data point. **(E)** Hybridization chain reaction RNA-FISH (HCR) from liver section of hFcRn^{Tg32}, hFcRn^{Tg32}-IFNAR$^{-/-}$, or hFcRn^{Tg32}-IFNLR$^{-/-}$ neonatal mice at 3dpi using probes against the E5 genome (green) and albumin (red). DAPI-stained nuclei are shown in blue. Scale bars shown at bottom right (100μm). In A-D, data are shown with significance determined with a Kruskal-Wallis test with a Dunn's test for multiple comparisons (*p<0.05, **p<0.005, ***p<0.0005, ****p<0.0001).

4.2.4 Type III IFNs limit persistent echovirus infection of the GI epithelium

Because we observed low levels of E5 replication in GI-derived tissues at 3 dpi, we next compared viral titers from tissues isolated at 7dpi to determine if there were differences in persistence compared to hFcRn^{Tg32}-IFNAR$^{-/-}$ mice. As hFcRn^{Tg32}-IFNAR$^{-/-}$ mice died from disease before 7dpi, they were excluded from these studies. At 7dpi, hFcRn^{Tg32}-IFNLR$^{-/-}$ mice were the only genotype with consistently detectable virus in tissues associated with the GI tract. Whereas select animals had detectable virus in the stomach (1 of 7 hFcRn^{Tg32} mice and 2 of 14 hFcRn^{Tg32}-IFNLR$^{-/-}$ mice) and large intestine (3 of 14 hFcRn^{Tg32}-IFNLR$^{-/-}$ mice), hFcRn^{Tg32}-IFNLR$^{-/-}$ animals had higher levels of virus in all regions of the small intestine including the duodenum (6 of 14 mice), jejunum (6 of 14 mice), and ileum (4 of 14 mice) (**Figure 23A-G**). Consistent with more persistent infection in the GI tract of hFcRn^{Tg32}-IFNLR$^{-/-}$ mice, these mice also contained higher levels of virus in stool (7 of 14 animals with detectable virus) compared to all other genotypes (**Figure 23F**). Male animals did contain higher viral titers than did female mice, although these differences were not significant (**Figure 49C**). However, even at 7dpi, we were unable to detect any virus in the blood, liver, pancreas, or brain of any genotype, including hFcRn^{Tg32}-IFNLR$^{-/-}$ (**Figure 51A, B, C, & D)**. These data show that type III IFNs do not control dissemination but limit persistent infection of the intestinal epithelium.

Visualization of intestinal replication of enteroviruses *in vivo* has been hindered by the lack of sensitive assays to monitor infection with low signal-to-noise. To overcome this limitation, we utilized HCR, a component of which includes signal amplification given the self-assembly of secondary detection hairpins into amplification polymers. We inoculated 7-day old hFcRn^{Tg32}-IFNAR$^{-/-}$ and hFcRn^{Tg32}-IFNLR$^{-/-}$ animals with 10^6 PFU of E5 by the oral route, sacrificed them at 3dpi, and then performed Swiss rolling of full intestinal tissue, which was sectioned and

processed for HCR. In contrast to viral titer data, which showed high levels of virus in the intestines of hFcRn^{Tg32}-IFNAR$^{-/-}$ animals, we did not detect any vRNA in any intestinal section of these animals **(Figure 23G)**. However, we observed clear areas of vRNA-containing cells in various regions of the small intestines of hFcRn^{Tg32}-IFNLR$^{-/-}$ animals **(Figure 23G)**. While vRNA was detected in both the duodenum and jejunum, there were more vRNA-containing cells in the ileum of the hFcRn^{Tg32}-IFNLR$^{-/-}$ animals **(Figure 23G and H)**, suggesting that there may be regional differences in echovirus persistence in the epithelium. Although we observed areas of viral replication within the epithelium, we do not see any damage to the epithelium. A blinded pathologist reviewed H&Es from uninfected, hFcRn^{Tg32}-IFNAR$^{-/-}$ and hFcRn^{Tg32}-IFNLR$^{-/-}$ animals and observed no significant changes or damage to the intestine following 3dpi E5 infection (**Figure 52A**). Additionally, we observed no change to the cellular composition of the epithelium as suggested by Periodic Acid Schiff (PAS) staining for goblet cells (**Figure 52B**).

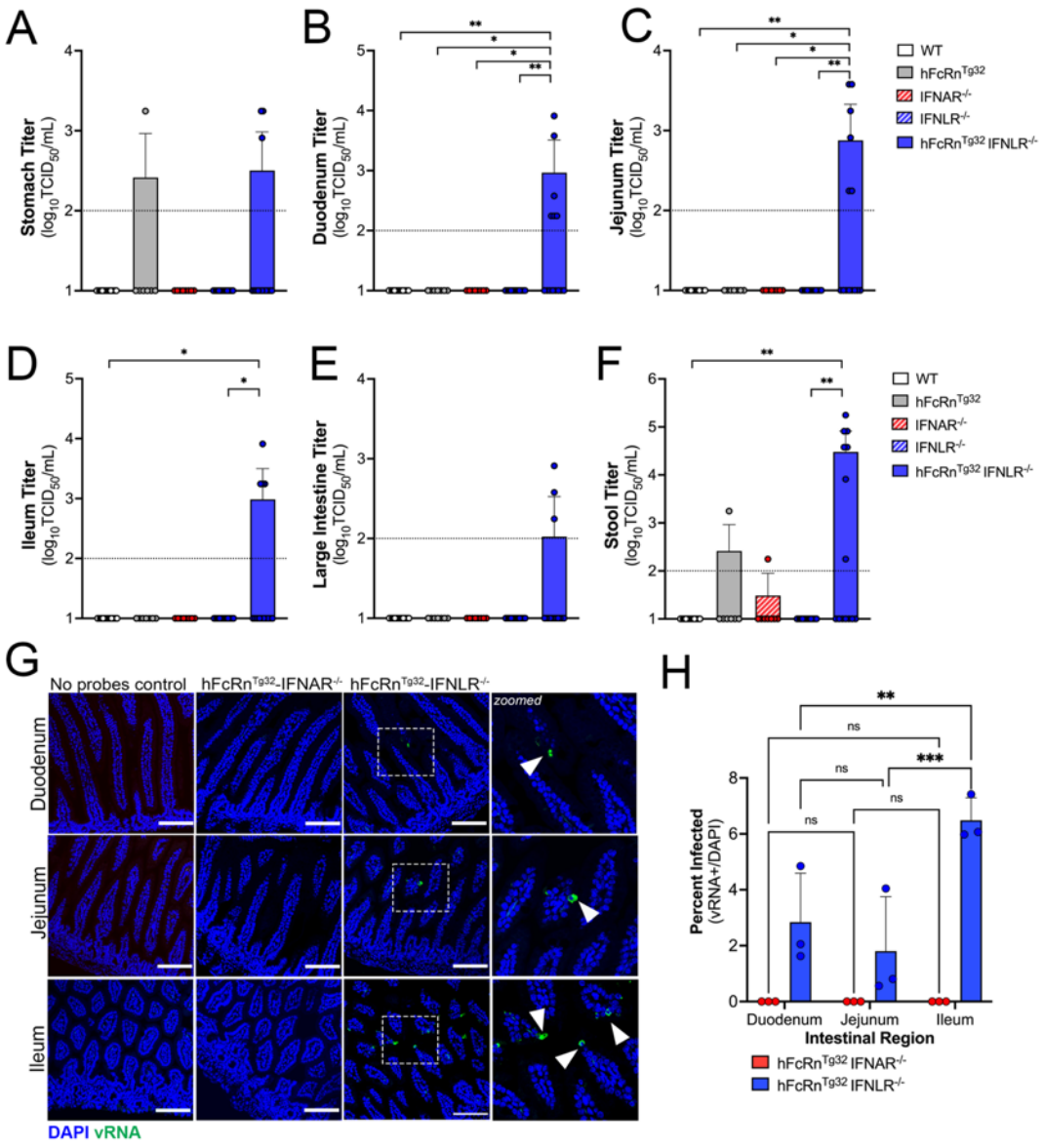

Figure 23 Type III IFNs restrict persistent echovirus infection in the GI epithelium.

7-day old neonatal were orally inoculated with 10^6 PFU of E5 and at 7dpi, animals were sacrificed for viral titration and tissue collection. **(A-F),** Viral titers are shown in stomach **(A)**, duodenum **(B)**, jejunum **(C)**, ileum **(D)**, large intestine **(E)**, and stool **(F)**. In all, titers are shown as log_{10}TCID50/mL with the limit of detection indicated by a dotted line. Data are shown as mean ± standard deviation with individual animals shown as each data point. Significance was determined using a Kruskal-Wallis test with a Dunn's test for multiple comparisons (*p<0.05, **p<0.005). **(G)** At 3dpi, animals were sacrificed and the entire GI tract was removed and swiss rolled following by histologic sectioned. HCR of hFcRn^{Tg32}-IFNAR$^{-/-}$ or hFcRn^{Tg32}-IFNLR$^{-/-}$ pups at the 3dpi using probes against the E5 genome (green) and DAPI (blue). Scale bars shown at bottom right (100µm). Zoom of specific regions in hFcRn^{Tg32}-IFNLR$^{-/-}$ images are shown to the right. **(H)** Quantification of three independent tile scans using confocal microscopy of each region

of the small intestines based on the number of villi that were positive for vRNA using the cell count function in FIJI. Data are shown as percent of vRNA positive villi over total villi per tile scan. Three independent tile scans were quantified (for an average of 144 villi in the duodenum, 224 villi in the jejunum, and 164 villi in the ileum). Significance was determined by a Two-way Anova with Šídák's multiple comparisons tests (*p<0.05, **p<0.005, ***p<0.0005, ****p<0.0001).

4.2.5 Enterocytes are the main cellular targets of echoviruses *in vivo*

We showed previously that echoviruses preferentially infect enterocytes and enteroendocrine cells in human stem cell-derived enteroids[49]. However, whether there is a cell type specificity of infection for echoviruses, or other enteroviruses, *in vivo* is unknown. To define the cellular tropism of echoviruses *in vivo*, we designed HCR probes targeting an enterocyte marker (alkaline phosphate intestinal, Alpi), goblet cell marker (mucin-2, Muc2), and enteroendocrine cell marker (chromogranin A, Chga). We confirmed the specificity of these probes in murine-derived intestinal tissue and found that they accurately labeled distinct cell populations in the epithelium (**Figure 24A**). Using probes directed against E5 and Alpi, Muc2, or Chga, we performed HCR in Swiss rolled intestinal tissue sections isolated from hFcRn^{Tg32}-IFNLR$^{-/-}$ animals orally infected with 10^6 E5 at 3dpi. We found that echovirus vRNA exclusively localized to Alpi-positive cells (**Figure 24B**) and was not observed in any Muc2-positive goblet cells (**Figure 24C**) or Chga-positive enteroendocrine cells (**Figure 24D**), as assessed by image analysis and quantification of confocal microscope-generated tile scans of ~4mm^2 of intestinal tissue (**Figure 24E and Figure 53**). These data show that enterocytes are the main targets of echoviruses following oral inoculation of hFcRn^{Tg32}-IFNLR$^{-/-}$ mice.

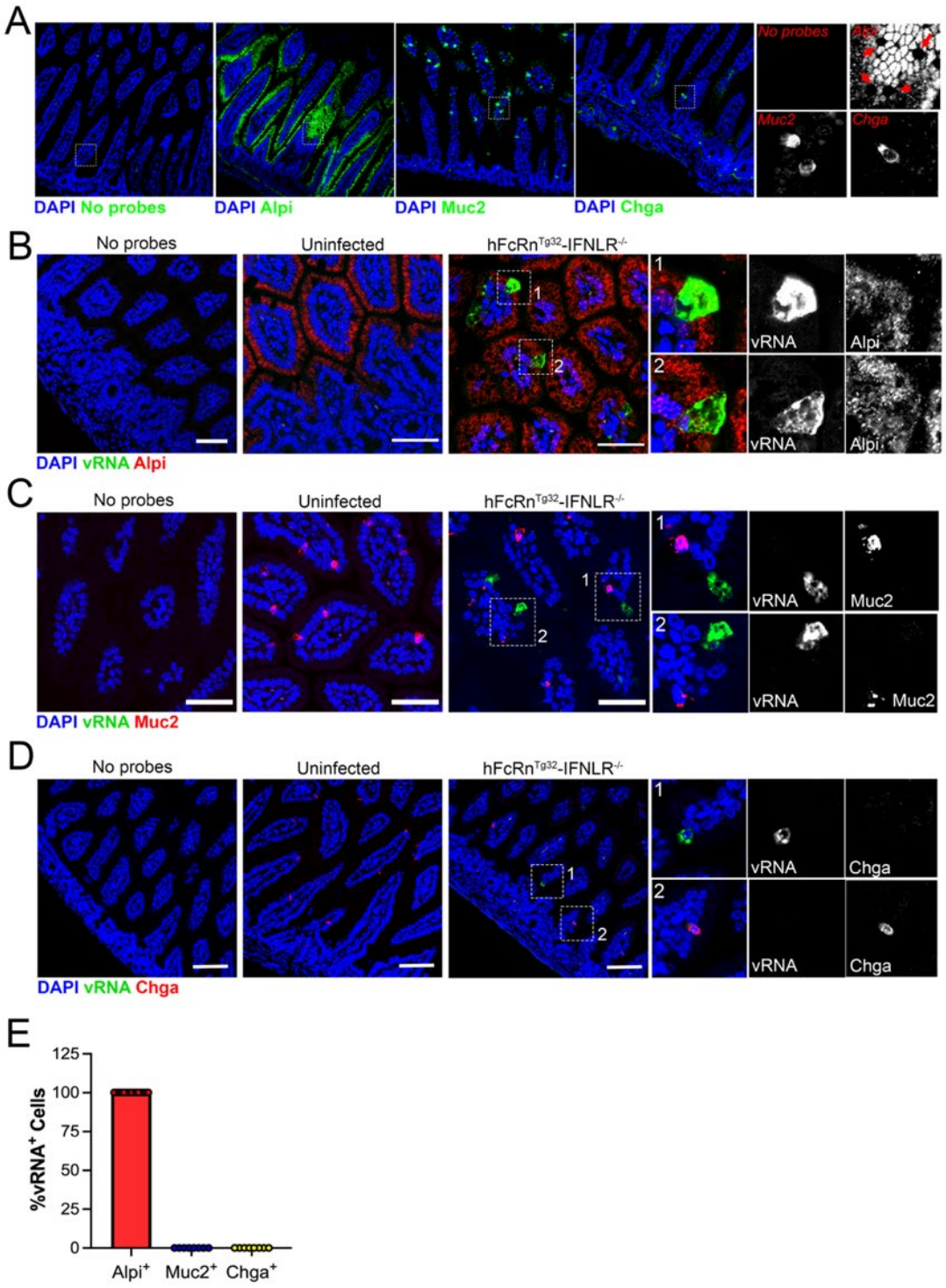

Figure 24 *In vivo* replication of echoviruses is specific for enterocytes.

(A) Hybridization chain reaction RNA-FISH (HCR) of uninfected small intestine sections using specific probes against Alpi, Muc2, or Chga (in green), as indicated at bottom. DAPI-stained nuclei are shown in blue. No probe containing control is shown at left. In all, white box is shown zoomed (~6x) at right using the probes indicated in red. Red arrows in Alpi section denote goblet cells

based on morphology that were not positive for Alpi, as expected. **(B-D)** 7-day old hFcRn^{Tg32}-IFNLR$^{-/-}$ neonatal mice were orally inoculated with 10^6 PFU of E5 and at 3dpi, animals were sacrificed and the entire small intestine removed and Swiss rolled for subsequent histologic sectioning. Shown are representative images of ileum tissue using probes to E5 (green in all) and either Alpi (B), Muc2 (C), or Chga (D) (red in all). DAPI-stained nuclei are shown in blue. In all, white boxes denote zoomed areas shown at right, which include black and white images as indicated. Scale bars shown at bottom right (50μm). **(E)** Quantification of confocal images was performed using Fiji and was quantified as the total percentage of vRNA positive cells that colocalized with Alpi (in red), Muc2 (in blue), or Chga (in green). Note that there was no colocalization between vRNA and either Muc2 or Chga.

4.3 Discussion

The events associated with enterovirus infections of the GI tract *in vivo* are largely unknown. Here, we defined the role of hFcRn and type-specific IFN signaling in mediating echovirus infections of the intestinal epithelium and dissemination to secondary tissue sites. We show that hFcRn is necessary and sufficient for echovirus infection of the intestinal epithelium in enteroids derived from humanized FcRn mice. However, *in vivo*, expression of hFcRn alone is not sufficient for echovirus infection by the enteral route. Using humanized FcRn mouse models deficient in either type I or III IFN signaling, we defined the differential roles of these IFNs in echovirus replication in and dissemination from the GI tract. These studies showed that type I IFNs limit dissemination of echoviruses from the GI tract and ablation of this signaling robustly increases viral replication at secondary sites, such as the liver. In contrast, type III IFNs suppress replication in the intestinal epithelium and deletion of the receptor for these IFNs prolongs intestinal echovirus replication and increases viral persistence. We further show that echoviruses preferentially infect enterocytes *in vivo*, which is enhanced in the absence of type III IFN signaling. Collectively, our work presented here provides key insights into the roles of FcRn and IFN signaling in echovirus pathogenesis in the GI tract.

Little is known regarding the mechanisms used by echoviruses to enter the intestinal epithelium. Our data support a model whereby hFcRn is necessary and sufficient for intestinal replication *in vitro*. While some echoviruses utilize decay accelerating factor (DAF/CD55) as an attachment factor *in vitro*[110], E5 does not bind DAF[109]. Moreover, DAF-binding echoviruses do not bind the murine homolog of DAF[110]. While a previous study predicted that echovirus binding to DAF might trigger viral internalization and particle delivery to endosomes, at which time FcRn-mediated uncoating would occur[128], the data presented here do not support such a model and suggest that DAF plays no role in echovirus infections of the intestinal epithelium *in vitro* or *in vivo*. Instead, our data suggest that FcRn is necessary and sufficient for echovirus infection of the intestinal epithelium and occurs independent of DAF binding. This is consistent with *in vivo* data from humanized mouse models of DAF, which show that expression of DAF does not impact intestinal replication of DAF-binding variants of CVB[278].

FcRn is unique in its ability to mediate the transcytosis of IgG and albumin across the intestinal epithelium. Interestingly, this transport functions in a bidirectional manner in cultured intestinal cell lines, suggesting that FcRn can sample contents from the apical or basolateral domains and mediate the transcytosis of cargo to the opposing domain[239]. This function of FcRn could have important implications during echovirus infections—FcRn could *(i)* mediate the internalization of viral particles into intracellular compartments that facilitate uncoating and subsequent replication and/or *(ii)* could mediate the direct transcytosis of viral particles across the intestinal epithelium from the lumen into underlying tissue. Given that FcRn mediates bidirectional transport across the epithelium, this raises the possibility that echoviruses could be transported from either the apical or basolateral domains to cross the intestinal barrier. We were unable to visualize active replication in the intestinal epithelium of hFcRn^{Tg32}-IFNAR$^{-/-}$ animals, despite

robust viral dissemination to secondary sites of infection. In contrast, we detected vRNA in ~6% of enterocytes in ileum tissue of hFcRn^{Tg32}-IFNLR$^{-/-}$ animals, in which there was no dissemination observed. These data suggest that in addition to facilitating viral entry and replication into enterocytes, it is possible that in some cases, FcRn might facilitate the transcytosis of echovirus particles across the epithelium and that ablation of type I IFN signaling promotes dissemination of these particles to secondary sites of infection.

Type III IFNs are important in antiviral defenses of many barrier tissues, including the GI tract[93,282]. For example, IFN-λs control rotavirus infection in the intestinal epithelium in adult and neonatal mice[46]. This study showed that whereas mice lacking IFNLR were more susceptible to rotavirus replication and viral-induced cytotoxicity, IFNAR$^{-/-}$ mice were comparable to immunocompetent WT mice. These data are distinct from our work presented here, which shows that type I IFNs are key host mediators that prevent echovirus dissemination following oral infection. Type III IFNs have also been implicated in restricting murine norovirus replication in the GI tract *in vivo*[48]. Similar to our findings with echoviruses, IFN-λs restrict persistent norovirus infection whereas type I IFNs restrict dissemination[48]. Previous studies with PV and EV71 suggest that type I IFNs control viral replication of these enteroviruses by the enteral route *in vivo*[197,277] whereas CVB infection is unchanged in animals deficient in IFNAR[278]. While the mechanistic basis for these differences is unknown, it is possible that the cell-type specific nature of enterovirus replication in the intestine may influence their dependence on IFN signaling. For example, in human enteroids, EV71 preferentially infects goblet cells whereas echoviruses are enriched in enterocytes[49,130]. In cell lines, previous work has suggested that PV transcytoses across M cells , suggesting it does not replicate in the epithelium[283]. Future studies on the cell-type specific nature of IFN signaling in distinct lineages of intestinal cells and the impact of these differences on

enterovirus replication will be essential to determine if the distinct cellular tropism of enteroviruses in the GI tract influences IFN-mediated signaling.

Our findings presented here define fundamental aspects of echovirus biology that enhance our understanding of how infection, tissue targeting, and disease occurs *in vivo*. We show that FcRn is necessary but not sufficient for echovirus infections of the GI tract in vivo and that type I and III IFNs differentially control echovirus persistence and dissemination. Collectively, these studies provide new insights into echovirus biology and the development of in vivo models that recapitulate distinct aspects of echovirus disease, which could potentially accelerate the development of therapies.

4.4 Materials and Methods

4.4.1 Cells and viruses

HeLa cells (clone 7B) were provided by Jeffrey Bergelson, Children's Hospital of Philadelphia, Philadelphia, PA, and cultured in MEM supplemented with 5% FBS, non-essential amino acids, and penicillin/streptomycin. Experiments were performed with echovirus 5 (Noyce strain, E5), which was obtained from the ATCC. Virus was propagated in HeLa cells and purified by ultracentrifugation over a 30% sucrose cushion, as described previously[245]. Enteroid experiments were performed with light-sensitive neutral red (NR) incorporated viral particles. E5 was propagated in the presence of NR (10μg/mL) in semi-dark conditions and was subsequently purified in semi-dark conditions by ultracentrifugation over a sucrose cushion[115]. All viruses were sequenced for viral stock purity following propagation. Purity of all viral stocks was confirmed by

Sanger sequencing of VP1 using enterovirus-specific primers[284]. Briefly, RNA extraction was performed on 10µl of purified virus stock, according to manufacturer's instructions (Qiagen Cat. 529904). RNA was reverse transcribed using SuperScript III reverse transcription kit, (Invitrogen cat. 18080093) according to manufacturer's instructions, with a pan enterovirus primer (vir21; ATAAGAATGCGGCCGCTTTTTTTTTTTTTTTTTTTTTTTT), followed by an RNaseH treatment for 20 minutes. PCR was performed with 5µl of the cDNA reaction using BioRad iTaq DNA polymerase (BioRad cat. 1708870). Virus specific primers were as follows: E5 forward 5'-TATCGCCAATTACAACGCGAA-3'; E5 reverse 5'-TTGGTTTGAAGTAAACCCTTA-3'.

4.4.2 Animals

All animal experiments were approved by the Duke University Animal Care and Use Committees, and all methods were performed in accordance with the relevant guidelines and regulations. C57BL/6J (WT, cat. no. 000664), B6.Cg-*Fcgr*$^{t\text{tm1Dcr}}$Tg(FCGRT)32Dcr/DcrJ (hFcRn^{Tg32}, cat. no. 014565), and B6.(Cg)-Ifnar1$^{tm1.2Ees}$/J (IFNAR$^{-/-}$, cat. no. 028288) mice were purchased from The Jackson Laboratory. hFcRn^{Tg32}-IFNAR$^{-/-}$ mice were generated as described previously[280]. B6.Ifnlr$^{-/-}$/J (IFNLR$^{-/-}$) mice were provided by Dr. Megan Baldridge (Washington University School of Medicine). hFcRn^{Tg32}-IFNLR$^{-/-}$ mice were generated by crossing B6.Cg-*Fcgr*$^{t\text{tm1Dcr}}$Tg(FCGRT)32Dcr/DcrJ (hFcRn^{Tg32}, cat. no. 014565) mice with B6.Ifnlr$^{-/-}$/J mice. Breeders were established that were deficient in mouse FcRn and IFNLR and were homozygous for the hFcRn transgene. All animals used in this study were genotyped by Transnetyx.

4.4.3 Enteroid isolation and passaging

Murine intestinal crypts were isolated using a protocol adapted from Stem Cell Technologies. Briefly, intestines were isolated from five 10-day old pups and connective tissue removed. Intestines were cut longitudinally and washed extensively in PBS. Intestines were cut into 5mm segments and washed again using a 10mL serological pipette until PBS was clear. Washed intestinal pieces were incubated in gentle cell dissociation reagent (Stem Cell Technologies Cat. 07174) for 15 minutes at room temperature. Crypts were released using 0.1% BSA and vigorous pipetting with a 10mL serological pipette. Crypts were filtered using a 70μm cell strainer and the resulting flow through centrifuged at 290xg for 5 minutes. Pellets were resuspended in Matrigel (Corning Cat. 356231) and 40μL of crypt-containing Matrigel 'domes' plated into each well of a 24 well plates (Corning 3526), placed in a 37ºC incubator to pre-polymerize for ~3 min, turned upside-down to ensure equal distribution of the isolated cells in domes for another 10 min, then carefully overlaid with 500 μL IntestiCult Organoid Growth Medium (Stem Cell Technologies Cat. 06005) supplemented with 1% penicillin/streptomycin, 50μg/mL gentamycin, and 0.2% amphotericin b, containing Y-27632 (Rock inhibitor, Sigma). Media was changed every 48hrs and Y-27632 was removed after the first media change.

Confluent enteroids were passaged by manual disruption of Matrigel domes with a P1000 pipette tip in PBS and centrifuged at 400xg for 5 minutes. The enteroid-containing pellet were resuspended in TrypLE (Invitrogen Cat. 12605010) and incubated in a water bath at 37°C for 8 minutes. Enzyme activity was quenched with DMEM containing 10% FBS and centrifuged at 400xg for 5 minutes. Pellets were resuspended in Matrigel and 40μL Matrigel domes in each well of a 24 well plate. Domes were allowed to solidify at 37°C for 10 minutes and then covered with IntestiCult Organoid Growth Medium, as described above. For infections, crypts were plated in

24-well plates pre-coated with 15uL of Matrigel using a P1000 tip and allowed to solidify for 30 minutes.

4.4.4 Enteroid infections

Enteroids plated on Matrigel coating as described above were allowed to differentiate for 5 days with media replaced every 48hrs. For infections, wells were infected with 10^6 PFU of NR-incorporated virus, generated as described above. Virus was pre-adsorbed for 1 hour at 16°C, enteroids washed three times with PBS, and media replaced. Infections were initiated by shifting enteroids to 37°C. At 6hpi, enteroids were exposed to light on a light box for 20 minutes to render intact viral particles non-infectious and infections performed for the times indicated. Plaque assays were performed in HeLa cells overlayed with 1:1 mixture of 1% agarose and 2x MEM (4% FBS, 2% pen/strep, 2% NEAA). Plaques were enumerated 40hpi by crystal violet staining.

4.4.5 RNA extraction and RNA sequencing

Total RNA was prepared using the Sigma GenElute total mammalian RNA miniprep kit with optional DNase step, according to the protocol of the manufacturer. RNA quality was assessed by Nanodrop and an Agilent RNA Screen Tape System, and 1ug was used for library preparation using RNA with Poly A selection kit (Illumina), as per the manufacturer's instructions. Sequencing was performed on an Illumina HiSeq. RNA-seq FASTQ data were processed and mapped to the mouse reference genome (GRCm38) using CLC Genomics Workbench 20 (Qiagen). Differential gene expression was performed using the DESeq2 package in R[249].

Heatmaps and volcano plots were made in GraphPad Prism 9. Raw sequencing files have been deposited in Sequence Read Archives.

4.4.6 Suckling pup infections

7-day-old mice were inoculated by the oral route with 10^6 PFU of E5. Oral gavage inoculation was performed using a 1mL disposable syringe and a 24-gauge round tipped needle in 50μL of 1X PBS. Mice were euthanized at either 3- or 7-days post inoculation and organs harvested into 0.5mL of DMEM and stored at -80°C. Tissue samples for viral titration were thawed and homogenized with a TissueLyser LT (Qiagen) for 5 minutes, followed by brief centrifugation for 5 minutes at 8000xg. Viral titers in organ homogenates were determined by TCID50 in HeLa cells and enumerated following crystal violet staining.

4.4.7 HCR and Imaging

HCR was performed following the Molecular Instruments HCR v3.0 protocol for FFPE human tissue sections[259,261]. Briefly, tissue sections were deparaffinized with xylene and rehydrated with decreasing concentrations of ethanol (100%, 95%, 80%). Antigen unmasking was performed with slides submerged in 10 mM citrate buffer (pH 6.0) and heated in a steamer for 20 minutes at ~90°C. Slides were cooled to room temperature. Sections were treated with 10 μg/mL Proteinase K for 10 min at 37°C and washed with RNase free water. Samples were incubated for 10 minutes at 37°C in hybridization buffer. Sections were incubated overnight in a humidified chamber at 37°C with 3 pmol of initiator probes in hybridization buffer. We designed probes for albumin (**Table 8**), E5 (**Table 10**), Muc2 (**Table 11**), and Chga (**Table 12**) in house. Custom

probes for Alpi were designed by Molecular Instruments (Lot PRI910). The next day, slides were washed in probe wash buffer and 5x SSCT for 4x 15 min, according to the manufacturer's instructions. Samples were incubated in a humidified chamber at 37°C for 30 minutes in amplification buffer. Fluorescent hair pins were heated to 95°C for 90 seconds and snap cooled at room temperature for 30 min. Hairpins and amplification buffer were added to the sample and incubated overnight at room temperature. Hairpins were washed off with 5x SSCT for 5 minutes, 15 minutes, 15 minutes, and 5 minutes followed by a wash with PBS containing DAPI. Slides were mounted in vectashield with DAPI. Slides were imaged on a Zeiss 880 with Airyscan inverted confocal microscope. Tile scans were performed at a 20x magnification using a 6 by 6 square area resulting in 36 total images. Each intestinal segment was tile scanned using three different areas for quantification. Image analysis was performed using FIJI.

4.4.8 Periodic Acid Schiff (PAS) staining

PAS staining was performed according to manufactures instructions (Abcam, ab150680). Slides were mounted with Cytoseal 60 (Thermo Scientific, 83104). Images were captured on an IX83 inverted microscope (Olympus) using a UC90 color CCD camera (Olympus).

4.4.9 Statistics

All statistical analysis was performed using GraphPad Prism version 8. Data are presented as mean ± SD. A one-way ANOVA was used to determine statistical significance, as described in the figure legends. Parametric tests were applied when data were distributed normally based on

D’Agostino–Pearson analyses; otherwise, nonparametric tests were applied. P values of <0.05 were considered statistically significant, with specific P values noted in the figure legends.

5.0 An *in vivo* model of echovirus-induced meningitis defines the differential roles of type I and III interferon signaling in CNS infection

Echoviruses are amongst the most common causes of aseptic meningitis worldwide, which can cause long-term sequelae and death, particularly in neonates. However, the mechanisms by which these viruses induce meningeal inflammation is poorly understood, owing at least in part to the lack of *in vivo* models that recapitulate this aspect of echovirus pathogenesis. Here, we developed an *in vivo* neonatal mouse model that recapitulates key aspects of echovirus-induced meningitis. We found that expression of the human homologue of the neonatal Fc receptor (FcRn), the primary echovirus receptor, in neonatal mice was not sufficient for infection of the brain. However, ablation of type I, but not III, IFN signaling in mice expressing human FcRn permitted high levels of echovirus replication in the brain, with corresponding clinical symptoms including delayed motor skills and hind limb weakness. We also defined the immunological response of the brain to echovirus infections and identified key cytokines induced by this infection. Lastly, we found that echoviruses robustly replicate in the leptomeninges, where they induce profound inflammation and cell death. Together, this work establishes an *in vivo* model of aseptic meningitis associated with echovirus infections and defines the specificity of echoviral infections within the meninges.

5.1 Introduction

Enteroviruses are the main causes of aseptic meningitis worldwide, which is characterized by meningeal inflammation not associated with any identifiable bacterial species in cerebrospinal fluid (CSF). Approximately 90% of aseptic meningitis cases in infants[285] and 50% in older children and adults[286] are caused by enteroviruses, with the group B enterovirus members coxsackievirus B (CVB) and echoviruses being amongst the most common[287,288]. Infants and young children are particularly vulnerable to complications of echovirus-associated neuronal complications, which can cause long-term sequelae including seizure disorders[289,290], and are associated with high rates of mortality, which occurs in as many as one-third of cases[291,292]. Despite the clear association between echoviruses and aseptic meningitis, the mechanisms by which these viruses induce meningeal inflammation is poorly understood, owing at least in part to the lack of *in vivo* models that recapitulate this aspect of echovirus pathogenesis.

Echoviruses are the largest subgroup of the Enterovirus genus and consist of approximately 30 serotypes. We and others have shown that the neonatal Fc receptor (FcRn) is the primary receptor for echoviruses[109,128]. FcRn transports and regulates the circulating half-life of immunoglobulin G (IgG) and albumin and is enriched in the endothelium of the central nervous system (CNS), including the blood-brain barrier (BBB), where it mediates the efflux of IgG from the brain[230,235,236,293,294]. Although several studies have investigated the possible mechanistic basis for CVB-associated neuronal dysfunction *in vitro* and *in vivo*[295–297], much less is known about echovirus-associated CNS complications. Intracerebral inoculation of newborn mice expressing VLA-2, a reported receptor for echovirus 1, exhibit paralysis and motor defects[258]. Other work suggests that type I interferons (IFNs) play a role in echovirus 11 CNS disease following intracranial inoculation[298]. We previously generated an *in vivo* mouse model of echovirus 11

pathogenesis using adult and neonatal mice and showed that expression of the human homologue of FcRn in mice lacking type I IFN signaling were susceptible to echovirus infection, including infection of the brain[280]. However, the consequences of echovirus infection including the induction of cytokines and cell death in the brains of these mice, as well as identification of the region(s) of the brain targeted by infection were not explored.

The meninges surround the brain and are composed of three distinct membranous layers which includes the dura, arachnoid, and pia mater. A hallmark of aseptic meningitis involves inflammation of the meninges, resulting in immune cell infiltration and swelling. In human cases of confirmed echovirus aseptic meningitis, infection is associated with a robust inflammatory response, as indicated by the presence of high levels of proinflammatory mediators in CSF[299–301]. Higher levels of type I IFNs are also present in CSF isolated from enterovirus-associated meningitis than from bacterial meningitis[302], suggesting that these IFNs play a prominent role in aseptic meningitis. Type I IFNs, which include IFNαs and IFN-β, provide key antiviral defenses from many neurotropic viruses, including flaviviruses, alphaviruses, and herpesviruses[303]. In some cases, type III IFNs (IFN-λs) also defend from CNS viral infections[56,304] and have been proposed to function by alterations in BBB permeability[56]. Whether type I and III IFNs play differential roles in echovirus infections of the CNS is unknown.

Here, we developed an *in vivo* model of echovirus-induced aseptic meningitis in neonatal mice which recapitulates many of the disease manifestations observed in humans. We show that expression of human FcRn alone is not sufficient to mediate echovirus infection of the brains of 7-day-old neonatal mice. In addition, the brains of mice deficient in either type I or III IFN signaling alone were not permissive to echovirus infection. In contrast, we found that humanized FcRn mice deficient in IFNAR, the type I IFN receptor, but not IFNLR, the type III IFN receptor,

exhibited high levels of echovirus replication in the brain, with corresponding clinical symptoms including hind limb weakness and paralysis. Using this model, we defined the immune response in the brains of echovirus-infected mice, which included the induction of high levels of IL-6, CXCL10, and granulocyte colony-stimulating factor (GSF)-3. Lastly, we show that echoviruses replicate in the leptomeninges and induce inflammation and cytotoxicity in these membranes, including activation of apoptotic cell death. Together, this work establishes an *in vivo* model of aseptic meningitis associated with echovirus infections and defines the specificity of echoviral infections in the meninges.

5.2 Results

5.2.1 Ablation of type I interferon signaling and human FcRn expression are required for echovirus infection of the brain

Previously, we developed a mouse model of echovirus pathogenesis through intraperitoneal (IP) inoculation using mice expressing the human homologue of hFcRn ($hFcRn^{Tg32}$) that are also ablated in type I IFN signaling by deletion of IFNAR ($hFcRn^{Tg32}$-$IFNAR^{-/-}$)[280]. $hFcRn^{Tg32}$ mice are deficient in expression of mouse FcRn and express human FcRn under the control of the native human promotor[227]. To determine if type III IFNs also play a role in echovirus infections at secondary sites of infection including the brain, we generated $hFcRn^{Tg32}$ mice deficient in IFNLR expression, the receptor for type III IFNs ($hFcRn^{Tg32}$-$IFNLR^{-/-}$)[305]. We used six genotypes of mice, including the hFcRn mice described above ($hFcRn^{Tg32}$, $hFcRn^{Tg32}$-$IFNAR^{-/-}$, and $hFcRn^{Tg32}$-$IFNLR^{-/-}$) and animals expressing murine FcRn that were

immunocompetent (C57/BL6, WT) or deficient in type I or III IFN signaling (IFNAR$^{-/-}$ or IFNLR$^{-/-}$, respectively) **(Figure 25A)**. Neonatal (7-day old) mice were inoculated with 10^4 PFU of echovirus 5 (E5) by the IP route and monitored for three days post-inoculation (dpi). We observed death in 100% of hFcRn^{Tg32}-IFNAR$^{-/-}$ animals by 2 dpi **(Figure 25B)**. In contrast, there were no clinical symptoms of illness in any other genotype and all animals survived until 3dpi **(Figure 25B)**. There were no significant differences in mortality between male and female hFcRn^{Tg32}-IFNAR$^{-/-}$ mice **(Figure 54A)**. We next determined the level of circulating virus in the blood and brains of these animals. We detected high levels of E5 in the blood (6 of 6 mice) and brains (12 of 12 mice) of hFcRn^{Tg32}-IFNAR$^{-/-}$ mice, but no detectable virus in any other genotype **(Figure 25C & D)**. There were no significant differences in E5 titer in the brains of male or female hFcRn^{Tg32}-IFNAR$^{-/-}$ mice **(Figure 54B)**.

Consistent with our previous findings with E11[280], we found that there was robust replication in the livers and pancreases of E5 infected hFcRn^{Tg32}-IFNAR$^{-/-}$ mice (12 of 12 mice) **(Figure 54C and D)**. However, in contrast to the brain, we found that hFcRn^{Tg32}-IFNLR$^{-/-}$ animals also contained virus in the liver (4 of 8 mice) and pancreas (8 of 8 mice) **(Figure 54C and D)**. We also detected low to mid-levels of E5 in the pancreases of immunocompetent hFcRn^{Tg32} mice (5 of 5 mice) and to a much lesser extent in liver (1 of 5 mice) **(Figure 54C and D)**. There was no detectable virus in any animals expressing the murine homologue of FcRn **(Figure 54C and D)**, consistent with our previous work[280]. Collectively, these data show that echovirus infections in the brain require expression of hFcRn and that the primary barrier to infection is type I IFN-mediated signaling.

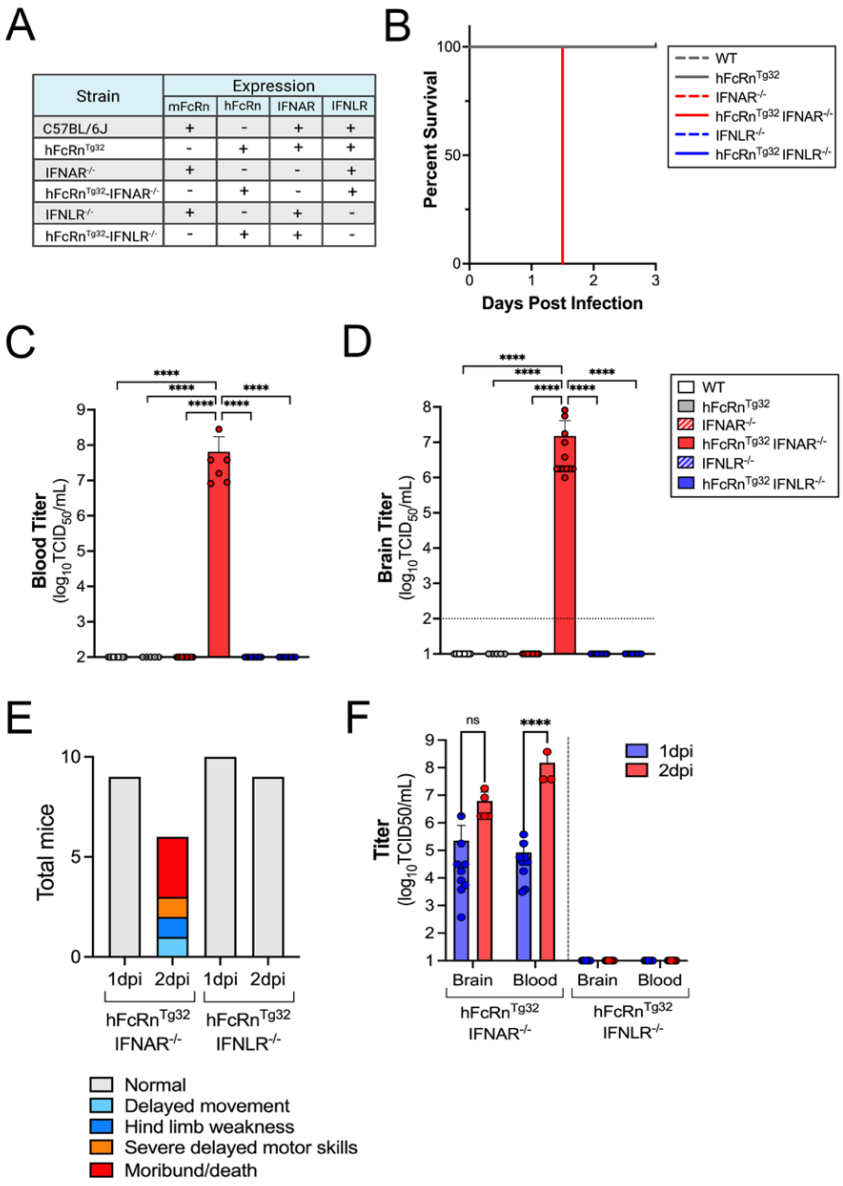

Figure 25 Ablation of type I interferon signaling and human FcRn expression are required for echovirus infection in the brain

(A) Table of the six genotypes used in this study. Shown is the expression of mouse or human FcRn, IFNAR, and IFNLR amongst these genotypes. **(B)** Survival of the indicated genotype of mice inoculated with 10^4 PFU E5 by the IP route and monitored for 3 days post-inoculation. The number of pups in each genotype are as follows: WT (17), hFcRn^{Tg32} (6), IFNAR$^{-/-}$ (17), hFcRn^{Tg32}-IFNAR$^{-/-}$ (12), IFNLR$^{-/-}$ (14), and hFcRn^{Tg32}-IFNLR$^{-/-}$ (8). The log-rank test was used to analyze the statistical difference of the survival rate. **(C and D)**. At 3dpi, animals were sacrificed and viral titers in blood **(C)** and brain **(D)** determined by TCID50 assays. Titers are shown as $\log_{10}$TCID50/mL with the limit of detection indicated by a dotted line. Data are shown as mean ± standard

deviation with individual animals shown as each data point. Data are shown with significance determined with a Kruskal-Wallis test with a Dunn's test for multiple comparisons. **(E and F)** hFcRn^{Tg32}-IFNAR$^{-/-}$ and hFcRn^{Tg32}-IFNLR$^{-/-}$ mice were inoculated with 10^3 PFU of E5 by the IP route and monitored for signs of disease. **(E)** Clinical symptoms observed of hFcRn^{Tg32}-IFNAR$^{-/-}$ or hFcRn^{Tg32}-IFNLR$^{-/-}$ pups at either one- or two-days post infection. **(F)** At 1 or 2dpi, animals were sacrificed and viral titers in blood and brain determined by TCID50 assays. Titers are shown as $\log_{10}$TCID50/mL with the limit of detection indicated by a dotted line. Data are shown as mean ± standard deviation with individual animals shown as each data point. Data are shown with significance determined with a Two-way Anova with Šídák's multiple comparisons tests (*p<0.05, **p<0.005, ***p<0.0005, ****p<0.0001).

5.2.2 Echovirus infections cause paralysis and motor defects in infected mice

Because we observed high levels of mortality in mice infected with 10^4 PFU E5 by the IP route, we investigated the neurotropism and neurovirulence of E5 in mice infected with a lower inoculum (10^3 PFU) of E5 by the IP route and monitored animals daily for 2 days. At this lower inoculum we observed death in approximately 50% of hFcRn^{Tg32}-IFNAR$^{-/-}$ animals by 1.5-2 days dpi compared to no mortality in hFcRn^{Tg32}-IFNLR$^{-/-}$ animals **(Figure 55A)**. There were no differences in mortality between male and female hFcRn^{Tg32}-IFNAR$^{-/-}$ mice **(Figure 55C)**. Infected animals were monitored for signs of illness (e.g., delayed movements, paralysis, discoloration, lack of nursing, lack of parental care, and death) throughout the duration of infection. There were no signs of clinical illness in echovirus-infected hFcRn^{Tg32}-IFNLR$^{-/-}$ animals at 1 or 2 dpi **(Figure 25E)**. There were also no obvious clinical symptoms in hFcRn^{Tg32}-IFNAR$^{-/-}$ animals at 1dpi. However, by 1.5-2dpi, there were clear defects in motor skills and various degrees of paralysis in hFcRn^{Tg32}-IFNAR$^{-/-}$ infected animals. There were a range of defects ranging from mild loss of motor function in one or more limb characterized by difficulty walking, hemiplegia that obstructed mobility or hind limb paralysis **(Figure 25E and Figure 55B)**. To correlate clinical symptoms with infection, we titrated virus from the brains of infected animals at 1 and 2 dpi, which

revealed similar titers at both days in brain and higher titers in blood at 2dpi in hFcRn^{Tg32}-IFNAR$^{-/-}$ animals **(Figure 25F)**. There were no differences in titers between male and female mice **(Figure 55D)**. Additionally, similar to the lack of clinical disease and low morality rates, no virus was detected in the blood or brains of hFcRn^{Tg32}-IFNLR$^{-/-}$ animals **(Figure 25F)**. These data show that echoviruses induce clinical symptoms of neurological disease, which occurs in an hFcRn-dependent manner and requires ablation of type I IFN signaling.

5.2.3 Immunological signature of echovirus infected brains

To define the immunological signature of echovirus infected brains, we harvest the brains of E5-infected mice expressing hFcRn (hFcRn^{Tg32}, hFcRn^{Tg32}-IFNAR$^{-/-}$, and hFcRn^{Tg32}-IFNLR$^{-/-}$) at 3dpi and performed multianalyte Luminex-based profiling of 27 cytokines and chemokines on brain tissue homogenates. We found that echovirus infection induced high levels of cytokines in brain tissue of hFcRn^{Tg32}-IFNAR$^{-/-}$ infected mice at 3dpi, including high levels of Granulocyte colony-stimulating factor-3 (GSF-3), which was the most abundant cytokine detected (~750-fold over uninfected) **(Figure 26A and C)**. Other highly induced cytokines included IL-6 (25-fold over uninfected), CXCL10 (17-fold over uninfected), monocyte chemoattractant protein-1 (MCP-1, 16-fold over uninfected), and keratinocyte-derived chemokine (KC, 12-fold over uninfected) **(Figure 26A and D-F)**. There was no significant induction of any cytokines in infected hFcRn^{Tg32} or hFcRn^{Tg32}-IFNLR$^{-/-}$ animals at 3dpi **(Figure 26A)**. We did not detect the type I IFNs IFN-α2 or IFN-β or the type III IFN IFN-λ1 in the brains of any mice **(Figure 56A-C)**.

We next assessed the kinetics of cytokine induction in echovirus infected brains isolated from hFcRn^{Tg32}-IFNAR$^{-/-}$ and hFcRn^{Tg32}-IFNLR$^{-/-}$ infected animals at 1 and 2dpi. Consistent with the overall low levels of virus in the brains of mice at 1dpi, we observed very little cytokine

induction in hFcRn^{Tg32}-IFNAR$^{-/-}$ animals at this time **(Figure 26B)**. However, by 2dpi, there were high levels of similar cytokines observed at 3dpi, including G-CSF (647-fold over uninfected), CXCL10 (33-fold over uninfected), IL-6 (28-fold over uninfected), and MCP-1 (23-fold over uninfected) **(Figure 26B, G-J)**. This cytokine induction paralleled the accumulation of viral RNA (vRNA) in the brain, as assessed by RT-qPCR for vRNA and the transcript for CXCL10 **(Figure 56D-E**). There were no cytokines significantly induced in infected hFcRn^{Tg32}-IFNLR$^{-/-}$ animals at either time point **(Figure 26B)**. These data show that echovirus infection of brain tissue results in an immunological response characterized by the induction of select pro-inflammatory cytokines and chemokines.

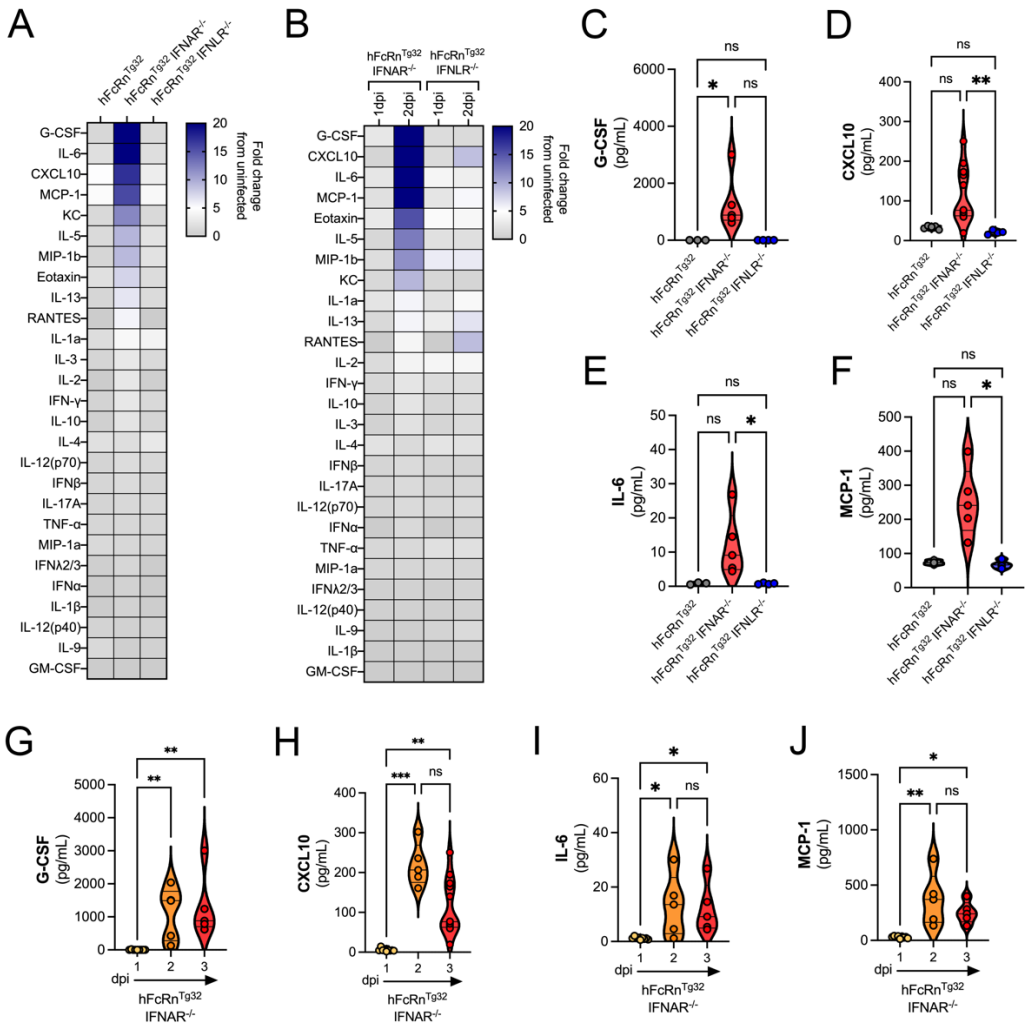

Figure 26 Immunological signature of echovirus infected brains.

Pups were IP inoculated and sacrificed either 1, 2, or 3dpi. Cytokine expression in brain tissue homogenates were analyzed by multiplex Luminex assays. **(A)** Heatmap demonstrating the induction (shown as fold-change from uninfected control) in E5-infected mice of the indicated genotype sacrificed at 3dpi. Blue denotes significantly increased cytokines in comparison to untreated. Grey or white denote little to no changes (scale at top right). **(B)** Heatmap demonstrating the induction (shown as fold-change from hFcRn^{Tg32} pups) in E5-infected mice of the indicated genotype sacrificed at 1 or 2dpi, as indicated. Blue denotes significantly increased cytokines in comparison to untreated. Grey or white denote little to no changes (scale at top right). **(C-F)** The top four cytokines induced from animals sacrificed at 3dpi from (A) including G-CSF **(C)**, CXCL10 **(D)**, IL-6 **(E)**, MCP-1 **(F)** shown as pg/mL. **(G-J)** The top four cytokines induced in hFcRn^{Tg32}-IFNAR$^{-/-}$ animals over the course of the infection time. Shown are G-CSF **(G)**, CXCL10 **(H)**, IL-6 **(I)**, and MCP-1 **(J)**. Data are shown as mean ± standard deviation and individual animals (points). Data are shown with significance determined with a Kruskal-Wallis test with a Dunn's test for multiple comparisons (*p<0.05, **p<0.005, ***p<0.0005, ****p<0.0001, ns-not significant).

5.2.4 Echoviruses replicate in the leptomeninges to induce meningeal inflammation

Very little is known regarding the cellular or structural targets of echovirus infections in the brain, including the meninges, which is composed of three membranous layers. To define the site(s) of echovirus replication in the brain, we infected hFcRn^{Tg32}, hFcRn^{Tg32}-IFNAR$^{-/-}$, and hFcRn^{Tg32}-IFNLR$^{-/-}$ mice with 10^4 PFU E5 for 3d to maximize infection. At this time, whole brains were removed, sectioned, and processed for hybridization chain reaction (HCR) using E5-specific probes. HCR allows for fluorescent quantitative RNA detection with enhanced sensitivity over conventional hybridization approaches given signal amplification resulting from the self-assembly of secondary detection hairpins into amplification polymers[259,261]. Whole brain confocal microscopy-based tile scanning of ~36mm^2 was then performed to define the region(s) and cell(s) infected by E5. We observed high levels of E5 vRNA in infected hFcRn^{Tg32}-IFNAR$^{-/-}$ brain tissue, but none in hFcRn^{Tg32} or hFcRn^{Tg32}-IFNLR$^{-/-}$ brains, at 3dpi, which was localized to a distinct region surrounding the brain **(Figure 27A, Figure 57A and B)**. This region was specific for the leptomeninges, which includes the two inner layers of the meninges **(Figure 27B and C)**. In addition, there were concentrated regions of high levels of E5 vRNA surrounding blood vessels localized throughout the meninges **(Figure 27D)**. Although the choroid plexus has been reported to express high levels of FcRn[294], we did not detect any infection in this region **(Figure 57C)**. To determine the timing of E5 vRNA in the meninges, we performed HCR in whole brains isolated from hFcRn^{Tg32}-IFNAR$^{-/-}$ mice infected with E5 for 1-3dpi. At 1dpi, we found that the levels of E5 vRNA were undetectable like uninfected controls, but by 2dpi, there were clear areas of E5 infection, which significantly increased by 3dpi **(Figure 27E and F)**.

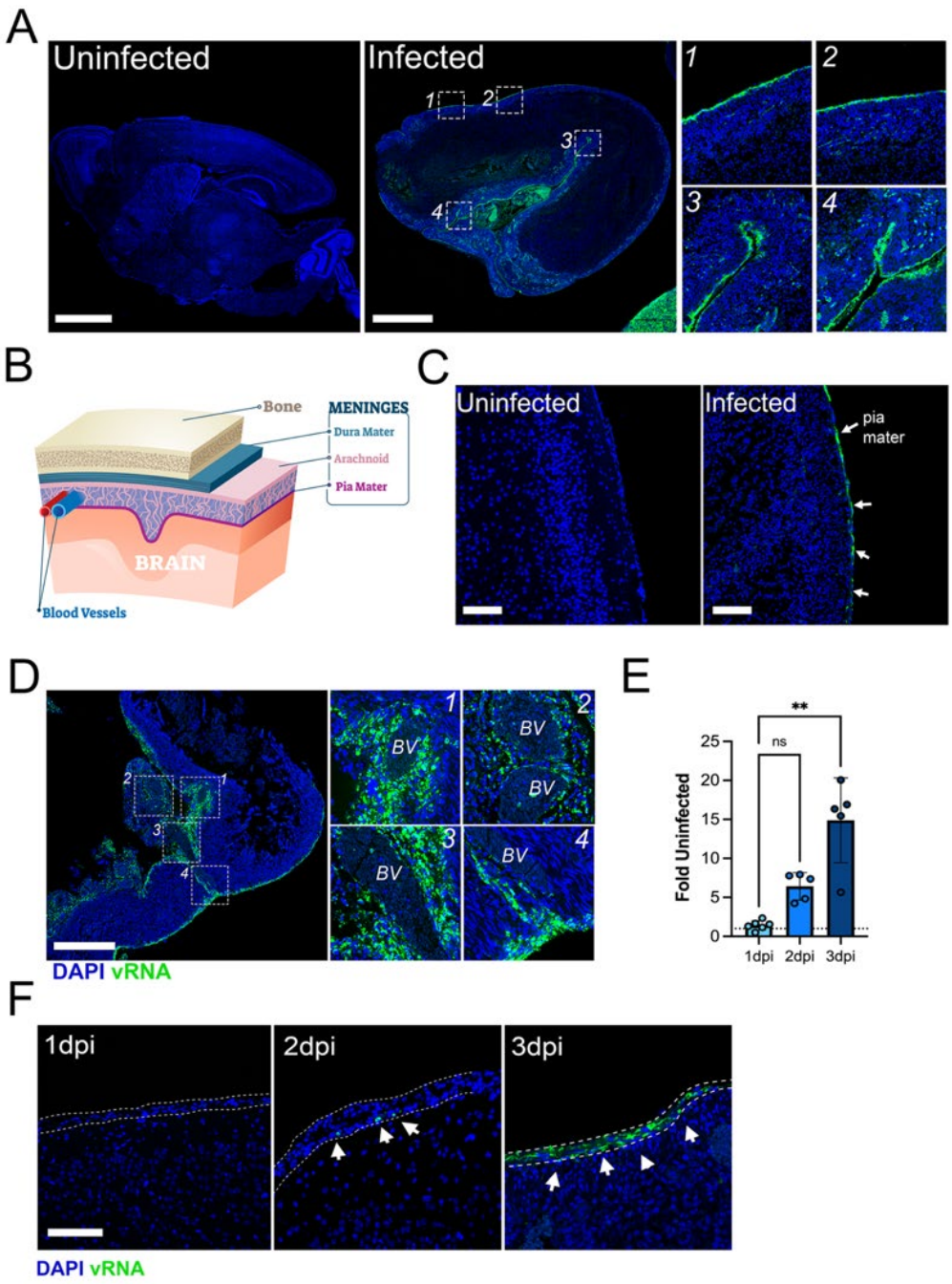

Figure 27 Echovirus replication in the leptomeninges

(A) Tile scan of the brains from an uninfected animal (left) and E5 infected hFcRn^{Tg32}-IFNAR$^{-/-}$ animal at 3dpi (middle) using Hybridization chain reaction RNA-FISH (HCR) for vRNA (in green) and DAPI (in blue). Numbered white boxes show zoomed areas to the right. **(B)** Schematic representation of the different layers of the meninges surrounding the brain. The dura mater in teal with the leptomeninges (arachnoid and pia mater) in shades of pink. **(C)** HCR for vRNA (in green) and DAPI (in blue) of a brain from an uninfected or an E5 infected hFcRn^{Tg32}-IFNAR$^{-/-}$ animal at 3dpi. White arrows denote areas of vRNA. **(D)** Tile scan of

HCR for E5 vRNA from a brain of an infected hFcRn^{Tg32}-IFNAR$^{-/-}$ animal at 3dpi of areas of infection surrounding blood vessels (BV). DAPI-stained nuclei in blue and vRNA in green. White boxes indicate zoomed images at right with numbers in the top right corner denoting the corresponding zoomed image. **(E)** Image analysis of the extent of vRNA signal in the brains of hFcRn^{Tg32}-IFNAR$^{-/-}$ animals at 1-3dpi as shown as a fold change from uninfected controls. Symbols represent unique regions used in quantification. Data are shown with significance determined with a Kruskal-Wallis test with a Dunn's test for multiple comparisons (**p<0.01, ns-not significant). **(F)** HCR for vRNA (in green) and DAPI (in blue) of the brains from infected hFcRn^{Tg32}-IFNAR$^{-/-}$ animals at 1, 2, or 3dpi, as indicated at top left. Dotted lines highlight the leptomeninges and arrows denote infected cells. Scale bars are as follows: 1mm (A), 100mm (C), 1mm (D), and 50mm (F).

To define the localization of FcRn within the brains of hFcRn^{Tg32} mice and to correlate this expression with E5 infection, we performed immunohistochemistry for hFcRn in hFcRn^{Tg32}-IFNAR$^{-/-}$ mice. We found that hFcRn was enriched in the leptomeninges of infected animals, where it was concentrated to regions associated with high levels of vRNA **(Figure 28A)**.

Next, we assessed the impacts of E5 infection on the integrity of the meninges. We noted instances of acute meningitis and inflammatory tissue damage in hFcRn^{Tg32}-IFNAR$^{-/-}$ mice infected with E5 for 3dpi, which included areas of immune cell infiltration **(Figure 28B)**. Areas of inflammation correlated with high levels of E5 replication, as indicated by aligning HCR and H&E images **(Figure 28C)**. Lastly, to determine whether E5 infection induces direct cell death or damage to the meninges, we performed immunohistochemistry for cleaved caspase-3, which revealed discrete areas of apoptosis as early as 2dpi, with more significant levels at 3dpi **(Figure 28D)**. Together, these data show that echovirus infection of the meninges induces pronounced tissue damage and inflammation.

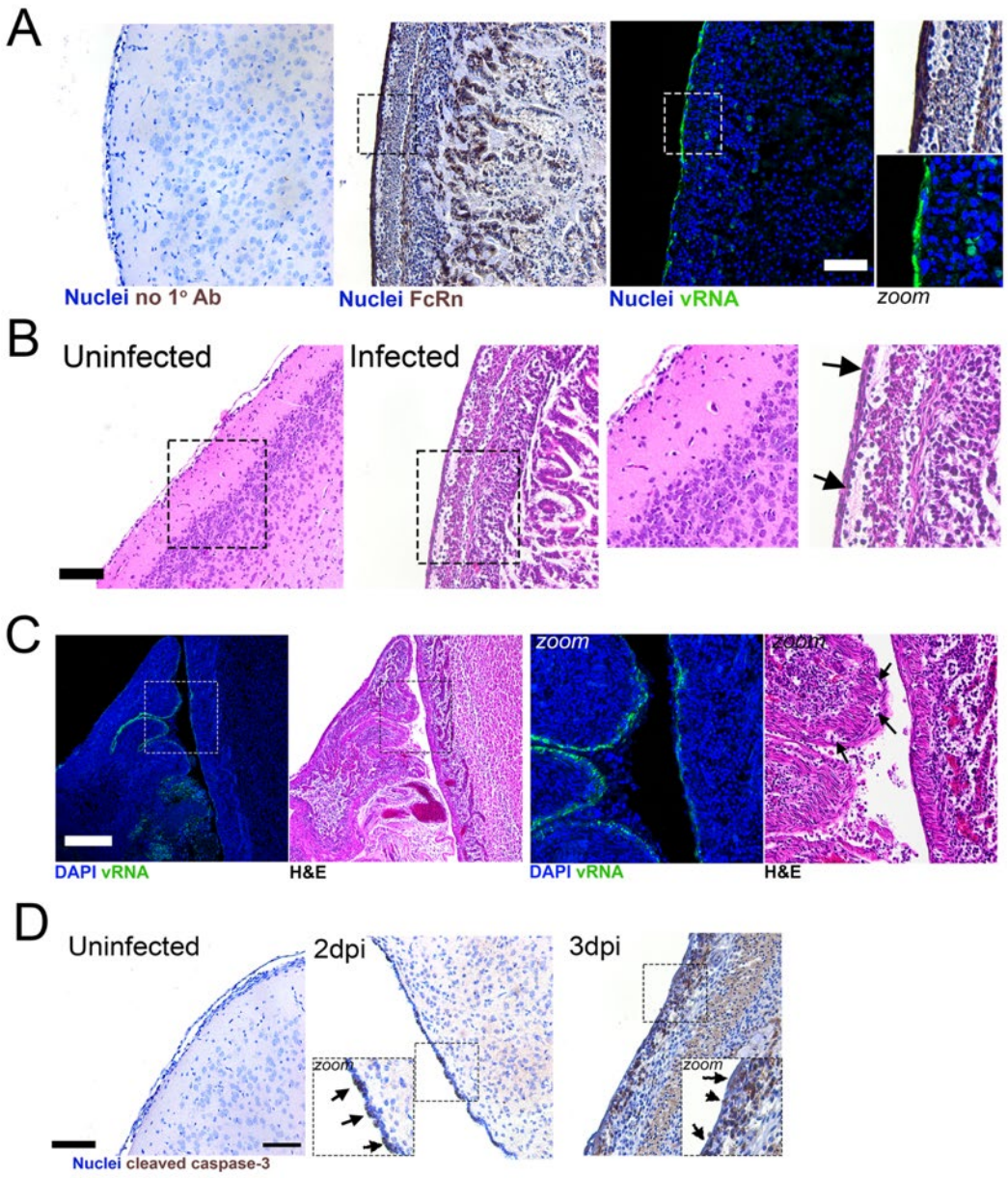

Figure 28 Echovirus replication in the meninges induces inflammation and cell death

(A) Immunohistochemistry for hFcRn and HCR for vRNA in the brain of a hFcRn^{Tg32}-IFNAR$^{-/-}$ animal infected with E5 for 3d. At left, no primary antibody control in an uninfected control animal. Middle, hFcRn IHC and right, HCR for vRNA (in green) and DAPI (in blue) from the same E5 infected hFcRn^{Tg32}-IFNAR$^{-/-}$ animal. Boxes indicate regions that are zoomed at right. **(B)** Hematoxylin and eosin staining of representative brain sections from an uninfected or E5 infected hFcRn^{Tg32}-IFNAR$^{-/-}$ animal. Black boxes show areas of zoomed images at right. Arrows denote regions of inflammation within the meninges. **(C)** HCR for E5 vRNA or hematoxylin and eosin staining of the cerebellum within the brain of a hFcRn^{Tg32}-IFNAR$^{-/-}$ animal at 3dpi. HCR shows vRNA (in green) and DAPI (in blue). Boxes denote areas of zoomed images at right. Arrows denote region of inflammation within

the meninges. **(D)** IHC for cleaved caspase 3 in uninfected, or hFcRn^{Tg32}-IFNAR$^{-/-}$ animals infected with E5 for 2dpi, or 3dpi. Arrows denote cells that are positive for cleaved caspase 3. Black boxes show zoomed images. Scale bars are as follows: 100mm (A, B, D) and 1mm (C).

5.3 Discussion

Echovirus infections are common causes of neonatal meningitis, which can be fatal. However, how these viruses infect the brain and their regional tropism within the brain remains unknown. Here, we developed an *in vivo* model of echovirus-induced meningitis and used this model to define the cellular targets and host immune pathways associated with echovirus infection within the brain. We show that expression of the human homologue of FcRn is necessary, but not sufficient, for echovirus infection of the brain. In addition, we show that type I IFNs, but not type III IFNs, provide a barrier to echovirus infections of the meninges and that ablation of this pathway sensitizes the brain to infection, which induces a robust immune response. Lastly, we define the specificity of echovirus replication in the brain and show that high levels of replication in the leptomeninges induced inflammation and cell death. These studies thus provide key insights into the events associated with echovirus-induced meningitis and an *in vivo* model that could be used to test echovirus therapeutics targeting echovirus-induced neuronal disease.

FcRn is expressed on the microvasculature of the blood-brain barrier[294], where it has been proposed to mediate the efflux of antibodies out of the brain[306]. In addition to this localization, FcRn is expressed in the epithelium of the choroid plexus[294]. This pattern of expression is conserved between humans and in hFcRn^{Tg32} mice[228]. In addition to these sites, our data show that FcRn is also expressed at distinct regions of the meninges. The meninges are composed of diverse cell types, with distinct patterns of expression regionally between the dura, arachnoid layer, and

pia mater, with the arachnoid and pia mater referred to as the leptomeninges[307]. The meningeal layers are primarily comprised of fibroblasts, with each subtype expressing their own unique transcriptional signature[307]. In addition to fibroblasts, the arachnoid layer also contains arachnoid barrier cells, which are epithelial-like in origin and separate the dura mater from the subarachnoid space in which CSF accesses the brain. The meninges also contain a large population of immune cells, including $CD4^+$ T cells and B cells. Notably, meningeal macrophages are a specialized subclass of macrophages which are long-lived in the leptomeninges[308]. We observed the highest levels of E5 infection restricted to the leptomeninges, the inner layer of the meninges containing the pia mater and arachnoid layers, which also expressed high levels of FcRn. Given the robust levels of E5 infection in the meninges, it is likely that fibroblasts are at least one target of infection. However, it is possible that other cell types, such as macrophages, are also permissive to infection and contribute to pathogenesis. Collectively, these data suggest that the regional expression of FcRn plays a direct role in the tropism of echoviruses in the brain and directly correlates with their high levels of replication in the meninges.

Several studies have investigated the levels of cytokines and chemokines within the CSF of infants and children with confirmed echovirus-induced meningitis. The CSF of children with echovirus 30-induced meningitis contain very high levels of MCP-1 and IL-6 compared to controls[300,309]. Our data show that $hFcRn^{Tg32}$-$IFNAR^{-/-}$ animals also induce very high levels of MCP-1 and IL-6 in brain tissue homogenates. MCP-1, also known as CCL2, is a monocyte chemoattractant responsible for recruiting monocytes and dendritic cells to the site of inflammation due to infection. IL-6 is a proinflammatory cytokine that is secreted by macrophages that have detected a viral infection. These immune mediators play important roles in alerting the immune system to a viral infection and recruiting immune cells to the sites of infection. However,

because we used brain tissue homogenates and human studies can are restricted to CSF, it is unclear which cytokines induced by echovirus infections mediate the influx of immune cells observed in echovirus-induced meningitis. Although the differential roles of type I and III IFNs has been established in the respiratory and intestinal epithelium during enterovirus infection[49,130,305,310], whether these IFNs play distinct roles in enterovirus-induced meningitis has remained unclear. Our data suggest that type I IFNs are the sole barrier to echovirus infection of the CNS, which is consistent with previous work defining indicating that these IFNs form at least one bottleneck to poliovirus access to the CNS[311]. However, type I IFNs were not detected in multiplex Luminex profiling of brain homogenates from echovirus-infected mice, suggesting that these IFNs are not produced locally in the brain. It is therefore likely that circulating IFNs produced at distal sites, such as the liver, trigger antiviral responses in the CNS that protect from echovirus infections.

In humans, neonates are at increased risks for echovirus-induced morbidity and mortality. For example, rates of echovirus-induced paralysis decreased with increased age at inoculation[312]. Our previous work showed that adult echovirus-infected mice exhibit low levels of infection in the brain following IP inoculation[280]. Our data presented here show that neonatal mice are highly sensitive to echovirus-induced neuronal dysfunction and contain high levels of viral infection within the meninges. The mechanistic basis for age-related differences in echovirus infection of the brain remains unclear. Given that BBB forms in mice prior to birth[313], this barrier is unlikely to participate in these age-related differences. Age-related differences in neuronal susceptibility to infections not specific to echoviruses and has also been shown for reovirus[314]. However, unlike this work, our data suggest that type I IFNs are not the primary drivers for differential age susceptibility given that both adult and neonatal animals in our work were deficient in IFNAR

expression. Other work has shown that age-related differences in susceptibility to cardiac infections by CVB may result from differences in receptor expression[315,316]. Age-related differences in FcRn expression in humans are unknown, but its expression in human liver is not dependent on age[317], suggesting this is unlikely to explain age-related differences in echovirus-associated neuronal infections. Therefore, it remains unclear which factors contribute to age-related difference in infection of the CNS.

Our findings presented here define key aspects of echovirus infection of the brain, including the sites of viral replication and the consequences of this infection. We show that FcRn is necessary but not sufficient for echovirus infection of the brain *in vivo* and that type I IFNs control infection within the meninges. Collectively, these studies develop a model of echovirus aseptic meningitis, which could aid in the testing of novel therapeutics.

5.4 Materials and Methods

5.4.1 Cell lines and viruses

HeLa cells (clone 7B) were provided by Jeffrey Bergelson, Children's Hospital of Philadelphia, Philadelphia, PA, and cultured in MEM supplemented with 5% FBS, non-essential amino acids, and penicillin/streptomycin. Experiments were performed with echovirus 5 (Noyce strain, E5), which was obtained from the ATCC. Virus was propagated in HeLa cells and purified by ultracentrifugation over a 30% sucrose cushion, as described previously[245]. All viruses were sequenced for viral stock purity following propagation. Purity of all viral stocks was confirmed by Sanger sequencing of VP1 using enterovirus-specific primers[284]. Briefly, RNA extraction was

performed on 10µl of purified virus stock, according to manufacturer's instructions (Qiagen Cat. 529904). RNA was reverse transcribed using SuperScript III reverse transcription kit, (Invitrogen cat. 18080093) according to manufacturer's instructions, with a pan enterovirus primer (vir21; ATAAGAATGCGGCCGCTTTTTTTTTTTTTTTTTTTTTTT), followed by an RNaseH treatment for 20 minutes at 37ºC. PCR was performed with 5µl of the cDNA reaction using BioRad iTaq DNA polymerase (BioRad cat. 1708870). Virus specific primers are as follows: E5 forward 5'-TATCGCCAATTACAACGCGAA-3'; E5 reverse 5'-TTGGTTTGAAGTAAACCCTTA-3'.

5.4.2 Animals

All animal experiments were approved by the Duke University Animal Care and Use Committees, and all methods were performed in accordance with the relevant guidelines and regulations. C57BL/6J (WT, cat. no. 000664), B6.Cg-*Fcgrt*^{tm1Dcr}Tg(FCGRT)32Dcr/DcrJ (hFcRn^{Tg32}, cat. no. 014565), and B6.(Cg)-Ifnar1$^{tm1.2Ees}$/J (IFNAR$^{-/-}$, cat. no. 028288) mice were purchased from The Jackson Laboratory. hFcRn^{Tg32}-IFNAR$^{-/-}$ mice were generated as described previously[280]. B6.Ifnlr$^{-/-}$/J (IFNLR$^{-/-}$) mice were provided by Dr. Megan Baldridge (Washington University School of Medicine). hFcRn^{Tg32}-IFNLR$^{-/-}$ mice were generated by crossing B6.Cg-*Fcgrt*^{tm1Dcr}Tg(FCGRT)32Dcr/DcrJ (hFcRn^{Tg32}, cat. no. 014565) mice with B6.Ifnlr$^{-/-}$/J mice[305]. Breeders were established that were deficient in mouse FcRn and IFNLR and were homozygous for the hFcRn transgene. All animals used in this study were genotyped by Transnetyx.

5.4.3 Suckling pup infections

7-day-old mice were inoculated by the IP route with 10^4 or 10^3 PFU of E5. Inoculation was performed using a 1mL disposable syringe and a 27-gauge needle in 50µL of 1X PBS. Mice were euthanized at either 1-, 2-, or 3-days post inoculation and organs harvested into 0.5mL of DMEM and stored at -80°C. Tissue samples for viral titration were thawed and homogenized with a TissueLyser LT (Qiagen) for 5 minutes, followed by brief centrifugation for 5 minutes at 8000xg. Viral titers in organ homogenates were determined by TCID50s in HeLa cells and enumerated following crystal violet staining.

5.4.4 Luminex assays

Luminex profiling was performed on whole brain tissue homogenates where were homogenized with a TissueLyser LT (Qiagen) for 5 minutes, followed by a centrifugation of 10,000xg for 10 minutes. Luminex kits that were used are as follows a custom mouse IFN kit (IFN alpha, IFN beta, IL-28, Invitrogen), mouse cytokine 23-plex (Bio-Rad, M60009RDPD), and mouse CXCL10 (Invitrogen, EPX01A-26018-901), according to the manufacturer's protocol. Assays were read on a BioPlex 200 by BioRad. Heat maps were generated using the fold change in concentration (picograms/milliliter) of each animal compared to the average of uninfected animals and was made in GraphPad Prism. Violin plots are shown as the concentration for each animal (one point) in picograms/milliliter.

5.4.5 RNA extraction and RT-qPCR

Total RNA was isolated from brains using the Sigma GenElute Total Mammalian RNA Miniprep Kit (Sigma, RTN350), according to the manufacturer protocol with the addition of a Sigma DNase digest reagent (Sigma, DNASE70). RNA (1 ug total) was reverse transcribed using iScript cDNA Synthesis Kit (Bio-Rad, 1708891) and diluted to 100 ul in ddH_2O for subsequent qPCR analyses. RT-qPCR was performed using the iTaq Universal SYBR Green Supermix (Bio-Rad, 1725121) on a CFX96 Touch Real-Time PCR Detection System (Bio-Rad, 1855195). Primer sequences can be found in **Table 13**.

5.4.6 Immunohistochemistry

Tissues were fixed in 10% buffered formalin for 24hrs and then transferred to 70% ethanol. Tissues were embedded in paraffin and sectioned. Slides were stained with cleaved caspase 3 (Asp175) (9661, Cell Signaling) or human FCGRT (Abcam, ab139152). Tissue sections were deparaffinized with xylene and rehydrated with decreasing concentrations of ethanol (100%, 95%, 80%), then washed with ddH_2O. Antigen unmasking was performed with slides submerged in 10 mM citrate buffer (pH 6.0) and heated in a steamer for 20 minutes at ~90˚C. Slides were cooled to room temperature and slides were immunostained with cleaved caspase 3 or FCGRT using Vectastain Elite ABC HRP (Vector Biolabs, PK-6100), according to the manufacturer's instructions. Slides were incubated in 6% H_2O_2 in methanol for 30 min then washed 3 times for 5 minutes in H_2O. Avidin block (Vector, SP-2001) was applied for 15 minutes and washed twice in H_2O followed by biotin block (Abcam, ab156024) for 15 minutes and washed twice in H_2O. Finally, serum-free protein block was applied for 10 minutes, and cleaved caspase 3 antibody was

diluted 1:100 and the FCGRT antibody was diluted to 1:200 in TBS-T (Tris-buffered saline, 0.1% Tween 20) and slides incubated overnight in a humidified chamber at 4C. Next, slides were washed three times for 5 min in PBST and exposed to the goat anti-rabbit biotinylated secondary antibody (Vector, BA-1000) for 30 min. Slides were rinsed in PBST three times for 5 min and the Vectastain Elite ABC HRP kit was applied for 30 min. Slides were rinsed in PBST for three times for 5 min and diaminobenzidine substrate for 5 mins, which was terminated with water incubation. Slides were counterstained with hematoxylin for 1 min, thoroughly rinsed with H_2O, and incubated in 0.1% sodium bicarbonate in H_2O for 5 mins. Slides were then dehydrated with increasing concentrations of ethanol, cleared with xylene and mounted with Cytoseal 60 (Thermo Scientific, 83104). Images were captured on an IX83 inverted microscope (Olympus) using a UC90 color CCD camera (Olympus).

5.4.7 HCR and Imaging

HCR was performed following the Molecular Instruments HCR v3.0 protocol for FFPE human tissue sections[259,261]. Briefly, tissue sections were deparaffinized with xylene and rehydrated with decreasing concentrations of ethanol (100%, 95%, 80%). Antigen unmasking was performed with slides submerged in 10 mM citrate buffer (pH 6.0) and heated in a steamer for 20 minutes at ~90°C. Slides were cooled to room temperature. Sections were treated with 10 µg/mL Proteinase K for 10 min at 37°C and washed with RNase free water. Samples were incubated for 10 minutes at 37°C in hybridization buffer. Sections were incubated overnight in a humidified chamber at 37°C with 3 pmol of initiator probes in hybridization buffer. We designed probes for E5 **(Table 10)**. The next day, slides were washed in probe wash buffer and 5x SSCT for 4x 15 min, according to the manufacturer's instructions. Samples were incubated in a humidified

chamber at 37°C for 30 minutes in amplification buffer. Fluorescent hair pins were heated to 95°C for 90 seconds and snap cooled at room temperature for 30 min. Hairpins and amplification buffer were added to the sample and incubated overnight at room temperature. Hairpins were washed off with 5x SSCT for 5 minutes, 15 minutes, 15 minutes, and 5 minutes followed by a wash with PBS containing DAPI. Slides were mounted in Vectashield with DAPI. Slides were imaged on a Zeiss 880 with Airyscan inverted confocal microscope. Image analysis was performed using FIJI.

5.4.8 Statistics

All statistical analysis was performed using GraphPad Prism version 9. Data are presented as mean ± SD. Parametric tests were applied when data were distributed normally based on D'Agostino–Pearson analyses; otherwise, nonparametric tests were applied. The log-rank test was used to analyze the statistical difference of the survival rate in Kaplan Meier curves. In most cases, a Kruskal-Wallis test with a Dunn's test for multiple comparisons or Two-way Anova with Šídák's multiple comparisons tests were used to determine statistical significance, as described in the figure legends. P values of <0.05 were considered statistically significant, *p<0.05, **p<0.005, ***p<0.0005, ***p<0.0001, as noted in figure legends.

6.0 Unbiased screening defines ISGs that function in pan-enterovirus and enterovirus-specific specific manners

Enteroviruses are restricted by type I or III interferons because of the hundreds of ISGs induced downstream of this signaling. The redundancy in the antiviral activity of ISGs is central to the broadly antiviral nature of interferon activity. Although several ISGs are known to suppress enterovirus replication, the broad activity of ISGs against members of the enterovirus family has not been defined. In addition, whether these ISGs function in cell-type specific manners to suppress enterovirus replication is unknown. In this work, we performed unbiased flow cytometry-based screening of hundreds of ISGs in two physiologically relevant cell types to define the anti-enterovirus activity of these ISGs. To determine whether ISGs restrict enterovirus replication in a virus-specific manner, we performed parallel screens using laboratory and clinical strains of coxsackievirus B (CVB), echovirus 11 (E11), and enterovirus 71 (EV71). In addition, we performed parallel screens using a library of human and macaque ISGs to define the evolutionary conservation of anti-enterovirus activity amongst ISGs. This screening revealed that select ISGs function in a pan-enterovirus manner and function to restrict enterovirus replication across cell types. In contrast, some ISGs restrict enterovirus replication in species-, cell-, and virus-specific manners. We also show that ISGs exert differential activity against laboratory and clinical isolates and that clinical isolates are more sensitive to the antiviral effects of ISGs. Lastly, we will determine whether enteroviruses antagonize ISG activity through viral protease-mediated cleavage to define the complex interplay between host restriction and viral evasion. This study reveals critical differences in enterovirus-specific ISGs as well as cell dependent mechanisms of ISG activity.

6.1 Introduction

Enteroviruses are small single-stranded RNA viruses that belong to the *Picornaviridae* family. Enteroviruses infect 10-15 million people in the United States annually and are a significant concern for public health[318]. The pediatric population are especially susceptible to enterovirus infections. Enteroviruses, which include poliovirus, echoviruses, coxsackievirus B (CVB), enterovirus D-68 (EV-D68), and enterovirus 71 (EV71)[82], primarily infect humans through the fecal-oral route[119]. These viruses enter the body through ingestion where they infect the gastrointestinal (GI) epithelium. Following primary infection, they disseminate into secondary sites of replication, where they typically cause clinical disease. Enterovirus-induced disease encompasses a broad range of symptoms from minor skin rashes to liver failure, acute flaccid myelitis, and meningitis[319].

IFNs and ISGs are important antiviral factors that control viral infection[46,47]. The IFN family is composed of three classes, type I (IFN-αs, IFN-β and others), type II (IFN-γ), and type III (IFN-λs). Both type I and III IFN signaling induces the expression of antiviral ISGs to suppress infection. Previous studies have shown that IFN expression is important for restriction of different enteroviruses[320]. We have previously shown that echovirus 11 (E11) specifically induces type III IFNs in human intestinal enteroids and recombinant type I and III IFN controls E11[130]. Others have shown that type I IFNs are important for the control of CVB[321]. Additionally, RNAseq shows that enteroviruses induce the expression of ISGs in primary cells and animals[59,130,280]. One previous study identified the role of the interferon-induced protein with tetratricopeptide repeats (IFIT) family of ISGs in the protection of cardiomyocytes from CVB infection[322]. Others have identified a role of RSAD2/viperin in the inhibition of EV71[323,324]. Furthermore, many studies have

investigated the role of the enterovirus-encoded viral proteases, $2A^{pro}$ or $3C^{pro}$ in the cleavage of RLRs, such as RIG-I, MDA5, and their adaptor MAVS, to inhibit the initiation of innate immune responses across many different enteroviruses[170,175–180,183]. While many studies have explored how enteroviruses are detected in cells, what ISGs are induced, and the mechanisms enteroviruses use to evade the IFN response, few studies have identified ISGs that exert enterovirus antiviral activity and how enteroviruses specifically evade them[320].

Here we developed a high-throughput flow cytometry-based screen to measure active replication of enteroviruses in order to identify antiviral ISGs based on a previously established ISG screening library[325]. We screened three different enteroviruses, CVB, E11, and EV71, in two physiologically relevant cell lines, human brain microvascular endothelial cells (HBMEC) and human colorectal adenocarcinoma cells (Caco-2), to identify antiviral factors in cell type-specific and virus-specific manners. To define the evolutionary conservation of anti-enterovirus activity of ISGs, we performed parallel screening with a library of human and macaque ISGs. These comparative screens identified proviral and antiviral ISGs that were shared amongst enteroviruses and those that exhibited specific effects. We also found ISGs that had species specific effects on replication when comparing the human and macaque libraries. Using clinical isolates of CVB, E11, and EV71, we found that anti-enterovirus ISGs were more robust at suppressing the replication of these isolates, suggesting that laboratory strains may have evolved mechanisms to evade this restriction. Together, these studies provide a broad identification of anti-enterovirus ISGs and suggest that ISGs exert differential activity against laboratory and clinical strains of these viruses.

6.2 Results

6.2.1 Establishment of a flow cytometry-based method of detecting viral RNA

A previous study utilized a GFP reporter-tagged CVB to identify human ISGs with anti-enterovirus activity within HeLa cells[326]. While this study identified several ISGs with anti-CVB activity, it did not perform comparative screens with closely related or divergent enteroviruses, compare antiviral activity across physiologically relevant cell types, determine the evolutionary conservation of ISG activity across human and macaque ISGs, or determine antiviral activity during *bona fide* replication not dependent on reporter viruses. Therefore, we developed a flow-cytometry based ISG screen to identify antiviral proteins against lab adapted and clinical isolates of enteroviruses. Because it is well known that reporter containing enteroviruses are attenuated in replication time and the ability to combat the IFN response, we decided to use nonreporter viruses, which has not been done before with enteroviruses. In order to do this, we had to establish a method of detecting viral replication by flow cytometry, a method that has not been well established for enteroviruses previously. We wanted to make sure we were detecting active viral replication instead of just any input virus so we utilized a double stranded RNA (dsRNA) antibody to detect replication intermediates within the cell. To establish this method of vRNA detection, we used a highly permissive cell line and infected different MOIs of CVB on a flat bottom 96 well plate. We trypsinized and fixed the cells after 8hpi. We were not sure the best method of staining for flow cytometry with this antibody, so we used multiple conditions to find the best one that yielded the lowest background to best positive signal. We compared blocking in 1% human serum to 1% BSA or no blocking, primary antibody for 1hr to an overnight incubation with primary the antibody at 4°C, and finally the secondary antibody. After many trials, we established this staining method

worked best with a 1% human serum in 1% BSA blocking step before an overnight primary antibody incubation in permeabilization buffer at 4°C coupled with an Alexa fluor conjugated secondary antibody for 1hr **(Figure 29)**.

6.2.2 Establishment of infectious inoculum for screening in HBMEC and Caco-2 cells

After we established our assay to measure viral replication by flow cytometry, we needed to establish our infection inoculum and length of infection for the screen. We wanted to perform the screen using two cell line models of physiologically relevant sites of enterovirus infection. The first is a model of the blood brain barrier, HBMEC, and the second is a model of the gastrointestinal epithelium, Caco-2. These are extremely important sites of infection in humans and may show differences between viral evasion in different cell types in addition to potential cell type specific ISGs. But because these two cell lines have different susceptibility to enteroviruses, we had to establish the infectious inoculum and the infection length separately for each cell line with each virus. We knew from working with each cell line previously that Caco-2 cells are overall more permissive to enteroviruses compared to HBMECs. Ideally, the screen is performed within the time that only one round of viral replication occurs to only detect ISGs that restrict replication and not other processes of viral infection, such as egress. This proves to be a unique balance between over and under infecting cells. We started with infecting Caco-2s for 8hrs and HBMECs for 16hrs. To figure out the infection dose, we did serial dilutions of each of the viruses in each cell type and used our staining protocol that was described above to determine what inoculum resulted in about 30% of the cells positive for vRNA. We chose the level of infection to be around 30% so we could accurately determine pro and antiviral ISGs without a large population of cells that were dead. The dilution of virus in each of the cell types that yielded around 30% detectable infection by the flow

cytometer was the dilution we would use in the screen (see methods for infection details). Because EV71 tends to replicate slightly slower, no matter which cell type was being used, EV71 infections occurred for 16hrs.

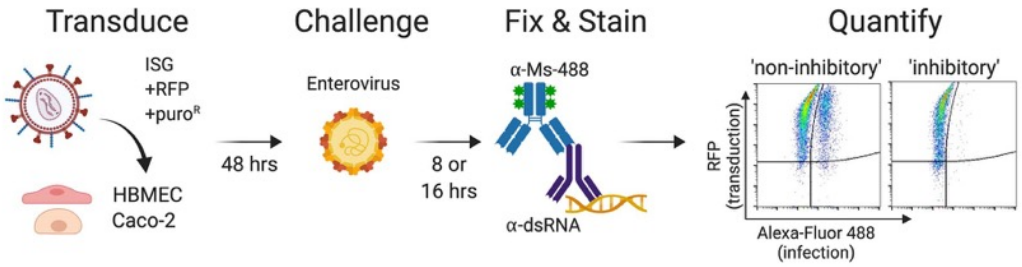

Figure 29 Schematic of ISG screen workflow

Schematic representation of the workflow of a flow cytometry based ISG screen. Either HBMEC or Caco-2 cells were plated in 96 well plates one day prior to transduction. Cells were transduced with the lentiviral library which contained an ISG. Cells were incubated for 48hrs before challenging with the respective enterovirus. 8 or 16hrs post infection, cells were trypsinized, fixed, permeabilized and stained overnight with an antibody recognizing double stranded RNA. Following an overnight incubation with the primary antibody, cells were washed and incubated with an anti-mouse secondary antibody which was conjugated to a 488 fluorophore. Samples were read on an attune flow cytometer with a 96 well autosampler. Figure was made with Biorender.com.

6.2.3 Optimization of lentivirus transduction of ISG library in HBMEC and Caco-2 cells

The last condition we had to optimize before starting our screen was transduction of the libraries in the two cell types. We used the two previously established human and macaque libraries in order to determine if any species specificity occurs in restrictive ISGs[325,326]. These libraries combine to test 491 unique ISGs. The human library is comprised of 399 ISGs while the macaque library is comprised of 346 ISGs. They both contain 254 dual ISGs which allows for testing of species differences between specific ISGs. Every cell line transduces with lentiviral particles at different efficiencies. In order to make sure our screens contained high numbers of transduced cells so we could quantify levels of infection, we optimized transduction of the lentiviral particles.

Similar to how we tested our enterovirus inoculum, we performed serial dilutions of the lentivirus particles to determine how much was needed to have 90% of the cells be transduced with the ISG and quantified this by flow cytometry. Because it would be impossible to titer all of the individual wells of the lentiviral library and add a different amount to every single well, the goal of having a transduction efficiency of 90% with an empty vector control lentiviral prep helped make sure that even with variation between wells of the lentivirus library, we would hopefully have at least 50% of cells that were transduced. We also tested whether polybrene would help increase transduction in each of the cell types. Our test determined that polybrene was not necessary for high efficiency transduction of either cell type and gave us an average volume of lentiviral supernatants required to produce high transduction efficiencies. Following this last test for transduction efficiency, we were able to perform our screen.

6.2.4 ISG screen data interpretation

Cells were transduced with the ISG library from either the human or macaque libraries followed by infection of the specified enterovirus for either 8 or 16hrs (see methods). Cells were stained using an antibody that recognizes double stranded RNA, a replication intermediate of enteroviruses, followed by a secondary antibody, and quantified by flow cytometry. The percentage of infected cells for each well was determined by taking the double positive cells and divided by the total RFP positive cells. In order to determine the level of ISG restriction, each wells' percentage of infected cells was divided by the average of the empty vector controls that are throughout the screen for the respective cell type and virus. This gave us a percentage of infection compared to control to determine if each ISG restricts infection, has not impact on infection, or is proviral. We called potential hits has ISGs that decreased infection by at least 2-

fold or increased infection by at least 3-fold **(Figure 30)**. Overall, the ISG screens identified both proviral and antiviral factors against CVB, E11, and EV71 in both cell types.

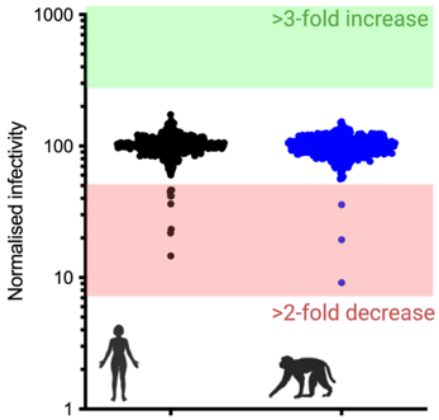

Figure 30 Example plot of potential hits

Example plot of how the data will be graphed. On the x axis is which species library which is shown (human black, macaque blue). The y axis will be the normalized infectivity percentages. An example of an antiviral hit would be in the highlighted red area, which shows a 2-fold decrease in replication. An example of a proviral hit would be in the highlighted green area, which shows a 3-fold increase in replication.

6.2.5 ISG screen identifies several pro-viral and antiviral host factors against CVB, E11, EV71 in human brain microvascular endothelial cells

In HBMECs, CVB had the least amount of identified antiviral factors (5 human, 8 macaque) **(Figure 31A, bottom, D, and E)** where as E11 (24 human, 7 macaque) and EV71 (22 human, 28 macaque) had many factors that reduced viral replication **(Figure 31B and C, bottom, D and E)**. Interestingly, EV71, in HBMECs, had several host factors that were pro-viral (11 human, 8 macaque) **(Figure 31C, top)**. One host factor that was meaningful was Scavenger Receptor Class B Member 2 (SCARB2), as it is the viral entry receptor. SCARB2 was included

when the library was established since it becomes upregulated when cells are treated with interferons and therefore is an ISG. SCARB2 being in both the human and macaque libraries validates that our screen is working properly for EV71 infection as when SCARB2, the viral receptor, is overexpressed infection should increase. In fact, in our screen both the human and macaque isoforms significantly increased infection. The macaque derived library also included an antiviral that helped validate that the screen was working as we expected, IFN beta (IFN-β). We expected that IFN-β would be a strong antiviral factor as it should turn on hundreds of ISGs, nonspecifically, that will act to restrict infection. This was the case where macaque IFN-β restricted all three viruses in HBMECs **(Figure 31)**. These two ISGs, while not intentionally included for this reason, helped validate the screen was giving us accurate data.

Within each species library, the viruses had several overlapping antiviral ISGs. In the human library, three genes were shared among all three enteroviruses, E74 Like ETS Transcription Factor 1 (ELF1), ISG20, and Lysosomal Associated Membrane Protein 3 (LAMP3) **(Figure 31D)**. Interestingly, four ISGs were shared between EV71 and E11 but did not impact CVB replication, Shiftless Antiviral Inhibitor of Ribosomal Frameshifting (C19orf66), BCL2 Like 14 (BCL2L14), Zinc Finger CCCH-Type Containing, Antiviral 1 (ZC3HAV1), and Fms Related Receptor Tyrosine Kinase 1 (FLT1). While CVB and E11, members of the same enterovirus family, shared only one ISG that restricted infection, Thrombomodulin (THBD) **(Figure 31D)**. CVB and EV71 did not share any antiviral ISGs in the human library. A similar trend occurred in the macaque library. All three viruses shared three ISGs, IFN-β, MKX, and BCL2L14 **(Figure 31E)**. While E11 shared many common hits with the other two viruses in the human library, in the macaque library, E11 only shared hits that overlapped with all three viruses and did not share hits with only one

other virus. Instead, EV71 and CVB had two common ISGs, C9orf52 and ZC3HAV1 **(Figure 31E)**.

In addition to comparing antiviral ISGs between the three different viruses within the same species library, our screen allows for comparison of hits between species to determine if these ISGs have any species specificity against enteroviruses. To do this we only analyzed ISGs that were in both libraries to compare the similarities and differences between human and macaque isoforms of each ISG. The comparison of CVB led to the interesting observation that despite the high number of dual coverage ISGs between the two libraries, none were shared in restricting CVB in HBMECs **(Figure 31F)**. However, three human ISGs restricted infection where the macaque isoform did not and three macaque ISGs restricted infection where the human isoform did not restrict. On the other hand, E11 and EV71 had a few shared hits between the libraries. E11 had three shared hits between the human and macaque libraries, TNF Receptor Superfamily Member 10a (TNFRSF10A), BCL2L14, and TNFSF10 **(Figure 31G)**. But still twelve human and two macaque ISGs that restricted infection but their other species counterpart did not. EV71 had four shared hits between the libraries, homeobox protein Mohawk (MKX), ELF1, BCL2L14, and ZC3HAV1 **(Figure 31H)**. Both libraries had eleven ISGs that restricted infection of EV71 but the cross-species isoform did not impact infection. These data suggest a role for species specific ISGs in restricting enteroviruses in HBMECs.

C19orf66 and LAMP3 were interesting ISGs that stuck out from this screen using HBMECs. C19orf66 was only in the human library so we were not able to assess any species differences, however, it only is antiviral against E11 and EV71 and does not impact CVB replication **(Figure 31D)**. Since C19orf66 does not impact CVB replication, it suggests this ISG is acting in a virus specific manner or that CVB has evolved a mechanism to overcome the antiviral

action of C19orf66. Another interesting ISG hit from this screen was LAMP3. LAMP3 was both species specific and enterovirus specific as only the human isoform was antiviral against only CVB and E11 **(Figure 31F and G).**

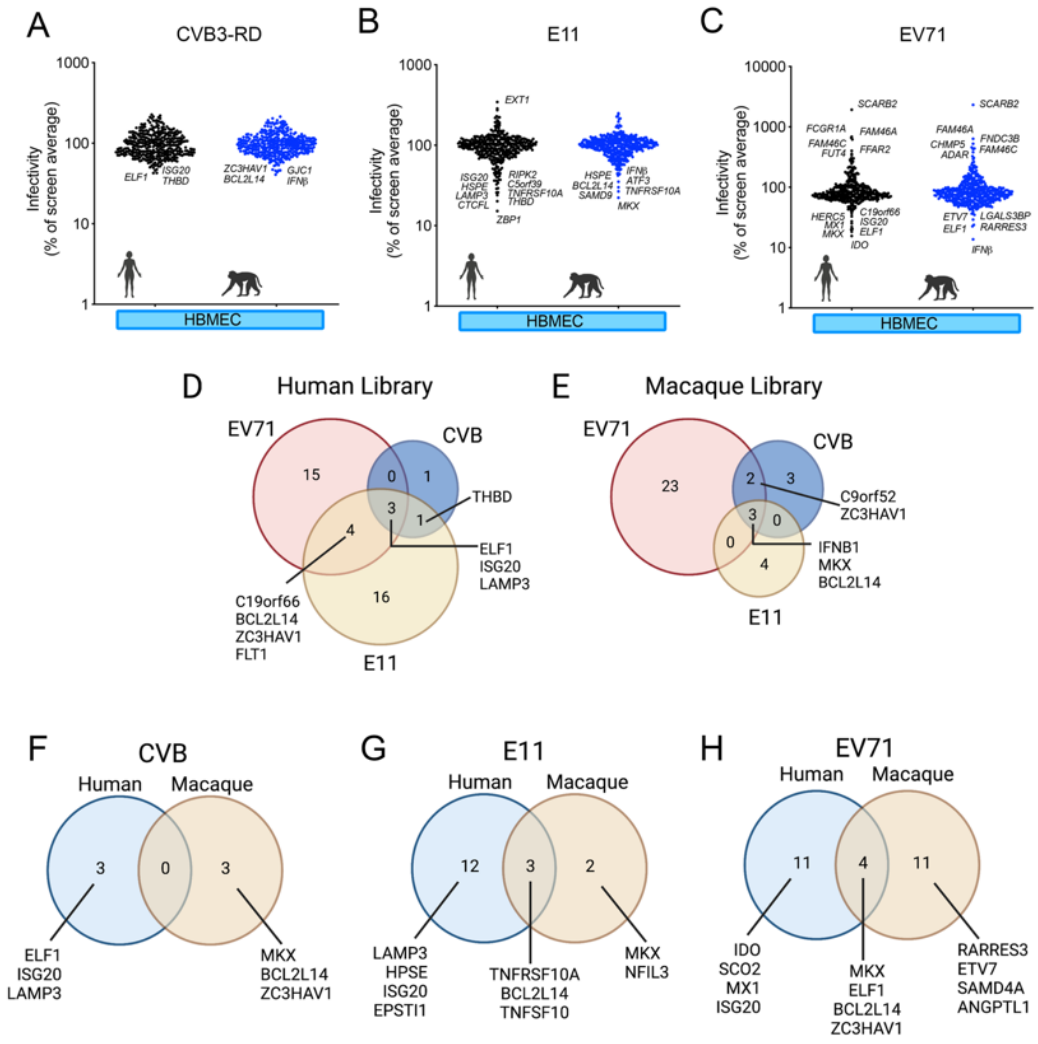

Figure 31 ISG screen identifies several pro-viral and antiviral factors against CVB, E11, and EV71 in human brain microendovascular cells

HBMECs were transduced with the lentiviral library containing an ISG for 48hrs and then infected with CVB **(A)**, E11 **(B)**, or EV71 **(C)** for 16hrs. Cells were washed, trypsinized, and stained with an antibody recognizing double stranded RNA followed by a secondary antibody conjugated to a 488 fluorophore. Percentage of double positive (RFP positive, 488 positive) cells were quantified and analyzed using an Attune Nxt flow cytometer using a 96 well autosampler. Data are shown as percent of infection of empty vector controls. Comparisons of overlapping hits between the viruses within the human (D) or macaque library (E) within

HBMECs. Comparisons of overlapping hits between the human and macaque library for CVB (F), E11 (G), EV71 (H) within HBMECs. Comparisons were made using Venny and Venn diagrams were made using BioRender.com.

6.2.6 ISG screen identifies several proviral and antiviral host factors against CVB, E11, EV71 in human intestinal derived cells, Caco-2 cells

The other cell type we decided to use in our screen were Caco-2 cells. Caco-2 cells have been used to study enterovirus biology of the intestine for many years. They can polarize leading to distinct apical and basolateral surfaces. This leads to localization of cellular proteins that are more like intestinal cells within the GI epithelium. Given that Caco-2 cells are polarized, this could alter ISG function to be more like how it normally acts, potentially helping eliminate false positive antiviral ISGs. These cells are very sensitive to nearly all enterovirus species making them a good model to express potentially restrictive genes. Following the same trend as in the HBMECs, CVB had a small number of ISGs that were antiviral (8 human, 3 macaque), however the factors that were antiviral had a very strong impact on infection reducing infection by 40% or more **(Figure 32A)**. Similarly, E11 only had a few ISGs that restricted infection, but these proteins had a strong antiviral phenotype (7 human, 3 macaque) **(Figure 32B)**. While EV71 had the most ISGs that restricted viral replication (20 human, 13 macaque) **(Figure 32C)**. Compared to the HBMECs, the viruses in Caco-2 cells had far more antiviral ISGs in the human library but fewer antiviral ISGs within the macaque library. Again, similar to HBMECs, SCARB2 increased infection for EV71 and macaque IFN-β restricted all three enteroviruses held true in the Caco-2 cells **(Figure 32)**.

The three viruses also had a higher number of ISGs that overlapped in the human library **(Figure 32D)**. ZC3HAV1 and MDA5 both were able to restrict all three of the viruses. CVB and

EV71 shared two ISG that were unique in controlling their replication, ISG20 and interferon regulatory factor 1 (IRF1). EV71 and E11 shared only one common ISG which was P21 activated kinase 3 (PAK3). E11 and CVB also only shared one common ISG, which was C19orf66 **(Figure 32D)**. While the human library in Caco-2 cells produced many ISG hits that were similar within the viruses, the macaque library yielded only three ISGs that had any commonality between the viruses **(Figure 32E)**. All three viruses were restricted by two common ISGs, ZC3HAV1 and IFN-β, while OAS1 was shared between E11 and CVB **(Figure 32E)**.

Again, we were interested in comparing not only hits between viruses but hits between species within the Caco-2 cells. We took ISGs that were in both libraries and compared the hits. Only one ISG overlapped between the human and macaque libraries as a hit for CVB, ZC3HAV1 **(Figure 32F)**. However, the human ISGs had five that were considered a hit while their macaque isoforms were not. On the other hand, the macaque library had one ISG, 2'-5'-oligoadenylate synthetase 1 (OAS1), that was able to restrict CVB infection **(Figure 32F)**. Along similar lines, E11 had one ISG that overlapped between human and macaque isoforms which also was ZC3HAV1, like CVB, and one macaque ISG that restricted infection while the human isoform did not, OAS1 **(Figure 32G)**. E11 also had four unique ISGs from the human library that restricted infection, including MDA5 and MX Dynamin Like GTPase 2 (MX2) **(Figure 32G)**. EV71 shared two ISGs that were antiviral within both libraries, ZC3HAV1 and IRF1 **(Figure 32H)**. While nine ISGs from the human library and 5 from the macaque library restricted EV71 **(Figure 32H)**.

One overlapping hit that stuck out was ZC3HAV1. Strikingly, both human and macaque ZC3HAV1 was the strongest antiviral factor in Caco-2 cells from the human library for all three viruses **(Figure 32F-H)**. Not surprisingly, ZC3HAV1 has been shown to be antiviral against other viruses such as human cytomegalovirus (CMV) and human immunodeficiency virus type I (HIV-

1)[327,328]. In addition to these two viruses, ZC3HAV1 has also been shown to inhibit echovirus 7 (E7) replication, which is closely related to E11[329]. Two examples of ISGs that exhibited a species specificity were MDA and OAS1. Interestingly, only the human isoform of MDA5, a known cytosolic sensor, was an antiviral hit for all three of the viruses, whereas the macaque isoform did not restrict infection **(Figure 32D)**. This could suggest some species specificity in the mechanism by which MDA5 restricts enterovirus infection. On the other hand, macaque OAS1 was another strong antiviral hit against CVB and E11 but not EV71 **(Figure 32E)**. Interestingly, the human OAS1 was not found to be an antiviral hit (within the cut off set) against any of the enteroviruses tested. Again, this may suggest a different mechanism of restriction leading to this species specificity.

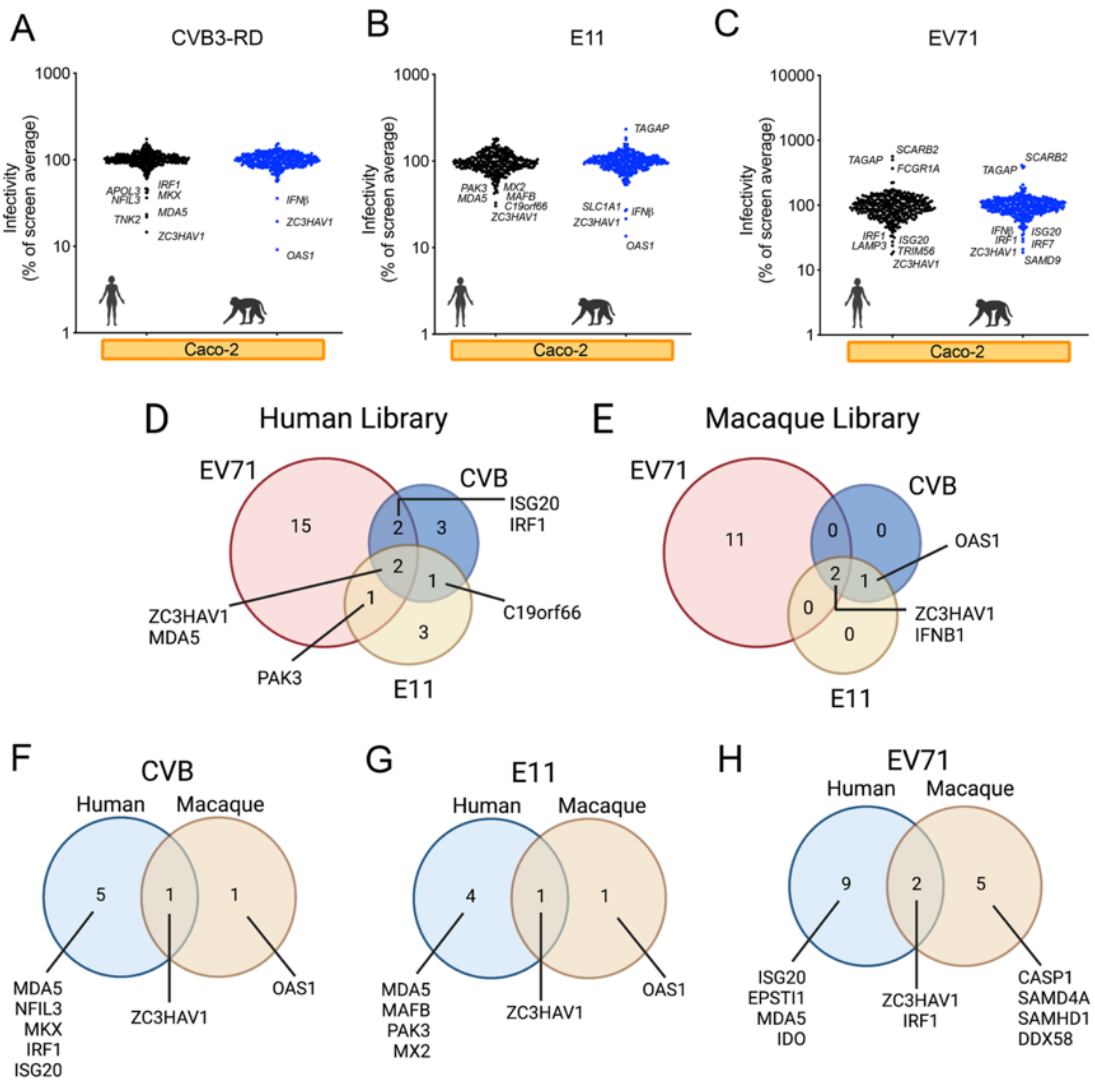

Figure 32 ISG screen identifies several pro-viral and antiviral factors against CVB, E11, and EV71 in human Caco-2 cells

Caco-2 cells were transduced with the lentiviral library containing an ISG for 48hrs and then infected with CVB **(A)** or E11 **(B)** for 8hrs or EV71 **(C)** for 16hrs. Cells were washed, trypsinized, and stained with an antibody recognizing double stranded RNA followed by a secondary antibody conjugated to a 488 fluorophore. Percentage of double positive (RFP positive, 488 positive) cells were quantified and analyzed using an Attune Nxt flow cytometer using a 96 well autosampler. Data are shown as percent of infection of empty vector controls. Comparisons of overlapping hits between the viruses within the human (D) or macaque library (E) within Caco-2 cells. Comparisons of overlapping hits between the human and macaque library for CVB (F), E11 (G), EV71 (H) within Caco-2 cells. Comparisons were made using Venny and Venn diagrams were made using BioRender.com.

6.2.7 Mini hits screen compares laboratory and clinical isolates of enteroviruses

Following analysis of the full screen, we wanted to validate our potential hits using a mini screen. To do this we took any factor that decreased infection by two-fold or more (a potential antiviral factor) or increased infection by 3-fold or more (a potential proviral factor) within any of the three viruses and in either of the two cell types and made a custom mini screen. In addition, if the ISG was a hit in one library but not the other, we included the other species isoform. The mini screen consisted of 79 human ISGs and 80 macaque ISGs. These plates also included many empty vector controls to normalize the screen. Using this mini screen, we wanted to retest our laboratory isolates of enteroviruses in HBMECs and Caco-2 cells to verify potential hit candidates. We also wanted to use this format to test CDC acquired clinical isolates of these same enteroviruses in the two different cell types **(Figure 33)**. Laboratory isolates of enteroviruses have been cultured and passaged for decades. We know that passaging of the virus can change their biology significantly. One example of this is the isolate we use in our screen. This isolate was passaged on rhabdomyosarcoma cells and gained affinity for binding DAF, an attachment factor used for entry[330]. Because laboratory isolates have been cultured and passaged for such a long period of time, we wanted to compare them to more clinically relevant isolates to determine if changes in susceptibility to ISGs have occurred over the passaging time. This screen has never been done to compare laboratory isolates to clinical isolates.

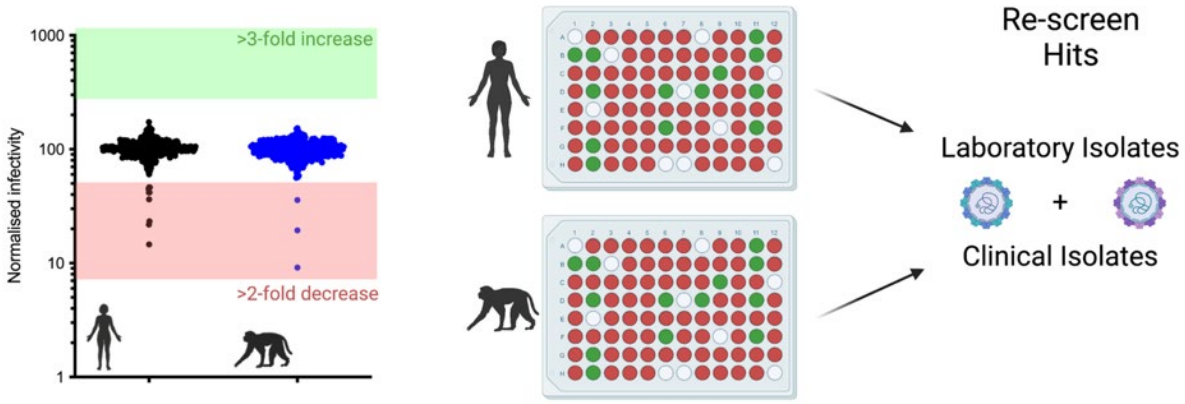

Figure 33 Schematic of the mini hits ISG screen

Visual representation of how factors were picked to be included in the mini hits screen. Any factor that decreased infection by 2-fold or more or increases infection by 3-fold or more was included in the mini hit library screen. This mini library of hits was rescreened with the same laboratory isolates as above as well as clinical isolates. Cells were transduced with the lentiviral library which contained the ISG. Cells were incubated for 48hrs before challenging with the respective enterovirus (laboratory or clinical isolates). 8 or 16hrs post infection, cells were trypsinized, fixed, permeabilized and stained overnight with an antibody recognizing double stranded RNA. Following an overnight incubation with the primary antibody, cells were washed and incubated with an anti-mouse secondary antibody which was conjugated to a 488 fluorophore. Samples were read on an attune flow cytometer with a 96 well autosampler. Figure was made with BioRender.com.

6.2.7.1 Mini hits screen in HBMECs shows similarities and differences of pro- and antiviral factors between lab and clinical isolates of enteroviruses

To validate hits in HBMECs, the mini hits screen as performed using hits that were determined as described above **(Figure 34)**. Many factors that were antiviral in the larger screen, were verified in this smaller targeted screen however some hits did not verify. CVB had five human and eight macaque potential antiviral hits in the original screen while two of those human hits and five of the macaque hits validated in the follow up screen, six additional human and two macaque

ISGs were antiviral **(Figure 34A)**. E11 had twenty-four human and seven macaque potential antiviral hits in the original screen while twelve of those human hits and four of the macaque hits validated in the follow up screen, seven additional human and twelve macaque ISGs were antiviral **(Figure 34B)**. EV71 had twenty-two human and twenty-eight macaque potential antiviral hits in the original screen while eight of those human hits and three of the macaque hits validated in the follow up screen, two additional human and four macaque ISGs were antiviral **(Figure 34C)**.

In addition to retesting the laboratory isolates in this mini screen as a validation method, we used CDC acquired clinical isolates to test their sensitivity to these different pro- and antiviral factors and thus compare them to their older lab adapted counter parts. Because lab isolates have been cultured and passaged for decades and have undergone biological changes that may impact their sensitivity to the antiviral activity of ISGs, we wanted to use clinical isolates which have been minimally passaged and may act differently than the classical lab used isolates. We used a CVB3 isolate that was isolated in 2018 and passaged once **(Figure 34D)**. The clinical isolate of E11 was also isolated in 2018 and passaged twice **(Figure 34E)**. Finally, the clinical isolate of EV71 was isolated in 2018 and passaged four times **(Figure 34F)**.

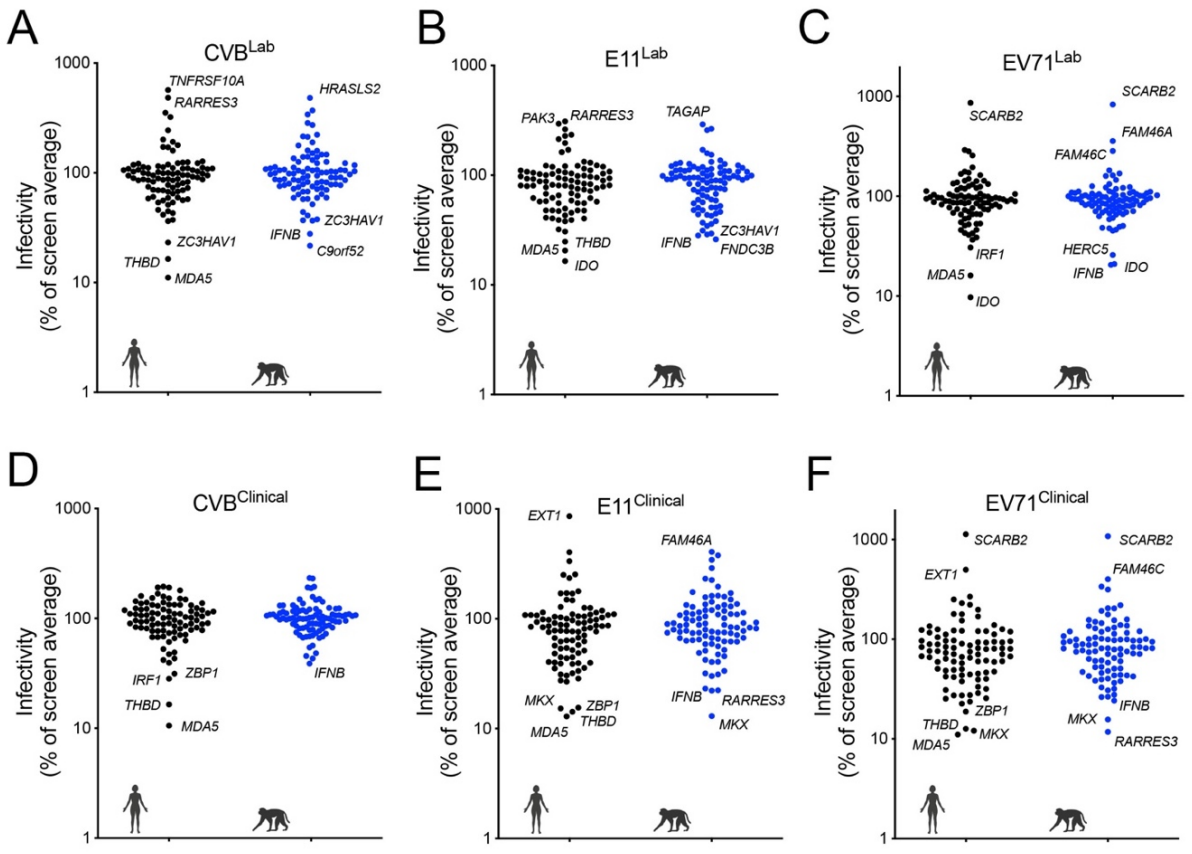

Figure 34 HBMEC hits screen shows similarities and differences between laboratory and clinical isolates

Cells were transduced with the lentiviral library which contained the ISG. Cells were incubated for 48hrs before challenging with the respective enterovirus (laboratory or clinical isolates). 8 or 16hrs post infection, cells were trypsinized, fixed, permeabilized and stained overnight with an antibody recognizing double stranded RNA. Following an overnight incubation with the primary antibody, cells were washed and incubated with an anti-mouse secondary antibody which was conjugated to a 488 fluorophore. Samples were read on an attune flow cytometer with a 96 well autosampler. Data are shown as percent of infection of empty vector controls.

The main goal of using these clinical isolates was to compare their susceptibility to specific ISGs to the laboratory isolates. In HBMECs, the clinical isolate of CVB showed overall slightly less sensitivity to ISGs that were antiviral against the clinical isolate but the main factors that limited replication of the laboratory isolate, also impacted the clinical isolate of CVB **(Figure 35A and D)**. Within the human library, both isolates of CVB were restricted by four ISGs, including

MDA5 and ZBP1 **(Figure 35A)**. While in the macaque library both isolates were restricted by two ISGs, IFN-β and C9orf52 **(Figure 35D)**. The isolates of CVB share a few common ISGs, that have many more that are different. Between both libraries the laboratory isolate of CVB had ten ISGs that did not impact the clinical isolate. On the other hand, the clinical isolate was restricted by seven different ISGs between the two libraries that did not impact the laboratory isolate **(Figure 35A and D)**. While the clinical isolate of CVB seemed to be less sensitive overall to these factors, the clinical isolate of E11 was the opposite and had many more antiviral factors compared to the laboratory isolate **(Figure 35B and E)**. Both isolates shared thirteen ISGs within the human library, including MDA5 and IDO, while sharing seven ISGs within the macaque library, including IFN-β and FNDC3B. The laboratory isolate of E11 was sensitive to fifteen ISGs within the human and macaque libraries **(Figure 35B and E)**. Whereas the clinical isolate of E11 was sensitive to seventeen ISGs **(Figure 35B and E)**. Along a similar trend as E11, the EV71 clinical isolate was much more sensitive to ISGs compared to the laboratory isolate of EV71. Together, between both libraries, both shared eleven common ISGs, including IDO from both libraries, MDA in the human library, and IFN-β from the macaque library **(Figure 35C and F)**. Between both libraries, the laboratory isolate of EV71 only had seven ISGs whereas the clinical isolate of EV71 was sensitive to thirty seven ISGs, twenty 21 human and 16 macaque **(Figure 35C and F)**.

Another goal of our screen was to compare potential similarities and differences between different species. We compared all ISGs that were in both libraries for potential antiviral hits against the clinical isolates. The mini screen contained fifty-three ISGs that were in both libraries. Of these dual coverage ISGs, none overlapped as hits between the human and macaque libraries for the clinical isolate of CVB. Whereas the human isoforms of MDA5 and IRF1 and the macaque isoform of TNFRSF10A were antiviral hits for the clinical isolate of CVB **(Figure 35G)**. The

clinical isolate of E11 had any more ISG hits that overlapped between species. A total of seven ISGs were antiviral for both the human and macaque isoforms of the ISG, which included MKX and LAMP3 **(Figure 35H)**. On the other hand, six human and four macaque ISGs were unique for restricting the clinical isolate of E11 **(Figure 35H)**. Similar to the clinical isolate of E11, the clinical isolate of EV71 also had many ISGs in which both the human and macaque isoforms were both antiviral. The human and macaque libraries had nine overlapping antiviral ISGs against the clinical isolate of EV71, which included MKX and LAMP3 **(Figure 35I)**. While the human library had seven ISGs that were antiviral where their matched macaque isoform was not, the macaque library had eight ISGs that were antiviral where their matched human isoform was not **(Figure 35I)**.

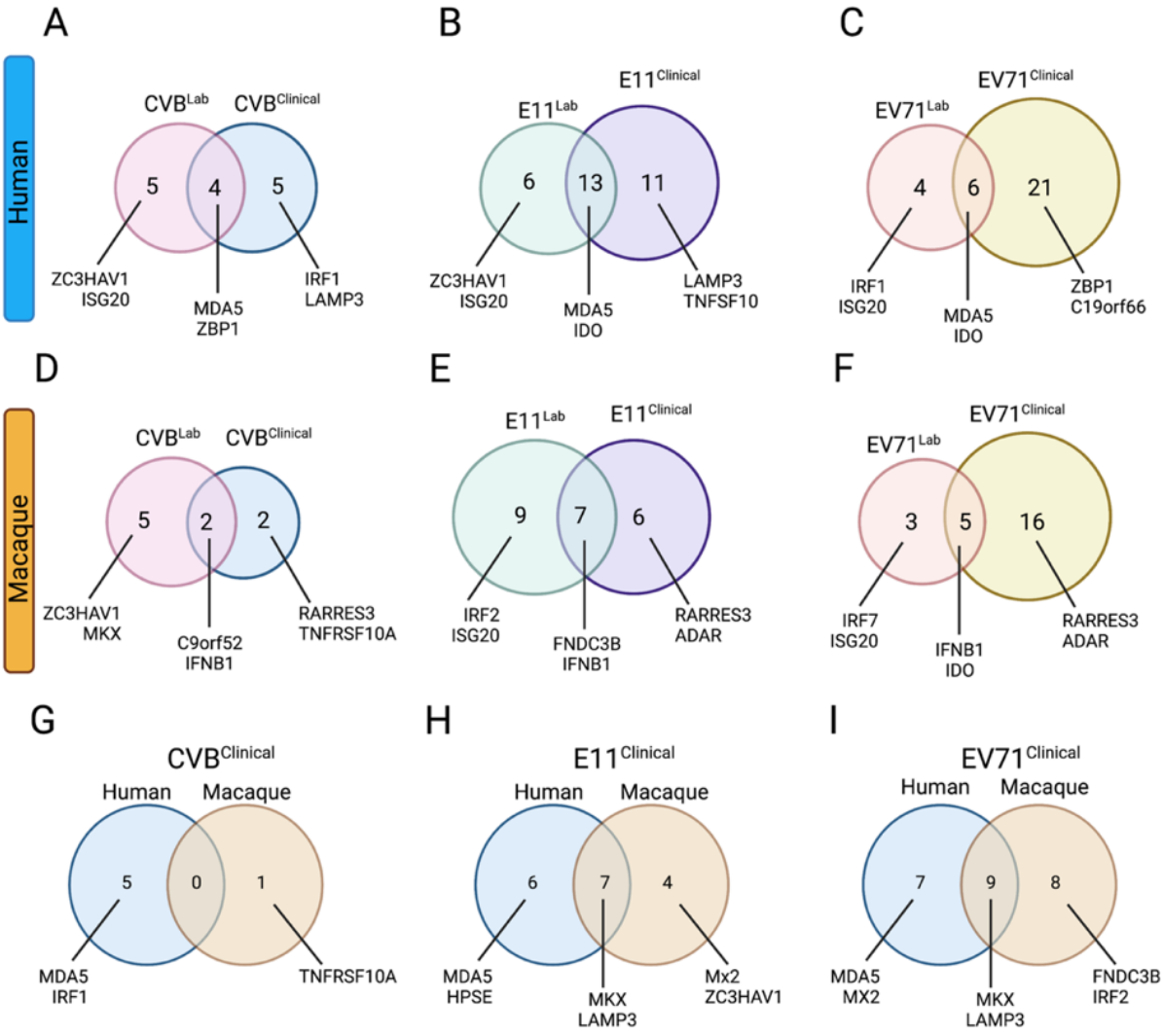

Figure 35 Visual comparision of hits between lab and clinical isolates and across species in HBMECs

Visual comparison of matching laboratory and clinical isolates within HBMECs. (A-C) Comparison of the human library with CVB (A), E11 (B), or EV71 (C) in HBMECs. (D-F) Comparison of the macaque library with CVB (D), E11 (E), or EV71 (F) in HBMECs. Comparisons of overlapping hits between the human and macaque library for the clinical isolates of CVB (G), E11 (H), EV71 (I) within HBMECs. Comparisons were made using Venny and Venn diagrams were made using BioRender.com.

6.2.7.2 Mini hits screen in Caco-2 cells shows similarities and differences in antiviral factors between laboratory and clinical isolates of enteroviruses

To validate hits in Caco2 cells, we used the same custom mini screen as shown in Figure 33 and discussed above. Of the eight human ISGs that were antiviral against CVB in the Caco-2 cells, two were validated in this follow up screen. The macaque library yielded three antiviral ISGs against CVB and all three of these verified in the follow up screen with an additional three that were antiviral in this screen **(Figure 36A)**. E11 had seven human and three macaque potential antiviral hits in the original screen while three of those human hits and three of the macaque hits validated in the follow up screen, three additional human and two macaque ISGs were antiviral **(Figure 36B)**. Of the twenty human ISGs that were antiviral against EV71, only four validated in the follow up screen and two additional ISGs were hits. In the macaque library, fourteen ISGs were antiviral against EV71 in the original screen while six of those validated and three additional ISGs were antiviral in the follow up screen **(Figure 36C)**. Again, because we wanted to determine if laboratory isolates have changed in their susceptibility to different ISGs from the many passages they have undergone, we used recently isolated, minimally passaged, clinical isolates of each virus **(Figure 36D, E, and F)**. The all three clinical isolates had more anti-viral factors compared to the laboratory isolates. The clinical isolate of CVB was very sensitive to C19orf66 and ZC3HAV1 **(Figure 36D)**. The clinical isolate of E11 was also sensitive to ZC3HAV1 and in addition was also sensitive to OAS1 **(Figure 36E)**. The clinical isolate of EV71 had the greatest number of factors it was sensitive to. Some of these included MDA5, MKX, and ZBP1 **(Figure 36F)**.

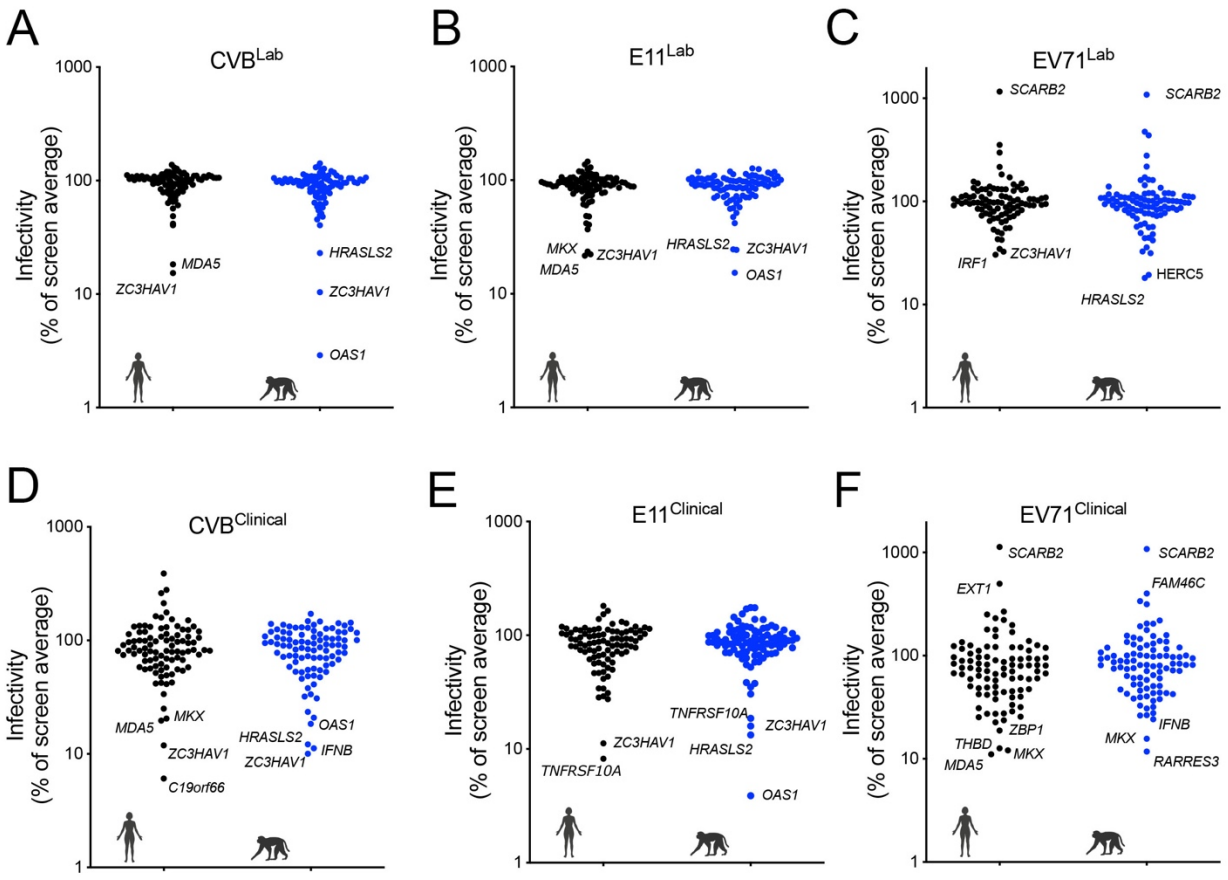

Figure 36 Caco-2 hits screen shows similarities and differences in antiviral factors between laboratory and clinical isolates

Cells were transduced with the lentiviral library which contained the ISG. Cells were incubated for 48hrs before challenging with the respective enterovirus (laboratory or clinical isolates). 8 or 16hrs post infection, cells were trypsinized, fixed, permeabilized and stained overnight with an antibody recognizing double stranded RNA. Following an overnight incubation with the primary antibody, cells were washed and incubated with an anti-mouse secondary antibody which was conjugated to a 488 fluorophore. Samples were read on an attune flow cytometer with a 96 well autosampler. Data are shown as percent of infection of empty vector controls.

The main goal of this mini screen was to validate any potential antiviral hits as well as compare laboratory and clinical isolates. While the laboratory and clinical isolates of CVB had some overlapping antiviral ISGs, the clinical isolate of CVB was sensitive to a higher number of

ISGs. Within the human library, the isolates shared four common antiviral ISGs, such as ZC3HAV1 and MDA5. While the laboratory isolate of CVB was sensitive to OAS1, the clinical isolate had eight antiviral hits, including MKX and DDX58 **(Figure 37A)**. In the macaque library, both isolates shared seven antiviral ISGs, including OAS1 and ZC3HAV1. The laboratory isolate did not have any unique ISGs, but the clinical isolate had seven that restricted infection in the Caco-2 cells **(Figure 37D)**. In both species libraries the isolates of E11 shared five common ISGs per library. Both libraries common hits included ZC3HAV1. The human library included ISGs such as MDA5 and the macaque library included ISGs such as OAS1 **(Figure 37B and E)**. The human library had quite a few different ISGs between the isolates. The laboratory isolate of E11 had three unique ISGs, while the clinical isolate of E11 had nine nonoverlapping ISGs in Caco-2 cells **(Figure 37B)**. Interestingly, EV71 had the least amount of shared antiviral ISGs in both libraries in the Caco-2 cells. In the human library, the EV71 isolates shared four common antiviral ISGs, such as IRF1 and ZC3HAV1. Each of the isolates had two unique ISG hits **(Figure 37C)**. The EV71 isolates only shared one ISG within the macaque library, HRASLS2. While the laboratory isolate of EV71 had eight unique antiviral ISGs and the clinical isolate only had one in the Caco-2 cells **(Figure 37F)**.

As mentioned earlier, one strength of this screen is that we used both a human and macaque ISG library to screen potential antiviral hits. This allows us to compare hits across species to look for species specific antiviral ISGs. The clinical isolate of CVB had an equal number of overlapping and different ISGs for each library **(Figure 37G)**. The human and macaque libraries overlapped with five ISGs, including MKX and ZC3HAV1. The human library had five ISGs that only the human isoform was antiviral against the clinical isolate of CVB, including IRF9 and MDA5. The macaque library had four ISGs that only the macaque isoform was able to restrict infection,

including OAS1 **(Figure 37G)**. The clinical isolate of E11 had three shared ISGs between the two species libraries, including TNFRSF10A and ZC3HAV1 **(Figure 37H)**. The human library has eight unique ISGs, such as MDA5 and IRF1, while the macaque library only had one antiviral ISG, OAS1, against the clinical isolate of E11 **(Figure 37H)**. Finally, the clinical isolate of EV71 only shared one cross species antiviral ISG, HRSL22 **(Figure 37I)**. The human library had five unique ISGs, which included IRF1 and MDA5. But the macaque library did not have any unique ISGs **(Figure 37I)**.

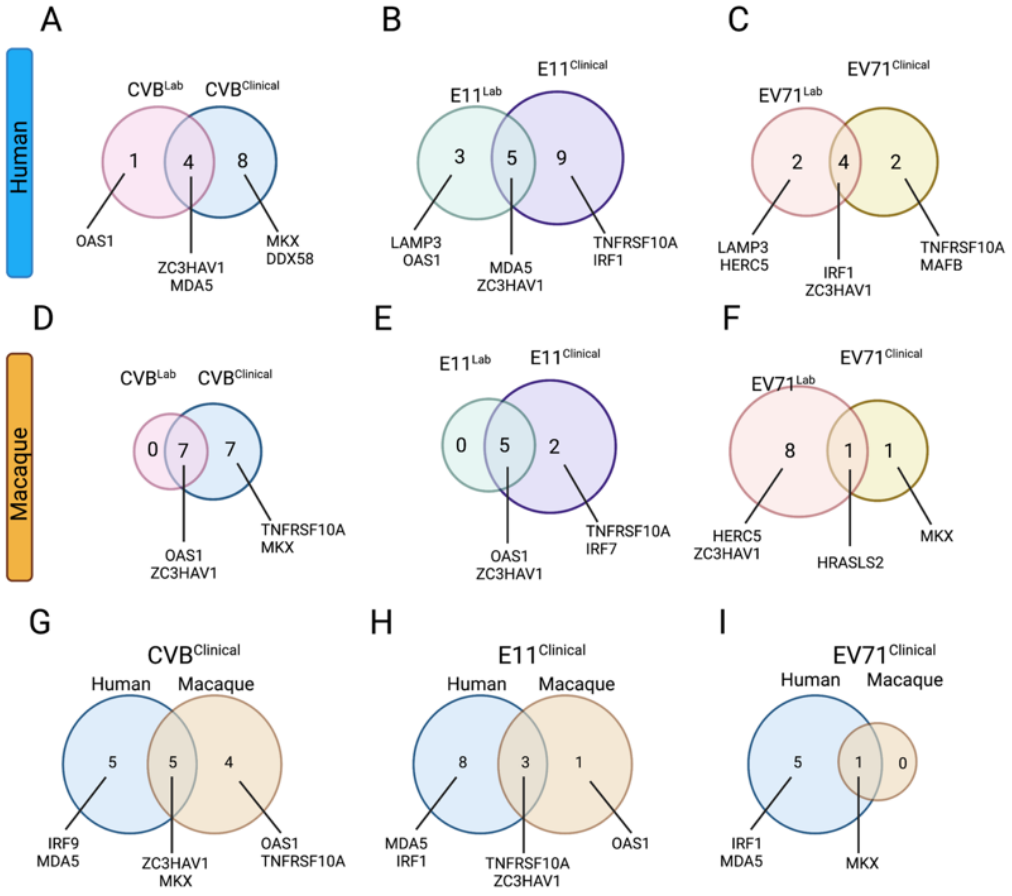

Figure 37 Visual comparision of hits between lab and clinical isolates and across species in Caco-2 cells

Visual comparison of matching laboratory and clinical isolates within Caco-2 cells. (A-C) Comparison of the human library with CVB (A), E11 (B), or EV71 (C) in Caco-2 cells. (D-F) Comparison of the macaque library with CVB (D), E11 (E), or EV71 (F) in Caco-2 cells. Comparisons of overlapping hits between the human and macaque library for the clinical isolates of CVB (G), E11 (H), EV71 (I) within Caco-2 cells. Comparisons were made using Venny and Venn diagrams were made using BioRender.com.

6.3 Discussion

Here, we applied flow cytometry-based comparative screening to identify ISGs that exert antiviral activity. This screening revealed the broad anti-enteroviral activity of a number of ISGs and highlighted the cell-, virus-, and species-selectivity of ISGs. Combined together between the two species libraries and both cell types, the laboratory isolate of CVB had twenty-eight antiviral hits, E11 had forty-eight antiviral hits, and EV71 had thirty-three antiviral hits. In comparison, the clinical isolates of each virus had more hits. The clinical isolate of CVB had thirty-nine antiviral hits, E11 had fifty-eight antiviral hits, and EV71 had fifty-six antiviral hits. These numbers combine both species libraries and cell types without accounting for overlap of genes. Therefore, the number of antiviral genes is likely much lower. However, this shows that we have identified many ISGs with a range of antiviral activity.

Two ISGs that had strong antiviral phenotypes were ZC3HAV1 and OAS1. One of the strongest antiviral factors in the screen was ZC3HAV1, also known as ZAP, which is a zinc finger protein that has been shown to be a cytosolic RNA sensor[331]. In addition, it is known to recruit cellular RNA degradation machinery to specific CG-rich viral RNA as a mechanism to degrade viral RNA and inhibit replication **(Figure 38)**[332]. Due to this known function of ZC3HAV1, it is not surprising that it would be a strong inhibitor of enterovirus replication. While it seems to restrict both laboratory and clinical isolates similarly, it was far more restrictive in Caco-2 cells compared to HBMECs. We don't yet understand why this would be the case. This could be due to timing of viral infection. Caco-2 infections were much shorter than HBMEC infection as Caco-2 cells are more permissive. It could be that the viruses are able to overcome the restriction of ZC3HAV1 during a longer infection cycle. Alternatively, it is possible that an essential binding partner of ZC3HAV1 is not as highly expressed in HBMECs compared to Caco-2 cells.

One binding partner that has been reported to be essential for ZC3HAV1 antiviral activity is TRIM25[333,334]. TRIM25 is an E3 ubiquitin ligase. It is still unclear exactly how TRIM25 interacts with ZC3HAV1 and how together they exhibit antiviral activity. But it is known that TRIM25 depletion significantly reduces ZC3HAV1 antiviral activity[335]. The lab has previously run RNAseq on both HBMECs and Caco-2 cells. Both cell types seem to have moderate levels of TRIM25 (10 RPKM in Caco-2 cells and about 11 RPKM in HBMECs)[59,184], so it does not seem to be the case that ZC3HAV1 activity would be impacted by not having TRIM25 expressed. Another binding partner that has been reported to interact with ZC3HAV1 is OAS3[336]. One study showed that ZC3HAV1 and OAS3 colocalize within infected cells[329]. Additionally, when OAS3 was depleted, ZC3HAV1 antiviral activity was decreased[329]. Within our RNAseq data sets, OAS3 is lowly expressed in both cell types (1 RPKM in Caco-2 and 2 RPKM in HBMECs). Although low expression overall, it seems each cell type has similar levels suggesting that lack of OAS3 expression does not account for the differences in ZC3HAV1 restriction between both cell types.

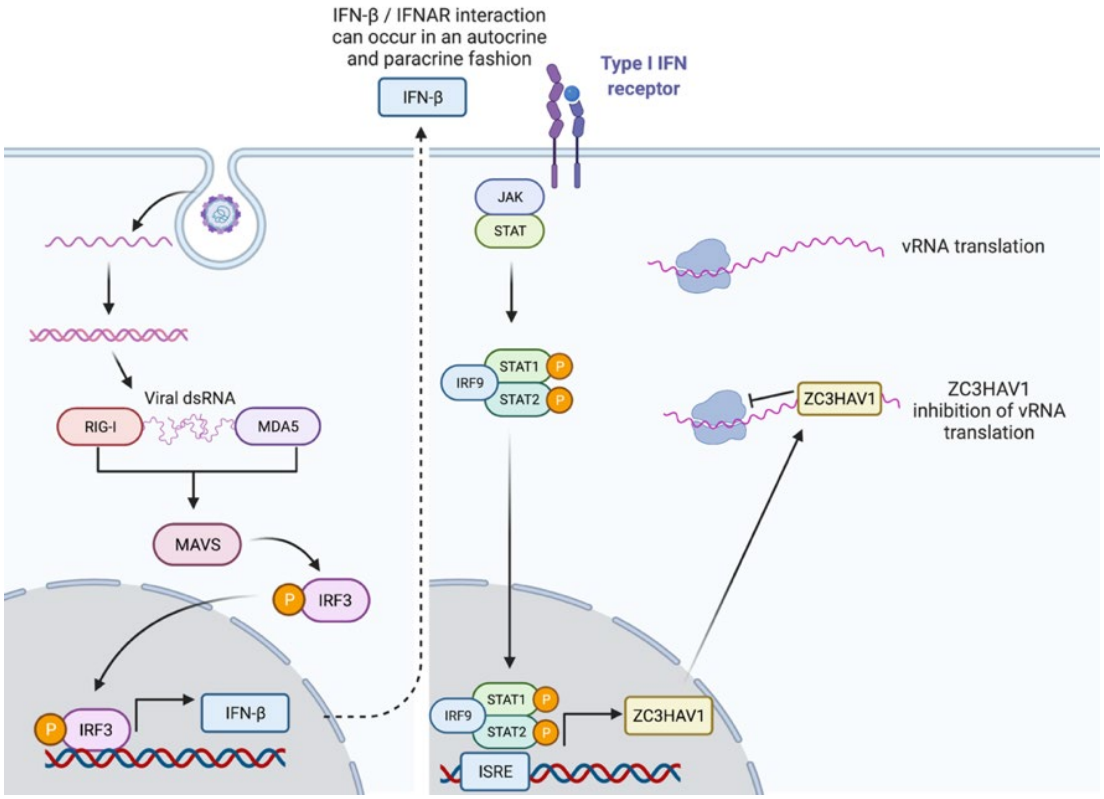

Figure 38 ZC3HAV1 mechanism of antiviral activity

Following virus entry into a cell, viral RNA undergoes replication. The replication intermediate of double stranded RNA (dsRNA) can be detected by many cytosolic host factors which triggers the production of IFN-β. When secreted, IFN-β can act in an autocrine or paracrine manner to induce the production of ISGs, in this case ZC3HAV1. Once induced, ZC3HAV1 binds CG rich RNA and inhibits ribosomal translation of both viral and host cellular RNA. This results in a nonspecific shut down of all translation in the cell, to limit viral replication.

In addition to ZC3HAV1, OAS1 was a major antiviral host factor that restricted CVB and E11 but not EV71. While the macaque isoform of OAS1 was a very strong hit, the human isoform only slightly restricted infection. OAS1, or 2′, 5′-oligoadenylate synthetase 1, is a cytosolic double stranded RNA (dsRNA) sensor which is a catalytically active enzyme. The detection of dsRNA by OAS1 triggers a conformational change in OAS1 to allow the enzymatic pocket to be exposed.

Once this pocket is exposed, OAS1 converts (ATP) to 2'-5'-oligoadenylates[337]. This leads to the activation of RNaseL which degrades cellular and viral RNA **(Figure 39)**[338]. The replication intermediate of enteroviruses is dsRNA, a potential trigger of OAS1 activation. As a result, it would be expected that OAS1 has some antiviral activity against enteroviruses. While human OAS1 has been shown to be antiviral against a broad class of viruses, it has only been shown to be antiviral against CVB and the mechanism is not well understood[339]. While no one has tested the macaque isoform of OAS1 to determine any impact any virus replication. In our screens, we show that the macaque isoform of OAS1 is much more restrictive than the human counterpart, although the human isoform still restricts infection mildly. This suggests a potential species-specific effect on viral replication. In addition, OAS1 is cell type specific with only antiviral activity in Caco-2 cells and not in HBMECs. One major binding partner that is essential for OAS1 antiviral effects is RNaseL. RNaseL is the executioner of RNA degradation of the OAS1 pathway and without this essential binding partner, OAS1 likely would not be able to have any antiviral functions. In Caco-2 cells expression of RNaseL by RNAseq is slightly higher than in HBMECs (2.3 RPKM in Caco-2 cells and 1 RPKM in HBMECs). Although this level of expression is not much different, this could explain why OAS1 seems to have a cell type specific antiviral effect. Interestingly, OAS1 has a virus-specific antiviral effect against CVB and E11 but not EV71. This could be due to the timing of replication. Historically, EV71 has slightly slower replication kinetics compared to CVB and E11 or it could be that EV71 may have evolved some mechanism to evade OAS1 specific antiviral activity. In addition, CVB and E11 are members of the same enterovirus group (enterovirus group B or EVB) where as EV71 is a member of a different enterovirus group (enterovirus group A or EVA). This could be why CVB and E11 are similarly restricted by OAS1 but EV71 is not.

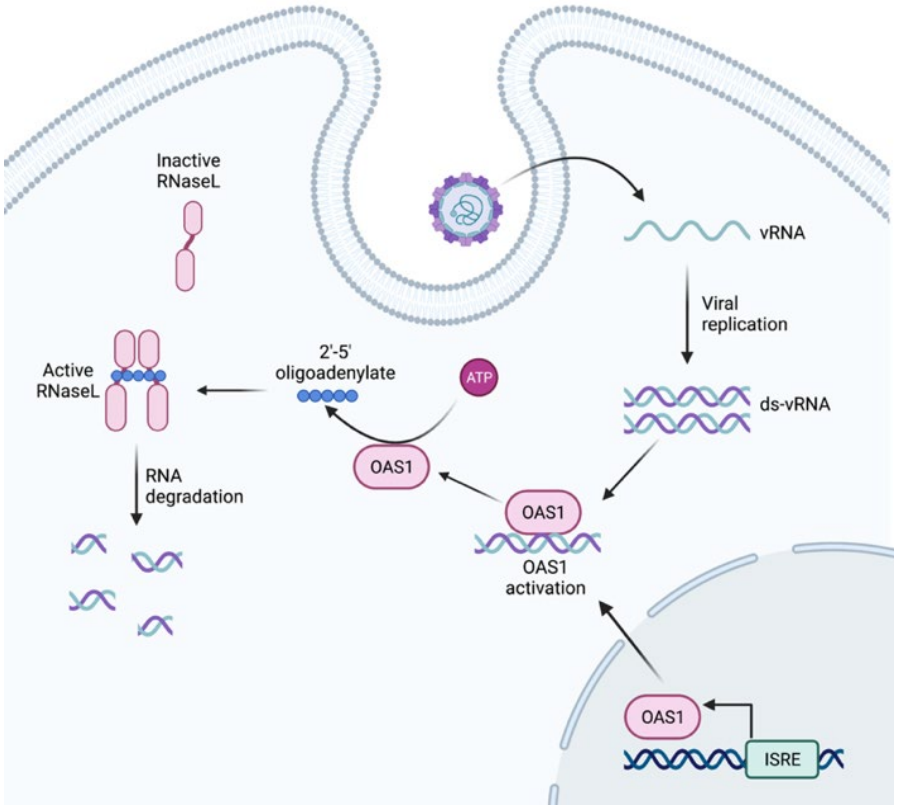

Figure 39 OAS1 mechanism of antiviral activity

As an enterovirus enters the cell and undergoes uncoating to expose its viral RNA. During replication, the double stranded RNA triggers a host innate immune response leading to the induction of hundreds of ISGs such as OAS1. OAS1 binds the double stranded viral RNA which leads to a confirmational change exposing the enzymatic binding pocket. Here, ATP is converted to 2'-5' oligoadenylate. This byproduct activates RNaseL leading to the degradation of both cellular and viral RNA.

While these two host factors seem to be strong antiviral candidates and would be interesting to follow up on more closely, we decided to take a bit broader approach to determine which host factors would be interesting for a follow up study. As mentioned before, enteroviruses encode two viral proteases, $2A^{pro}$ and $3C^{pro}$. These proteases cleave the viral polyprotein after translation as well as act to cleave host proteins. Several studies have mapped the potential protein cleavage sequences of each of the viral proteases[340,341]. While historical studies have suggested that $2A^{pro}$ preferentially cleaves between tyrosine-glycine pairs and $3C^{pro}$ cleaves between glutamine-glycine

pairs[341], other studies have shown the cleavage sites can be more variable. We believe that although some of these host factors are antiviral when overexpressed in the context of our ISG screen, that in the context of a natural infection, the proteases may cleave some of these host factors to try to evade the innate immune response. To investigate this, we took all the ISGs that restricted infection by 60 percent in either cell line or any of the six viruses and mapped potential protease cleavage sites for each host protein **(Table 3)**. Future studies will investigate how these viruses potentially overcome these antiviral ISGs.

Table 3 Potential enterovirus protease cleavage sites

Gene	2A	3C
C19orf66	1	1
IDO	None	None
LAMP3	2	2
MKX	2	3
THBD	4	3
ZBP1	10	None
ZC3HAV1	5	2
ELF1	2	None
Mx1	None	1
Mx2	1	1
OAS1	None	1
HERC5	None	1
ADAR	6	8
CD80	None	1
CTCFL	2	None
DDX58	1	1
HPSE	4	1
RIPK2	1	2
TNFSF10	2	2
TRIM25	1	2
FLT1	1	None
TCF7L2	2	2
MDA5	None	None
IRF1	None	None
ISG20	1	None

6.4 Materials and Methods

6.4.1 Cell lines

HBMECs were obtained from Kwang Sik Kim, Johns Hopkins University, Baltimore, MD, described previously[243], and grown in RPMI-1640 supplemented with 10% FBS (Invitrogen), 10% NuSerum (Corning), non-essential amino acids (Invitrogen), sodium pyruvate, MEM vitamin solution (Invitrogen), and penicillin/streptomycin. Caco-2 cells were purchased from the American Type Culture Collection (ATCC) and cultured in MEM supplemented with 10% FBS, non-essential amino acids, sodium pyruvate, and penicillin/streptomycin. HeLa cells (clone 7B) were provided by Jeffrey Bergelson, Children's Hospital of Philadelphia, PA, and cultured in MEM supplemented with 5% FBS, non-essential amino acids, and penicillin/streptomycin. HEK 293T were purchased from the American Type Culture Collection (ATCC) and cultured in DMEM supplemented with 10% FBS with gentamicin.

6.4.2 Enteroviruses

Experiments were performed with CVB3 (RD strain) and echovirus 11 (Gregory) that were provided by Jeffrey Bergelson and originally obtained from the ATCC. Enterovirus 71 (EV71, 1095) which was obtained from the American Type Culture Collection (ATCC). Clinical isolates used were provided under an MTA with the Centers for Disease Control. The clinical isolates used were CVB3 (USA/2018-2303/STSPRD3 1/18/2019), E11 (USA/2018-23290/STSPRD3 1/15/2019), and EV71 (USA/2018-23092/STSPRD3 1/15/2019). Enteroviruses were propagated

in HeLa cells and purified by ultracentrifugation over a sucrose cushion, as described previously[245].

6.4.3 ISG Screens

The production of ISG-expressing lentiviral pseudoparticles were performed as described previously[325,342,343]. Briefly, ISG-encoding lentiviral vectors (SCRPSY) were generated by cotransfection of 293T cells using polyethyleneimine with 25ng HIV-1 Gag-Pol and 5ng VSV-G expression vectors, along with 250ng of each SCRPSY-based ISG expression vector in a 96-well plate format ($0.35x10^5$ cells/well). Thereafter, culture supernatants were used to transduce the relevant susceptible target cells. HBMEC and Caco-2 cells were plated 24hrs prior to transduction ($1x10^3$ cells/well). Transduced ISG-expressing cells were challenged 48 hours later with the virus and MOI in **Table 4 and Table 5**. Infection was allowed to occur for various amounts of time dependent on the virus and cell type. At the indicated timepoint, cells were washed with 1xdPBS and dissociated using 0.05% trypsin-EDTA for 10 minutes at 37°C. Once disassociated, cells were transferred to a v-bottom 96-well plate. Cells were pelleted at 1000xg for 5 minutes and rinsed in cold 0.5% BSA in PBS. Cells were pelleted and fixed for 20 minutes in IC fixation buffer (Invitrogen). Fixed cells were then pelleted again and resuspended in blocking buffer (0.5% BSA + 1% human serum in 1xPBS) for 15 minutes. The primary antibody against dsRNA was diluted in 1x IC permeabilization buffer (Invitrogen) and incubated overnight at 4°C. The following day, cells were pelleted, washed twice in 0.5% BSA in 1xPBS, and then incubated for 1hr at room temperature with Alexa-Fluor-conjugated secondary antibody (Goat anti-mouse total IgG, 488, Invitrogen). Following incubation, cells were washed twice with 0.5% BSA in 1XPBS and run on

an Attune Nxt flow cytometer (Invitrogen) where the percentage of TagRFP+ and Alexa-Fluor-488+ cells were quantified.

Table 4 Infection conditions for ISG screen in HBMECs

HBMEC		
CVB3-RD	50 pfu/cell	16hrs
E11	100 pfu/cell	16hrs
EV71	10 pfu/cell	16hrs
CDC CVB3	50 pfu/cell	16hrs
CDC E11	100 pfu/cell	16hrs
CDC EV71	300 $TCID_{50}$/cell	16hrs

Table 5 Infection conditions for ISG screen in Caco-2 cells

Caco-2		
CVB3-RD	3 pfu/cell	8hrs
E11	5 pfu/cell	8hrs
EV71	5 pfu/cell	16hrs
CDC CVB3	0.66 pfu/cell	8hrs
CDC E11	6 pfu/cell	8hrs
CDC EV71	1.76 $TCID_{50}$/cell	16hrs

6.4.4 Antibodies

The following antibodies or reagents were used—recombinant anti-dsRNA antibody (provided by Abraham Brass, University of Massachusetts) and described previously[246].

Appendix A Supplementary Figures

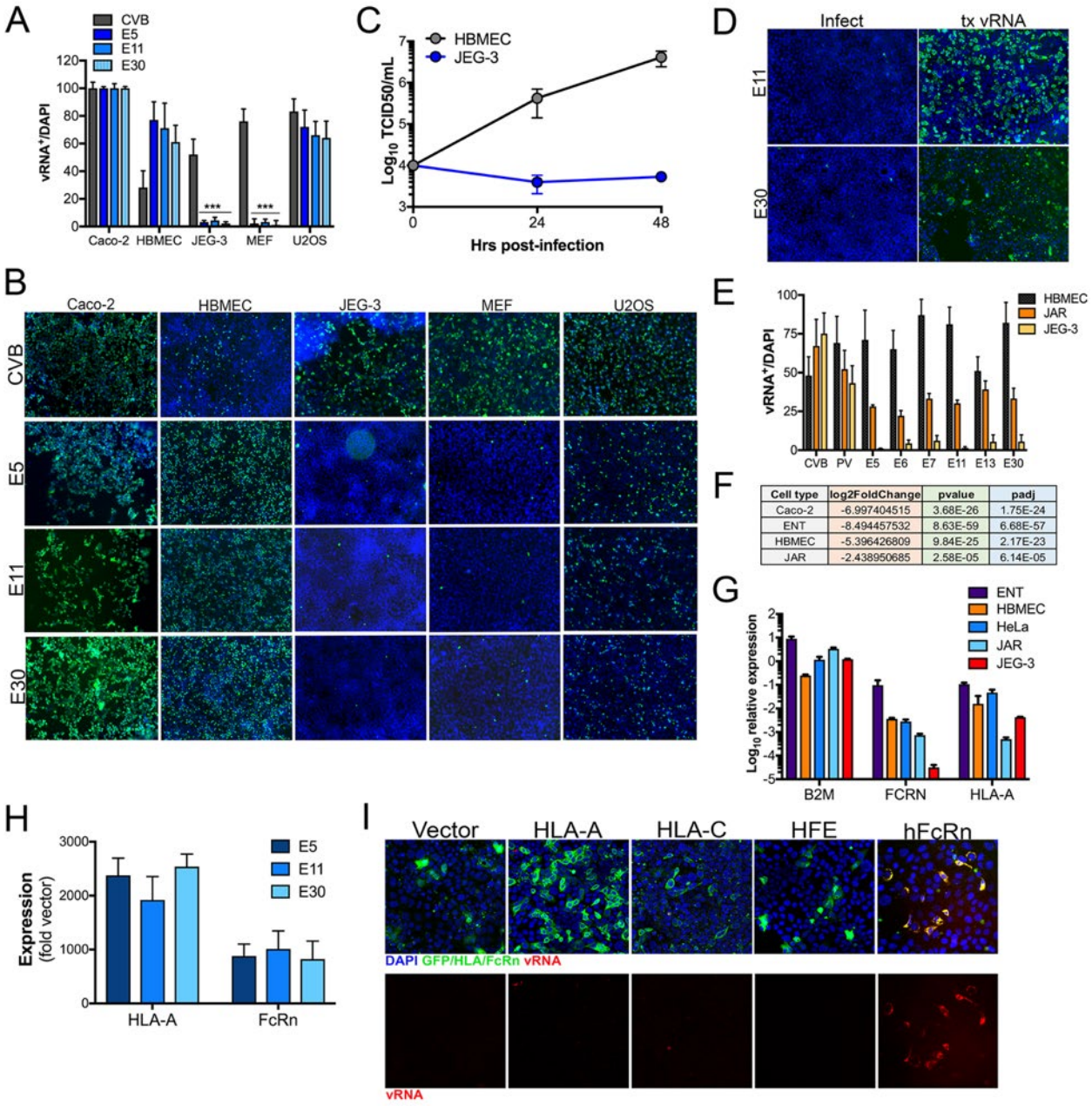

Cell type	log2FoldChange	pvalue	padj
Caco-2	-6.997404515	3.68E-26	1.75E-24
ENT	-8.494457532	8.63E-59	6.68E-57
HBMEC	-5.396426809	9.84E-25	2.17E-23
JAR	-2.438950685	2.58E-05	6.14E-05

Figure 40 JEG-3 cells resist echovirus infection and express low levels of FcRn

(A), The extent of infection of coxsackievirus B (CVB, grey bars) or the indicated echoviruses (blue bars) in Caco-2 cells, HBMEC, JEG-3 cells, mouse embryonic fibroblasts (MEFs), or U2OS cells was assessed by

immunofluorescence microscopy for double-stranded viral RNA at 24hrs post-infection. Shown is quantification of the percent of DAPI-positive nuclei that were also positive for vRNA ($vRNA^+$/DAPI) from a total of >1000 cells. Data are shown as mean ± standard deviation with significance determined with a Kruskal-Wallis test with Dunn's test for multiple comparisons (***$p<0.001$) compared to CVB-infected controls. **(B),** Representative images from the experiments described in (A). DAPI-stained nuclei are shown in blue and vRNA in green. **(C),** Production of infectious E11 from HeLa or JEG-3 cells (shown as $\log_{10}$ TCID50/mL) at the indicated hours post-infection. **(D),** JEG-3 cells were infected with E11 or E30 for 24hrs or were transfected with 100ng of infectious vRNA for 24hrs. The extent of viral replication was assessed by immunostaining for double-stranded vRNA (green). DAPI-stained nuclei are shown in blue. **(E),** Comparison of infection of HBMEC, JAR cells, or JEG-3 cells by CVB, poliovirus (PV), or the indicated echovirus. The extent of infection was assessed at 24hrs post-infection by immunofluorescence microscopy for vRNA as described in (A). Data are shown as mean ± standard deviation from >1000 quantified cells. **(F),** Differential expression analysis of FcRn between JEG-3 cells and either Caco-2 cells, primary human enteroids (ENT), HBMEC, or JAR cells as determined by the DeSeq2 package in R. Shown is the log2 fold change, p-value, and adjusted p-value (p_{adj}). **(G),** RT-qPCR profiling of the level of expression of β2M (B2M), FcRn, or HLA-A in the indicated cell type. Data are shown as $\log_{10}$ relative expression normalized to actin and are shown as mean ± standard deviation. **(H),** Expression of HLA-A and FcRn as assessed by RT-qPCR analyses 24hrs following transfection of JEG-3 cells with cDNA expression vectors expressing HLA-A or FcRn. The level of expression is normalized to vector-transfected cells and was normalize to actin using the delta C_t method. **(I),** JEG-3 cells were transfected with vector control (pcDNA-EGFP), HLA-A, HLA-C, EGFP-fused HFE, or FcRn, infected with E11 24hrs post-infection, then infection assessed 24hrs post-infection by immunofluorescence microscopy for double-stranded vRNA (red, bottom). The extent of transfection was assessed using an antibody against HLA-A, HLA-C, or FcRn (in green) or by EGFP fluorescence (vector control and HFE).

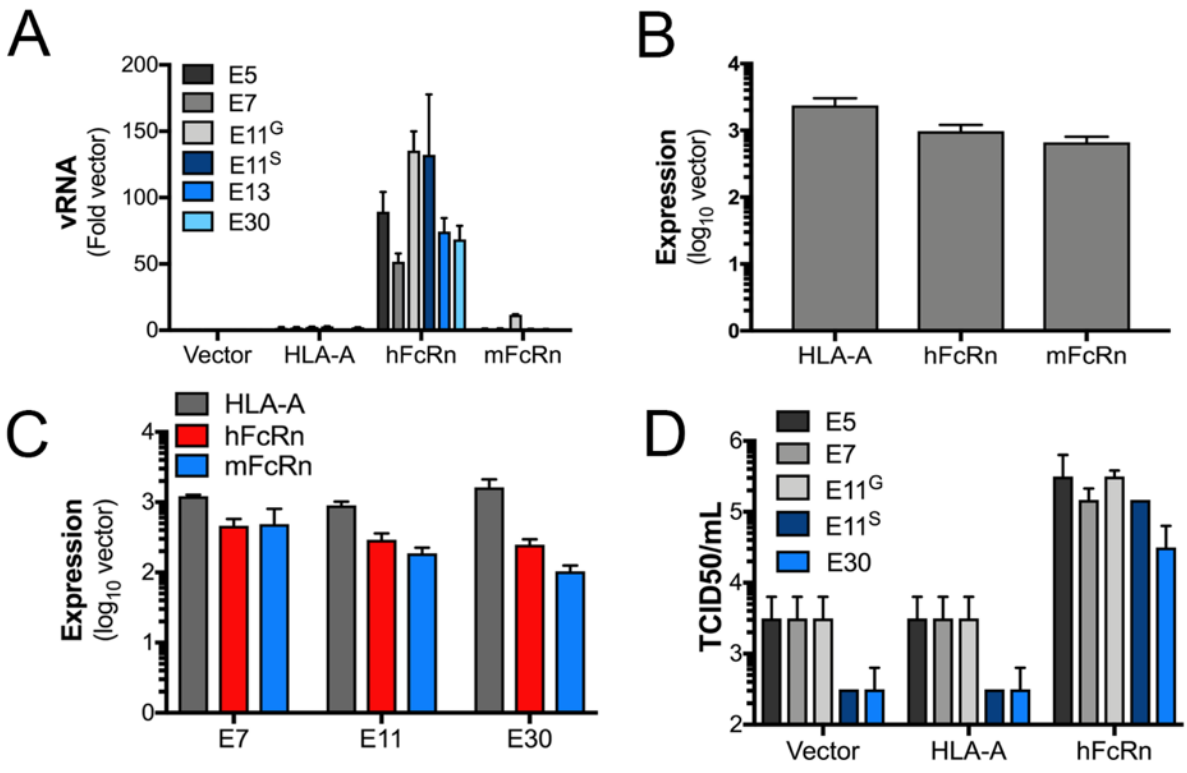

Figure 41 Expression of human, but not mouse, FcRn restores echovirus infection in human and mouse cells

(A), JEG-3 cells were transfected with vector control (pcDNA), human HLA-A, human FcRn (hFcRn), or mouse FcRn (mFcRn) for 24hrs and then infected with the indicated echovirus for 24h ($E11^G$ Gregory strain and $E11^S$ Silva strain). Viral replication was assessed by RT-qPCR for vRNA and is shown as mean ± standard deviation normalized to vector-transfected controls. **(B),** The relative expression of HLA-A, hFcRn, and mFcRn in JEG-3 cells transfected with vector control, HLA-A, hFcRn, or mFcRn as assessed by RT-qPCR for the indicated transcript 24hrs following transfection. Data are shown as mean ± standard deviation normalized to vector-transfected controls. **(C),** The relative expression of HLA-A, hFcRn, and mFcRn in MEFs transfected with vector control, HLA-A, hFcRn, or mFcRn as assessed by RT-qPCR for the indicated transcript 24hrs following transfection. Data are shown as mean ± standard deviation normalized to vector-transfected controls. **(D),** CHO cells were transfected with vector control (pcDNA), human HLA-A or human FcRn (hFcRn) for 24hrs and then infected with the indicated echovirus for 24hrs. Viral titers (log_{10} TCID50/mL) are shown as mean ± standard deviation with significance determined.

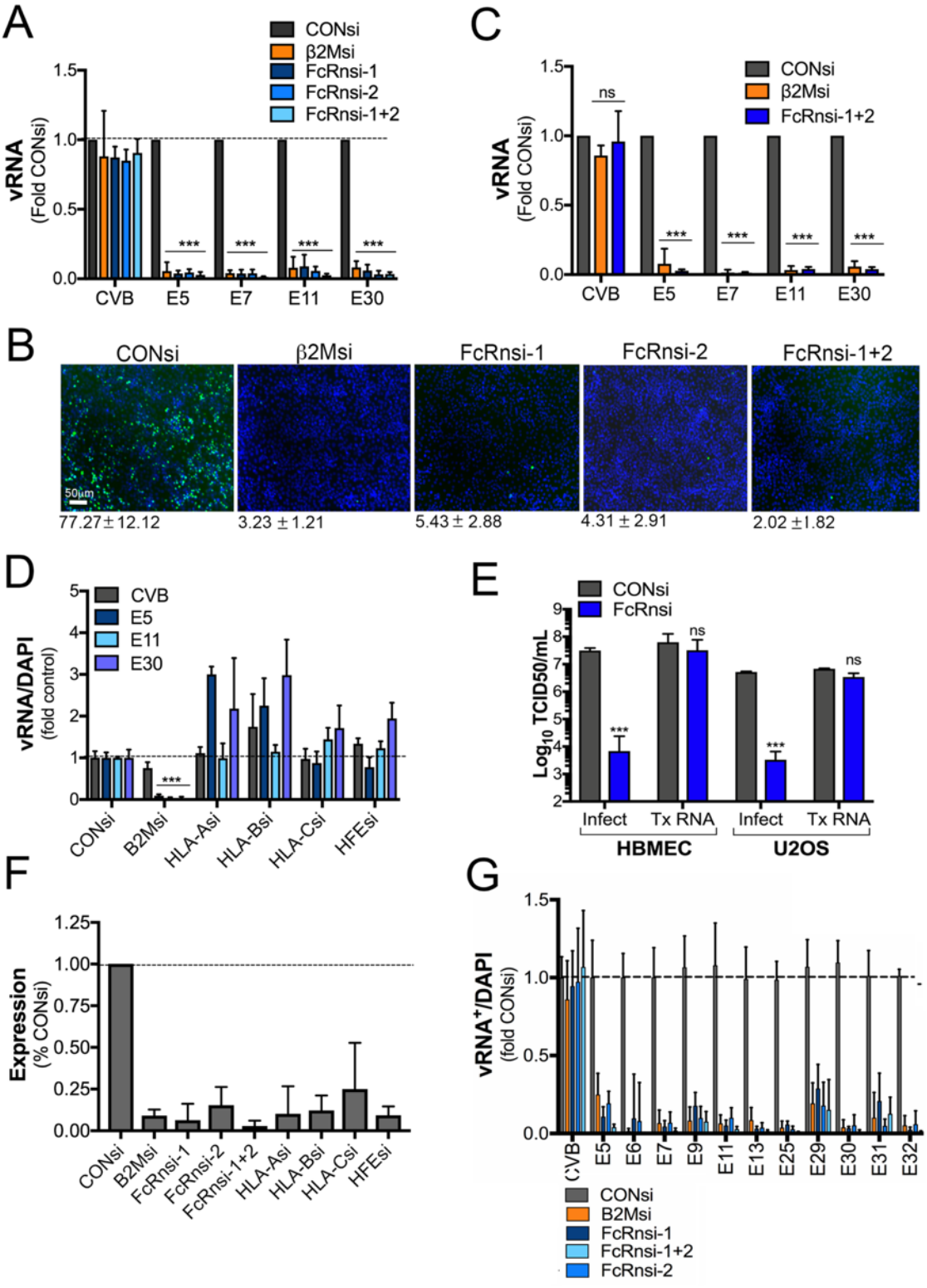

Figure 42 Loss of FcRn expression reduces echovirus infection

(A), HBMEC were transfected with an siRNA against β2M (orange bar) or two independent siRNAs against in combination (FcRn 1+2) (blue bars), or scrambled control siRNA (CONsi, grey bars) for 48hrs and then infected with CVB or the indicated echovirus for an additional 16hrs. Shown is the extent of viral replication as assessed by RT-qPCR for viral RNA. Data are shown as mean ± standard deviation percent change from CONsi-transfected cells. Significance determined with a Kruskal-Wallis test with Dunn's test for multiple comparisons (***p<0.001). **(B),** HBMEC transfected with siRNAs as described in (A) were infected with E11 for 24hrs and then infection assessed by immunofluorescence microscopy for double stranded viral RNA (a replication intermediate, in green). DAPI-stained nuclei are shown in blue. The average level of infection (as determined by the percent of DAPI-stained nuclei that were positive for vRNA is shown at bottom as mean ± standard deviation. **(C),** U2OS cells were transfected with an siRNA against β2M (orange bar) or two independent siRNAs against FcRn (FcRn-1 and FcRn-2) alone or in combination (FcRn 1+2) (blue bars), or scrambled control siRNA (CONsi, grey bars) for 48hrs and then infected with CVB or the indicated echovirus for an additional 16hrs. Shown is the extent of viral replication as assessed by RT-qPCR for viral RNA. Data are shown as mean ± standard deviation percent change from CONsi-transfected cells. Significance determined with a Kruskal-Wallis test with Dunn's test for multiple comparisons (***p<0.001). **(D),** HBMEC were transfected with an siRNA against β 2M or siRNAs against HLA-A, HLA-B, HLA-C, or HFE for 48hrs and then infected with CVB (grey bars) or the indicated immunofluorescence microscopy for double-stranded viral RNA at 24hrs post-infection. Shown is quantification of the percent of DAPI-positive nuclei that were also positive for vRNA ($vRNA^+$/DAPI) from a total of >1000 cells. Data are shown as mean ± standard deviation percent change from CONsi-transfected cells. Significance determined with a Kruskal-Wallis test with Dunn's test for multiple comparisons (***p<0.001**). (E)**HBMEC transfected with scrambled control siRNA (CONsi) or FcRn siRNA (FcRnsi-1) for 48hrs were infected with E11 or transfected with infectious E11 viral RNA for an additional 24hrs. Shown are viral titers (log_{10} TCID50/mL) as mean ± standard deviation with significance determined with a t-test (***p<0.001, ns not significant). **(F),** Efficiency of silencing of β2M, FcRn, HLA-A, HLA-B, HLA-C, or HFE in HBMEC transfected with the indicated siRNA for 48hrs. Data are shown as mean ± standard deviation percent change from CONsi-transfected cells. Level of knockdown of target transcripts was assessed in each experiment described, with data across experiments shown here. **(G),** High-content based RNAi screening in 96-well plates for infection in HBMEC transfected with an siRNA against B2M (orange bar) or two independent siRNAs against FcRn (FcRn-1 and FcRn-2) alone or in combination (FcRn 1+2) (blue bars), or scrambled control siRNA (CONsi, grey bars) for 48hrs

and then infected with CVB or the indicated echovirus for an additional 16hrs. Cells were fixed and immunostained for double-stranded viral RNA and counterstained with DAPI. Automated image analysis using an inverted IX83 Olympus microscope and CellSens software using the MultiPoint module was performed from four independent sites from three independent wells and the extent of infection measured as the percent of $vRNA^{+}$ cells over total cells (DAPI) using the CellSens Count and Measure module. Data are shown as mean ± standard deviation percent change from CONsi-transfected cells from >2000 total cells.

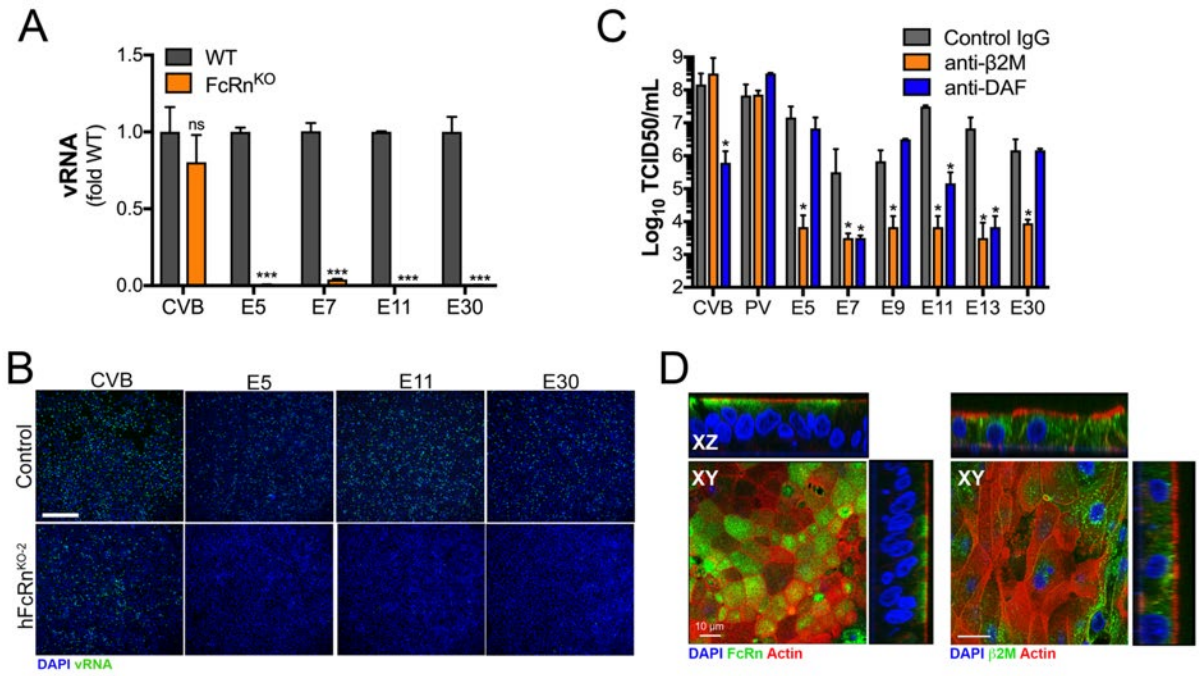

Figure 43 Loss of FcRn expression and blocking antibodies against B2M reduce echovirus infection

(A,B), Control (wild-type, WT) U2OS cells or cells lacking FcRn expressing by CRISPR/Cas9-mediated gene editing ($FcRn^{KO}$) were infected with the indicated echoviruses, or with CVB as a control, and infection assessed by RT-qPCR for viral RNA (A) or immunostaining for double stranded viral RNA (in green, B) ~20hrs post-infection. DAPI-stained nuclei are shown in blue in (B). Data in (A) are shown as mean ± standard deviation as fold change from WT with significance determined with a Kruskal-Wallis test with Dunn's test for multiple comparisons **(C),** U2OS cells were incubated with anti- β2M or anti-DAF (IF7 clone) monoclonal antibodies or control IgG for 60min at 4oC, then pre-adsorbed with coxsackievirus B (CVB), poliovirus (PV), or the indicated echovirus in the presence of the indicated antibody for an additional 1hr at 4°C. Cells were washed with 1x PBS or media (IF7) and then infected at 37°C for 24hrs. Shown are viral titers (log10 TCID50/mL) as mean ± standard deviation with Significance determined with a Kruskal-Wallis test with Dunn's test for multiple comparisons (*$p<0.05$). **(D),** Confocal micrographs of fetal-derived primary human intestinal epithelial (HIE) cells immunostained for FcRn (left, green) or β2M (right, green) and counterstained for actin (left and right, red). DAPI-stained nuclei are shown in blue. Three-dimensional cross-sections are shown at top and right. Scale bars at bottom left.

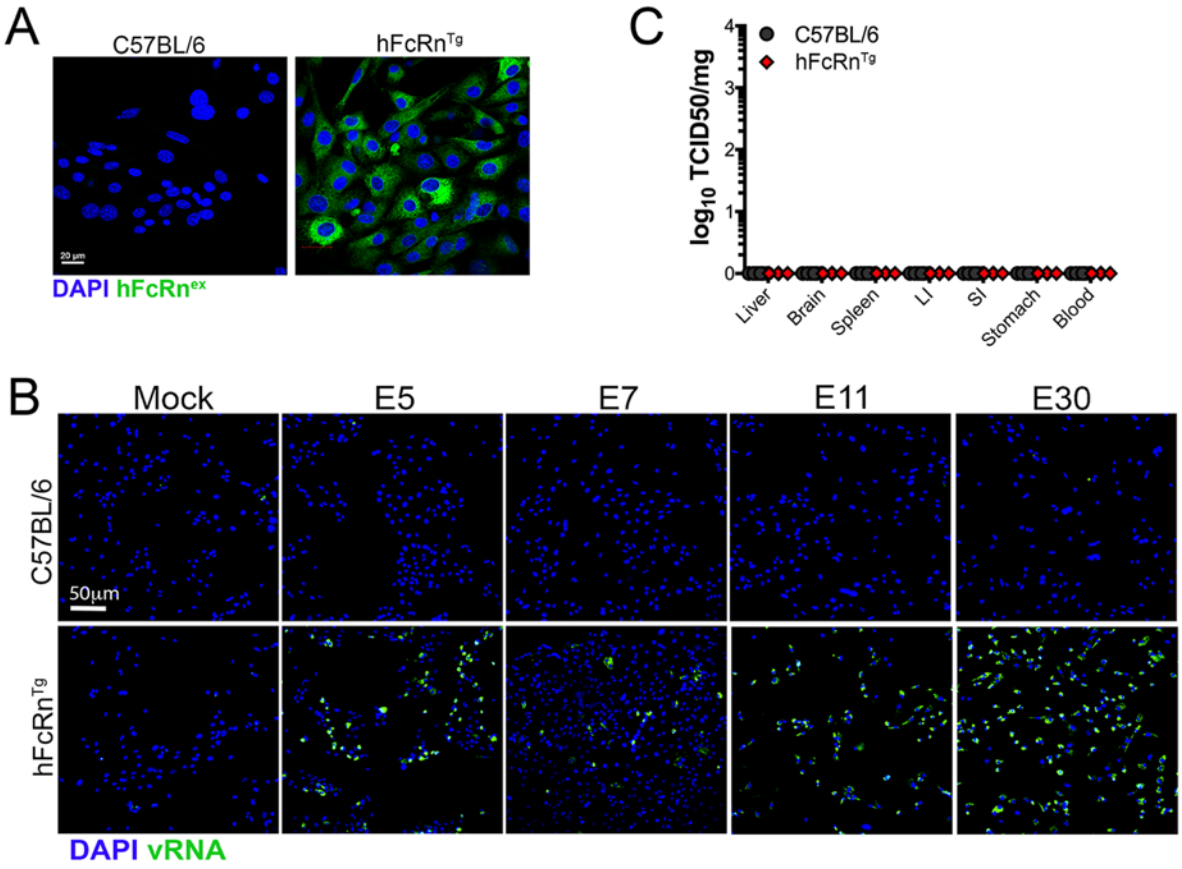

Figure 44 Expression of hFcRn in primary mouse cells renders cells sensitive to infection

(A), Primary fibroblasts were isolated from wild-type C57Bl/6 mice or mice expressing human FcRn ($hFcRn^{Tg}$) were immunostained with an antibody recognizing the extracellular domain of hFcRn (in green). DAPI-stained nuclei are shown in blue. **(B),** Primary fibroblasts isolated from WT or $hFcRn^{Tg}$ mice were infected with the indicated echovirus, or mock infected as a control, and then the level of viral replication assessed at 6hrs post-infection by immunofluorescence microscopy for double-stranded viral RNA (a replication intermediate, in green). DAPI-stained nuclei in blue. (**C**), E11 titers in the indicated tissues as determined by TCID50 assays from WT C57Bl/6 mice (5 total) of $hFcRn^{Tg}$ mice (5 total) infected for 3 days by oral gavage with 10^6 E11 particles.

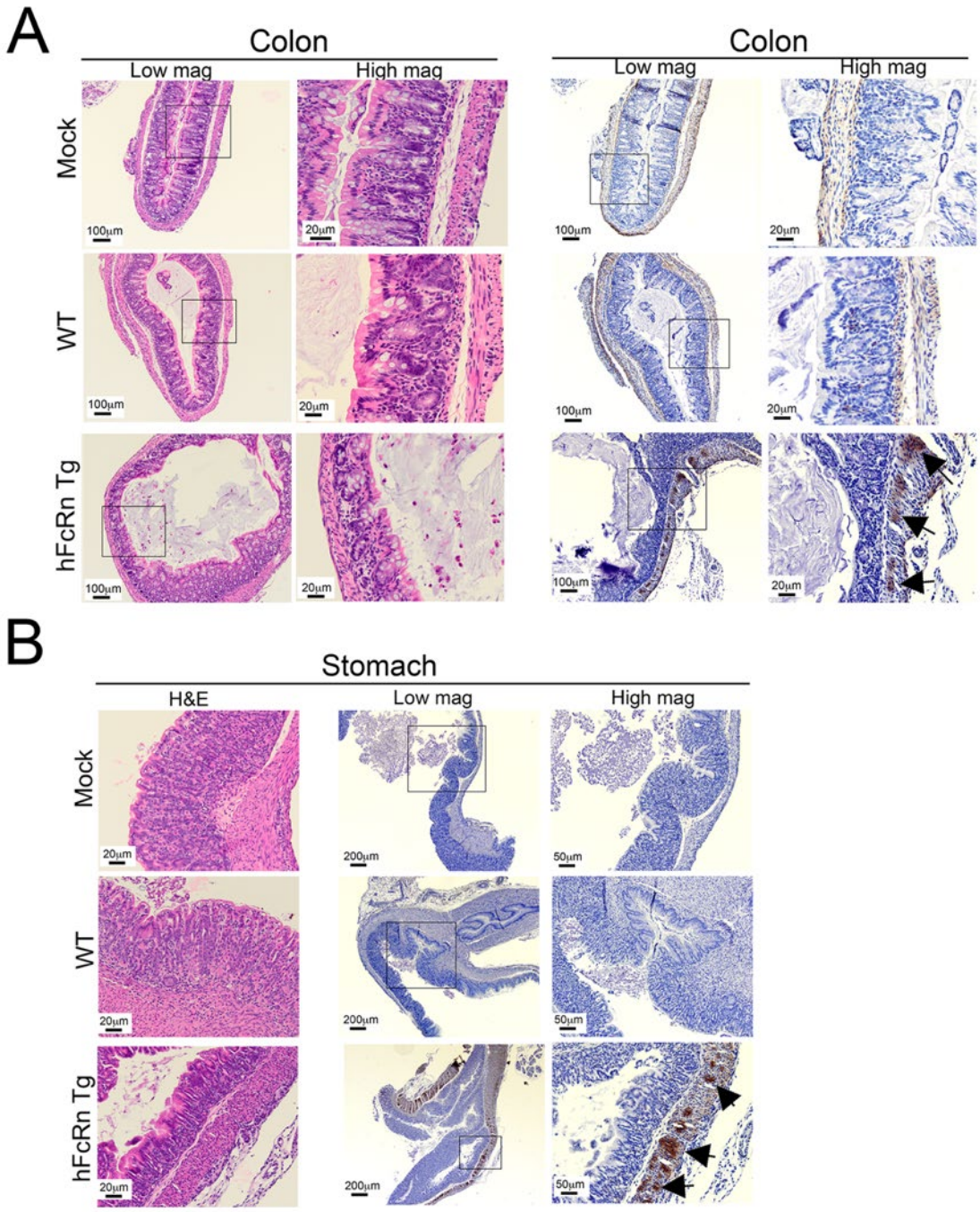

Figure 45 E11 infection in tissue isolated from hFcRn mice by immunohistochemistry

(A, B) Immunohistochemistry for E11 using an antibody recognizing the VP1 capsid protein from WT or hFcRn^{Tg} inoculated by oral gavage. Shown are H&E (left) and IHC (right) from colon (A) or stomach (B) in animals infected for 7 days. Black arrows denote positive staining for VP1. Scale bars are shown at bottom left.

Table 6 RT-qPCR primers used in the study

Target	Forward Primer	Reverse Primer
B2M	AAGGACTGGTCTTTCTATCTC	GATCCCACTTAACTATCTTGG
FcRn	GAAACCTGGAGTGGAAGGAG	CGGAGGGTAGAAGGAGAAGG
HFE	CAGGGTTCAAGAGGAGC	TCTAGTTTTGTCTCCTTCCC
HLA-A	CTTGTAAAGTGAGACAGC	CTTCAAGTCACAAAGCGAAG
HLA-B	CTGAGATGCAGGATTTCTTC	GAACAAGAAAGATGACTGGG
HLA-C	CATCACTTGTAAAGCCTGAG	CTCTTGAAGTCACAAAGGAG

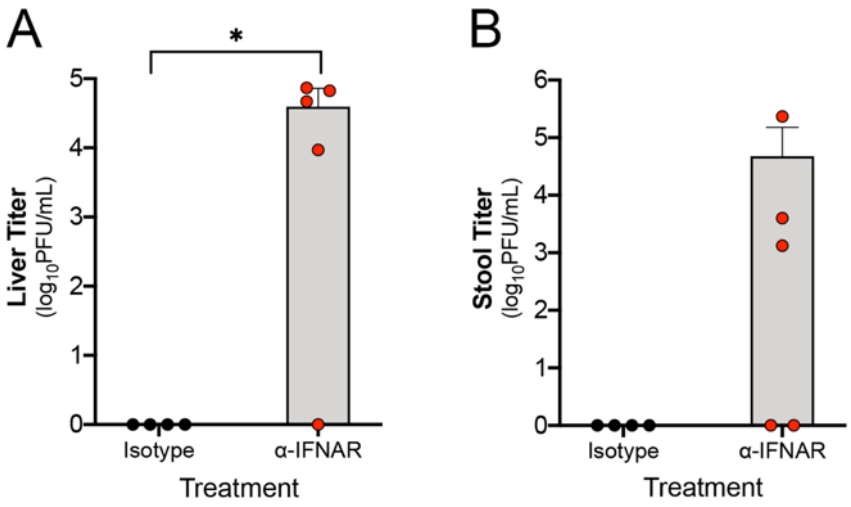

Figure 46 Treatment with an anti-IFNAR blocking antibody renders hFcRn^{Tg32} animals susceptible to E11

hFcRn^{Tg32} adult animals treated with an isotype antibody (black, 4 animals) or an anti-IFNAR blocking antibody (red, 5 animals) were inoculated with E11 by the IP route and sacrificed 72 hours post inoculation. Viral titers in the liver **(A)** or stool **(B)**. Data are shown with significance determined with a Mann-Whitney test (*$p<0.05$).

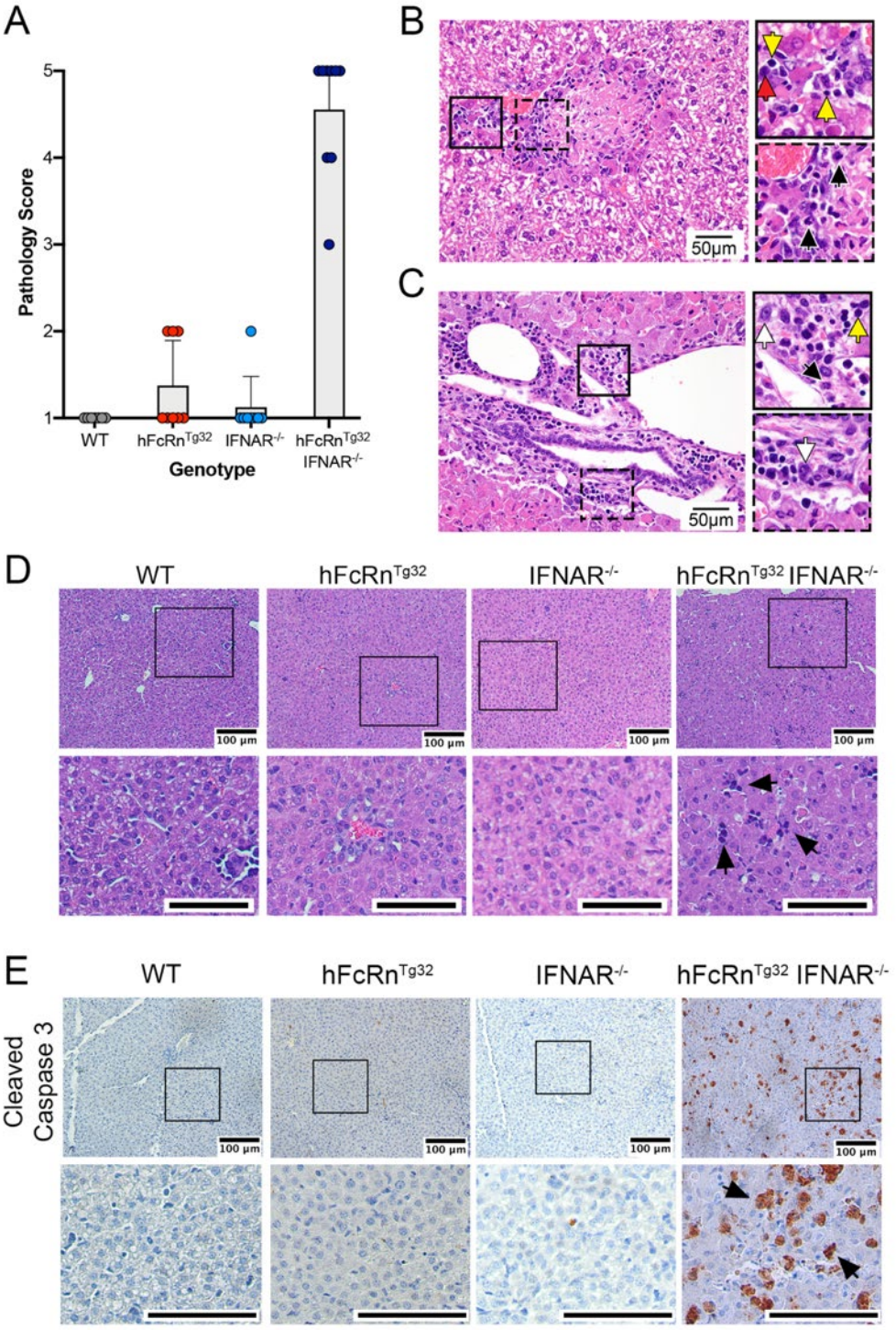

Figure 47 hFcRn^{Tg32}-IFNAR$^{-/-}$ animals have immune infiltrates and cell death in the liver

WT (grey, 7 animals), hFcRn^{Tg32} (light blue, 8 animals), IFNAR$^{-/-}$ (dark blue, 8 animals), and hFcRn^{Tg32}-IFNAR$^{-/-}$ (red, 6 animals) adult mice were inoculated with E11 by the IP route and sacrificed 72 hours post inoculation. H&E sections were scored blinded to genotype based on severity of pathology using the following descriptors—1: retention of normal architecture and cord

pattern of liver cells, 2: Immune infiltration, 3: spotty/random hepatocytolysis, 4: punctate aggregates of hepatocyte necrosis/death, and 5: confluent areas of hepatocyte necrosis and death. **(B)** Representative image of an hFcRn^{Tg32}-IFNAR$^{-/-}$ adult animal with areas of necrosis are often associated with neutrophils (black arrows) around the edge, along with lymphocytes (yellow arrows), and plasma cells (red arrows). **(C)** Representative image of an hFcRn^{Tg32}-IFNAR$^{-/-}$ adult animal around the portal areas with macrophages (white arrows), lymphocytes (yellow arrows), and neutrophils (black arrows). **(D)** H&E staining of the livers in suckling mice. C57Bl/6 (WT), hFcRn^{Tg32}, IFNAR$^{-/-}$, and hFcRn^{Tg32}-IFNAR$^{-/-}$ suckling mice were IP inoculated with 10^4 E11 and sacrificed 72 hours post inoculation. Black arrows denote areas of immune infiltration. **(E)** Immunohistochemistry using an antibody recognizing the cleaved form of caspase 3 from the livers of a representative suckling mouse of each genotype as indicated. Black arrows denote positive staining. Scale bars (100μm) are shown at bottom right.

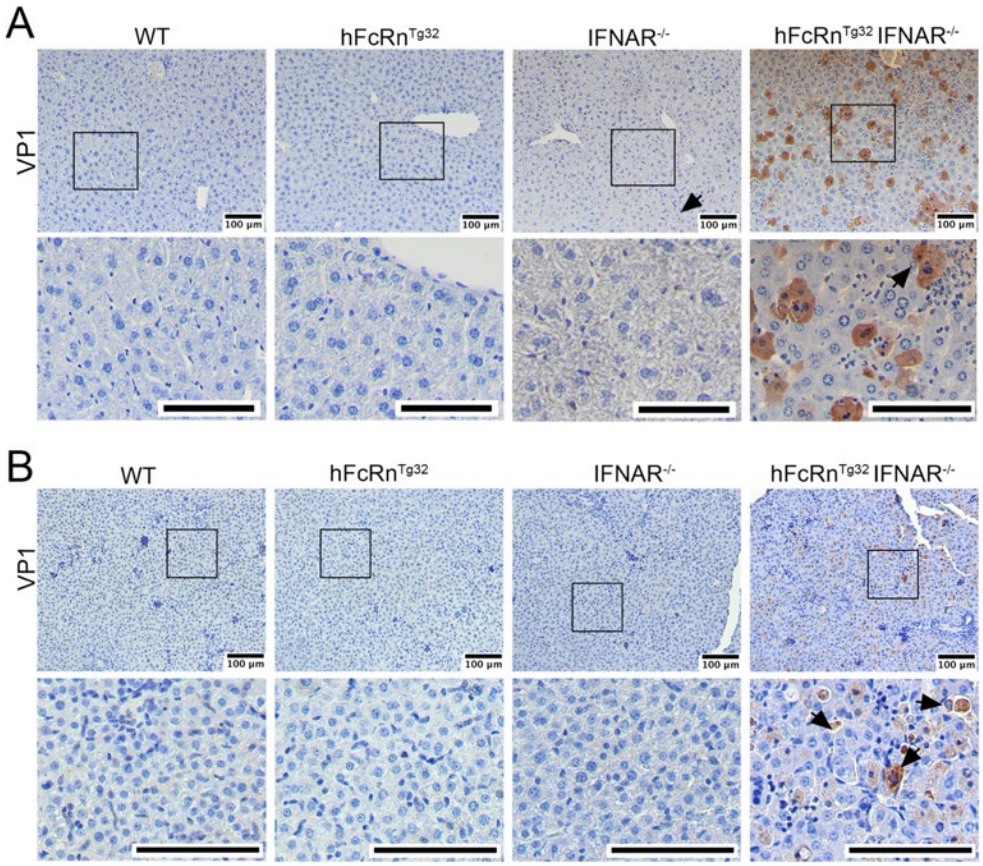

Figure 48 The liver hFcRn^{Tg32}-IFNAR$^{-/-}$ animals has replicating E11

WT, hFcRn^{Tg32}, IFNAR$^{-/-}$, and hFcRn^{Tg32}-IFNAR adult **(A)** or suckling mice **(B)** were inoculated with E11 by the IP route and sacrificed 72 hours post-inoculation. Shown are representative images from immunohistochemistry for E11 using an antibody recognizing the VP1 capsid protein from the livers of a representative animal of each genotype.

Table 7 Probes used to detect echovirus 11 RNA

Probe Pair		
B4P1	CCTCAACCTACCTCCAAC AATTTGTGTTGATACTTGCGCTCCCAT	TCAAGCCGGTTTCATGCGCACCGG TATTCTCACCATATTCGCTTC
B4P2	CCTCAACCTACCTCCAACAAC TG CCTATTTGCCGAGTTGGATGC	TGAACTTACCAGGGTCTTGTGAAAA ATTCTCACCATATTCGCTTC
B4P3	CCTCAACCTACCTCCAACAATGTC ACTGTACCCACACTCTTCAGC	AGTTACCTAGTGTTATGGATCGCA CATTCTCACCATATTCGCTTC
B4P4	CCTCAACCTACCTCCAACAAT GGC CTCATTGTCTTTCAGGTACTC	CAGGGTGGGTTGGTTGATCTTCAG CATTCTCACCATATTCGCTTC
B4P5	CCTCAACCTACCTCCAACAAC CGGGAATTTCCACCACCACCCGGG	CGAAGAGCCCCATATCTTTTAGGG CATTCTCACCATATT CGCTTC
B4P6	CCTCAACCTACCTCCAACAACCTG ATGGAATTTAGATGCATTACA	CCGGTACACAGACCACTAGCAAGC AATTCTCACCATATTCGCTTC
B4P7	CCTCAACCTACCTCCAACAAA GAATTTCTTAGCGGTCTCCCCCTC	TGTTGGTCCCATTTGTGCTGGTAG AATTCTCACCATATTCGCTTC
B4P8	CCTCAACCTACCTCCAACAAAATT TATCCACTGATGTGGGTATAT	CGATGGTGGCGCAGTTATTGGTGC GATTCTCACCATATTCGCTTC
B4P9	CCTCAACCTACCTCCAACAAGTAC AAAGGGAATAATCATTAGTGT	TGGATGAATCTGAAGAATAGTCTA AATTCTCACCATATTCGCTTC
B4P10	CCTCAACCTACCTCCAACAAATCC TTGCAATGAGGTTGAGAGCCT	TGCTACCCGGTGTATTCATGACAG GATTCTCACCATATTCGCTTC

Table 8 Probes used to detecct mouse albumin RNA

Probe Pair		
B1P1	GAGGAGGGCAGCAAACGGAA GAGGAGGAGGAGAAAGGTTACCCAC	CCTGGAAAAAGCAGAGCCGGAGACG TA GAAGAGTCTTCCTTTACG
B1P2	GAGGAGGGCAGCAAACGGAA TGCTCATCGTATGAGCATTTCTGGA	TCTGTTACTTCCTGCACTAATTTGG TA GAAGAGTCTTCCTTTACG
B1P3	GAGGAGGGCAGCAAACGGAA TCACGGAGGTTTGGAATGGCACACA	CAGCAGTCAGCCAGTTCACCATAGT TA GAAGAGTCTTCCTTTACG
B1P4	GAGGAGGGCAGCAAACGGAA GGCATAGAAATAAGGATGTCTTCTG	CTGCTCAGCATAGTAAAGAAGTTCT TA GAAGAGTCTTCCTTTACG
B1P5	GAGGAGGGCAGCAAACGGAA CACTCCTTGTTGACTTTGGTCAGGT	GCGCATTCCAGCAGGTCACCATGGC TA GAAGAGTCTTCCTTTACG
B1P6	GAGGAGGGCAGCAAACGGAA CTTGCACACTTCCTGGTCCTCAACA	GAAGACATCCTTGGCCTCAGCATAG TA GAAGAGTCTTCCTTTACG
B1P7	GAGGAGGGCAGCAAACGGAA GCTCTTCTACAAGAGGCTGAAATTC	CACAGTTGGTTTTGACCAAGTTCTT TA GAAGAGTCTTCCTTTACG
B1P8	GAGGAGGGCAGCAAACGGAA AGACAGATAGTCTTCCACACAAGGC	CAGCAGACACACACGGTTCAGGATT TA GAAGAGTCTTCCTTTACG
B1P9	GAGGAGGGCAGCAAACGGAA TCTCAGCTTTAAACTCTTTGGGGAC	TGCAGATATCAGAGTGGAAGGTGAA TA GAAGAGTCTTCCTTTACG
B1P10	GAGGAGGGCAGCAAACGGAA GAGAAGGTTGTGGTTGTGATGTGTT	TCATGTCTTTTTTTCTCAGGGTAGC TA GAAGAGTCTTCCTTTACG

Table 9 Probes used to detect mouse IFN-β RNA

Probe Pair		
B1P1	GAGGAGGGCAGCAAACGGAA AGCCTGGCTTCCATCATGAACAACA	GCAGGAACGCAGCGTGGAGGATCCA TAGAAGAGTCTTCCTTTACG
B1P2	GAGGAGGGCAGCAAACGGAA GAGGTTGATCTTTCCATTCAGCTGC	AGGGATCTTGAAGTCCGCCCTGTAG TAGAAGAGTCTTCCTTTACG
B1P3	GAGGAGGGCAGCAAACGGAA CTTGGATGGCAAAGGCAGTGTAACT	AGACAAGAAAGACATTCTGGAGCAT TAGAAGAGTCTTCCTTTACG
B1P4	GAGGAGGGCAGCAAACGGAA GTACTGTCTTCAGAAACACTGTCTG	TCAATCTTTCCTCTTGCTTTTCCTC TAGAAGAGTCTTCCTTTACG
B1P5	GAGGAGGGCAGCAAACGGAA TGCACCCTCCAGTAATAGCTCTTCA	TTGTACTTCATGAGTTTAAGGTACC TAGAAGAGTCTTCCTTTACG
B1P6	GAGGAGGGCAGCAAACGGAA GCATCAACTGACAGGTCTTCAGTTT	TTGCCTGCAACCACCACTCATTCTG TAGAAGAGTCTTCCTTTACG
B1P7	GAGGAGGGCAGCAAACGGAA TAAAAAGTAGAAAATAATTTAAATT	TTATTTTCTGAGGTTAAAAAGTTTA TAGAAGAGTCTTCCTTTACG

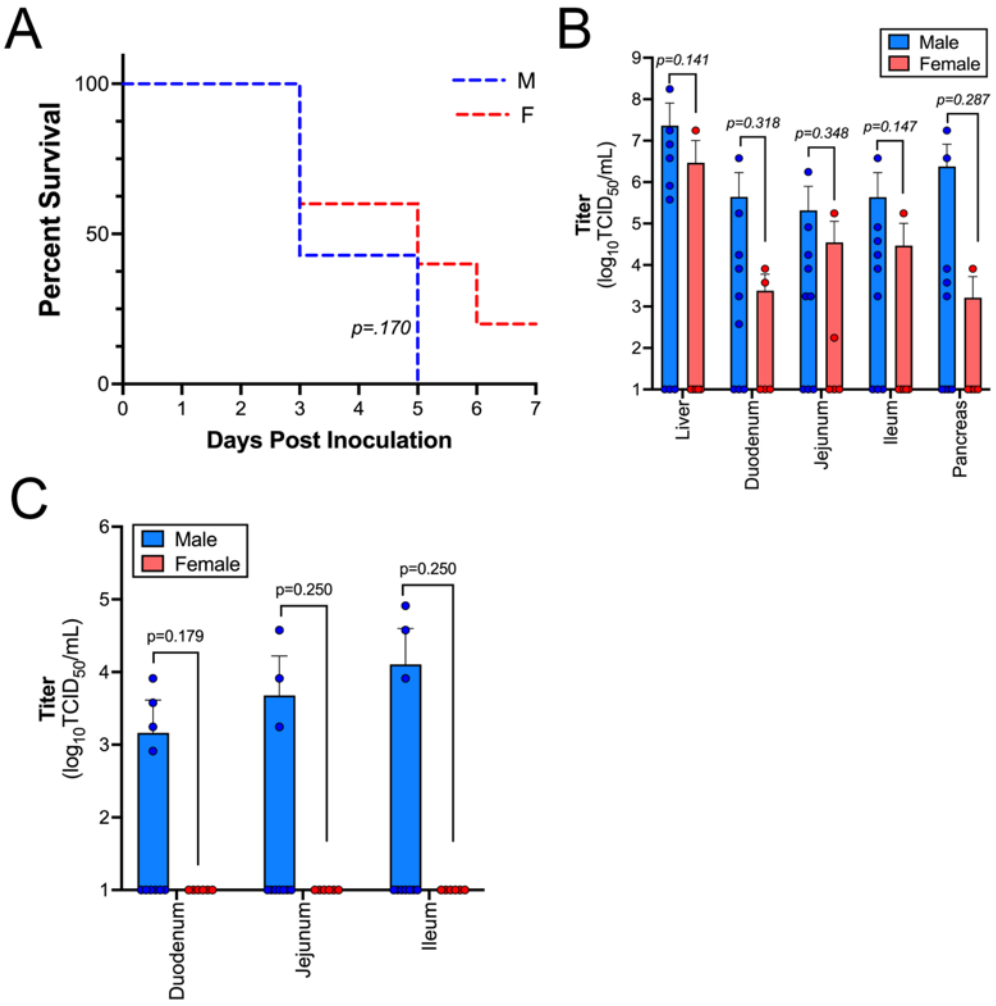

Figure 49 Sex differences

7-day old pups were orally inoculated with 10^6 PFU of E5. **(A)** Survival curve of hFcRn^{Tg32}-IFNAR$^{-/-}$ animals broken down by sex. A log-rank test was used to analyze the statistical difference of the survival rate. **(B)** Viral titers of hFcRn^{Tg32}-IFNAR$^{-/-}$ animals at 3dpi broken down by sex. **(C)** Viral titers of hFcRn^{Tg32}-IFNLR$^{-/-}$ animals at 7dpi broken down by sex. Significance was determined by Mann-Whitney U test (p values shown). Each symbol represents an individual animal.

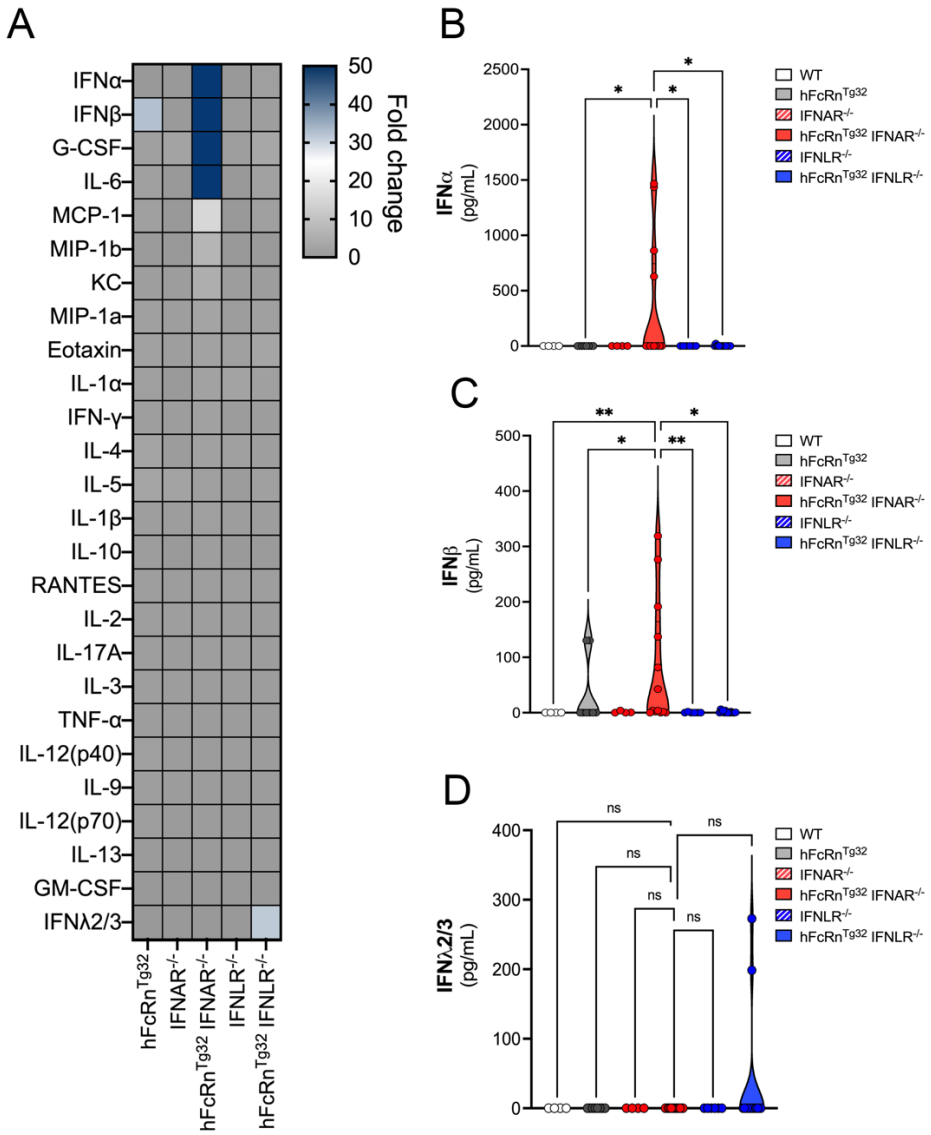

Figure 50 Luminex from blood of orally inoculated mice

Neonatal mice were inoculated by the oral route with 10^6 PFU of E5 and sacrificed 3 dpi. Luminex-based multianalyte profiling of 26 cytokines was then performed from whole blood. **(A)** Heatmap demonstrating the induction (shown as fold-change from uninfected control) in E5-infected mice of the indicated genotype. Blue denotes significantly increased cytokines in comparison to untreated. Grey or white denote little to no changes (scale at top right). The IFNs are shown to the right as pg/mL IFNα **(B)**, IFNβ **(C)**, and IFNλ2/3 **(D)**. Data are shown as mean ± standard deviation and individual animals (points). Data are shown with significance determined with a Kruskal-Wallis test with a Dunn's test for multiple comparisons (*p<0.05, **p<0.005, ns-nt significant). Each symbol represents an individual animal.

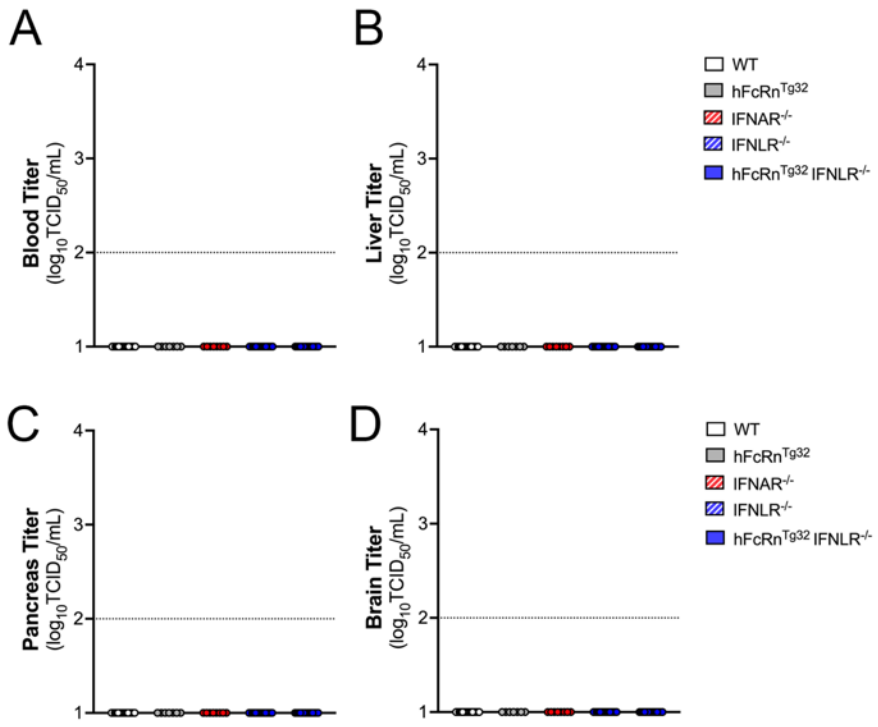

Figure 51 No dissemination of orally inoculated pups at 7dpi

7-day old pups were orally inoculated with 10^6 PFU of E5. At 7dpi, animals were sacrificed to measure viral replication in tissues. Viral titers are shown as log_{10}TCID50/mL in the blood **(A)**, liver **(B)**, pancreas **(C)**, and brain **(D)**. Data are shown as mean ± standard deviation and individual animals (points). Data are shown with significance determined with a Kruskal-Wallis test with a Dunn's test for multiple comparisons (*p<0.05, **p<0.005). Each symbol represents an individual animal.

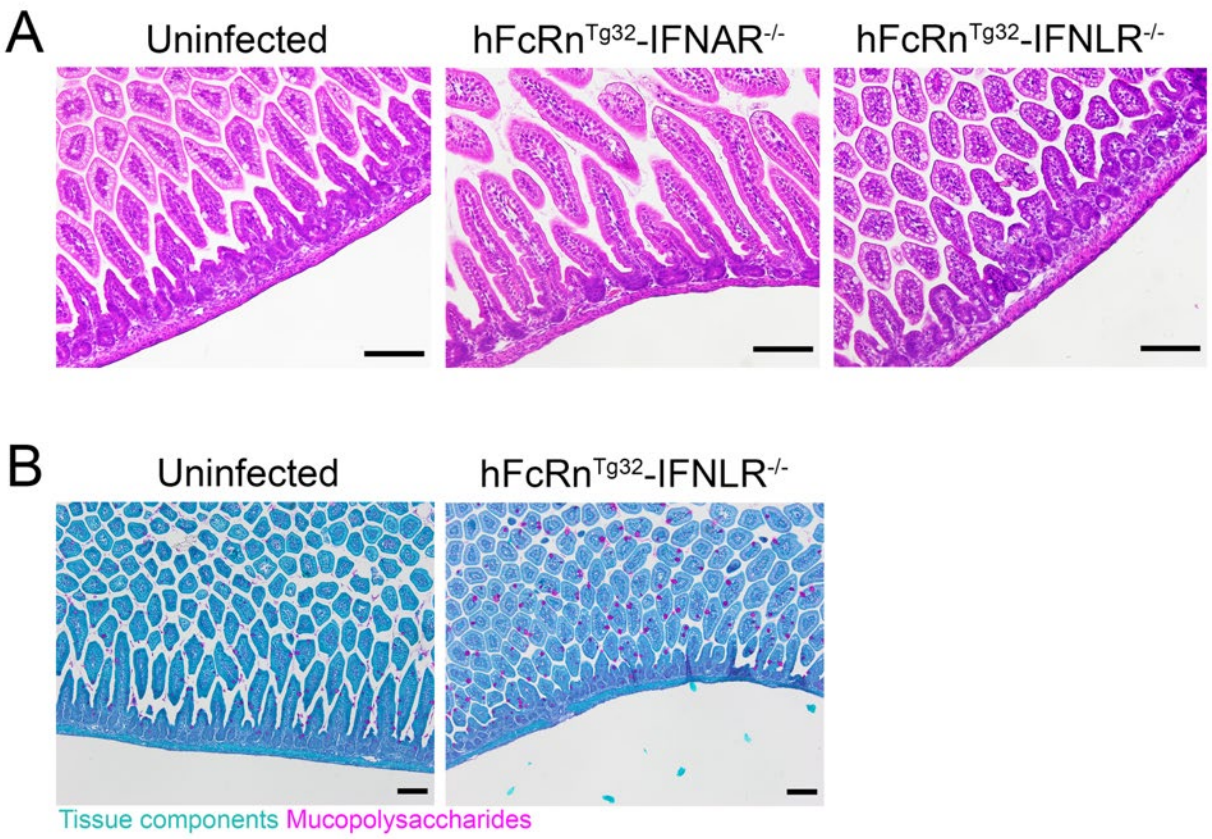

Figure 52 No significant histological changes following oral inoculation

7-day old pups were orally inoculated with 10^6 PFU of E5. At 3dpi, animals were sacrificed and intestines were collected for histology. **(A)** Hematoxylin and eosin staining of representative intestinal sections from uninfected, hFcRn^{Tg32}-IFNAR$^{-/-}$, or hFcRn^{Tg32}-IFNLR$^{-/-}$ animals. **(B)** Periodic Acid Schiff staining of representative intestinal sections uninfected or hFcRn^{Tg32}-IFNLR$^{-/-}$ animals to identify goblet cells. Scale bars at bottom right (100mm).

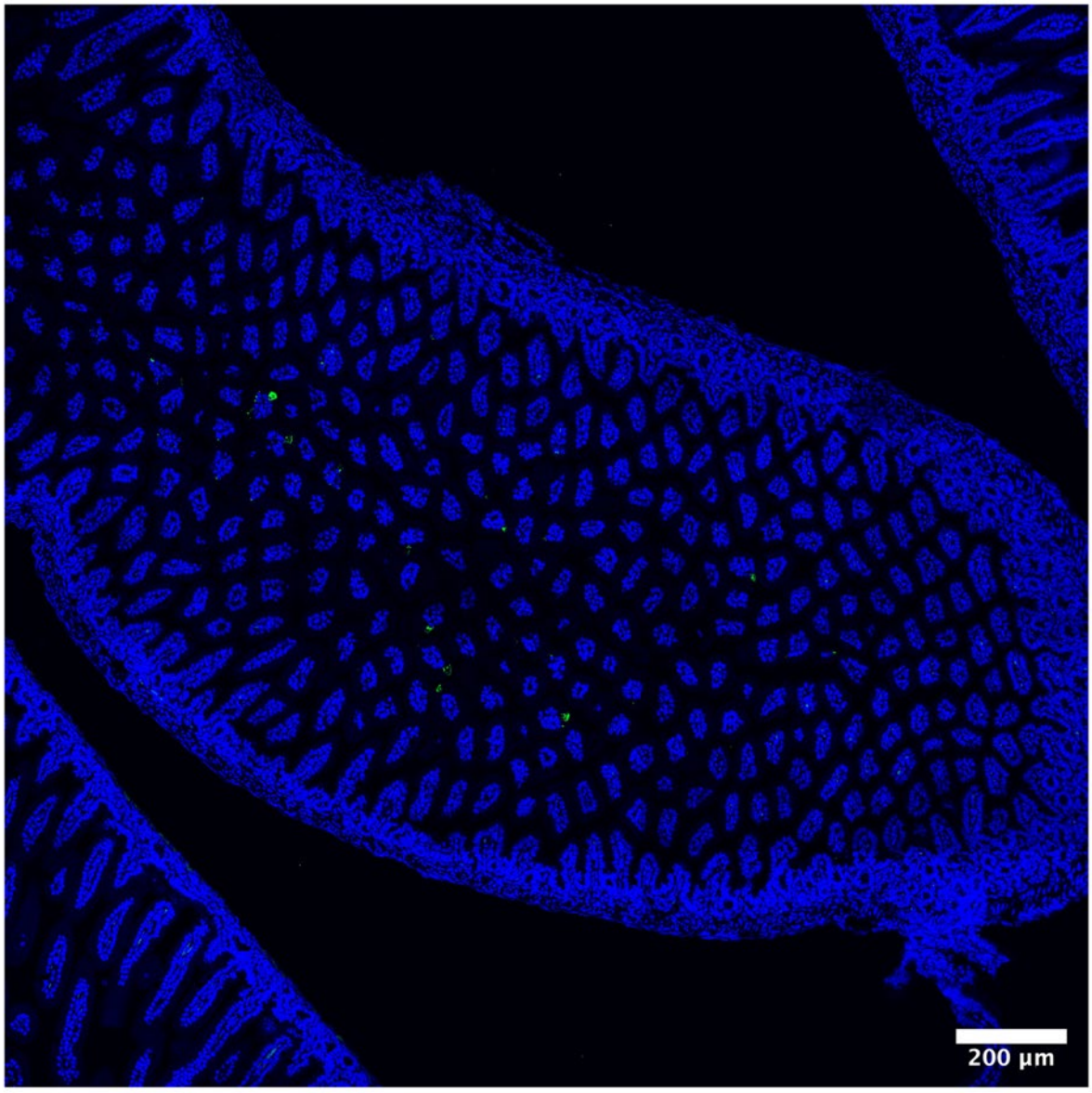

Figure 53 Tile scan of intestinal section

Representative tile scan of an ileum from a hFcRn^{Tg32}-IFNLR$^{-/-}$ pup with vRNA shown in green and DAPI in blue. Tile scan was done at a 20x magnification with an area of 6 by 6 tiles combined for a total of 36 individual images that were stitched together. The total area of view is 4mm^2 per image.

Table 10 HCR probes to detect echovirus 5 RNA

Probe Pair		
B4P1	CCTCAACCTACCTCCAACAAGGG CTCAGTAAACTTTCCCGGGTCT	CATGGATTTGATCATAAGGTCCTT CATTCTCACCATATTCGCTTC
B4P2	CCTCAACCTACCTCCAACAAAGC CCTGATGGAACTTAGATGCGTT	CTTCAGGCACACACACCACCAGGA GATTCTCACCATATTCGCTTC
B4P3	CCTCAACCTACCTCCAACAAGCA TTACTATGGTGGCACAATTGTT	TGTCCATCGGTACGCTATTAATGT AATTCTCACCATATTCGCTTC
B4P4	CCTCAACCTACCTCCAACAATGC TGCACCATCCTATAGTGGGTTT	ATGTAGCCTGCTGCTGAGTATTCA TATTCTCACCATATTCGCTTC
B4P5	CCTCAACCTACCTCCAACAAGTT ATGCTCAGACTTGGGCACGTCA	TTGGCCAAAGGCTCCATATGTGTG CATTCTCACCATATTCGCTTC
B4P6	CCTCAACCTACCTCCAACAAGTG ATCAGGTCATCGTGATTTCTTA	CCAATGAGGGCTAGTGTGGCAGTC AATTCTCACCATATTCGCTTC
B4P7	CCTCAACCTACCTCCAACAAGAT CTTCCAATTAGATTTGTTGCTA	ACTGAGCTGTTAAGCTTTTCAGCT AATTCTCACCATATTCGCTTC
B4P8	CCTCAACCTACCTCCAACAACTC CCTGTATAACGGTGGTCCCTGA	TGTCTCTGGTGCAACACTAATTTTG ATTCTCACCATATTCGCTTC
B4P9	CCTCAACCTACCTCCAACAATTA GTGGGCGTGCCGCCCAGGTTTA	GTGGGGAAGTTATACATGAGCATT CATTCTCACCATATTCGCTTC
B4P10	CCTCAACCTACCTCCAACAAAGC GCTTCAAGACCCTCAGTACCGT	TGGGTAACCGGCGCTCGTTGTTAG ATATTCTCACCATATTCGCTTC
B4P11	CCTCAACCTACCTCCAACAATGC ACAAGTAGTCAATGTAGTTAGT	GCTTGTCTCTGTACAGGTGATGGG AATTCTCACCATATTCGCTTC
B4P12	CCTCAACCTACCTCCAACAATTT CACGAATGTTGATCTCCCACCT	TCTCACACTTTCTACGTAGTTGCAC ATTCTCACCATATTCGCTTC

Table 11 HCR probes to detect mouse Muc2 RNA

Probe Pair		
B1P1	GAGGAGGGCAGCAAACGGAAGAG AGGCCGGCCCGAGAGTAGACCT	AGTGCATCTTCCCGGTTCCACATG ATAGAAGAGTCTTCCTTTACG
B1P2	GAGGAGGGCAGCAAACGGAACGC AGGGCGAGCTGCTCTCCAGGTA	TAACCTCCAGATGTGAGCATGTGT CTAGAAGAGTCTTCCTTTACG
B1P3	GAGGAGGGCAGCAAACGGAAAGT CTTCAGGCAGGTCTGCTTGTCT	CTTCTTGTCGTCAGTCAACAGCAC GTAGAAGAGTCTTCCTTTACG
B1P4	GAGGAGGGCAGCAAACGGAAGGA ACACCAGTGCTCAGCGTAGTTG	AAAGGGCGTCTCTGACCTCTTCAG GTAGAAGAGTCTTCCTTTACG
B1P5	GAGGAGGGCAGCAAACGGAAATA CACTCAGTATGGTAATAGCCAG	AGTCCATCGGGACACACACAGCCA CTAGAAGAGTCTTCCTTTACG
B1P6	GAGGAGGGCAGCAAACGGAAAGG TACTGACCCACTTCCCGTGTGA	ATGATGCCGGAGCTGGCTTCCACC ATAGAAGAGTCTTCCTTTACG
B1P7	GAGGAGGGCAGCAAACGGAAGAA CTCCCAGTAGCAGAAGATACCA	TTGCCCCACTGTTCCATTGGGGCC GTAGAAGAGTCTTCCTTTACG
B1P8	GAGGAGGGCAGCAAACGGAATTA ATGGGGTGGTTGGTGAAGTAGT	TTGTTGGTGAGGTGGTTGGTGAGG TTAGAAGAGTCTTCCTTTACG
B1P9	GAGGAGGGCAGCAAACGGAAAGA TGGTTGGTGAGGTGGTTGAAGG	TAGGAGAGATGGTTGATGTTGTTA TTAGAAGAGTCTTCCTTTACG
B1P10	GAGGAGGGCAGCAAACGGAAGTG AACTGGTTGATGGAGTGGTAGG	TTGGTGAGGTGGTTGATGGGGTGG TTAGAAGAGTCTTCCTTTACG
B1P11	GAGGAGGGCAGCAAACGGAAAGG CACGAAGGCGTGGCACTGGGA	CAGGCAAGCTTCATAGTAGTGCTT GTAGAAGAGTCTTCCTTTACG
B1P12	GAGGAGGGCAGCAAACGGAATAC AGGGCACATGGGTACAGGAGAT	GCTCAAAGCCAGAGCTGCAGGAG ATTAGAAGAGTCTTCCTTTACG

Table 12 HCR probes to detect mouse CHGA RNA

Probe Pair		
B1P1	GAGGAGGGCAGCAAACGGAAGCA ATGCTATGCCGGCTTTTATATA	ATGGTGGCGGTGGCGGCGGCAGCA GTAGAAGAGTCTTCCTTTACG
B1P2	GAGGAGGGCAGCAAACGGAAGAA AGAGTGGACGAGCTGCTGCAGG	GGAGCGCATAGCGAGCCGGACGG TGTAGAAGAGTCTTCCTTTACG
B1P3	GAGGAGGGCAGCAAACGGAAGTC GGAGATGACTTCCAGGACGCAC	AGGCATGGGGCTGGGTTTGGACAG CTAGAAGAGTCTTCCTTTACG
B1P4	GAGGAGGGCAGCAAACGGAAGCT GCTGCTGCTGCTGCTGCTGCT	TCAAAGCTGCTGTGTTGCTGCTCCT TAGAAGAGTCTTCCTTTACG
B1P5	GAGGAGGGCAGCAAACGGAATCT TGGTTAGGCTCTGGAAAGGCCT	GACTCACTGTCTCCCATCATGGGG GTAGAAGAGTCTTCCTTTACG
B1P6	GAGGAGGGCAGCAAACGGAACCT TCTCTCTAGCCACAGCCTCCTC	CTGCAGTGGGGACTTCTTCAGGCC CTAGAAGAGTCTTCCTTTACG
B1P7	GAGGAGGGCAGCAAACGGAAGGT CCCTACCATGGCCTCTTCCCCA	CCCGCCTTGGGGGAAGAGACCTTG GTAGAAGAGTCTTCCTTTACG
B1P8	GAGGAGGGCAGCAAACGGAACGG GTCCGGAAGGAGAGCTTCATGG	GGCCCAGGATCTCTGAAGCCATAG GTGAAGAGTCTTCCTTTACG
B1P9	GAGGAGGGCAGCAAACGGAAGCT CTCTAGCTCCTGGTCCTCTGCT	CTCCAGCTCTGCCTCGATGGCTGA CTAGAAGAGTCTTCCTTTACG
B1P10	GAGGAGGGCAGCAAACGGAAAAG TGTCCAGGGCAGGGGCTGAGAA	GTGCTGACATTCAGGGCTGCCCTG CTAGAAGAGTCTTCCTTTACG

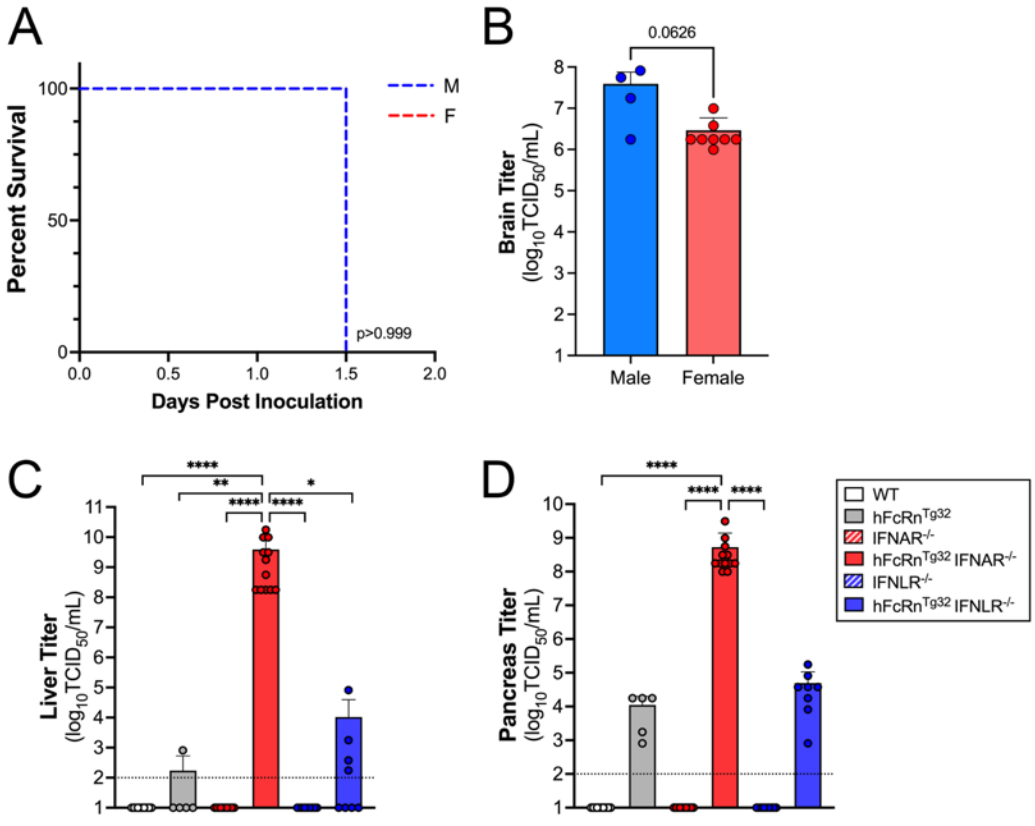

Figure 54 Animals inoculated with a high dose of E5

(A) Survival of hFcRn^{Tg32}-IFNAR$^{-/-}$ mice inoculated with 10^4 PFU of E5 by the IP route and monitored for 3 days post-inoculation. Animals are broken down by sex (M-male, F-female) to represent any potential sex differences in mortality. The log-rank test was used to analyze the statistical difference of the survival rate with p value shown. **(B)** Brain titers from hFcRn^{Tg32}-IFNAR$^{-/-}$ animals broken down by sex. Data are shown with significance determined with a Mann-Whitney U test with p value shown. **(C and D)** The indicated genotype of mice inoculated with 10^4 E5 by the IP route. At 3dpi, animals were sacrificed and viral titers in liver **(C)** and pancreas **(D)** determined by TCID50 assays. Titers are shown as $\log_{10}$TCID50/mL with the limit of detection indicated by a dotted line. Data are shown as mean ± standard deviation with individual animals shown as each data point. Data are shown with significance determined with a Kruskal-Wallis test with a Dunn's test for multiple comparisons (*p<0.05, **p<0.005, ***p<0.0005, ***p<0.0001).

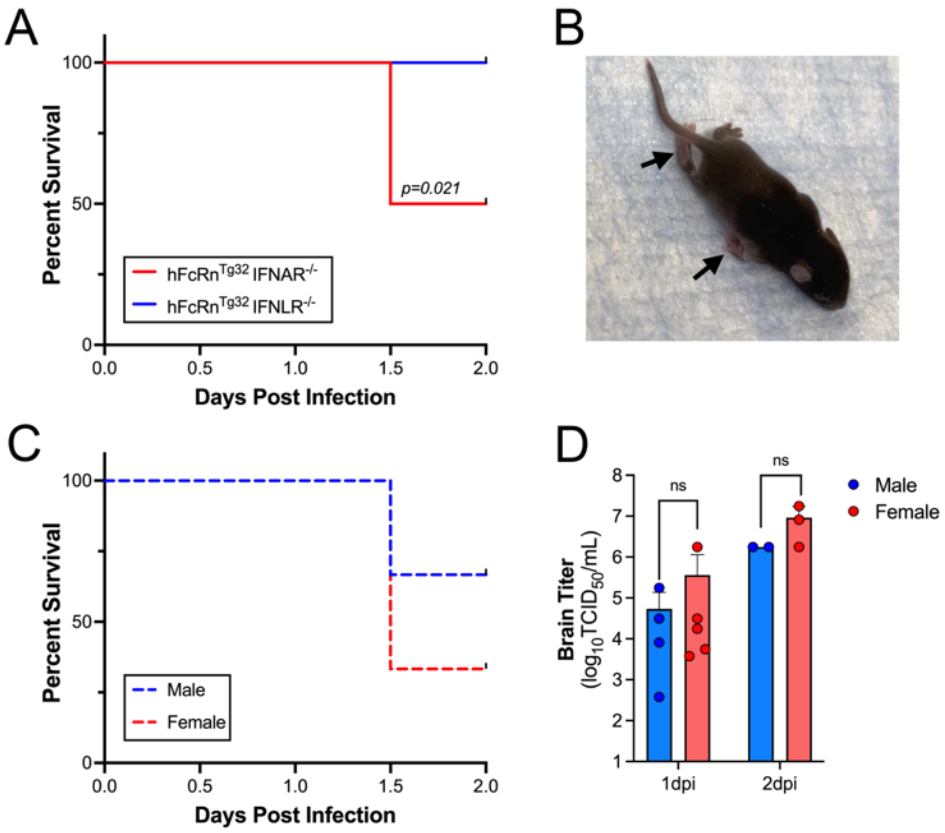

Figure 55 Animals inoculated with a low dose of E5

(A) Survival of hFcRn^{Tg32}-IFNAR$^{-/-}$ and hFcRn^{Tg32}-IFNLR$^{-/-}$ mice which were inoculated with 10^3 PFU of E5 by the IP route and monitored for 2 days post-inoculation. The number of pups in each genotype are as follows: hFcRn^{Tg32}-IFNAR$^{-/-}$ (6) and hFcRn^{Tg32}-IFNLR$^{-/-}$ (9). The log-rank test was used to analyze the statistical difference of the survival rate of hFcRn^{Tg32}-IFNAR$^{-/-}$ or hFcRn^{Tg32}-IFNLR$^{-/-}$ pups. **(B)** Representative image of a hFcRn^{Tg32}-IFNAR$^{-/-}$ mouse with hemiplegia. Arrows denote limbs that are impacted. **(C)** Survival of hFcRn^{Tg32}-IFNAR$^{-/-}$ mice broken down by sex which were inoculated with 10^3 PFU of E5 by the IP route and monitored for 2 days post-inoculation. The log-rank test was used to analyze the statistical difference of the survival rate of between males and females with the p value shown. **(D)** Brain titers from hFcRn^{Tg32}-IFNAR$^{-/-}$ animals broken down by sex at either 1 or 2dpi. Data are shown with significance determined with a Mann-Whitney U test, ns-not significant.

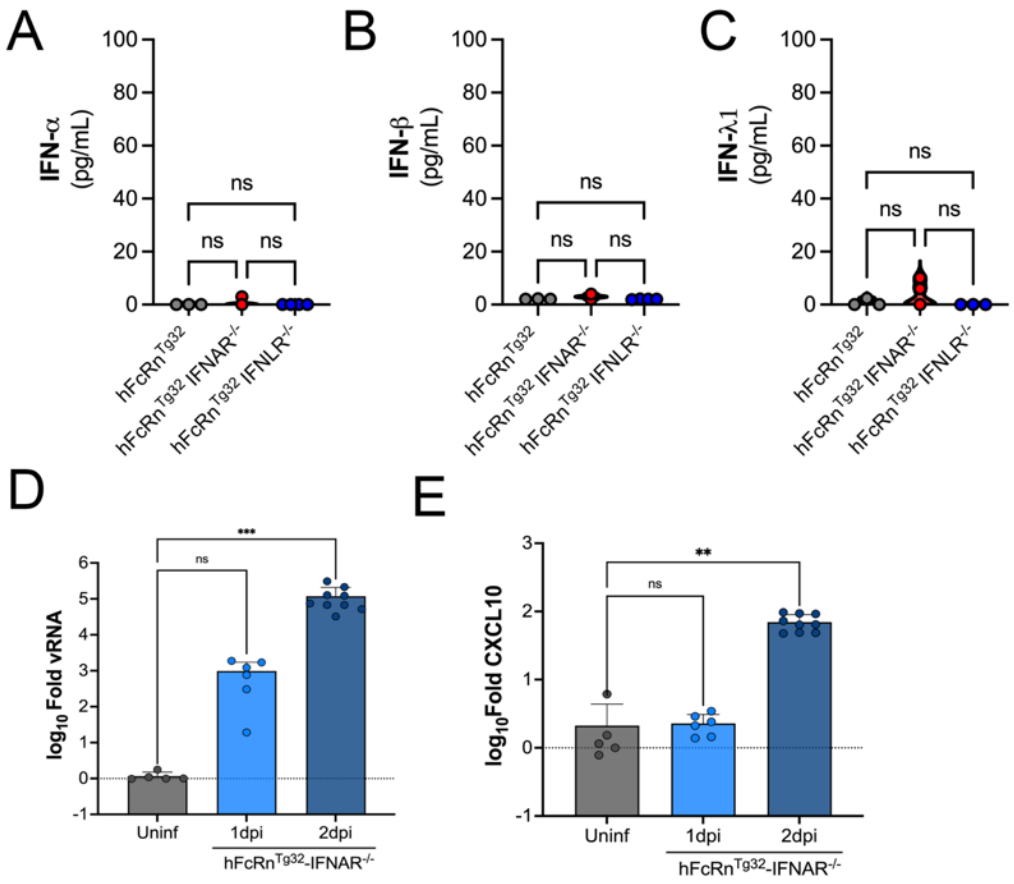

Figure 56 Luminex and RT-qPCR from infected brains

(A-C) Luminex multiplex assays from brain tissue homogenates of hFcRn^{Tg32}, hFcRn^{Tg32}-IFNAR$^{-/-}$, and hFcRn^{Tg32}-IFNLR$^{-/-}$ animals that were IP inoculated and sacrificed at 3dpi. Shown as the concentration in pg/mL IFN-α **(A)**, IFN-β **(B)**, and IFNλ1 **(C)**. RT-qPCR for viral RNA **(D)** or CXCL10 **(E)** from the brains of uninfected, 1dpi, or 2dpi hFcRn^{Tg32}-IFNAR$^{-/-}$ animals. Data are shown with the significance determined with a Kruskal-Wallis test with a Dunn's test for multiple comparisons (**p<0.005, ***p<0.0005, ns-not significant).

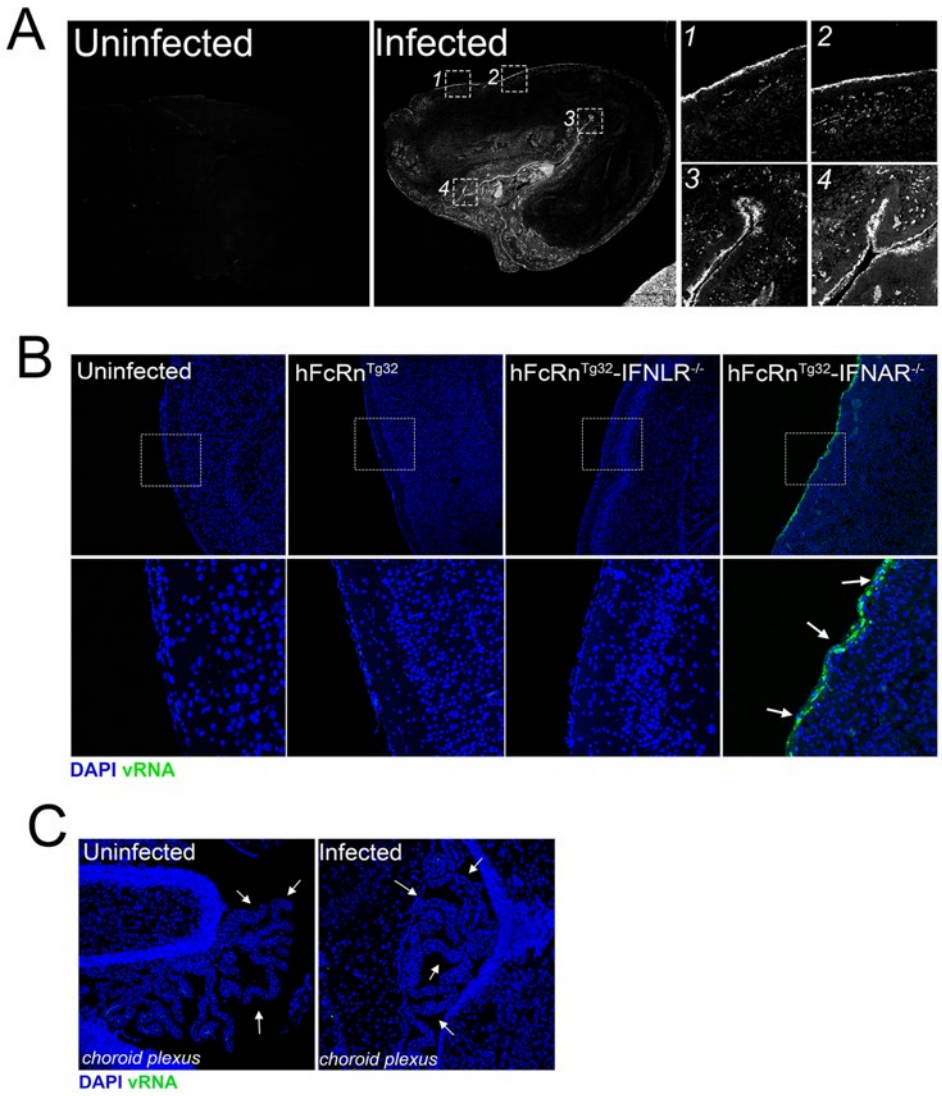

Figure 57 HCR of E5 infected brains

(A) Tile scan of the brains from an uninfected (left) and E5 inoculated at 3dpi (middle) hFcRn^{Tg32}-IFNAR$^{-/-}$ animal using Hybridization chain reaction RNA-FISH (HCR) from figure 4A. vRNA is shown in white. **(B)** HCR of brain sections from hFcRn^{Tg32}, hFcRn^{Tg32}-IFNAR$^{-/-}$, and hFcRn^{Tg32}-IFNLR$^{-/-}$ animals at 3dpi. E5 viral RNA (vRNA) is shown in green and DAPI-stained nuclei are shown in blue. White box is shown as a zoomed image below. White arrows at right denote areas of E5 vRNA. **(C)** Choroid plexus region within the brain from an uninfected (left) and E5 inoculated at 3dpi (right) hFcRn^{Tg32}-IFNAR$^{-/-}$ animal using HCR with vRNA (in green) and DAPI (in blue). White arrows show the choroid plexus.

Table 13 RT-qPCR primers used in this study

Target	Forward Primer	Reverse Primer
GAPDH	AGGTCGGTGTGAACGGATTTG	TGTAGACCATGTAGTTGAGGTCA
Echovirus 5	ACCCTACYGYAYTAACCGAAC	CCGCACCGAAYGCGGAKAATTTAC
CXCL10	AAAAAGGTCTAAAAGGGCTC	AATTAGGACTAGCCATCCAC

Appendix B Copyright Permissions

Chapters 1, 2, and 3 were previously published and are presented herein in a modified form under the Creative Commons BY license (*Viruses, Trends in Immunology, PNAS, PLOS Pathogens*):

Wells, A. I. & Coyne, C. B. Enteroviruses: A Gut-Wrenching Game of Entry, Detection, and Evasion. *Viruses* **11**, 1–20 (2019).

Wells, A. I. & Coyne, C. B. Type III Interferons in Antiviral Defenses at Barrier Surfaces. *Trends Immunol.* **39**, 848–858 (2018).

Morosky, S. Wells, A. I., Lemon, K. Evans, A. S., Schamus, S., Bakkenist, C. J., Coyne, C. B. The neonatal Fc receptor is a pan-echovirus receptor. *Proc. Natl. Acad. Sci.* **116**, 3758–3763 (2019).

Wells, A. I. *et al.* Human FcRn expression and Type I Interferon signaling control Echovirus 11 pathogenesis in mice. *PLOS Pathog.* **17**, e1009252 (2021).

Bibliography

1. Kay, H., Nelson, M. & Wang, Y. *The Placenta: From Development to Disease*. (Wiley-Blackwell, 2011).

2. Cornick, S., Tawiah, A. & Chadee, K. Roles and regulation of the mucus barrier in the gut. *Tissue Barriers* **3**, (2015).

3. Delorme-Axford, E. & Coyne, C. B. The Actin Cytoskeleton as a Barrier to Virus Infection of Polarized Epithelial Cells. *Viruses* **3**, 2462–2477 (2011).

4. Schneider, W. M., Chevillotte, D. & Rice, C. M. Interferon-Stimulated Genes: A Complex Web of Host Defenses. *Annu. Rev. Immunol* **32**, 513–545 (2014).

5. Isaacs, A. & Lindenmann, J. Virus interference. I. The interferon. *J. Interferon Res.* **7**, 429–438 (1987).

6. Hardy, M. P., Owczarek, C. M., Jermiin, L. S., Ejdebäck, M. & Hertzog, P. J. Characterization of the type I interferon locus and identification of novel genes. *Genomics* **84**, 331–345 (2004).

7. Henco, K. *et al.* Structural relationship of human interferon alpha genes and pseudogenes. *J. Mol. Biol.* **185**, 227–260 (1985).

8. Díaz, M. O. *et al.* Structure of the Human Type-I Interferon Gene Cluster Determined from a YAC Clone Contig. *Genomics* vol. 22 540–552 (1994).

9. Kotenko, S. V *et al.* IFN-λs mediate antiviral protection through a distinct class II cytokine receptor complex. *Nat. Immunol.* **4**, 69–77 (2003).

10. Sheppard, P. *et al.* Il-28, IL-29 and their class II cytokine receptor IL-28R. *Nat. Immunol.* **4**, 63–68 (2003).

11. Prokunina-Olsson, L. *et al.* A variant upstream of IFNL3 (IL28B) creating a new interferon gene IFNL4 is associated with impaired clearance of hepatitis C virus. *Nat. Genet.* **45**, 164–171 (2013).

12. Hamming, O. J. *et al.* Interferon lambda 4 signals via the IFNλ receptor to regulate antiviral activity against HCV and coronaviruses. *EMBO J.* **32**, 3055–3065 (2013).

13. Wack, A., Terczynska-Dyla, E. & Hartmann, R. Guarding the frontiers: the biology of type III interferons. *Nat. Immunol.* **16**, 802–809 (2015).

14. Kotenko, S. V. & Durbin, J. E. Contribution of type III interferons to antiviral immunity: Location, location, location. *J. Biol. Chem.* **292**, 7295–7303 (2017).

15. Sabat, R. IL-10 family of cytokines. *Cytokine Growth Factor Rev.* **21**, 315–324 (2010).

16. Walter, M. R. The Molecular Basis of IL-10 Function: From Receptor Structure to the Onset of Signaling. *Curr. Top. Microbiol. Immunol.* **380**, 191–212 (2014).

17. Sommereyns, C., Paul, S., Staeheli, P. & Michiels, T. IFN-Lambda Is Expressed in a Tissue-Dependent Fashion and Primarily Acts on Epithelial Cells In Vivo. *PLoS Pathog* **4**, (2008).

18. Kelly, A. *et al.* Immune Cell Profiling of IFN-lambda Response Shows pDCs Express Highest Level of IFN-lR1 and Are Directly Responsive via the JAK-STAT Pathway. *J. Interf. Cytokine Res.* **36**, 671–680 (2016).

19. Blazek, K. *et al.* IFN-λ resolves inflammation via suppression of neutrophil infiltration and IL-1β production. *J. Exp. Med.* **212**, 845–853 (2015).

20. Broggi, A., Tan, Y., Granucci, F. & Zanoni, I. IFN-λ suppresses intestinal inflammation by non-translational regulation of neutrophil function. *Nat. Immunol.* **18**, 1084–1093 (2017).

21. Uematsu, S. & Akira, S. Toll-like receptors and innate immunity. *J. Mol. Med.* **84**, 712–725 (2006).

22. Durbin, R. K., Kotenko, S. V. & Durbin, J. E. Interferon induction and function at the mucosal surface. *Immunol. Rev.* **255**, 25–39 (2013).

23. Maniatis, T. *et al.* Structure and function of the interferon-beta enhanceosome. *Cold Spring Harb. Symp. Quant. Biol.* **63**, 609–20 (1998).

24. Thomson, S. J. P. *et al.* The role of transposable elements in the regulation of IFN-lambda1 gene expression. *Proc. Natl. Acad. Sci. U. S. A.* **106**, 11564–11569 (2009).

25. Seth, R. B., Sun, L. & Chen, Z. J. Antiviral innate immunity pathways. *Cell Res. Cell Res.* **16**, (2006).

26. De Weerd, N. A. & Nguyen, T. The interferons and their receptors-distribution and regulation. *Immunol. Cell Biol.* **90**, 483–491 (2012).

27. Ingle, H. I. D., Peterson, S. T. & Baldridge, M. T. Distinct Effects of Type I and III Interferons on Enteric Viruses. *Viruses* **10**, 1–23 (2018).

28. Bolen, C. R., Ding, S., Robek, M. D. & Kleinstein, S. H. Dynamic expression profiling of type I and type III interferon- stimulated hepatocytes reveals a stable hierarchy of gene expression. *Hepatology* **59**, 1262–1272 (2014).

29. Selvakumar, T. A. *et al.* Identification of a Predominantly Interferon-λ-Induced Transcriptional Profile in Murine Intestinal Epithelial Cells. *Front. Immunol* **8**, (2017).

30. Bhushal, S. *et al.* Cell polarization and epigenetic status shape the heterogeneous response to type III interferons in intestinal epithelial cells. *Front. Immunol.* **8**, (2017).

31. Kojima, T. *et al.* Regulation of tight junctions in upper airway epithelium. *Biomed Res. Int.* **2013**, 1–11 (2012).

32. Yaghi, A. & Dolovich, M. Airway Epithelial Cell Cilia and Obstructive Lung Disease. *Cells* **5**, 1–19 (2016).

33. Jewell, N. A. *et al.* Lambda Interferon Is the Predominant Interferon Induced by Influenza A Virus Infection In Vivo. *J. Virol.* **84**, 11515–11522 (2010).

34. Mordstein, M. *et al.* Lambda Interferon Renders Epithelial Cells of the Respiratory and Gastrointestinal Tracts Resistant to Viral Infections. *J. Virol.* **84**, 5670–5677 (2010).

35. Andreakos, E., Salagianni, M., Galani, I. E. & Koltsida, O. Interferon- λs: Front-Line Guardians of immunity and Homeostasis in the Respiratory Tract. *Front. Immunol* **8**, 1–7 (2017).

36. Davidson, S. *et al.* IFNλ is a potent anti-influenza therapeutic without the inflammatory side effects of IFNα treatment. *EMBO Mol. Med.* **8**, 1099–1112 (2016).

37. Fox, J. M., Crabtree, J. M., Sage, L. K., Tompkins, S. M. & Tripp, R. A. Interferon Lambda Upregulates IDO1 Expression in Respiratory Epithelial Cells After Influenza Virus Infection. *J. Interf. Cytokine Res.* **35**, 554–562 (2015).

38. Iwasaki, A. & Pillai, P. S. Innate immunity to influenza virus infection. *Nat. Publ. Gr.* **14**, (2014).

39. Wang, J. *et al.* Human Alveolar Type II Cells Secrete Antiviral IL-29 (IFN-λ1) in Response to Influenza A Infection. *J Immunol* **182**, 1296–1304 (2009).

40. Travar, M., Miroslav Petkovic, B., Antonija Verhaz, B. & Hirszfeld, Ó. L. Type I, II, and III Interferons: Regulating Immunity to Mycobacterium tuberculosis Infection. *Arch. Immunol. Ther. Exp.* **64**, 19–31 (2016).

41. Villenave, R. *et al.* Induction and Antagonism of Antiviral Responses in Respiratory Syncytial Virus-Infected Pediatric Airway Epithelium. *J. Virol.* **89**, 12309–12318 (2015).

42. Galani, I. E. *et al.* Interferon-λ Mediates Non-redundant Front-Line Antiviral Protection against Influenza Virus Infection without Compromising Host Fitness. *Immunity* **46**, 875-890.e6 (2017).

43. Mordstein, M. *et al.* Interferon-λ contributes to innate immunity of mice against influenza A virus but not against hepatotropic viruses. *PLoS Pathog.* **4**, 1–7 (2008).

44. Sambuy, Y. *et al.* The Caco-2 cell line as a model of the intestinal barrier : Influence of cell and culture-related factors on Caco-2 cell functional characteristics. *Cell Biol. Toxicol.* **21**, 1–26 (2005).

45. Kotredes, K. P., Thomas, B. & Gamero, A. M. The Protective Role of Type I interferons in

the Gastrointestinal Tract. *Front. Immunol* **8**, 1–10 (2017).

46. Pott, J. *et al.* IFN-λ determines the intestinal epithelial antiviral host defense. *PNAS* **108**, 7944–7949 (2011).

47. Baldridge, M. T. *et al.* Expression of Ifnlr1 on Intestinal Epithelial Cells Is Critical to the Antiviral Effects of Interferon Lambda against Norovirus and Reovirus. *J. Virol.* **91**, 1–14 (2017).

48. Nice, T. J. *et al.* Interferon Lambda cures persistent murine norovirus infection in the absence of adaptive immunity. *Science (80-.).* **347**, 269–273 (2015).

49. Drummond, C. G. *et al.* Enteroviruses infect human enteroids and induce antiviral signaling in a cell lineage-specific manner. *PNAS* **114**, 1672–1677 (2017).

50. Hakim, M. S. *et al.* Basal interferon signaling and therapeutic use of interferons in controlling rotavirus infection in human intestinal cells and organoids. *Sci. Rep.* **8**, (2018).

51. Saxena, K. *et al.* A paradox of transcriptional and functional innate interferon responses of human intestinal enteroids to enteric virus infection. *PNAS* E570--E579 (2017) doi:10.1073/pnas.1615422114.

52. Pervolaraki, K. *et al.* Type i and Type iii interferons Display Different Dependency on Mitogen- activated Protein Kinases to Mount an antiviral state in the human gut. *Front. Immunol* **8**, (2017).

53. Mahlakõiv, T., Hernandez, P., Gronke, K., Diefenbach, A. & Staeheli, P. Leukocyte-Derived IFN-α/β and Epithelial IFN-λ Constitute a Compartmentalized Mucosal Defense System that Restricts Enteric Virus Infections. *PLoS Pathog.* (2015) doi:10.1371/journal.ppat.1004782.

54. Yin, X. *et al.* Engineering Stem Cell Organoids. *Cell Stem Cell* **18**, 25–38 (2016).

55. Abbott, N. J., Patabendige, A. A. K., Dolman, D. E. M., Yusof, S. R. & Begley, D. J. Structure and function of the blood–brain barrier. *Neurobiol. Dis.* **37**, 13–25 (2009).

56. Lazear, H. M. *et al.* Interferon-l restricts West Nile virus neuroinvasion by tightening the blood-brain barrier. *Sci. Transl. Med.* **7**, (2015).

57. Daniels, B. P. & Klein, R. S. Knocking on Closed Doors: Host Interferons Dynamically Regulate Blood-Brain Barrier Function during Viral Infections of the Central Nervous System. *PLoS Pathog.* (2015) doi:10.1371/journal.ppat.1005096.

58. Douam, F. *et al.* Type III Interferon-Mediated Signaling Is Critical for Controlling Live Attenuated Yellow Fever Virus Infection In Vivo. *MBio* **8**, 1–22 (2017).

59. Bramley, J. C. *et al.* A Three-Dimensional Cell Culture System To Model RNA Virus Infections at the Blood-Brain Barrier. *mSphere* **2**, (2017).

60. Division of Viral Diseases CDC. Non-polio enterovirus infection. https://www.cdc.gov/non-polio-enterovirus/index.html.

61. Pons-Salort, M., Parker, E. P. K. K. & Grassly, N. C. The epidemiology of non-polio enteroviruses: Recent advances and outstanding questions. *Curr. Opin. Infect. Dis.* **28**, 479–487 (2015).

62. Lie, S.-L. *et al.* Comparative epidemiology and virology of fatal and nonfatal cases of hand, foot and mouth disease in mainland China from 2008 to 2014. *Rev. Med. Virol.* **25**, 115–128 (2015).

63. Wang, J., Atchison, R. W., Walpusk, J. & Jaffe, R. Echovirus hepatic failure in infancy: report of four cases with speculation on the pathogenesis. *Pediatr. Dev. Pathol.* **4**, 454–60 (2001).

64. Huber, S. & Ramsingh, A. I. Coxsackievirus-Induced Pancreatitis. *Viral Immunol.* **17**, 358–369 (2004).

65. Ph Syriopoulou, V. *et al.* Clinical and epidemiological aspects of an enterovirus outbreak in a neonatal unit. *J. Hosp. Infect.* **51**, 275–280 (2002).

66. Haston, J. C. & Dixon, T. C. Nonpolio Enterovirus Infections in Neonates. *Pediatr. Ann.* **44**, e103–e107 (2015).

67. Isaacs, D. *et al.* Conservative Management of an Echovirus 11 Outbreak in a Neonatal Unit. *Lancet* **333**, 543–545 (1989).

68. Civardi, E. *et al.* Viral outbreaks in neonatal intensive care units: What we do not know. *Am. J. Infect. Control* **41**, 854–856 (2013).

69. Naing, Z. *et al.* Prevalence of viruses in stool of premature neonates at a neonatal intensive care unit. *J. Paediatr. Child Health* **49**, (2013).

70. Xing, W. *et al.* Hand, foot, and mouth disease in China, 2008-12: An epidemiological study. *Lancet Infect. Dis.* **14**, 308–318 (2014).

71. Cassidy, H., Poelman, R., Knoester, M., Van Leer-Buter, C. C. & Niesters, H. G. M. M. Enterovirus D68 -the new polio? *Front. Microbiol.* **9**, 1–11 (2018).

72. Centers for Disease Control & Prevention. Acute Flaccid Myelitis.

73. Sejvar, J. J. *et al.* Acute Flaccid Myelitis in the United States, August-December 2014: Results of Nationwide Surveillance. *Clin. Infect. Dis.* **63**, 737–745 (2016).

74. Zhu, R. *et al.* Serological survey of neutralizing antibodies to eight major enteroviruses among healthy population. *Emerg. Microbes Infect.* **7**, (2018).

75. Wallace, G. S., Curns, A. T., Weldon, W. C. & Oberste, M. S. Seroprevalence of Poliovirus

Antibodies in the United States Population, 2009-2010. *BMC Public Health* **16**, 1–8 (2016).

76. Sabin, A. B. Oral Poliovirus Vaccine: History of Its Development and Use and Current Challenge to Eliminate Poliomyelitis from the World. *J. Infect. Dis.* **151**, 420–436 (1985).

77. Dey, A. *et al.* Human circulating antibody-producing B cell as a predictive measure of mucosal immunity to poliovirus. *PLoS One* **11**, 1–14 (2016).

78. Bearden, D., Collett, M., Quan, P. L., Costa-Carvalho, B. T. & Sullivan, K. E. Enteroviruses in X-Linked Agammaglobulinemia: Update on Epidemiology and Therapy. *J. Allergy Clin. Immunol. Pract.* **4**, 1059–1065 (2016).

79. Luk, A. D. W. *et al.* Type I and III interferon productions are impaired in X-linked agammaglobulinemia patients toward poliovirus but not influenza virus. *Front. Immunol.* **9**, 1–16 (2018).

80. Mena, I. *et al.* The role of B lymphocytes in coxsackievirus B3 infection. *Am. J. Pathol.* **155**, 1205–1215 (1999).

81. Cherry, J. & Krogstad, P. *Enteroviruses, Parechoviruses, and Saffold Viruses*. *Feigin and Cherry's Textbook of Pediatric Infectious Diseases* (Elsevier Inc., 2019). doi:10.1016/B978-0-323-37692-1.00166-0.

82. Knipe, D. *et al. Fields Virology*. (Wolters Kluwer/Lippincott Williams & Wilkins Health, 2013).

83. Liu, M. Y. *et al.* Characterization of enterovirus 71 infection and associated outbreak of Hand, Foot, and Mouth Disease in Shawo of China in 2012. *Nat. Publ. Gr.* (2016) doi:10.1038/srep38451.

84. Rapmund, G., Gauld, J. R., Rogers, N. G. & Holmes, G. E. Neonatal Myocarditis and Meningoencephalitis Due to Coxsackie Virus Group B, Type 4. *N. Engl. J. Med.* **260**, 819–821 (1959).

85. Vanek, J., Lukes, J., Potuznik, V., Polednikova, I. & Vilim, V. Myocarditis and encephalitis in newborn infants, caused by Coxsackie B virus. *J. Hyg. Epidemiol. Microbiol. Immunol.* **3**, 283–91 (1959).

86. Centers for Disease Control & Prevention. Enterovirus surveillance-United States 2002-2004. *MMWR Morb. Mortal. Wkly. Rep.* **55**, 153–156.

87. Williams, J. M. *et al.* Epithelial Cell Shedding and Barrier Function: A Matter of Life and Death at the Small Intestinal Villus Tip. *Vet. Pathol.* **52**, 445–455 (2015).

88. Makala, L. H. C., Suzuki, N. & Nagasawa, H. Peyer's patches: Organized lymphoid structures for the induction of mucosal immune responses in the intestine. *Pathobiology* **70**, 55–68 (2002).

89. Heel, A. K., McCauley, R., Papadimitriou, J. M. & Hall, J. C. Review: Peyer's patches. *J. Gastroenterol.* **12**, 122–136 (1997).

90. Finke, D. & Kraehenbuhl, J. P. Formation of Peyer's patches. *Curr. Opin. Genet. Dev.* **11**, 561–567 (2001).

91. Farquhar, M. G. & Palade, G. E. Junctional complexes in various epithelia. *J. Cell Biol.* **17**, 375–412 (1963).

92. Green, K. J., Getsios, S., Troyanovsky, S. & Godsel, L. M. Intercellular junction assembly, dynamics, and homeostasis. *Cold Spring Harb. Perspect. Biol.* **2**, 1–24 (2010).

93. Wells, A. I. & Coyne, C. B. Type III Interferons in Antiviral Defenses at Barrier Surfaces. *Trends Immunol.* **39**, 848–858 (2018).

94. Zanoni, I. *et al.* identification of a Predominantly interferon-λ-induced Transcriptional Profile in Murine intestinal epithelial cells. *Front. Immunol* **8**, 13023389–1302 (2017).

95. Henning, S. J. & Von Furstenberg, R. J. GI stem cells – new insights into roles in physiology and pathophysiology. *J Physiol* **594**, 4769–4779 (2016).

96. Barker, N. *et al.* Identification of stem cells in small intestine and colon by marker gene Lgr5. *Nature* **449**, 1003–1007 (2007).

97. Nephrol, W. J. Paneth cells in intestinal physiology and pathophysiology. *World J. Gastrointest. Pathophysiol.* **8**, (2017).

98. Sato, T. *et al.* Paneth cells constitute the niche for Lgr5 stem cells in intestinal crypts. *Nature* **469**, 415–418 (2011).

99. Karpus, O. N. *et al.* Colonic CD90+ Crypt Fibroblasts Secrete Semaphorins to Support Epithelial Growth. *Cell Rep.* **26**, 3698–3708 (2019).

100. Neutra, M. R. Current Concepts in Mucosal Immunity V. Role of M cells in transepithelial transport of antigens and pathogens to the mucosal immune system. *Am J Physiol Gastrointest Liver Physiol* **274**, 785–791 (1998).

101. Cheng, H. & Leblond, C. P. Origin, differentiation and renewal of the four main epithelial cell types in the mouse small intestine. *Am. J. Anat.* **141**, 537–561 (1974).

102. Yamayoshi, S. *et al.* Scavenger receptor B2 is a cellular receptor for enterovirus 71. *Nat. Med.* **15**, 798–802 (2009).

103. Nishimura, Y. *et al.* Human P-selectin glycoprotein ligand-1 is a functional receptor for enterovirus 71. *Nat. Microbioloy* **15**, 794–798 (2009).

104. Yamayoshi, S., Ohka, S., Fujii, K. & Koike, S. Functional Comparison of SCARB2 and PSGL1 as Receptors for Enterovirus 71. *J. Virol.* **87**, 3335–3347 (2013).

105. Bergelson, J. M. *et al.* Isolation of a Common Receptor for Coxsackie B Viruses and Adenoviruses 2 and 5. *Science (80-.).* **275**, 1320–1324 (1997).

106. Carson, S. D., Chapman, N. N. & Tracy, S. M. Purification of the putative coxsackievirus B receptor from HeLa cells. *Biochem. Biophys. Res. Commun.* **233**, 325–328 (1997).

107. Tomko, R. P., Xu, R. & Philipson, L. HCAR and MCAR: The human and mouse cellular receptors for subgroup C adenoviruses and group B coxsackieviruses. *Proc. Natl. Acad. Sci.* **94**, 3352–3356 (1997).

108. Mendelsohn, C. L., Wimmer, E. & Racaniello, V. R. Cellular receptor for poliovirus: Molecular cloning, nucleotide sequence, and expression of a new member of the immunoglobulin superfamily. *Cell* **56**, 855–865 (1989).

109. Morosky, S. *et al.* The neonatal Fc receptor is a pan-echovirus receptor. *Proc. Natl. Acad. Sci.* **116**, 3758–3763 (2019).

110. Bergelson, J. M. *et al.* Decay-accelerating factor (CD55), a glycosylphosphatidylinositol-anchored complement regulatory protein, is a receptor for several. *Proc Natl Acad Sci U S A* **91**, 6245–6248 (1994).

111. Bergelson, J. M. *et al.* Coxsackievirus B3 adapted to growth in RD cells binds to decay-accelerating factor (CD55). *J. Virol.* **69**, 1903–6 (1995).

112. Coyne, C. B. & Bergelson, J. M. Virus-induced Abl and Fyn kinase signals permit coxsackievirus entry through epithelial tight junctions. *Cell* **124**, 119–131 (2006).

113. Rubbia-Brandt, L., Brown, T. D. K., Stuart, A. D., McKee, T. A. & Sobo, K. Decay-Accelerating Factor Binding Determines the Entry Route of Echovirus 11 in Polarized Epithelial Cells. *J. Virol.* **85**, 12376–12386 (2011).

114. Brandenburg, B. *et al.* Imaging poliovirus entry in live cells. *PLoS Biol.* **5**, 1543–1555 (2007).

115. Crowther, D. & Melnick, J. L. The incorporation of neutral red and acridine orange into developing poliovirus particles making them photosensitive. *Virology* **14**, 11–21 (1961).

116. Coyne, C. B., Kim, K. S. & Bergelson, J. M. Poliovirus entry into human brain microvascular cells requires receptor-induced activation of SHP-2. *EMBO J.* **26**, 4016–4028 (2007).

117. Lulla, V. *et al.* An upstream protein-coding region in enteroviruses modulates virus infection in gut epithelial cells. *Nat. Microbiol.* (2018) doi:10.1038/s41564-018-0297-1.

118. Van Der Schaar, H. M., Dorobantu, C. M., Albulescu, L., Strating, J. R. P. M. & Van Kuppeveld, F. J. M. Fat(al) attraction: Picornaviruses Usurp Lipid Transfer at Membrane Contact Sites to Create Replication Organelles. (2016) doi:10.1016/j.tim.2016.02.017.

119. Baggen, J., Thibaut, H., P M Strating, J. R. & van Kuppeveld, F. J. The life cycle of non-polio enteroviruses and how to target it. *Nat. Rev. Microbiol.* **16**, (2018).

120. Feng, Z. *et al.* A pathogenic picornavirus acquires an envelope by hijacking cellular membranes. *Nature* **496**, 367–371 (2013).

121. Chen, Y. H. *et al.* Phosphatidylserine vesicles enable efficient en bloc transmission of enteroviruses. *Cell* **160**, 619–630 (2015).

122. Bird, S. W., Maynard, N. D., Covert, M. W. & Kirkegaard, K. Nonlytic viral spread enhanced by autophagy components. *Proc. Natl. Acad. Sci.* **111**, 13081–13086 (2014).

123. Nishimura, Y. & Shimizu, H. Cellular receptors for human enterovirus species A. *Front. Microbiol.* **3**, 1–5 (2012).

124. Staring, J. *et al.* KREMEN1 Is a Host Entry Receptor for a Major Group of Enteroviruses. *Cell Host Microbe* (2018) doi:10.1016/j.chom.2018.03.019.

125. Su, P.-Y. *et al.* Cell surface sialylation affects binding of enterovirus 71 to rhabdomyosarcoma and neuroblastoma cells. *BMC Microbiol.* **12**, 162 (2012).

126. Wei, W. *et al.* ICAM-5/Telencephalin Is a Functional Entry Receptor for Enterovirus D68. *Cell Host Microbe* **20**, 631–641 (2016).

127. Bergelson, J. M. *et al.* Identification of the Integrin VLA-2 as a Receptor for Echovirus 1. *Science (80-.).* **255**, 1718–1720 (1992).

128. Zhao, X. *et al.* Human Neonatal Fc Receptor Is the Cellular Uncoating Receptor for Enterovirus B. *Cell* **177**, 1553-1565.e16 (2019).

129. Chi, C. *et al.* Robust antiviral responses to enterovirus 71 infection in human intestinal epithelial cells. *Virus Res.* **176**, 53–60 (2013).

130. Good, C., Wells, A. I. & Coyne, C. B. Type III interferon signaling restricts Enterovirus 71 infection of goblet cells. *Sci. Adv.* **5**, 1–11 (2019).

131. Jensen, S. & Thomsen, A. R. Sensing of RNA Viruses: a Review of Innate Immune Receptors Involved in Recognizing RNA Virus Invasion. *J. Virol.* (2012) doi:10.1128/JVI.05738-11.

132. Akira, S. & Takeda, K. Toll-like receptor signalling. *Nat. Rev. Immunol.* **4**, 499–511 (2004).

133. Bryant, C. E. *et al.* Advances in Toll-like receptor biology: Modes of activation by diverse stimuli. *Crit. Rev. Biochem. Mol. Biol.* **50**, 359–379 (2015).

134. Brubaker, S. W., Bonham, K. S., Zanoni, I. & Kagan, J. C. *Innate Immune Pattern Recognition: A Cell Biological Perspective*. *Annual Review of Immunology* vol. 33 (2015).

135. Alexopoulou, L., Czopik Holt, A., Medzhitov, R. & Flavell, R. A. Recognition of double-

stranded RNA and activation of NF-kappa B by Toll-like receptor 3. *Nature* **413**, 732–738 (2001).

136. Xu, J., Yang, A. Y., Wang, A. C. & Jiang, A. B. Rotavirus and coxsackievirus infection activated different profiles of toll-like receptors and chemokines in intestinal epithelial cells. *Inflamm. Res.* **58**, 585–592 (2009).

137. Abe, Y. *et al.* The Toll-Like Receptor 3-Mediated Antiviral Response Is Important for Protection against Poliovirus Infection in Poliovirus Receptor Transgenic Mice. *J. Virol.* 185–194 (2012) doi:10.1128/JVI.05245-11.

138. Yang, J. *et al.* Type I Interferons Triggered through the Toll-Like Receptor 3-TRIF Pathway Control Coxsackievirus A16 Infection in Young Mice. *J. Virol.* **89**, 10860–7 (2015).

139. Negishi, H. *et al.* A critical link between Toll-like receptor 3 and type II interferon signaling pathways in antiviral innate immunity. *Proc. Natl. Acad. Sci. U. S. A.* **105**, 20446–20451 (2008).

140. Oshiumi, H. *et al.* The TLR3/TICAM-1 Pathway Is Mandatory for Innate Immune Responses to Poliovirus Infection. *J. Immunol.* **187**, 5320–5327 (2011).

141. Wang, C. *et al.* Differential Regulation of TLR Signaling on the Induction of Antiviral Interferons in Human Intestinal Epithelial Cells Infected with Enterovirus 71. *PLoS One* **11**, (2016).

142. Gorbea, C. *et al.* A role for toll-like receptor 3 variants in host susceptibility to enteroviral myocarditis and dilated cardiomyopathy. *J. Biol. Chem.* **285**, 23208–23223 (2010).

143. Belkaya, S. *et al.* Autosomal Recessive Cardiomyopathy Presenting as Acute Myocarditis. *J. Am. Coll. Cardiol.* **69**, 1653–1665 (2017).

144. Satoh, M. *et al.* Expression of Toll-like receptor 4 is associated with enteroviral replication in human myocarditis. *Clin. Sci.* **104**, 577–84 (2003).

145. Satoh, M. *et al.* Toll-like receptor 4 is expressed with enteroviral replication in myocardium from patients with dilated cardiomyopathy. *Lab. Investig.* **84**, 173–81 (2004).

146. Trianta, K. & Trianta, M. Coxsackievirus B4-Induced Cytokine Production in Pancreatic Cells Is Mediated through Toll-Like Receptor 4. *J. Virol.* **78**, 11313–11320 (2004).

147. Hornung, V. *et al.* Sequence-specific potent induction of IFN-$α$ by short interfering RNA in plasmacytoid dendritic cells through TLR7. *Nat. Med.* **11**, 263–270 (2005).

148. Li, B. *et al.* Expression and significance of toll-like receptors 7 and 8 in brain and lung tissues of death cases caused by EV71 infection. *Chinese J. Contemp. Pediatr.* **17**, 1051–1055 (2015).

149. Triantafilou, K. *et al.* Human cardiac inflammatory responses triggered by Coxsackie B

viruses are mainly Toll-like receptor (TLR) 8-dependent. *Cell. Microbiol.* **7**, 1117–1126 (2005).

150. Satoh, M. *et al.* Association between toll-like receptor 8 expression and adverse clinical outcomes in patients with enterovirus-associated dilated cardiomyopathy. *Am. Heart J.* **154**, 581–588 (2007).

151. Yoneyama, M. *et al.* Shared and Unique Functions of the DExD/H-Box Helicases RIG-I, MDA5, and LGP2 in Antiviral Innate Immunity. *J. Immunol.* **175**, 2851–2858 (2005).

152. Hornung, V. *et al.* 5'-Triphosphate RNA is the Ligand for RIG-I. *Science (80-.).* **314**, (2006).

153. Francisco, E., Suthar, M., Gale, M., Rosenfeld, A. B. & Racaniello, V. R. Cell-type specificity and functional redundancy of RIG-I-like receptors in innate immune sensing of Coxsackievirus B3 and encephalomyocarditis virus. *Virology* **528**, 7–18 (2019).

154. Feng, Q., Langereis, M. A., Olagnier, D., Chiang, C. & Van De Winkel, R. Coxsackievirus Cloverleaf RNA Containing a 59 Triphosphate Triggers an Antiviral Response via RIG-I Activation. *PLoS One* **9**, 95927 (2014).

155. Abe, Y. *et al.* The Toll-Like Receptor 3-Mediated Antiviral Response Is Important for Protection against Poliovirus Infection in Poliovirus Receptor Transgenic Mice. *J. Virol.* **86**, 185–194 (2012).

156. Pichlmair, A. *et al.* Activation of MDA5 Requires Higher-Order RNA Structures Generated during Virus Infection. *J. Virol.* **83**, 10761–10769 (2009).

157. Kato, H. *et al.* Length-dependent recognition of double-stranded ribonucleic acids by retinoic acid–inducible gene-I and melanoma differentiation–associated gene 5. *J. Exp. Med.* **205**, 1601–1610 (2008).

158. Wu, B. *et al.* Structural basis for dsRNA recognition, filament formation, and antiviral signal activation by MDA5. *Cell* **152**, 276–289 (2013).

159. Triantafilou, K. *et al.* Visualisation of direct interaction of MDA5 and the dsRNA replicative intermediate form of positive strand RNA viruses. *J. Cell Sci.* **125**, 4761–4769 (2012).

160. Kuo, R. L., Kao, L. T., Lin, S. J., Wang, R. Y. L. & Shih, S. R. MDA5 Plays a Crucial Role in Enterovirus 71 RNA-Mediated IRF3 Activation. *PLoS One* **8**, (2013).

161. Wang, J. P. *et al.* MDA5 and MAVS Mediate Type I Interferon Responses to Coxsackie B Virus. *J. Virol.* **84**, 254–260 (2010).

162. Feng, Q. *et al.* MDA5 Detects the Double-Stranded RNA Replicative Form in Picornavirus-Infected Cells. *Cell Rep.* **2**, 1187–1196 (2012).

163. Pang, L. *et al.* A polymorphism in melanoma differentiation-associated gene 5 may be a risk factor for enterovirus 71 infection. *Clin. Microbiol. Infect.* **20**, O711–O717 (2014).

164. Hühn, M. H. *et al.* Melanoma differentiation-associated protein-5 (MDA-5) limits early viral replication but is not essential for the induction of type 1 interferons after Coxsackievirus infection. *Virology* **401**, 42–48 (2010).

165. Gack, M. U. *et al.* TRIM25 RING-finger E3 ubiquitin ligase is essential for RIG-I-mediated antiviral activity. *Nature* **446**, 916–920 (2007).

166. Oshiumi, H., Matsumoto, M., Hatakeyama, S. & Seya, T. Riplet/RNF135, a RING finger protein, ubiquitinates RIG-I to promote interferon-beta induction during the early phase of viral infection. *J. Biol. Chem.* **284**, 807–817 (2009).

167. Hou, F. *et al.* MAVS forms functional prion-like aggregates to activate and propagate antiviral innate immune response. *Cell* **146**, 448–461 (2011).

168. Patel, J. R. & García-Sastre, A. Activation and regulation of pathogen sensor RIG-I. *Cytokine Growth Factor Rev.* **25**, 513–523 (2014).

169. Zhang, Q. M. *et al.* Over-expression of mitochondrial antiviral signaling protein inhibits coxsackievirus B3 infection by enhancing type-I interferons production. *Virol. J.* **9**, 2–11 (2012).

170. Mukherjee, A. *et al.* The Coxsackievirus B 3C pro Protease Cleaves MAVS and TRIF to Attenuate Host Type I Interferon and Apoptotic Signaling. *PLoS Pathog.* **7**, (2011).

171. Xiang, Z. *et al.* Enterovirus 68 3C Protease Cleaves TRIF To Attenuate Antiviral Responses Mediated by Toll-Like Receptor 3. *J. Virol.* **88**, 6650–6659 (2014).

172. Lei, X. *et al.* Cleavage of the Adaptor Protein TRIF by Enterovirus 71 3C Inhibits Antiviral Responses Mediated by Toll-Like Receptor 3. *J. Virol.* **85**, 8811–8818 (2011).

173. Alirezaei, M., Flynn, C. T. & Whitton, J. L. Interactions between enteroviruses and autophagy in vivo. *Autophagy* **8**, 973–975 (2012).

174. Song, J. *et al.* Suppression of the toll-like receptor 7-dependent type I interferon production pathway by autophagy resulting from enterovirus 71 and coxsackievirus A16 infections facilitates their replication. *Arch. Virol.* **163**, 135–144 (2017).

175. Feng, Q. *et al.* Enterovirus 2Apro Targets MDA5 and MAVS in Infected Cells. *J. Virol.* **88**, 3369–3378 (2014).

176. Rui, Y. *et al.* Disruption of MDA5-Mediated Innate Immune Responses by the 3C Proteins Coxsackievirus A16, Coxsackievirus A6, and Enterovirus D68. *J. Virol.* **91**, 546–563 (2017).

177. Barral, P. M. *et al.* MDA-5 Is Cleaved in Poliovirus-Infected Cells. *J. Virol.* **81**, 3677–3684

(2007).

178. Barral, P. M., Sarkar, D., Fisher, P. B. & Racaniello, V. R. RIG-I is cleaved during picornavirus infection. *Virology* **391**, 171–176 (2009).

179. Chen, N. *et al.* Enterovirus 71 inhibits cellular type I interferon signaling by inhibiting host RIG-I ubiquitination. *Microb. Pathog.* **100**, 84–89 (2016).

180. Maelfait, J. & Beyaert, R. Emerging Role of Ubiquitination in Antiviral RIG-I Signaling. *Microbiol. Mol. Biol. Rev.* **76**, 33–45 (2012).

181. Friedman, C. S. *et al.* The tumour suppressor CYLD is a negative regulator of RIG-I-mediated antiviral response. *EMBO Rep.* **9**, 930–936 (2008).

182. Xu, C. *et al.* Downregulation of MicroRNA miR-526a by Enterovirus Inhibits RIG-I-Dependent Innate Immune Response. *J. Virol.* **88**, 11356–11368 (2014).

183. Wang, B. *et al.* Enterovirus 71 Protease 2Apro Targets MAVS to Inhibit Anti-Viral Type I Interferon Responses. *PLoS Pathog.* **9**, (2013).

184. Drummond, C. G., Nickerson, C. A. & Coyne, C. B. A Three-Dimensional Cell Culture Model To Study Enterovirus Infection of Polarized Intestinal Epithelial Cells. *mSphere* **1**, (2015).

185. McCracken, K. W., Howell, J. C., Wells, J. M. & Spence, J. R. Generating human intestinal tissue from pluripotent stem cells in vitro. *Nat. Protoc.* **6**, 1920–1928 (2011).

186. Spence, J. R. *et al.* Directed differentiation of human pluripotent stem cells into intestinal tissue in vitro. *Nature* **470**, 105–110 (2011).

187. Stelzner, M. *et al.* A nomenclature for intestinal in vitro cultures. *AJP Gastrointest. Liver Physiol.* **302**, G1359–G1363 (2012).

188. Kretzschmar, K. & Clevers, H. Organoids: Modeling Development and the Stem Cell Niche in a Dish. (2016) doi:10.1016/j.devcel.2016.08.014.

189. Saxena, K. *et al.* Human Intestinal Enteroids: a New Model To Study Human Rotavirus Infection, Host Restriction, and Pathophysiology. *J. Virol* **90**, 43–56 (2016).

190. Ettayebi, K. *et al.* Replication of human noroviruses in stem cell-derived human enteroids. *Science (80-.).* **353**, 1387–1394 (2016).

191. Moon, C., VanDussen, K., Miyoshi, H. & Stappenbeck, T. Development of a primary mouse intestinal epithelial cell monolayer culture system to evaluate factors that modeulate IgA transcytosis. *Mucosal Immunol.* **7**, 818–828 (2014).

192. Erickson, A. K. *et al.* Bacteria Facilitate Enteric Virus Co-infection of Mammalian Cells and Promote Genetic Recombination. *Cell Host Microbe* **23**, 77-88.e5 (2018).

193. Aguilera, E. R., Nguyen, Y., Sasaki, J. & Pfeiffer, K. Bacterial Stabilization of a Panel of Picornaviruses. *mSphere* **4**, e00183-19 (2019).

194. Ren, R., Costantini, F., Gorgacz, E. J., Lee, J. J. & Racaniello, V. R. Transgenic mice expressing a human poliovirus receptor: A new model for poliomyelitis. *Cell* **63**, 353–362 (1990).

195. Fujii, K. *et al.* Transgenic mouse model for the study of enterovirus 71 neuropathogenesis. doi:10.1073/pnas.1217563110.

196. Wang, Y. & Pfeiffer, J. K. Emergence of a large-plaque variant in mice infected with coxsackievirus B3. *MBio* **7**, 1–10 (2016).

197. Ohka, S. *et al.* Establishment of a Poliovirus Oral Infection System in Human Poliovirus Receptor-Expressing Transgenic Mice That Are Deficient in Alpha/Beta Interferon Receptor. *J. Virol.* **81**, 7902–7912 (2007).

198. Robinson, C. M., Wang, Y. & Pfeiffer, J. K. Sex-Dependent Intestinal Replication of an Enteric Virus. *J. Virol.* **91**, e02101-16 (2017).

199. Bopegamage, S. *et al.* Coxsackie B virus infection of mice: Inoculation by the oral route protects the pancreas from damage, but not from infection. *J. Gen. Virol.* **86**, 3271–3280 (2005).

200. Yang, C.-H. *et al.* A Novel Murine Model Expressing a Chimeric mSCARB2/hSCARB2 Receptor is Highly Susceptible to Oral Infection with Clinical Isolates of EV71. *J. Virol.* JVI.00183-19 (2019) doi:10.1128/JVI.00183-19.

201. Chen, Y. C. *et al.* A murine oral enterovirus 71 infection model with central nervous system involvement. *J. Gen. Virol.* **85**, 69–77 (2004).

202. Zhang, Y. *et al.* Pathogenesis study of enterovirus 71 infection in rhesus monkeys. *Lab. Investig.* **91**, 1337–1350 (2011).

203. Hashimoto, I. & Hagiwara, A. N. D. A. Pathogenicity of a Poliomyelitis-like disease in monkeys infected orally with Enterovirus 71: a model for human infection. *Neuropathol. Appl. Neurobiol.* **8**, 149–156 (1982).

204. Liu, L. *et al.* Neonatal rhesus monkey is a potential animal model for studying pathogenesis of EV71 infection. *Virology* **412**, 91–100 (2011).

205. Cammock, C. E. *et al.* Myocarditis, Disseminated Infection, and Early Viral Persistence Following Experimental Coxsackievirus B Infection of Cynomolgus Monkeys. *PLoS One* **8**, 1–8 (2013).

206. London, W. T., Curfman, B. L., Brown, R. L. & Notkins, A. L. Coxsackie Virus B4 Produces Transient Diabetes in Nonhuman Primates. *Diabetes* **35**, 712–716 (1986).

207. Bachtold, J. G., Gebhardt, L. P. & Bubel, H. C. Cellular Immunity of Monkeys versus Antibody Titers Following Oral Inoculation with Poliomyelitis Virus. *J. Immunol.* **75**, (1955).

208. Coid, C. & Beswick, T. The sensitivity of monkeys to subcutaneous inoculation of the Brunenders strain of type-I poliomyelitis virus. *J. Pathol. Bacteriol.* **79**, 325–30 (1960).

209. Coid, C. R., Beswick, T. S. L. & Tobin, J. O. h. The virulence of strains of poliovirus for cynomolgus monkeys after subcutaneous injection. *J. Hyg. (Lond).* **59**, 387–394 (1961).

210. Shen, L. *et al.* Pathogenic Events in a Nonhuman Primate Model of Oral Poliovirus Infection Leading to Paralytic Poliomyelitis. *J. Virol.* **91**, 1–15 (2017).

211. Nagata, N. *et al.* Differential localization of neurons susceptible to enterovirus 71 and poliovirus type 1 in the central nervous system of cynomolgus monkeys after intravenous inoculation. *J. Gen. Virol.* **85**, 2981–2989 (2004).

212. Sabin, A. B. Immunization of Chimpanzees and Human Beings With Avirulent Strains of Poliomyelitis Virus. *Ann. N. Y. Acad. Sci.* **61**, 1050–1056 (1955).

213. Horstmann, D., Melnick, J., Ward, R. & Fletias. The susceptibility of infant rhesus monkeys to poliomyelitis virus administered by mouth. *J. Exp. Med.* **4**, (1947).

214. Khetsuriani, N., Lamonte-Fowlkes, A., Oberst, S. & Pallansch, M. A. Enterovirus surveillance--United States, 1970-2005. *MMWR. Surveill. Summ. Morb. Mortal. Wkly. report. Surveill. Summ. / CDC* (2006).

215. Tebruegge, M. & Curtis, N. Enterovirus infections in neonates. *Semin. Fetal Neonatal Med.* **14**, 222–227 (2009).

216. Pedrosa, C., Lage, M. J. & Virella, D. Congenital echovirus 21 infection causing fulminant hepatitis in a neonate. *BMJ Case Rep.* (2013) doi:10.1136/bcr-2012-008394.

217. Tassin, M. *et al.* A case of congenital Echovirus 11 infection acquired early in pregnancy. *J. Clin. Virol.* **59**, 71–73 (2014).

218. Viskari, H. R. *et al.* Maternal first-trimester enterovirus infection and future risk of type 1 diabetes in the exposed fetus. *Diabetes* **51**, 2568–2571 (2002).

219. Garcia, A. G., Basso, N. G., Fonseca, M. E. & Outani, H. N. Congenital echo virus infection--morphological and virological study of fetal and placental tissue. *J. Pathol.* **160**, 123–7 (1990).

220. Basso, N. G. *et al.* Enterovirus isolation from foetal and placental tissues. *Acta Virol.* **34**, 49–57 (1990).

221. Nielsen, J. L., Berryman, G. K. & Hankins, G. D. V. Intrauterine Fetal Death and the Isolation of Echovirus 27 from Amniotic Fluid. *J. Infect. Dis.* **158**, 501–502 (1988).

222. Bergelson, J. M. *et al.* Decay-accelerating factor (CD55), a glycosylphosphatidylinositolanchored complement regulatory protein, is a receptor for several echoviruses. *Proc. Natl. Acad. Sci.* **91**, 6245–6248 (1994).

223. Chevaliez, S. *et al.* Role of class I human leukocyte antigen molecules in early steps of echovirus infection of rhabdomyosarcoma cells. *Virology* **381**, 203–214 (2008).

224. Ward, T. *et al.* Role for β2-Microglobulin in Echovirus Infection of Rhabdomyosarcoma Cells. *J. Virol.* **72**, 5360–5365 (1998).

225. Goodfellow, I. G. *et al.* Echovirus infection of rhabdomyosarcoma cells is inhibited by antiserum to the complement control protein CD59. *J. Gen. Virol.* **81**, 1393–1401 (2000).

226. Petkova, S. B. *et al.* Enhanced half-life of genetically engineered human IgG1 antibodies in a humanized FcRn mouse model: Potential application in humorally mediated autoimmune disease. *Int. Immunol.* **18**, 1759–1769 (2006).

227. Roopenian, D. C., Christianson, G. J., Proetzel, G. & Sproule, T. J. Human FcRn Transgenic Mice for Pharmacokinetic Evaluation of Therapeutic Antibodies. *Methods Mol. Biol.* **1438**, 103–114 (2016).

228. Latvala, S., Jacobsen, B., Otteneder, M. B., Herrmann, A. & Kronenberg, S. Distribution of FcRn Across Species and Tissues. *J. Histochem. Cytochem.* **65**, 321–333 (2017).

229. Fan, Y. Y. *et al.* Tissue expression profile of human neonatal Fc receptor (FcRn) in Tg32 transgenic mice. *MAbs* **8**, 848–853 (2016).

230. Pyzik, M., Rath, T., Lencer, W. I., Baker, K. & Blumberg, R. S. FcRn: The Architect Behind the Immune and Nonimmune Functions of IgG and Albumin. *J. Immunol.* **194**, 4595–4603 (2015).

231. Arora, N., Sadovsky, Y., Dermody, T. S. & Coyne, C. B. Microbial Vertical Transmission during Human Pregnancy. *Cell Host Microbe* **21**, 561–567 (2017).

232. Roopenian, D. C. & Akilesh, S. FcRn: The neonatal Fc receptor comes of age. *Nat. Rev. Immunol.* **7**, 715–725 (2007).

233. Jones, E. A. & Waldmann, T. A. The mechanism of intestinal uptake and transcellular transport of IgG in the neonatal rat. *J. Clin. Invest.* **51**, 2916–2927 (1972).

234. Cianga, C., Cianga, P., Plamadeala, P. & Amalinei, C. Nonclassical major histocompatibility complex I-like Fc neonatal receptor (FcRn) expression in neonatal human tissues. *Hum. Immunol.* **72**, 1176–1187 (2011).

235. Pyzik, M. *et al.* Hepatic FcRn regulates albumin homeostasis and susceptibility to liver injury. *Proc. Natl. Acad. Sci.* **114**, E2862–E2871 (2017).

236. Chaudhury, C. *et al.* The Major Histocompatibility Complex–related Fc Receptor for IgG

(FcRn) Binds Albumin and Prolongs Its Lifespan. *J. Exp. Med.* **197**, 315–322 (2003).

237. Ward, T., Powell, R. M., Evans, D. J. & Almond, J. W. Serum albumin inhibits echovirus 7 uncoating. *J. Gen. Virol.* **80**, 283–290 (1999).

238. Chaudhury, C., Brooks, C. L., Carter, D. C., Robinson, J. M. & Anderson, C. L. Albumin binding to FcRn: Distinct from the FcRn-IgG interaction. *Biochemistry* **45**, 4983–4990 (2006).

239. Dickinson, B. L. *et al.* Bidirectional FcRn-dependent IgG transport in a polarized human intestinal epithelial cell line. *J. Clin. Invest.* **104**, 903–911 (1999).

240. Simister, N. E. & Mostov, K. E. An Fc receptor structurally related to MHC class I antigens. *Nature* vol. 337 184–187 (1989).

241. Leach, J. L. *et al.* Isolation from human placenta of the IgG transporter, FcRn, and localization to the syncytiotrophoblast: implications for maternal-fetal antibody transport. *J. Immunol.* **157**, 3317 LP – 3322 (1996).

242. Sockolosky, J. T. & Szoka, F. C. The neonatal Fc receptor, FcRn, as a target for drug delivery and therapy. *Adv. Drug Deliv. Rev.* **91**, 109–124 (2015).

243. Stins, M. F., Badger, J. & Sik Kim, K. Bacterial invasion and transcytosis in transfected human brain microvascular endothelial cells. *Microb. Pathog.* **30**, 19–28 (2001).

244. Bayer, A. *et al.* Type III Interferons Produced by Human Placental Trophoblasts Confer Protection against Zika Virus Infection. *Cell Host Microbe* **19**, 705–712 (2016).

245. Morosky, S., Lennemann, N. J. & Coyne, C. B. BPIFB6 Regulates Secretory Pathway Trafficking and Enterovirus Replication. *J. Virol.* **90**, 5098–5107 (2016).

246. Savidis, G. *et al.* The IFITMs Inhibit Zika Virus Replication. *Cell Rep.* **15**, 2323–2330 (2016).

247. Oberste, M. S. *et al.* Species-specific RT-PCR amplification of human enterovirus: A tool for rapid species identification of uncharacterized enteroviruses. *J. Gen. Virol.* **87**, 119–128 (2006).

248. Babicki, S. *et al.* Heatmapper: web-enabled heat mapping for all. *Nucleic Acids Res.* **44**, W147–W153 (2016).

249. Love, M. I., Huber, W. & Anders, S. Moderated estimation of fold change and dispersion for RNA-seq data with DESeq2. *Genome Biol.* **15**, 1–21 (2014).

250. Giannetti, A. M. & Björkman, P. J. HFE and transferrin directly compete for transferrin receptor in solution and at the cell surface. *J. Biol. Chem.* **279**, 25866–25875 (2004).

251. Morens, D. M. Enteroviral disease in early infancy. *J. Pediatr.* (1978) doi:10.1016/S0022-

3476(78)80422-3.

252. Civardi, E. *et al.* Viral outbreaks in neonatal intensive care units: What we do not know. *Am. J. Infect. Control* **41**, 854–856 (2013).

253. Verboon-Maciolek, M. A., Krediet, T. G., Gerards, L. J., Fleer, A. & Van Loon, T. M. Clinical and epidemiologic characteristics of viral infections in a neonatal intensive care unit during a 12-year period. *Pediatr. Infect. Dis. J.* **24**, 901–904 (2005).

254. Ho, S. Y. *et al.* Investigation and successful control of an echovirus 11 outbreak in neonatal intensive care units. *Pediatr. Neonatol.* **61**, 180–187 (2019).

255. Zhao, X. *et al.* Human Neonatal Fc Receptor Is the Cellular Uncoating Receptor for Enterovirus B. *Cell* **177**, 1–13 (2019).

256. Khan, S. *et al.* Poliomyelitis in transgenic mice expressing CD155 under the control of the Tage4 promoter after oral and parenteral poliovirus inoculation. *J. Gen. Virol.* **95**, 1668–1676 (2014).

257. Koestner, W. *et al.* Interferon-beta expression and type I interferon receptor signaling of hepatocytes prevent hepatic necrosis and virus dissemination in Coxsackievirus B3-infected mice. *PLoS Pathog.* **14**, 1–23 (2018).

258. Hughes, S. A., Thaker, H. M. & Racaniello, V. R. Transgenic mouse model for echovirus myocarditis and paralysis. *Proc. Natl. Acad. Sci. U. S. A.* **100**, 15906–15911 (2003).

259. Choi, H. M. T. *et al.* Third-generation in situ hybridization chain reaction: Multiplexed, quantitative, sensitive, versatile, robust. *Dev.* **145**, 1–10 (2018).

260. Dirks, R. M. & Pierce, N. A. Triggered amplification by hybridization chain reaction. *Proc. Natl. Acad. Sci. U. S. A.* **101**, 15275–15278 (2004).

261. Choi, H. M. T. *et al.* Mapping a multiplexed zoo of mRNA expression. *Dev.* **143**, 3632–3637 (2016).

262. Shah, U. *et al.* Distribution of the IgG Fc receptor, FcRn, in the human fetal intestine. *Pediatr. Res.* **53**, 295–301 (2003).

263. Israel, E. J. *et al.* Expression of the neonatal Fc receptor, FcRn, on human intestinal epithelial cells. *Immunology* **92**, 69–74 (1997).

264. Blumberg, R. S. *et al.* A major histocompatibility complex class I- related Fc receptor for IgG on rat hepatocytes. *J Clin Invest. Clin. Invest* **95**, 2397–2402 (1995).

265. Bersani, I. *et al.* Neonatal acute liver failure due to enteroviruses: a 14 years single NICU experience. *J. Matern. Neonatal Med.* (2020) doi:10.1080/14767058.2018.1555806.

266. Morgan, C., Thomson, S. J., Legg, J. & Narat, S. A Case of Fulminant Hepatitis due to

Echovirus 9 in a Patient on Maintenance Rituximab Therapy for Follicular Lymphoma. *Case Rep. Hematol.* **2015**, 1–4 (2015).

267. Lefterova, M. I., Rivetta, C., George, T. I. & Pinsky, B. A. Severe hepatitis associated with an echovirus 18 infection in an immune-compromised adult. *J. Clin. Microbiol.* **51**, 684–687 (2013).

268. Bajema, K. L. *et al.* Acute Liver Failure Due to Echovirus 9 Associated With Persistent B-Cell Depletion From Rituximab. *Open Forum Infect. Dis.* **4**, 9–11 (2017).

269. Laassri, M. *et al.* Evolution of echovirus 11 in a chronically infected immunodeficient patient. *PLoS Pathog.* **14**, 1–18 (2018).

270. Ventura, K. C., Hawkins, H., Smith, M. B. & Walker, D. H. Fatal neonatal echovirus 6 infection: Autopsy case report and review of the literature. *Mod. Pathol.* (2001) doi:10.1038/modpathol.3880260.

271. Tripathi, A. *et al.* The gut-liver axis and the intersection with the microbiome. *Nat. Rev. Gastroenterol. Hepatol.* **15**, 397–411 (2018).

272. Ohtani, N. & Kawada, N. Role of the Gut-Liver Axis in Liver Inflammation, Fibrosis, and Cancer: A Special Focus on the Gut Microbiota Relationship. *Hepatol. Commun.* **3**, 456–470 (2019).

273. Abedi, G. R., Watson, J. T., Nix, W. A., Oberste, M. S. & Gerber, S. I. Morbidity and Mortality Weekly Report Enterovirus and Parechovirus Surveillance-United States, 2014-2016. *MMWR. Morb. Mortal. Wkly. Rep.* **67**, 515–18 (2018).

274. Bubba, L. *et al.* A 4-year Study on Epidemiologic and Molecular Characteristics of Human Parechoviruses and Enteroviruses Circulating in Children Younger Than 5 Years in Northern Italy. *Pediatr. Infect. Dis. J.* **36**, 13–19 (2017).

275. Cabrerizo, M. *et al.* Molecular epidemiology of enterovirus and parechovirus infections according to patient age over a 4-year period in Spain. *J. Med. Virol.* **89**, 435–442 (2017).

276. Rodà, D. *et al.* Clinical characteristics and molecular epidemiology of Enterovirus infection in infants <3 months in a referral paediatric hospital of Barcelona. *Eur. J. Pediatr.* **174**, 1549–1553 (2015).

277. Khong, W. X. *et al.* A Non-Mouse-Adapted Enterovirus 71 (EV71) Strain Exhibits Neurotropism, Causing Neurological Manifestations in a Novel Mouse Model of EV71 Infection. *J. Virol.* **86**, 2121–2131 (2012).

278. Pan, J. *et al.* Expression of Human Decay-Accelerating Factor on Intestinal Epithelium of Transgenic Mice Does Not Facilitate Infection by the Enteral Route. *J. Virol.* **89**, 4311–4318 (2015).

279. Nice, T. J. *et al.* Type I Interferon Receptor Deficiency in Dendritic Cells Facilitates

Systemic Murine Norovirus Persistence Despite Enhanced Adaptive Immunity. *PLoS Pathog.* **12**, 1–19 (2016).

280. Wells, A. I. *et al.* Human FcRn expression and Type I Interferon signaling control Echovirus 11 pathogenesis in mice. *PLOS Pathog.* **17**, e1009252 (2021).

281. Knudsen Sand, K. M. *et al.* Unraveling the interaction between FcRn and albumin: Opportunities for design of albumin-based therapeutics. *Front. Immunol.* **6**, 1–21 (2015).

282. Schoggins, J. W. Interferon-Stimulated Genes: What Do They All Do? *Annu. Rev. Virol.* **6**, 567–584 (2019).

283. Ouzilou, L. *et al.* Poliovirus transcytosis through M-like cells. *J. Gen. Virol.* **83**, 2177–2182 (2002).

284. Oberste, M. S., Nix, W. A., Maher, K. & Pallansch, M. A. Improved molecular identification of enteroviruses by RT-PCR and amplicon sequencing. *J. Clin. Virol.* **26**, 375–377 (2003).

285. Modlin, J. F. *et al.* Aseptic Meningitis in Infants <2 Years of Age: Diagnosis and Etiology. *J. Infect. Dis.* **168**, 888–892 (1993).

286. Huang, C. *et al.* Multiple-year experience in the diagnosis of viral central nervous system infections with a panel of polymerase chain reaction assays for detection of 11 viruses. *Clin. Infect. Dis.* **39**, 630–635 (2004).

287. Rotbart, H. Enteroviral infections of the central nervous system. *Clin. Infect. Dis.* **20**, 971–981 (1995).

288. Centers for Disease Control & Prevention. Outbreaks of Aseptic Meningitis Associated with Echoviruses 9 and 30 and Preliminary Surveillance Reports on Enterovirus Activity --- United States, 2003. *MMWR Morb Mortal Wkly Rep* **52**, 761–764 (2003).

289. Lee, H. Y. *et al.* Clinical features of echovirus 6 and 9 infections in children. *J. Clin. Virol.* **49**, 175–179 (2010).

290. Kim, H. J. *et al.* Epidemics of viral meningitis caused by echovirus 6 and 30 in Korea in 2008. *Virol. J.* **9**, 38 (2012).

291. Chuang, Y. Y. & Huang, Y. C. Enteroviral infection in neonates. *J. Microbiol. Immunol. Infect.* **52**, 851–857 (2019).

292. Modlin, J. F. Perinatal echovirus infection: insights from a literature review of 61 cases of serious infection and 16 outbreaks in nurseries. *Rev. Infect. Dis.* **8**, 918–926 (1986).

293. Zhang, Y. & Pardridge, W. M. Mediated efflux of IgG molecules from brain to blood across the blood-brain barrier. *J. Neuroimmunol.* **114**, 168–172 (2001).

294. Schlachetzki, F., Zhu, C. & Pardridge, W. M. Expression of the neonatal Fc receptor (FcRn) at the blood-brain barrier. *J. Neurochem.* **81**, 203–206 (2002).

295. Ahn, J. *et al.* Susceptibility of mouse primary cortical neuronal cells to coxsackievirus B. *J. Gen. Virol.* **85**, 1555–1564 (2004).

296. Feuer, R. *et al.* Coxsackievirus targets proliferating neuronal progenitor cells in the neonatal CNS. *J. Neurosci.* **25**, 2434–2444 (2005).

297. Feuer, R. *et al.* Coxsackievirus B3 and the neonatal CNS: The roles of stem cells, developing neurons, and apoptosis in infection, viral dissemination, and disease. *Am. J. Pathol.* **163**, 1379–1393 (2003).

298. Zhang, G. *et al.* Pathological features of echovirus-11-associated brain damage in mice based on rna-seq analysis. *Viruses* **13**, 1–14 (2021).

299. Nishikawa, M. *et al.* Abnormalities of brain perfusion in echovirus type 30 meningitis. *J. Neurol. Sci.* **179**, 122–126 (2000).

300. Wang, S. M. *et al.* Cerebrospinal fluid cytokines in enterovirus 71 brain stem encephalitis and echovirus meningitis infections of varying severity. *Clin. Microbiol. Infect.* **13**, 677–682 (2007).

301. Ichiyama, T. *et al.* Analysis of cytokine levels in cerebrospinal fluid in mumps meningitis: Comparison with echovirus type 30 meningitis. *Cytokine* **30**, 243–247 (2005).

302. Chonmaitree, T. & Baron, S. Bacteria and viruses induce production of interferon in the cerebrospinal fluid of children with acute meningitis: a study of 57 cases and review. *Rev. Infect. Dis.* **13**, 1061–1065 (1991).

303. Singh, H., Koury, J. & Kaul, M. Innate immune sensing of viruses and its consequences for the central nervous system. *Viruses* **13**, 1–42 (2021).

304. Li, Y. *et al.* Interferon-λ attenuates rabies virus infection by inducing interferon-stimulated genes and alleviating neurological inflammation. *Viruses* **12**, 1–22 (2020).

305. Wells, A. I., Grimes, K. A. & Coyne, C. B. Enterovirus replication and dissemination are differentially controlled by type I and III interferons in the GI tract. *bioRxiv* (2022) doi:10.4103/jispcd.JISPCD.

306. Cooper, P. R. *et al.* Efflux of monoclonal antibodies from rat brain by neonatal Fc receptor, FcRn. *Brain Res.* **1534**, 13–21 (2013).

307. DeSisto, J. *et al.* Single-Cell Transcriptomic Analyses of the Developing Meninges Reveal Meningeal Fibroblast Diversity and Function. *Dev. Cell* **54**, 43-59.e4 (2020).

308. Kierdorf, K., Masuda, T., Jordão, M. J. C. & Prinz, M. Macrophages at CNS interfaces: ontogeny and function in health and disease. *Nat. Rev. Neurosci.* **20**, 547–562 (2019).

309. Matsubara, T. *et al.* Mononuclear cells and cytokines in the cerebrospinal fluid of echovirus 30 meningitis patients. *Scand. J. Infect. Dis.* **32**, 471–474 (2000).

310. Freeman, M. C. *et al.* Respiratory and intestinal epithelial cells exhibit differential susceptibility and innate immune responses to contemporary EV-D68 isolates. *eLife* (2021) doi:10.1101/2021.01.05.425225.

311. Kuss, S. K., Etheredge, C. A. & Pfeiffer, J. K. Multiple host barriers restrict poliovirus trafficking in mice. *PLoS Pathog.* **4**, (2008).

312. Bultmann, B. D., Eggers, H. J., Galle, J. & Haferkamp, O. Age dependence of paralysis induced by echovirus type 9 in infant mice. *J. Infect. Dis.* **147**, 999–1005 (1983).

313. O'Brown, N. M., Pfau, S. J. & Gu, C. Bridging barriers: A comparative look at the blood-brain barrier across organisms. *Genes Dev.* **32**, 466–478 (2018).

314. Wu, A. G. *et al.* Age-dependent susceptibility to reovirus encephalitis in mice is influenced by maturation of the type-I interferon response. *Pediatr. Res.* **83**, 1057–1066 (2018).

315. Lyden, D., Olszewski, J. & Huber, S. Variation in susceptibility of Balb/c mice to coxsackievirus group B type 3-induced myocarditis with age. *Cell. Immunol.* **105**, 332–339 (1987).

316. Khatib, R., Chason, J. L., Silberberg, B. K. & Lerner, A. M. Age-dependent pathogenicity of group B coxsackieviruses in Swiss-Webster mice: Infectivity for myocardium and pancreas. *J. Infect. Dis.* **141**, 394–403 (1980).

317. Qiu, X. & Wang, M. Z. Quantification of neonatal fc receptor and beta-2 microglobulin in human liver tissues by ultraperformance liquid chromatography-multiple reaction monitoring-based targeted quantitative proteomics for applications in biotherapeutic physiologically-based p. *Drug Metab. Dispos.* **48**, 925–933 (2020).

318. Center for Disease Control. Non Polio Enterovirus. *CDC Website* (2017).

319. Yang, T. *et al. Clinical features and factors of unfavorable outcomes for non-polio enterovirus infection of the central nervous system in northern Taiwan, 1994-2003*. *J Microbiol Immunol Infect* vol. 38 https://pdfs.semanticscholar.org/7aac/8ae41c738011e085f4b066e775ecc6a32465.pdf (2005).

320. Wells, A. I. & Coyne, C. B. Enteroviruses: A Gut-Wrenching Game of Entry, Detection, and Evasion. *Viruses* **11**, 1–20 (2019).

321. Deonarain, R., Cerullo, D., Fuse, K., Liu, P. P. & Fish, E. N. Protective role for interferon-β in coxsackievirus B3 infection. *Circulation* **110**, 3540–3543 (2004).

322. Id, T. K., Flynn, C. T., Alirezaei, M., Sen, G. C. & J, L. W. Biphasic and cardiomyocyte-specific IFIT activity protects cardiomyocytes from enteroviral infection. *PLoS Pathog.* **15**,

1–22 (2019).

323. Wei, C. *et al.* Viperin inhibits enterovirus A71 replication by interacting with viral 2C protein. *Viruses* **11**, (2019).

324. Rivera-Serrano, E. E. *et al.* Viperin Reveals Its True Function. *Annual Review of Virology* vol. 7 421–446 (2020).

325. Kane, M. *et al.* Identification of Interferon-Stimulated Genes with Antiretroviral Activity. *Cell Host Microbe* **20**, 392–405 (2016).

326. Schoggins, J. W. *et al.* Pan-viral specificity of IFN-induced genes reveals new roles for cGAS in innate immunity. *Nature* **505**, 691–695 (2014).

327. Transcripts, U. L. U. L. *et al.* The Zinc Finger Antiviral Protein ZAP Restricts Human. *MBio* **12**, 1–23 (2021).

328. Takata, M. A. *et al.* CG dinucleotide suppression enables antiviral defence targeting non-self RNA. *Nature* **550**, 124–127 (2017).

329. Goonawardane, N., Nguyen, D. & Simmonds, P. Association of Zinc Finger Antiviral Protein Binding to Viral Genomic RNA with Attenuation of Replication of Echovirus 7. *mSphere* **6**, (2021).

330. Reagan, K. J., Goldberg, B. & Crowell, R. L. Altered receptor specificity of coxsackievirus B3 after growth in rhabdomyosarcoma cells. *J. Virol.* **49**, 635–640 (1984).

331. Lee, H. *et al.* Zinc-finger antiviral protein mediates retinoic acid inducible gene I-like receptor-independent antiviral response to murine leukemia virus. *Proc. Natl. Acad. Sci. U. S. A.* **110**, 12379–12384 (2013).

332. Meagher, J. L. *et al.* Structure of the zinc-finger antiviral protein in complex with RNA reveals a mechanism for selective targeting of CG-rich viral sequences. *Proc. Natl. Acad. Sci. U. S. A.* **116**, 24303–24309 (2019).

333. Choudhury, N. R., Heikel, G. & Michlewski, G. TRIM25 and its emerging RNA-binding roles in antiviral defense. *Wiley Interdiscip. Rev. RNA* **11**, 1–14 (2020).

334. Ficarelli, M., Neil, S. J. D. & Swanson, C. M. Targeted Restriction of Viral Gene Expression and Replication by the ZAP Antiviral System. *Annu. Rev. Virol.* **8**, 265–283 (2021).

335. Li, M. M. H. *et al.* TRIM25 Enhances the Antiviral Action of Zinc-Finger Antiviral Protein (ZAP). *PLoS Pathog.* **13**, 1–25 (2017).

336. Odon, V. *et al.* The role of ZAP and OAS3/RNAseL pathways in the attenuation of an RNA virus with elevated frequencies of CpG and UpA dinucleotides. *Nucleic Acids Res.* **47**, 8061–8083 (2019).

337. Lohöfener, J. *et al.* The activation mechanism of 2′-5′-oligoadenylate synthetase gives new insights into OAS/cGAS triggers of innate immunity. *Structure* **23**, 851–862 (2015).

338. Han, Y. *et al.* Structure of human RNase L reveals the basis for regulated RNA decay in the IFN response. *Science (80-.).* **343**, 1244–1248 (2014).

339. Soveg, F. W. *et al.* Endomembrane targeting of human OAS1 p46 augments antiviral activity. *Elife* **10**, 1–29 (2021).

340. Blom, N., Hansen, J., Blaas, D. & Brunak, S. Cleavage site analysis in picornaviral polyproteins: Discovering cellular targets by neural networks. *Protein Sci.* **5**, 2203–2216 (1996).

341. Krausslich, H. G. & Wimmer, E. VIRAL PROTEINASES. *Annu. Rev. Biochem.* **57**, 701–754 (1988).

342. Schoggins, J. W. *et al.* A diverse range of gene products are effectors of the type i interferon antiviral response. *Nature* **472**, 481–485 (2011).

343. Dittmann, M. *et al.* A serpin shapes the extracellular environment to prevent influenza a virus maturation. *Cell* **160**, 631–643 (2015).